Spin-charge coupled transport in two- and three-dimensional Rashba systems

Dissertation

zur Erlangung des akademischen Grades

Dr. rer. nat.

eingereicht an der

Mathematisch-Naturwissenschaftlich-Technischen Fakultät

der Universität Augsburg

von

Sebastian Tölle

Augsburg, Mai 2018

Erstgutachter:	Prof. Dr. Ulrich Eckern
Zweitgutachter:	Prof. Dr. Thilo Kopp
Drittgutachter:	Prof. Dr. Gerrit E. W. Bauer
Tag der mündlichen Prüfung:	26. Juli 2018

Contents

Abstract

Spintronics is an emerging field with the central objective of utilizing simultaneously the spin and charge degrees of freedom. The exploitation of the spin, in addition to the charge, offers the opportunity to overcome limitations of traditional electronics, especially for data storage and transfer. In this context, the fundamental tasks are the generation, manipulation, and detection of spin densities and spin currents. Experimentally, an implementation of these tasks can be achieved by attaching a spin-orbit active material to a ferromagnet. Particularly interesting examples of spin-orbit active materials are systems with Rashba spin-orbit coupling. In this thesis, we theoretically investigate the spin-charge coupled dynamics in such systems for three special geometries.

First, a quasi two-dimensional Rashba system with a proximity induced magnetization is considered. Due to a dynamical magnetic texture an effective force acting on the charge carriers is found. We identify each contribution by its origin, spin density or spin current, highlighting a novel 'inverse-spin-filter' contribution. The latter arises from a spin current polarized parallel to the magnetization as a result of a consistent treatment of spin-orbit contributions to the Elliott-Yafet spin relaxation mechanism.

In the second geometry, a two-dimensional Rashba system laterally attached to a ferromagnet, the boundary conditions at the interface are significantly affected by current-induced spin polarizations. Therefore, the magnetization-dependence of the magnetoresistance is non-trivial and asymmetric, and, in particular, features a characteristic magnetization angle where the ferromagnetic contribution to the magnetoresistance vanishes. The thermal analogue of the magnetoresistance, the magnetothermopower, turns out to be very small due to a cancellation of electrical and thermal contributions.

The Rashba system in the third setup is extended to the third dimension, and placed on top of a ferromagnetic insulator. Due to the spin-transfer torque, the current-induced spin polarization acquires a characteristic magnetization dependence which manifests itself in the signal of the magnetoresistance. Our theoretical results reproduce several features of the experiments, at least qualitatively. In particular, the anisotropy of the spin relaxation, enhanced due to the mass anisotropy, plays a major role for the interpretation of the observed signals.

1

Introduction

This thesis is devoted to the investigation of the active control of spin degrees of freedom in Rashba systems. In general, via spin-orbit coupling, an electric field can generate a transverse spin current, the spin Hall effect [1–4], and a current-induced spin polarization [5–10], to name the two most prominent phenomena in the field of spintronics [11, 12]. The latter is also referred to as inverse spin galvanic, Rashba-Edelstein, or simply Edelstein effect. Their thermal analogues, exchanging the electrical field with a thermal gradient, are the spin Nernst effect [13–17] and the thermally induced spin polarization [17–19], respectively, both belonging to the field of spin caloritronics [20]. Spin currents and spin densities can further be manipulated by exploiting the exchange coupling between the magnetization of a ferromagnet and the spin of charge carriers as the latter exerts a torque on the magnetization. Vice versa, a time-dependent magnetization is able to induce nonequilibrium spin densities and spin currents which by themselves can be observed as signatures in the charge currents.

As an overview, table 1.1 provides a short summary of the most relevant effects related to spin-orbit interaction. Here, each effect is named ("Effect"), together with the qualitative relation of the relevant observable to its driving source ("Definition"), the year of its experimental observation ("Experiment"), and some additional information ("Remarks"). A summation over multiple indices is implied, and ε_{iak} is the Levi-Civita symbol. The quantities appearing in the table are denoted as follows.

a-polarized spin current in i direction:	j_i^a
Spin current in i direction:	$\mathbf{j}_i$
Nonequilibrium part of the spin density:	$\delta\mathbf{s}$
Electric field:	$\mathbf{E}$
Temperature gradient:	∇T
Magnetization direction:	$\mathbf{n}$

Effect	Definition	Experiment	Remarks
Spin galvanic	$\mathbf{E} \perp \delta\mathbf{s}$	2001 [21]	Also referred to as inverse Edelstein effect [22]
Spin Hall	$j_i^a \sim \varepsilon_{iak} E_k$	2004 [3, 4]	
Inverse spin galvanic	$\delta\mathbf{s} \perp \mathbf{E}$	2004 [9, 10]	Also referred to as Edelstein or Rashba-Edelstein effect
Inverse spin Hall	$E_i \sim \varepsilon_{iak} j_k^a$	2006 [23–25]	Gives rise to the spin Hall magnetoresistance and the spin Nernst magnetothermopower
Spin Nernst	$j_i^a \sim \varepsilon_{iak} \nabla_k T$	2017 [26, 27]	Indirectly observed through the spin Nernst magnetothermopower
Thermally induced spin polarization	$\delta\mathbf{s} \perp \nabla T$	—	Also referred to as thermal Edelstein effect
Inverse spin filter	$E_i \sim \mathbf{n} \cdot \mathbf{j}_i$	—	Predicted in Ref. 28

TABLE 1.1.: Effects related to spin-orbit coupling.

Historically, the first experiments on the spin Hall effect were performed on semiconductor heterostructures [3, 4]. The two-dimensional electron gas (2DEG) that is formed at the interface of such structures shows strong spin-orbit coupling which can be classified as intrinsic or extrinsic depending on its origin, the band/device structure or the presence of impurities, respectively. Low-dimensional systems, and in particular two-dimensional systems are known to exhibit special physical phenomena such as the quantum Hall effect [29], the Kosterlitz-Thouless transition [30–32], or Anderson localization [33]. One important result of the scaling theory of localization [34] is that in two dimensions all states are localized for arbitrarily small impurity concentration. However, this is only the case for a system of infinite size due to the fact that the localization length is exponentially large in the case of weak disorder [35]. Therefore, transport mea-

surements for a 2D electron gas show metallic behavior even when a certain amount of impurities is present as long as the sample size does not exceed the localization length.

One particularly important type of intrinsic spin-orbit interaction, known as Rashba spin-orbit coupling [36, 37], arises due to a structural inversion asymmetry across the interface of a heterostructure. There exist a variety of possible microscopic origins, depending on the materials employed to achieve this type of spin-orbit coupling. For example, oxide heterostructures can exhibit a metallic interface [38–40], where the Rashba spin-orbit coupling originates primarily in the hybridization of t_{2g} orbitals due to spin-orbit splitting [41]. On the other hand, in conventional semiconductor heterostructures the interfacial 2DEG is formed by the s-orbital electron states with the Rashba spin splitting resulting from the asymmetric confining potential in the valance band [42].

The generation of a spin current by a dynamical magnetization is known as spin pumping [43–46]. The tool of choice for detecting these spin-pumping-induced spin currents is the inverse spin Hall effect, i.e., the build-up of an electric field transverse to the spin current [23–25, 46–49]. The typical spin pumping situation is as follows: in a magnet/normal-metal bilayer the magnetization of the magnetic material is driven such that it performs a conical precession which in turn leads to a spin current perpendicular to the interface. The inverse spin Hall effect allows to detect this spin current by measuring the inverse spin Hall voltage which is associated with the spin Hall angle θ_{SH}, the ratio of the spin Hall and charge conductivities. In this context, experimental investigations have so far concentrated on heavy-metal/ferromagnetic-insulator bilayers [50–55], since thin films of heavy metals such as Au, Pt, Ta, or W exhibit a large spin Hall conductivity [47, 49, 52, 56–61].

Apart from the magnet/normal-metal system discussed above, other spin pumping setups are possible. One particular interesting example is a Fe/GaAs bilayer, where the Fe/GaAs interface can be modelled as a spin-polarized effective two-dimensional electron gas [62, 63]. This heterostructure is known to exhibit Rashba spin-orbit coupling at the interface, which allows to generate an in-plane spin current in the spin pumping situation. In addition to spin currents, also a nonequilibrium spin density can be induced by the dynamic magnetization, which in turn generates an electric field perpendicular to its polarization. The latter describes the reciprocal of the inverse spin galvanic effect, the spin galvanic effect [21, 64, 65], which is also referred to as inverse Edelstein effect

[22, 66]. It was further shown that the inverse spin galvanic effect and the spin Hall effect are related to each other in Rashba systems [28, 67–69]. Note that in typical spin pumping setups, the magnetization is homogeneous. However, in this work, Chap. 4, we consider the more general case where the driving is due to a time-dependent magnetic texture, leading to a more complex situation [70–73].

Heterostructures consisting of spin-orbit active materials and a ferromagnet can also be employed for the investigation of the reciprocal situation where a spin current is generated by other means, e.g., an electric field. Here, the spin current can enter the magnetic material by exerting a spin torque on the ferromagnet's magnetization, a phenomena known as spin-transfer torque [74–76]. Together with the inverse spin Hall effect one can observe an indirect signature of the polarization-dependent spin currents by measuring the resistance of the metal layer for a varying magnetization direction, the so-called spin Hall magnetoresistance [50, 77]. Recently, the same principle was utilized to observe an indirect signature of the spin Nernst effect by measuring the magnetization-dependent thermopower, the spin Nernst magnetothermopower [26, 27].

In a two-dimensional Rashba system which is laterally connected to a ferromagnet, in-plane spin currents can be manipulated effectively by changing the polarization direction of the ferromagnet due to the spin-transfer torque. In this context, we theoretically investigate the spin Hall magnetoresistance and the spin Nernst magnetothermopower. Since the spin-transfer torque depends on the spin density at the interface, it is apparent that the inverse spin galvanic effect has a strong influence on the spin currents across the interface. As presented in Ref. 78, the results for both the spin Hall magnetoresistance and the spin Nernst magnetothermopower exhibit a more subtle and complex behavior in such a Rashba system than the results obtained for heavy-metal/ferromagnet bilayers using a purely phenomenological approach [77].

Recently, a new class of spin-orbit active materials has been discovered, namely bulk Rashba metals [79–84]. These three-dimensional materials exhibit a rather large Rashba spin-orbit coupling due to their noncentrosymmetric crystal structure, i.e., in this case, in the absence of a structure inversion asymmetry. These metals are promising candidates for an angular dependent magnetoresistance in a Rashba-metal/ferromagnet bilayer structure, similar to the heavy-metal/ferromagnet bilayer structure originally employed to measure the spin Hall magnetoresistance [50, 77].

Outline of this thesis

This thesis is organized as follows.

Chapter 2:
This chapter sets the stage by establishing the theoretical framework. We derive a generalized Boltzmann equation from the Keldysh Green's function formalism with particular focus on collision operators which describe momentum and spin relaxation due to impurities.

Chapter 3:
The systems under consideration is introduced, and the associated relevant phenomena are discussed: namely spin-orbit coupling, a proximity induced magnetization, and the spin-transfer torque.

Chapter 4:
Here, we present our results, published in Ref. 28, on the spin-charge coupled dynamics in a Rashba system with a time-dependent magnetic texture. A general force acting on the charge carriers is derived, featuring a novel contribution which we denote as inverse spin filter contribution. As an example, the typical spin pumping configuration is considered.

Chapter 5:
Based on Ref. 78, a two-dimensional Rashba system where one side is in contact with an insulating ferromagnet is discussed. We investigate the dependence of the spin currents and spin densities on the magnetization direction, as well as their signatures in the charge sector, i.e., the spin Hall magnetoresistance and the spin Nernst magnetothermopower.

Chapter 6:
In this chapter, we investigate the magnetoresistance of a three-dimensional Rashba metal attached to a ferromagnetic insulator. We show that the magnetization dependence of the current-induced spin polarization completely determines the magnetoresistance. The latter is discussed in the limiting cases of a purely damping-like and a purely field-like torque, respectively.

Chapter 7:
We close this thesis with a summary and an outlook on possible future investigations on spin-charge dynamics of Rashba systems coupled to a ferromagnet.

Appendices:
Appendices A, B, and C provide further technical details, relevant for Chap. 2, concerning the time-evolution operator, the gradient expansion, and the Elliott-Yafet collision operator, respectively. In App. D we derive a Landau-Lifshitz-Gilbert equation on the basis of the momentum integrated spin sector of the Boltzmann equation. Additional information for Chap. 4 is given in App. E, where the spin currents in a narrow wire is discussed. Appendix F provides supplementary material for Chap. 5, with a derivation of coupled spin diffusion equations, an application of the boundary conditions to this set of equations for large system sizes, and a derivation of Mott-like formulas for the spin transport coefficients. Details of Chap. 6 are given in App. G, in particular, the Elliott-Yafet collision operator for an anisotropic three-dimensional system, and the solution of the spin diffusion equations.

Finally, I wish to state that some of the main results of this thesis have already been published in Refs. 17, 28, 78, and 85. A list of own publications is given on page 163.

2

Kinetic theory

In this rather technical chapter, we set the stage for describing spin-charge coupled transport phenomena in the presence of spin-orbit coupling and a dynamical magnetic texture. For this purpose, we derive a Boltzmann equation for the distribution function $f = f^0 + \mathbf{f}\cdot\boldsymbol{\sigma}$, where f^0 is the particle distribution function, and $\mathbf{f}$ is the spin distribution function, where $\boldsymbol{\sigma} = (\sigma^x, \sigma^y, \sigma^z)$ denotes the vector of Pauli matrices. In order to obtain the Boltzmann equation we assume quasiclassical conditions, i.e., the spatial and temporal profiles of external fields are smooth on the Fermi wavelength and energy scales, respectively. Similarly, the spin-orbit energy splitting Δ_{SO} is assumed to be small, $\Delta_{\mathrm{SO}} \ll \epsilon_{\mathrm{F}}$.

The outline of this chapter is as follows: We first provide the basis by defining Green's functions in an equilibrium situation within the second quantization formalism. Next, we consider a nonequilibrium system and introduce the contour-ordered Green's function and the Keldysh formalism. We then employ diagrammatic perturbation theory, which allows to account for imperfections in our system, described by a random potential and the associated self-energy. Up to this point, common textbook knowledge will be presented [86–96], while we mainly follow the lines of Refs. 94–96. With these ingredients, we are able to derive the Boltzmann equation within the SU(2) formulation introduced in Ref. 97 by employing the gradient expansion [94, 98]. We close this chapter by deriving the collision operators of the Boltzmann equation. In particular, we present novel developments [28, 99] regarding the SU(2) description of the Elliott-Yafet collision operator, which itself describes a spin-flip relaxation mechanism due to spin-orbit coupling with impurities [100, 101].

2.1. Equilibrium Green's functions

This section provides the basis of the Green's function formalism by introducing the framework of second quantization –also known as canonical quantization– and defining the various Green's functions which we investigate within this whole chapter. Furthermore, we discuss the fluctuation-dissipation theorem and derive the spectral function for a free electron gas.

Second quantization

Let us first introduce the technique of second quantization as an appropriate formalism to deal with a many-body problem of identical particles. Within this formalism, particles are described by the fermionic field operators[1]

$$\hat{\Psi}(\mathbf{r}) = \sum_k \varphi_k(\mathbf{r})\hat{c}_k \ , \quad \hat{\Psi}^\dagger(\mathbf{r}) = \sum_k \varphi_k^*(\mathbf{r})\hat{c}_k^\dagger \, . \tag{2.1}$$

The operators $\hat{c}_k$ and $\hat{c}_k^\dagger$ annihilate and create a particle in state k, respectively, and obey the following anticommutation relations:

$$\begin{aligned} \left\{\hat{c}_k,\, \hat{c}_{k'}^\dagger\right\} &= \delta_{kk'} \, , \\ \left\{\hat{c}_k,\, \hat{c}_{k'}\right\} &= \left\{\hat{c}_k^\dagger,\, \hat{c}_{k'}^\dagger\right\} = 0 \, . \end{aligned} \tag{2.2}$$

Here, $\{\cdot,\, \cdot\}$ denotes the anticommutator and $\delta_{kk'}$ is the Kronecker delta. The wave functions $\varphi_k(\mathbf{r})$ in Eq. (2.1) form a complete set of single-particle eigenfunctions. Thus, together with the relations (2.2), the field operators fulfill the following anticommutation relations:

$$\begin{aligned} \left\{\hat{\Psi}(\mathbf{r}),\, \hat{\Psi}^\dagger(\mathbf{r}')\right\} &= \delta(\mathbf{r}-\mathbf{r}') \, , \\ \left\{\hat{\Psi}(\mathbf{r}),\, \hat{\Psi}(\mathbf{r}')\right\} &= \left\{\hat{\Psi}^\dagger(\mathbf{r}),\, \hat{\Psi}^\dagger(\mathbf{r}')\right\} = 0 \, . \end{aligned} \tag{2.3}$$

[1] Since we deal with spin-$1/2$ particles it is in principle implied that $\hat{\Psi}$ has also a spin structure, for example a 2×2 matrix structure in the basis of Pauli matrices. Nevertheless, since the expressions derived in the following are of general nature we suppress the spin degree of freedom for the time being.

Now, let us assume a single-particle Hamiltonian given in the spatial representation by

$$\mathcal{H}(\mathbf{r}) = -\frac{\hbar^2}{2m}\nabla^2 + V(\mathbf{r})\,. \tag{2.4}$$

In the field theoretical language with the field operators defined in Eq. (2.1) we obtain the following Hamiltonian:

$$\hat{H} = \int \mathrm{d}^3 r\, \hat{\Psi}^\dagger(\mathbf{r})\mathcal{H}(\mathbf{r})\hat{\Psi}(\mathbf{r})\,. \tag{2.5}$$

The operator $\hat{H}$ is now a many-particle operator, acting on Fock states denoted by $|\{n_\alpha\}\rangle \equiv |n_1, n_2, \ldots, n_k, \ldots\rangle$, meaning that the single-particle state $|k\rangle$ is occupied by n_k particles. In order to show that Eq. (2.5) is consistent with the statement, that the field describes independent fermions in single-particle modes, we assume that the single-particle wave functions φ_k are eigenfunctions of $\mathcal{H}$ with eigenvalues ϵ_k. By inserting Eq. (2.1) into Eq. (2.5) we obtain

$$\hat{H} = \sum_k \epsilon_k \hat{n}_k\,, \tag{2.6}$$

where $\hat{n}_k = \hat{c}_k^\dagger \hat{c}_k$ is the occupation number operator with the property $\hat{n}_k\,|\{n_\alpha\}\rangle = n_k\,|\{n_\alpha\}\rangle$. Thus, the Fock states are eigenstates of the Hamiltonian such that Eq. (2.5) is the correct field theoretical description.

Time-ordered Green's function

Using the language of second quantization described above, we now introduce the Green's function formalism. In classical physics, Green's functions are used as a method to solve inhomogeneous differential equations. Similarly, the Green's function formalism can be adopted to many-body physics as a very useful tool for describing the dynamics of physical observables. Let us start by defining the time-ordered Green's function

$$G^T(1,1') = -\mathrm{i}\,\langle T\left\{\hat{\Psi}_H(1)\hat{\Psi}_H^\dagger(1')\right\}\rangle\,. \tag{2.7}$$

The coordinates 1 and $1'$ denote space-time points $(t_1, \mathbf{r}_1)$ and $(t_{1'}, \mathbf{r}_{1'})$, respectively. We have also introduced the time-ordering operator $T\{\ldots\}$ defined for a set of Fermi operators $\{\hat{A}_\alpha\}$ by

$$T\left\{\hat{A}_1(t_1)\hat{A}_2(t_2)\ldots\hat{A}_n(t_n)\right\} = (-1)^P \hat{A}_j(t_j)\hat{A}_k(t_k)\ldots\hat{A}_m(t_m)\,, \tag{2.8}$$

where $t_j > t_k > \cdots > t_m$ and P counts the number of permutations necessary to rearrange the operators. Explicitly, the time-ordering in Eq. (2.7) reads

$$T\left\{\hat{\Psi}_H(1)\hat{\Psi}_H^\dagger(1')\right\} = \theta(t_1 - t_{1'})\hat{\Psi}_H(1)\hat{\Psi}_H^\dagger(1') - \theta(t_{1'} - t_1)\hat{\Psi}_H^\dagger(1')\hat{\Psi}_H(1)\,. \tag{2.9}$$

The field operators encountered in Eq. (2.7) are now time-dependent and given in the Heisenberg picture by

$$\hat{\Psi}_H(1) = \hat{U}_H^\dagger(t_1, t_0)\hat{\Psi}(\mathbf{r}_1)\hat{U}_H(t_1, t_0)\,, \tag{2.10}$$

where

$$\hat{U}_H(t_1, t_0) = T\left\{\exp\left(-\frac{\mathrm{i}}{\hbar}\int_{t_0}^{t_1}\mathrm{d}t'\,\hat{H}(t')\right)\right\} \tag{2.11}$$

is the time-evolution operator and t_0 is a reference time where the Schrödinger and the Heisenberg picture coincide. Note that for the time-ordering in Eq. (2.11) we do not have to worry about factors of (-1) since in a particle-number conserving Hamiltonian the Fermi operators always appear in pairs. For the time being, we assume a time-independent Hamiltonian $\hat{H}(t) = \hat{H}$ such that the time-evolution operator reduces to $\hat{U}_H(t_1, t_0) = \exp(-\mathrm{i}\hat{H}(t_1 - t_0)/\hbar)$.

Assuming thermodynamic equilibrium with a reservoir temperature T, the state of the system can be described with the statistical operator in the grand-canonical ensemble,

$$\hat{\rho} = \frac{\mathrm{e}^{-\beta\left(\hat{H}-\mu\hat{N}\right)}}{\mathrm{Tr}\left[\mathrm{e}^{-\beta\left(\hat{H}-\mu\hat{N}\right)}\right]}\,, \tag{2.12}$$

where $\beta = 1/k_\mathrm{B}T$ (k_B is the Boltzmann constant), μ is the chemical potential, $\hat{N} = \int\mathrm{d}^3r\,\hat{\Psi}^\dagger(\mathbf{r})\hat{\Psi}(\mathbf{r})$ is the total number operator, and Tr denotes the trace in the many-body space. The average $\langle\hat{O}\rangle$ of an operator $\hat{O}$ as encountered in Eq. (2.7) is then given by

$$\langle\hat{O}\rangle = \mathrm{Tr}\left[\hat{\rho}\,\hat{O}\right]\,. \tag{2.13}$$

In the following, we derive the equation of motion for the Green's function. The time derivative of $G^T(1, 1')$ with respect to t_1 reads

$$\mathrm{i}\hbar\frac{\partial}{\partial t_1}G^T(1, 1') = \hbar\delta(1 - 1') + \hbar\,\langle T\left\{\frac{\partial\hat{\Psi}_H(1)}{\partial t_1}\hat{\Psi}_H^\dagger(1')\right\}\rangle\,, \tag{2.14}$$

where the δ-function on the r.h.s., $\delta(1-1') = \delta(t_1 - t_{1'})\delta(\mathbf{r}_1 - \mathbf{r}_{1'})$, arises from the time derivative of the θ-function in the time-ordering operator and the first anticommutation relation (2.3). The time derivative of the field operator appearing on the r.h.s. of Eq. (2.14) can be rewritten by considering the Heisenberg equation of motion,

$$\mathrm{i}\hbar\frac{\partial\hat{\Psi}_H(1)}{\partial t_1} = \left[\hat{\Psi}_H(1),\, \hat{H}\right] = \mathcal{H}(\mathbf{r}_1)\hat{\Psi}_H(1)\,, \tag{2.15}$$

where $\mathcal{H}(\mathbf{r}_1)$ is the spatial representation of the single-particle Hamiltonian, analogously to the discussion around Eq. (2.5). We insert Eq. (2.15) into Eq. (2.14), rearrange the terms, and arrive at the equation of motion of the time-ordered Green's function

$$\left(\mathrm{i}\hbar\frac{\partial}{\partial t_1} - \mathcal{H}(\mathbf{r}_1)\right) G^T(1,1') = \hbar\delta(1-1')\,. \tag{2.16}$$

Thus, the time-ordered Green's function is the solution of the Schrödinger equation with a δ-inhomogeneity. Similarly, the anti-time-ordered Green's function $G^{\tilde{T}}$ fulfills

$$\left(\mathrm{i}\hbar\frac{\partial}{\partial t_1} - \mathcal{H}(\mathbf{r}_1)\right) G^{\tilde{T}}(1,1') = -\hbar\delta(1-1')\,, \tag{2.17}$$

where $\tilde{T}$ orders operators according to their time arguments oppositely to T.

Definitions

Obviously, many different Green's functions can be defined by all possible combinations of the field operator with its adjunct. Here, we focus on the so-called retarded, advanced, lesser, and greater Green's functions, defined by

$$G^R(1,1') = -\mathrm{i}\theta(t_1 - t_{1'})\,\langle\left\{\hat{\Psi}_H(1),\, \hat{\Psi}_H^\dagger(1')\right\}\rangle\,, \tag{2.18}$$

$$G^A(1,1') = \mathrm{i}\theta(t_{1'} - t_1)\,\langle\left\{\hat{\Psi}_H(1),\, \hat{\Psi}_H^\dagger(1')\right\}\rangle\,, \tag{2.19}$$

$$G^<(1,1') = \mathrm{i}\,\langle\hat{\Psi}_H^\dagger(1')\hat{\Psi}_H(1)\rangle\,, \tag{2.20}$$

$$G^>(1,1') = -\mathrm{i}\,\langle\hat{\Psi}_H(1)\hat{\Psi}_H^\dagger(1')\rangle\,, \tag{2.21}$$

respectively. Due to the anticommutator in their definitions, the retarded and advanced Green's functions are solutions of the inhomogeneous Schrödinger equation just like the time-ordered Green's function,

$$\left(\mathrm{i}\hbar\frac{\partial}{\partial t_1} - \mathcal{H}(\mathbf{r}_1)\right) G^{R,A}(1,1') = \hbar\delta(1-1')\,. \tag{2.22}$$

In contrast, the lesser and greater Green's functions, $G^<$ and $G^>$, are solutions of the homogeneous Schrödinger equation,

$$\left(\mathrm{i}\hbar\frac{\partial}{\partial t_1} - \mathcal{H}(\mathbf{r}_1)\right) G^{>,<}(1,1') = 0\,. \tag{2.23}$$

The various Green's functions introduced in this section are related to each other and it is worth to mention that the time-ordered, the anti-time-ordered, the retarded, and the advanced Green's functions can be written in terms of the lesser and greater Green's functions:

$$G^T(1,1') = \theta(t_1 - t_{1'})G^>(1,1') + \theta(t_{1'} - t_1)G^<(1,1')\,, \tag{2.24}$$

$$G^{\tilde{T}}(1,1') = \theta(t_{1'} - t_1)G^>(1,1') + \theta(t_1 - t_{1'})G^<(1,1')\,, \tag{2.25}$$

$$G^R(1,1') = \theta(t_1 - t_{1'})\left[G^>(1,1') - G^<(1,1')\right]\,, \tag{2.26}$$

$$G^A(1,1') = -\theta(t_{1'} - t_1)\left[G^>(1,1') - G^<(1,1')\right]\,. \tag{2.27}$$

Furthermore, at equal times, $t_1 = t_{1'}$, $G^>$ and $G^<$ are directly linked to physical observables. For example, the particle density is given by

$$\langle\hat{n}(1)\rangle = -\mathrm{i}G^<(1,1)\,. \tag{2.28}$$

Fluctuation-dissipation theorem

In the following, we show how $G^<$ and $G^>$ are linked to the spectral function which is defined by

$$A(\mathbf{p},\epsilon) = \mathrm{i}\left[G^R(\mathbf{p},\epsilon) - G^A(\mathbf{p},\epsilon)\right] = \mathrm{i}\left[G^>(\mathbf{p},\epsilon) - G^<(\mathbf{p},\epsilon)\right]\,. \tag{2.29}$$

Utilizing the cyclic invariance of the trace and the commutation relation $\left[\hat{\Psi}^\dagger(\mathbf{r}),\,\hat{N}\right] = -\hat{\Psi}^\dagger(\mathbf{r})$ we obtain

$$G^<(\mathbf{r},t,\mathbf{r}',t') = -\mathrm{e}^{\beta\mu}G^>(\mathbf{r},t-\mathrm{i}\hbar\beta,\mathbf{r}',t')\,. \tag{2.30}$$

Since the Hamiltonian is assumed to be time-independent, the equilibrium Green's functions are invariant under time translations and therefore they only depend on the difference between the times, $t-t'$. Let us now assume that the equilibrium state is translationally invariant in space as well. Then, the Fourier transformation $[(t-t',\mathbf{r}-\mathbf{r}') \to (\epsilon,\mathbf{p})]$

of relation (2.30) takes the form

$$G^{<}(\mathbf{p},\epsilon) = -\mathrm{e}^{-\beta(\epsilon-\mu)}G^{>}(\mathbf{p},\epsilon)\,. \tag{2.31}$$

With use of the spectral function, Eq. (2.29), we can solve for the lesser and the greater Green's function, respectively, and obtain

$$G^{<}(\mathbf{p},\epsilon) = \mathrm{i}f(\epsilon)A(\mathbf{p},\epsilon)\,, \tag{2.32}$$

$$G^{>}(\mathbf{p},\epsilon) = -\mathrm{i}\left[1-f(\epsilon)\right]A(\mathbf{p},\epsilon)\,, \tag{2.33}$$

where

$$f(\epsilon) = \frac{1}{\mathrm{e}^{\beta(\epsilon-\mu)}+1} \tag{2.34}$$

is the Fermi function. The spectral function is the imaginary part of G^R in momentum space, corresponding to a decay in the time domain and therefore dissipation. Thus, Eqs. (2.32) and (2.33) link the correlation functions $G^{<,>}$ (and thus also G^T, G^R, and G^A) with the dissipative part A, which is commonly known as the fluctuation-dissipation theorem [95, 102, 103].

Spectral function

Last, we explicitly derive the spectral function for the case of a free electron gas. The one-particle Hamiltonian $\mathcal{H}$ is then given by

$$\mathcal{H}(\mathbf{r}) = -\frac{\hbar^2}{2m}\nabla^2\,. \tag{2.35}$$

Thus, the Fourier transformation of the equation of motion (2.22) for the retarded Green's function with respect to $\mathbf{r}-\mathbf{r}'$ becomes

$$\left(\mathrm{i}\hbar\frac{\partial}{\partial t} - \epsilon_{\mathbf{p}}\right)G^R(\mathbf{p},t-t') = \hbar\delta(t-t')\,, \tag{2.36}$$

where $\epsilon_{\mathbf{p}} = \mathbf{p}^2/2m$. The solution of this differential equation is given by

$$G^R(\mathbf{p},t-t') = -\mathrm{i}\theta(t-t')\mathrm{e}^{-\frac{\mathrm{i}}{\hbar}\epsilon_{\mathbf{p}}(t-t')}\,. \tag{2.37}$$

One method to obtain the Fourier transform with respect to $t-t'$ is to insert the integral representation of the θ-function,

$$\theta(t-t') = \mathrm{i}\int\frac{\mathrm{d}\epsilon'}{2\pi}\,\frac{\mathrm{e}^{-\frac{\mathrm{i}}{\hbar}\epsilon'(t-t')}}{\epsilon'+\mathrm{i}0^+}\,, \tag{2.38}$$

and substitute $\epsilon' = \epsilon - \epsilon_{\mathbf{p}}$. We obtain

$$G^R(\mathbf{p}, t - t') = \int \frac{\mathrm{d}\epsilon}{2\pi\hbar} \frac{\hbar}{\epsilon - \epsilon_{\mathbf{p}} + \mathrm{i}0^+} \mathrm{e}^{-\frac{\mathrm{i}}{\hbar}\epsilon(t-t')} , \tag{2.39}$$

where the Fourier-transformed retarded Green's function can be read out directly,

$$G^R(\mathbf{p}, \epsilon) = \frac{\hbar}{\epsilon - \epsilon_{\mathbf{p}} + \mathrm{i}0^+} . \tag{2.40}$$

The advanced Green's function is obtained in an analogous manner and is the complex conjugate of retarded Green's function:

$$G^A(\mathbf{p}, \epsilon) = \left[G^R(\mathbf{p}, \epsilon)\right]^* = \frac{\hbar}{\epsilon - \epsilon_{\mathbf{p}} - \mathrm{i}0^+} . \tag{2.41}$$

With use of the identity

$$\frac{1}{x + \mathrm{i}0^+} = \frac{1}{x} - \mathrm{i}\pi\delta(x) , \tag{2.42}$$

where on the r.h.s. the Cauchy principal value is assumed, and by inserting Eqs. (2.40) and (2.41) into the definition of the spectral function, Eq. (2.29), we end up with

$$A(\mathbf{p}, \epsilon) = 2\pi\hbar\delta(\epsilon - \epsilon_{\mathbf{p}}) . \tag{2.43}$$

The spectral function for a free electron gas is sharply peaked at the single-particle energy $\epsilon_{\mathbf{p}}$. In general, interactions lead to a broadening of the spectral function. However, for sufficiently weak interacting systems one can still approximate the spectral function to be a δ-shaped function which is commonly known as the quasi-particle approximation.

2.2. Nonequilibrium theory

The objective of this section is to provide a basis for a perturbative expansion of the Green's function when a time-dependent perturbation is present. For this, we consider the time-evolution with respect to the unperturbated Hamiltonian and introduce the closed time path formalism, which allows to take advantage of the diagrammatic expansion.

Hamiltonian and expectation values

Let us consider a system which is in thermal equilibrium at temperature T with a time-independent Hamiltonian $\hat{H}_1$ prior to a time t_0. The Hamiltonian $\hat{H}_1$ is assumed to be of the form

$$\hat{H}_1 = \hat{H}_0 + \hat{H}^i \,, \tag{2.44}$$

where $\hat{H}_0$ is quadratic in the field operators and $\hat{H}^i$ represents an arbitrary interaction. Then, at time t_0 the system will be disconnected from the reservoir and be exposed to a disturbance, represented by $\hat{H}'(t)$. The total Hamiltonian is therefore given by

$$\hat{H}(t) = \hat{H}_1 + \hat{H}'(t) \,, \tag{2.45}$$

where $\hat{H}'(t) = 0$ for $t \leq t_0$. The state of the system for $t < t_0$ is described by the statistical operator

$$\hat{\rho}_1 = \frac{\mathrm{e}^{-\beta\left(\hat{H}_1 - \mu\hat{N}\right)}}{\mathrm{Tr}\left[\mathrm{e}^{-\beta\left(\hat{H}_1 - \mu\hat{N}\right)}\right]} \,. \tag{2.46}$$

The statistical operator for times $t > t_0$ evolves according to

$$\hat{\rho}(t) = \hat{U}(t, t_0)\hat{\rho}_1\hat{U}^\dagger(t, t_0) \,, \tag{2.47}$$

such that the average value of an arbitrary operator $\hat{A}$ in the Heisenberg picture is given by

$$\langle \hat{A}(t) \rangle = \mathrm{Tr}\left[\hat{\rho}_1 \hat{A}_H(t)\right] \,, \tag{2.48}$$

where $\hat{A}_H(t)$ is the time evolution of $\hat{A}$ with respect to the total Hamiltonian $\hat{H}$, analogously to Eq. (2.10).

Time evolution

With the Hamiltonian of the form as given in Eq. (2.45), we can factorize the time-evolution operator by utilizing the properties of the time-ordering operator as follows (see App. A.1 for details):

$$\hat{U}_H(t, t_0) = \hat{U}_{H_1}(t, t_0)\hat{S}(t, t_0) \,, \tag{2.49}$$

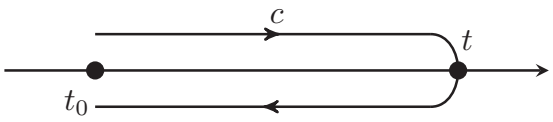

FIG. 2.1.: The closed time path contour c.

where the reference time within the time-evolution operator is conveniently t_0 and

$$\hat{U}_{H_1}(t,t_0) = \exp\left(-\frac{\mathrm{i}}{\hbar}\hat{H}_1(t-t_0)\right)\,, \tag{2.50}$$

$$\hat{S}(t,t_0) = T\left\{\exp\left(-\frac{\mathrm{i}}{\hbar}\int_{t_0}^{t}\mathrm{d}t'\,\hat{H}'_{H_1}(t')\right)\right\}. \tag{2.51}$$

Here, $\hat{H}'_{H_1}(t')$ is the time evolution of $\hat{H}'$ with respect to the Hamiltonian $\hat{H}_1$.In the following we stick to this notation, i.e., the respective Hamiltonian to which the time evolution of some operator is performed is indicated by the subscript of the operator under consideration. The time evolution of an arbitrary operator $\hat{O}$ is given by

$$\hat{O}_H(t) = \hat{S}^\dagger(t,t_0)\hat{O}_{H_1}(t)\hat{S}(t,t_0)\,. \tag{2.52}$$

Closed time path formalism

In order to obtain a convenient basis for perturbation theory, let us introduce the closed time path formalism, which allows to rewrite Eq. (2.52) as follows (see App. A.2):

$$\hat{O}_H(t) = T_c\left\{\exp\left[-\frac{\mathrm{i}}{\hbar}\int_c\mathrm{d}\tau\,\hat{H}'_{H_1}(\tau)\right]\hat{O}_{H_1}(t)\right\}. \tag{2.53}$$

Here, the integral in the exponent is performed along a closed contour c with the variable τ proceeding from t_0 to t and back again to t_0 along the real-time axis as depicted in Fig. 2.1. The operator T_c is the contour-ordering operator, i.e, $\hat{T}_c$ orders products of operators according to the position of the time argument on the contour,

$$T_c\left\{\hat{A}(\tau)\hat{B}(\tau')\right\} = \begin{cases}\hat{A}(\tau)\hat{B}(\tau') & \text{for } \tau >_c \tau' \\ \pm\hat{B}(\tau')\hat{A}(\tau) & \text{for } \tau <_c \tau'\,,\end{cases} \tag{2.54}$$

where $\tau >_c \tau'$ ($\tau <_c \tau'$) denotes that τ' follows (precedes) τ along the contour c; the upper (lower) sign corresponds to Bose (Fermi) operators. Similarly to the time-ordered

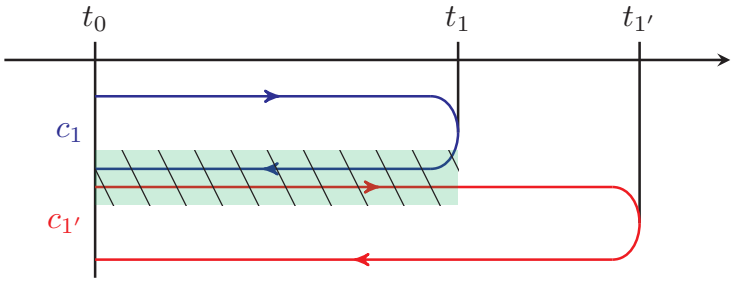

FIG. 2.2.: The contours c_1 and $c_{1'}$. Within the shaded area, the contour evolution operators cancel each other in Eq. (2.57).

Green's function, we introduce the contour-ordered Green's function by replacing the time-ordering operator with the contour-ordering operator ($T \to T_c$) and the respective time variables by the contour variables ($t \to \tau$):

$$G_c(1,1') = -\frac{\mathrm{i}}{\hbar}\langle T_c\left\{\hat{\Psi}_H(1)\hat{\Psi}_H^\dagger(1')\right\}\rangle \ . \tag{2.55}$$

According to the definition of the greater and lesser Green's functions, Eqs. (2.20) and (2.21), the contour-ordered Green's function is either the greater or lesser Green's function, depending on the time variables:

$$G_c(1,1') = \begin{cases} G^<(1,1') & \text{for } \tau_1 <_c \tau_{1'} \\ G^>(1,1') & \text{for } \tau_1 >_c \tau_{1'} \ . \end{cases} \tag{2.56}$$

Employing the properties of the contour-ordering operator we see

$$\begin{aligned} G^>(1,1') &= -\frac{\mathrm{i}}{\hbar}\langle T_{c_1}\left\{\mathrm{e}^{-\frac{\mathrm{i}}{\hbar}\int_{c_1}\mathrm{d}\tau\,\hat{H}'_{H_1}(\tau)}\hat{\Psi}_{H_1}(1)\right\}T_{c_{1'}}\left\{\mathrm{e}^{-\frac{\mathrm{i}}{\hbar}\int_{c_{1'}}\mathrm{d}\tau\,\hat{H}'_{H_1}(\tau)}\hat{\Psi}^\dagger_{H_1}(1')\right\}\rangle \\ &= -\frac{\mathrm{i}}{\hbar}\langle T_{c_1+c_{1'}}\left\{\mathrm{e}^{-\frac{\mathrm{i}}{\hbar}\int_{c_1+c_{1'}}\mathrm{d}\tau\,\hat{H}'_{H_1}(\tau)}\hat{\Psi}_{H_1}(1)\hat{\Psi}^\dagger_{H_1}(1')\right\}\rangle \ , \end{aligned} \tag{2.57}$$

where the contours c_1 and $c_{1'}$ start at t_0, have their reversal point at t_1 and $t_{1'}$, respectively, and return to t_0. The combined contour $c_1 + c_{1'}$, as found in the last equation, starts at t_0, passes through $\min(t_1, t_{1'})$, goes back to t_0, passes through $\max(t_1, t_{1'})$, and finally returns to t_0. However, since the field operators at t_1 and $t_{1'}$ are not involved for the return branch of c_1 and the forward branch of $c_{1'}$ up to t_1 (shaded part in Fig. 2.2), the contour-ordering only affects the exponent in Eq. (2.57), and thus the two branches cancel each other.

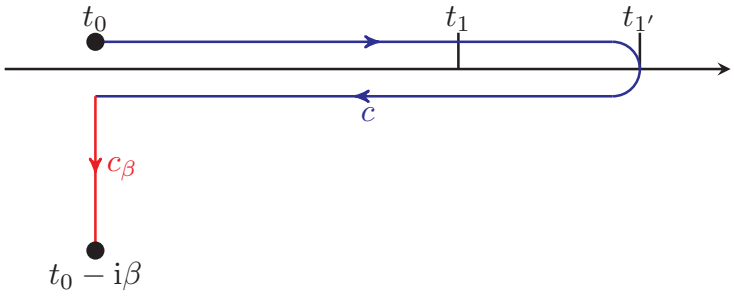

FIG. 2.3.: The joined contour c_i, combing c (blue) and c_β (red).

By a similar consideration for $G^<$ one obtains for the contour-ordered Green's function

$$G_c(1,1') = -i\left\langle T_c\left\{\mathrm{e}^{-\frac{\mathrm{i}}{\hbar}\int_c \mathrm{d}\tau\, \hat{H}'_{H_1}(\tau)}\hat{\Psi}_{H_1}(1)\hat{\Psi}^\dagger_{H_1}(1')\right\}\right\rangle , \tag{2.58}$$

where the contour c now starts at t_0, has its reversal point at $\max(\mathrm{t}_1, \mathrm{t}_{1'})$, and returns to t_0. We have now managed that the ordering operation acts on all operators within the expectation value, in principle a very useful form for deriving the perturbation theory as we will see in the next section. However, we recall that the Hamiltonian $\hat{H}_1$ also consists of the interaction part $\hat{H}^i$. Our aim is to perform a perturbative expansion in $\hat{H}'$ as well as in $\hat{H}^i$. Therefore, we further transform the time-evolution of the operators with respect to $\hat{H}_1$ to time-evolutions with respect to the quadratic Hamiltonian $\hat{H}_0$. Similarly to the previous manipulations, we find for an operator $\hat{O}$ in the Heisenberg picture

$$\hat{O}_H(t) = T_c\left\{\mathrm{e}^{-\frac{\mathrm{i}}{\hbar}\int_c \mathrm{d}\tau\left[\hat{H}^i_{H_0}(\tau)+\hat{H}'_{H_0}(\tau)\right]}\hat{O}_{H_0}(t)\right\} . \tag{2.59}$$

Explicitly, the contour-ordered Green's function then reads

$$G_c(1,1') = -\mathrm{i}\frac{\mathrm{Tr}\left[\mathrm{e}^{-\beta\left(\hat{H}_1-\mu\hat{N}\right)}T_c\left\{\mathrm{e}^{-\frac{\mathrm{i}}{\hbar}\int_c \mathrm{d}\tau\left[\hat{H}^i_{H_0}(\tau)+\hat{H}'_{H_0}(\tau)\right]}\hat{\Psi}_{H_0}(1)\hat{\Psi}^\dagger_{H_0}(1')\right\}\right]}{\mathrm{Tr}\left[\mathrm{e}^{-\beta\left(\hat{H}_1-\mu\hat{N}\right)}\right]} , \tag{2.60}$$

where we have also written out the average according to Eq. (2.48). The Boltzmann weighting factor $\exp(-\beta\hat{H}_1)$ in Eq. (2.60) can be expressed by

$$\mathrm{e}^{-\beta\left(\hat{H}_1-\mu\hat{N}\right)} = \mathrm{e}^{-\beta\left(\hat{H}_0-\mu\hat{N}\right)}T_{c_\beta}\left\{\mathrm{e}^{-\frac{\mathrm{i}}{\hbar}\int_{c_\beta}\mathrm{d}\tau\,\hat{H}^i_{H_0}(\tau)}\right\} , \tag{2.61}$$

where the contour c_β stretches parallel to the imaginary axis from t_0 to $t_0 - \mathrm{i}\beta$. By

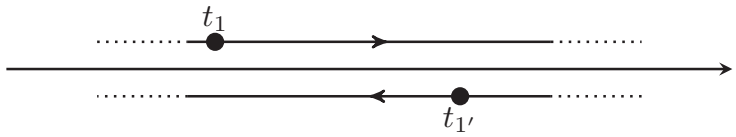

FIG. 2.4.: The Schwinger-Keldysh contour c_K, starting at $-\infty$ (upper path, first branch), returning at ∞, and going back to $-\infty$ (lower path, second branch).

extending the contour c with c_β to a new contour c_i, see Fig. 2.3, we obtain

$$G_{c_i}(1,1') = -\mathrm{i}\frac{\mathrm{Tr}\left[\mathrm{e}^{-\beta\left(\hat{H}_0-\mu\hat{N}\right)}T_{c_i}\left\{\mathrm{e}^{-\frac{\mathrm{i}}{\hbar}\int_{c_i}\mathrm{d}\tau\,\hat{H}^i_{H_0}(\tau)}\mathrm{e}^{-\frac{\mathrm{i}}{\hbar}\int_{c}\mathrm{d}\tau\,\hat{H}'_{H_0}(\tau)}\hat{\Psi}_{H_0}(1)\hat{\Psi}^\dagger_{H_0}(1')\right\}\right]}{\mathrm{Tr}\left[\mathrm{e}^{-\beta\left(\hat{H}_0-\mu\hat{N}\right)}T_{c_\beta}\left\{\mathrm{e}^{-\frac{\mathrm{i}}{\hbar}\int_{c_\beta}\mathrm{d}\tau\,\hat{H}^i_{H_0}(\tau)}\right\}\right]}\,. \tag{2.62}$$

Keldysh formalism

The Keldysh formalism is based on the closed Schwinger-Keldysh contour c_K, introduced in Ref. 104 by L. V. Keldysh after pioneering work of J. Schwinger [105]. As depicted in Fig. 2.4, the contour c_K stretches from $-\infty$ to ∞ and back again to $-\infty$. The extension of the contour beyond the largest time ($t_{1'}$ in Fig. 2.4) can be done by utilizing the unitarity of the time-development operator. Under the assumption that the interactions are switched on adiabatically, we can set $t_0 \to -\infty$ and neglect the contribution of the contour c_β, which is related to the neglect of initial correlations. Now, the interaction contribution can be treated exactly the same way as the external contribution and the contour-ordered Green's function becomes

$$G_{c_K}(1,1') = -\mathrm{i}\mathrm{Tr}\left[\hat{\rho}_0 T_{c_K}\left\{\mathrm{e}^{-\frac{\mathrm{i}}{\hbar}\int_{c_K}\mathrm{d}\tau\left[\hat{H}^i_{H_0}(\tau)+\hat{H}'_{H_0}(\tau)\right]}\hat{\Psi}_{H_0}(1)\hat{\Psi}^\dagger_{H_0}(1')\right\}\right]\,, \tag{2.63}$$

where

$$\hat{\rho}_0 = \frac{\mathrm{e}^{-\beta\left(\hat{H}_0-\mu\hat{N}\right)}}{\mathrm{Tr}\left[\mathrm{e}^{-\beta\left(\hat{H}_0-\mu\hat{N}\right)}\right]} \tag{2.64}$$

is the statistical operator for the non-interacting system in thermal equilibrium with temperature T.

We can write the Green's function as a 2×2 matrix,

$$G_{c_K}(1,1') \mapsto \tilde{G}(1,1') = \begin{pmatrix} G_{11}(1,1') & G_{12}(1,1') \\ G_{21}(1,1') & G_{22}(1,1') \end{pmatrix} , \tag{2.65}$$

depending on where on c_K the two time variables of the Green's function reside: the indices i, j of $G_{ij}(1,1')$ indicate that t_1 and $t_{1'}$ lie on the i-th and j-th branch of the contour, respectively. The matrix elements G_{ij} in Eq. (2.65) can be also expressed by

$$G_{11}(1,1') = G^T(1,1') , \tag{2.66}$$

$$G_{12}(1,1') = G^<(1,1') , \tag{2.67}$$

$$G_{21}(1,1') = G^>(1,1') , \tag{2.68}$$

$$G_{22}(1,1') = G^{\tilde{T}}(1,1') . \tag{2.69}$$

The above 2×2 matrix representation can be further transformed to a triangular matrix $\check{G}$ with the consequence that the triangular structure is preserved under matrix multiplications. This transformation was introduced by A. I. Larkin and Yu. Ovchinnikov [106] and is given by

$$\check{G} = L\tau_3 \tilde{G} L^\dagger , \tag{2.70}$$

where $L = (\tau_0 - \mathrm{i}\tau_2)/\sqrt{2}$ and τ_i are the Pauli matrices with τ_0 being the 2×2 unit matrix.[2] The result of the transformation is

$$\check{G}(1,1') = \begin{pmatrix} G^R(1,1') & G^K(1,1') \\ 0 & G^A(1,1') \end{pmatrix} , \tag{2.71}$$

where $G^K(1,1')$ is the Keldysh Green's function related to $G^<$ and $G^>$ by

$$G^K(1,1') = G^<(1,1') + G^>(1,1') . \tag{2.72}$$

In the following, we refer to the Keldysh space when considering the triangular matrix formalism.

In equilibrium, we can use the fluctuation-dissipation theorem, Eqs. (2.32) and (2.33), such that the Keldysh Green's function becomes

$$G^K(\mathbf{p},\epsilon) = -\mathrm{i}A(\mathbf{p},\epsilon)\left[1 - 2f(\epsilon)\right] . \tag{2.73}$$

[2] The notation τ_i instead of σ^i is used on purpose as τ_i has just the same mathematical structure as σ^i, whereas σ^i has also a physical interpretation as the spin degree of freedom.

In Sec. 2.4 we use this relation under the further assumption that it also holds in the nonequilibrium case, i.e, we assume that the population of the spectrum reshuffles, $f(\epsilon) \to f(\mathbf{p}, \epsilon)$, but not the spectrum itself.

2.3. Perturbation theory

In this section, we derive the perturbative expansion of the Green's function, based on Wick's theorem, and introduce the diagrammatic representation of the resulting series. In addition, we consider a random potential with the corresponding self-energy, which finally leads to the Dyson equation.

Wick's theorem

The contour-ordered Green's function on the Schwinger-Keldysh contour, Eq. (2.63), allows us to apply Wick's theorem [107]. It implies that for a noninteracting Hamiltonian $\hat{H}_0$ the expectation value of a contour-ordered product of creation and annihilation operators equals the sum over all pairwise products that can be formed [87–90]. For example, contour-ordered products like

$$\langle T_{c_K} \left\{ \hat{\Psi}_{H_0}(x_1) \hat{\Psi}^\dagger_{H_0}(y_1) \hat{\Psi}_{H_0}(x_2) \hat{\Psi}^\dagger_{H_0}(y_2) \dots \hat{\Psi}_{H_0}(x_n) \hat{\Psi}^\dagger_{H_0}(y_n) \right\} \rangle \ , \tag{2.74}$$

as can be encountered in Eq. (2.63), reduce to

$$\sum_{\text{a.p.p.}} \prod_{i,j} (-1)^P \langle T_{c_K} \left\{ \hat{\Psi}_{H_0}(x_i) \hat{\Psi}^\dagger_{H_0}(y_j) \right\} \rangle = \mathrm{i} \sum_{\text{a.p.p.}} \prod_{i,j} (-1)^P G_0(x_i, y_j) \, , \tag{2.75}$$

where a.p.p. denotes all possible pairings among the n field operators and P is the number of permutations needed to arrange the field operators in the same order as they appear on the l.h.s. of Eq. (2.75). Here, we have also introduced the free contour-ordered Green's function,

$$G_0(1, 1') = -\mathrm{i} \langle T_{c_K} \left\{ \hat{\Psi}_{H_0}(1) \hat{\Psi}^\dagger_{H_0}(1') \right\} \rangle \ . \tag{2.76}$$

Apparently, the usefulness of Wick's theorem is that complicated contour-ordered products of field operators can be decomposed into products of the "simple" free contour-ordered Green's function.

Diagrammatic representation

Let us now consider the particular case of a potential $U(\mathbf{r},t)$ and a vanishing initial interaction Hamiltonian, i.e.,

$$\begin{aligned}\hat{H}^i &= 0\,,\\ \hat{H}' &= \int \mathrm{d}^3 r\, \hat{\Psi}^\dagger(\mathbf{r}) U(\mathbf{r},t) \hat{\Psi}(\mathbf{r})\,.\end{aligned} \tag{2.77}$$

Expanding the exponential function in Eq. (2.63) and applying Wick's theorem, the contour-ordered Green's function can be written as a perturbation series in the external potential,

$$G_{c_K}(1,1') = G_0(1,1') + G_1(1,1') + G_2(1,1') + \dots\,, \tag{2.78}$$

where the index on the Green's functions on the r.h.s. denotes the power of the potential in the respective terms. For example, the first order Green's function explicitly reads

$$\begin{aligned}G_1(1,1') &= -\frac{1}{\hbar}\mathrm{Tr}\left[\hat{\rho}_0 T_{c_K}\left\{\int \mathrm{d}^3 r_2 \int_{c_K} \mathrm{d}\tau_2\, \hat{\Psi}^\dagger_{H_0}(2) U(2) \hat{\Psi}_{H_0}(2) \hat{\Psi}_{H_0}(1) \hat{\Psi}^\dagger_{H_0}(1')\right\}\right]\\ &= \frac{1}{\hbar}\int \mathrm{d}^3 r_2 \int_{c_K} \mathrm{d}\tau_2 \left[G_0(1,2)U(2)G_0(2,1') - G_0(2,2)U(2)G_0(1,1')\right].\end{aligned} \tag{2.79}$$

Employing the integration along the forward and the return parts of c_K one can show that pairings with equal time arguments vanish, such that the first order Green's function reduces to

$$G_1(1,1') = \frac{1}{\hbar}\int \mathrm{d}^3 r_2 \int_{c_K} \mathrm{d}\tau_2\, G_0(1,2)U(2)G_0(2,1'). \tag{2.80}$$

The second order term G_2 consists of six field operators and results therefore in $3!$ terms due to the possible pairings. Among these we encounter three equal time pairings which give no contribution. Furthermore, by splitting the contour c_K into its forward and return parts we see that

$$G_0(1,1') \int_{c_K} \mathrm{d}\tau_2 \int_{c_K} \mathrm{d}\tau_3\, U(2) G_0(2,3) U(3) G_0(3,2) = 0\,, \tag{2.81}$$

thus leaving us with only two nonvanishing pairings. The remaining two possible pairings are equal, and hence the second order Green's function reads

$$G_2(1,1') = \frac{1}{\hbar^2}\int \mathrm{d}^3 r_2 \int \mathrm{d}^3 r_3 \int_{c_K} \mathrm{d}\tau_2 \int_{c_K} \mathrm{d}\tau_3\, G_0(1,2)U(2)G_0(2,3)U(3)G_0(3,1')\,. \tag{2.82}$$

Higher order Green's function have an analogous form with an integration over the inner variables $2 \dots k$ of the integrand

$$\frac{1}{\hbar^k} G_0(1,2) U(2) G_0(2,3) U(3) G_0(3,4) \dots U(k) G_0(k,1') \,. \tag{2.83}$$

A very convenient way to express the unhandy terms within the series expansion of the full Green's function is the diagrammatic technique as invented by R. P. Feynman [108]. For this, we define the following diagrams, the potential vertex

$$\overset{\times}{1} = \frac{U(1)}{\hbar} \,, \tag{2.84}$$

the free contour-ordered Green's function

$$1 \longleftarrow 1' = G_0(1,1') \,, \tag{2.85}$$

and the full contour-ordered Green's function

$$1 \Longleftarrow 1' = G_{c_K}(1,1') \,. \tag{2.86}$$

The series in Eq. (2.78) can now be written as

$$1 \Longleftarrow 1' \;=\; 1 \longleftarrow 1' \;+\; 1 \longleftarrow \overset{\times}{2} \longleftarrow 1' \;+\; 1 \longleftarrow \overset{\times}{2} \longleftarrow \overset{\times}{3} \longleftarrow 1' \;+ \dots \,, \tag{2.87}$$

where an integration over the inner variables is implied, according to the discussion around Eqs. (2.78)–(2.83).

The diagrammatic representation can be used analogously for the Keldysh formalism by replacing the vertices and Green's functions with their respective objects in Keldysh space and further implying a matrix multiplication at the inner variables. We show this by considering the n-th order Green's function G_n. By splitting the upper and lower path of the time integration we can write G_n within the 2×2 space defined in Eq. (2.65) as

$$\tilde{G}_n(1,1') = \frac{1}{\hbar} \int \mathrm{d}^3 r_2 \int \mathrm{d}t_2 \, \tilde{G}_0(1,2) \tau_3 U(2) \tilde{G}_{n-1}(2,1') \,. \tag{2.88}$$

Transforming to Keldysh space and by inserting $L^\dagger L = 1$ between $\tilde{G}_0$ and τ_3 in the integrand one obtains

$$\check{G}_n(1,1') = \frac{1}{\hbar}\int \mathrm{d}^3 r_2 \int \mathrm{d}t_2\, \check{G}_0(1,2)\check{U}(2)\check{G}_{n-1}(2,1')\,, \tag{2.89}$$

where $\check{U} = \tau_0 U$ is the potential in Keldysh space. The respective diagrams in Keldysh space are therefore given by

$$\overset{\times}{1} = \frac{\check{U}(1)}{\hbar}\,, \tag{2.90}$$

$$1 \longleftarrow 1' = \check{G}_0(1,1')\,, \tag{2.91}$$

$$1 \Longleftarrow 1' = \check{G}(1,1')\,. \tag{2.92}$$

Random potential model

In the following, we consider a static random potential $V(\mathbf{r})$ which captures the effect of impurities or defects. Assuming N_i identical impurities the interaction Hamiltonian reads

$$\hat{H}^i = \int \mathrm{d}^3 r\, \hat{\Psi}^\dagger(\mathbf{r}) V(\mathbf{r}) \hat{\Psi}(\mathbf{r}) = \sum_{i=1}^{N_i} \int \mathrm{d}^3 r\, \hat{\Psi}^\dagger(\mathbf{r}) V_{\mathrm{imp}}(\mathbf{r}-\mathbf{r}_i)\hat{\Psi}(\mathbf{r})\,, \tag{2.93}$$

where $V_{\mathrm{imp}}(\mathbf{r}-\mathbf{r}_i)$ is the potential of a single impurity located at $\mathbf{r}_i$. With the impurities being distributed randomly, we have to average over their positions. Under the assumption that they are evenly distributed in space the average boils down to

$$\langle V(\mathbf{r})\rangle_{\mathrm{imp}} = 0\,, \tag{2.94}$$

$$\langle V(\mathbf{r})V(\mathbf{r}')\rangle_{\mathrm{imp}} = n_i \int \mathrm{d}^3 x\; V_{\mathrm{imp}}(\mathbf{r}-\mathbf{x})V_{\mathrm{imp}}(\mathbf{r}'-\mathbf{x})\,, \tag{2.95}$$

where n_i is the impurity density. We remark that in general the random potential $V(\mathbf{r})$ can have a nonzero mean value [109], which however can be absorbed into the definition of the chemical potential. In addition, the impurity correlator, Eq. (2.95), already implies the assumption that the correlation between two different impurities vanishes. Thus, the second order average is fully determined by the impurity density n_i and a

single impurity, located at the origin for simplicity reasons. Higher order averages regarding the same single impurity are neglected by treating the random potential model within the Born approximation, i.e., $\hbar/p_{\mathrm{F}}l \ll 1$. Here, l is the mean free path, associated with the square of the Fourier transform of the single impurity potential and the impurity density. Furthermore, we assume that the impurity average is Gaussian,

$$\langle \prod_{i=1}^{2n-1} V(\mathbf{r}_i) \rangle_{\mathrm{imp}} = 0 \,, \tag{2.96}$$

$$\langle \prod_{i=1}^{2n} V(\mathbf{r}_i) \rangle_{\mathrm{imp}} = \sum \prod \langle V(\mathbf{r}_i) V(\mathbf{r}_j) \rangle_{\mathrm{imp}} \,, \tag{2.97}$$

where $\sum \prod$ implies a sum over all distinct ways of splitting $V(\mathbf{r}_1) \ldots V(\mathbf{r}_{2n})$ into pairs $V(\mathbf{r}_i)V(\mathbf{r}_j)$ with each summand being a product of the n pairs. Hence, the impurity average of any product of random potentials vanishes for odd moments and reduces to products of the impurity correlator, Eq. (2.95), for even moments. For a more rigorous discussion of the random potential model see, for example, Ref. 109.

By expressing the single impurity potential through its Fourier transform,

$$V_{\mathrm{imp}}(\mathbf{r}) = \int \frac{\mathrm{d}^3 p}{(2\pi\hbar)^3} \, V_{\mathrm{imp}}(\mathbf{p}) \mathrm{e}^{-\frac{\mathrm{i}}{\hbar}\mathbf{p}\cdot\mathbf{r}} \,, \tag{2.98}$$

the impurity correlator, Eq. (2.95), can be rewritten as

$$\langle V(\mathbf{r}) V(\mathbf{r}') \rangle_{\mathrm{imp}} = n_i \int \frac{\mathrm{d}^3 p}{(2\pi\hbar)^3} \, V_{\mathrm{imp}}(\mathbf{p}) V_{\mathrm{imp}}(-\mathbf{p}) \mathrm{e}^{-\frac{\mathrm{i}}{\hbar}\mathbf{p}\cdot(\mathbf{r}-\mathbf{r}')} \,. \tag{2.99}$$

In addition, we assume that the Fourier transform of the single impurity potential varies sufficiently weak, such that we can approximate it as constant, $V_{\mathrm{imp}}(\mathbf{p}) \approx v_0$. This corresponds to the simple case of δ-shaped impurity potentials with amplitude v_0. The impurity correlator simplifies to

$$\langle V(\mathbf{r}) V(\mathbf{r}') \rangle_{\mathrm{imp}} \approx n_i v_0^2 \delta(\mathbf{r} - \mathbf{r}') \,. \tag{2.100}$$

Let us now represent the impurity averaged Green's function diagrammatically. The diagram for the impurity correlator is defined by

$$\underset{\mathbf{r}}{\times} \text{----} \underset{\mathbf{r}'}{\times} = \frac{1}{\hbar^2} \langle V(\mathbf{r}) V(\mathbf{r}') \rangle_{\mathrm{imp}} \,. \tag{2.101}$$

According to the Gaussian average, Eqs. (2.96) and (2.97), the number of diagrams containing n impurity correlators is given by $(2n-1)!!$. The various diagrams can be classified according to their topological structure. We illustrate this in the example case of second-order diagrams. Suppressing space-time coordinates, the resulting three diagrams are given by

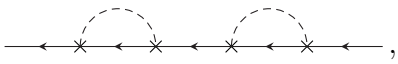

, (2.102)

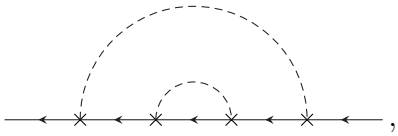

, (2.103)

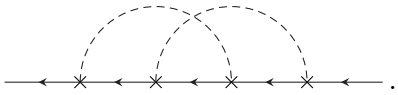

. (2.104)

The first diagram is reducible, i.e., it consists of at least one Green's function (disregarding the external ones) which is not enclosed by any impurity correlator. Vice versa, diagrams of the type (2.103) and (2.104) are called irreducible. The advantage of this classification is that any reducible diagram can be written as a product of irreducible diagrams connected with the free Green's function. Diagrams with crossing impurity lines, see (2.104), are a particular sub-class of irreducible diagrams.

Considering the momentum representation of the diagram (2.103) one can see that the diagram yields an integration over two momenta $\mathbf{p}'$ and $\mathbf{p}''$, where the angle integration can be separated. Conversely, the angle integration for the occurring momenta in the momentum representation of diagram (2.104) cannot be separated as they are restricted due to the crossed impurity correlations. As a result, the contribution of (2.104) is about $\hbar/p_{\mathrm{F}}l$ times smaller than the contribution of (2.103), see Refs. 87 and 109. Therefore, we neglect crossed diagrams in the following, analogously to the neglect of higher orders in the impurity correlation within the Born approximation. However, we would like to mention that the diagrams, where the impurity lines cross a maximal number of times, form a special subclass of crossed diagrams as their sum results in a singular behavior. This leads to quantum corrections to the conductivity known as weak localization, a precursor effect to the localization mentioned in the introduction.

Self-energy

Let us now introduce the self-energy Σ as the sum over all possible irreducible diagrams. Diagrammatically, it is expressed by

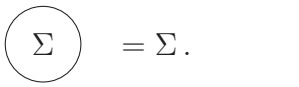

(2.105)

Neglecting crossed diagrams, the self-energy reads

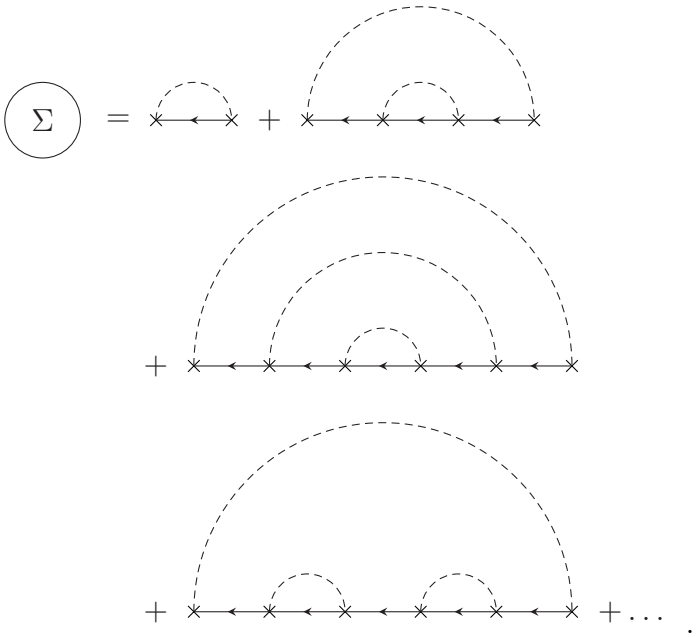

(2.106)

Note the topological structure of the diagrams: as a result of neglecting crossed diagrams we solely obtain diagrams whose start and end points are connected by a dashed line. The inner diagrams which are encircled by this dashed line are again a combination of irreducible diagrams connected by the free Green's function. Since we deal with an infinite sum of all possible connections of irreducible diagrams with the free Green's function, the sum over the diagrams beneath the outer dashed line is nothing else but the impurity average of the full Green's function:

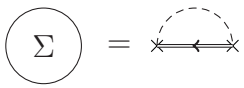

(2.107)

Note that we have omitted the indication of the impurity average, $\langle \ldots \rangle_{\mathrm{imp}}$, for the full Green's function. From now on, we shall always deal with impurity averaged quantities, and therefore we omit this indication in the following as well.

The full Green's function can now be expressed in terms of the self-energy as the infinite sum

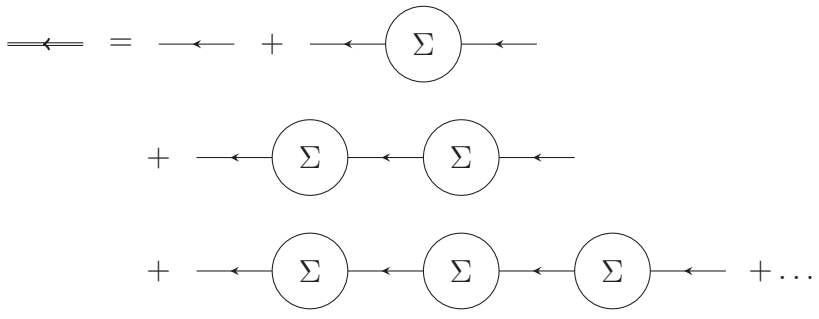

, (2.108)

which we can again iterate in order to obtain the Dyson equation

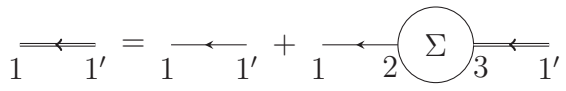

(2.109)

or equivalently,

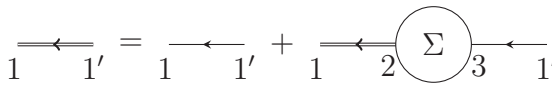

. (2.110)

Equations (2.109) and (2.110) will provide the basis for the derivation of the generalized Boltzmann equation as we see in the following section.

2.4. Generalized Boltzmann equation

In this section, we recapitulate the derivation of the generalized Boltzmann equation of Ref. 97 in a detailed way with the use of a compact relativistic notation as done in Ref. 110. The employed approach relies on the introduction of SU(2) gauge fields which allows to treat linear-in-momentum spin-orbit coupling in a unified way. One obtains a U(1)×SU(2) covariant Boltzmann equation, which has the advantage that charge and spin degrees of freedom are handled on equal footing. Similarly to Ref. 97, we perform the gradient expansion first and transform the resulting objects into their covariant form afterwards. The opposite way, transforming first to locally covariant objects and then performing the gradient expansion, is of course also possible. However, we find the way presented in this section more transparent, see App. B.2 for a comparison.

Hamiltonian

In order to set the stage, we start by introducing the Hamiltonian in the spatial representation,

$$\mathcal{H}(1) = \mathcal{H}_0(1) + \mathcal{H}_{\text{imp}}(\mathbf{r}_1)\,, \tag{2.111}$$

where $\mathcal{H}_{\text{imp}}$ is time-independent and describes the effect of impurities within the random potential model. However, we do not need to specify $\mathcal{H}_{\text{imp}}$ until we consider the collision operator of the Boltzmann equation. The Hamiltonian $\mathcal{H}_0$ corresponds to the free Green's function and is given by

$$\mathcal{H}_0(1) = \frac{1}{2m}\left[-\mathrm{i}\hbar\nabla_{\mathbf{r}_1} + e\mathbf{A}(1) + \boldsymbol{\mathcal{A}}^a(1)\frac{\sigma^a}{2}\right]^2 - e\Phi(1) - \Psi^a(1)\frac{\sigma^a}{2}\,, \tag{2.112}$$

where $\mathbf{A}$ and Φ are the common U(1) vector and scalar potentials, respectively. Due to the noncommutative spin algebra the a-th Pauli matrix σ^a has to be coupled to non-Abelian SU(2) potentials $\boldsymbol{\mathcal{A}}^a$ and Ψ^a. These potentials describe intrinsic spin-orbit coupling due to the band and/or device structure and Zeeman/exchange interaction, respectively. A summation over repeated indices is implied.

Quantum kinetic equation

In Keldysh space, the equation of motion for the full and the free Green's functions, according to Eqs. (2.22) and (2.23), reads

$$\left(\mathrm{i}\hbar\frac{\partial}{\partial t_1} - \mathcal{H}(1)\right)\check{G}(1,1') = \hbar\tau_0\delta(1-1')\,, \tag{2.113}$$

$$\left(\mathrm{i}\hbar\frac{\partial}{\partial t_1} - \mathcal{H}_0(1)\right)\check{G}_0(1,1') = \hbar\tau_0\delta(1-1')\,, \tag{2.114}$$

respectively. For convenience, we introduce the notation

$$\left(\check{A}\otimes\check{B}\right)(1,1') = \int\mathrm{d}^3r_2\int\mathrm{d}t_2\,\check{A}(1,2)\check{B}(2,1')\,, \tag{2.115}$$

which implies a convolution and a matrix multiplication of arbitrary objects $\check{A}$ and $\check{B}$ in Keldysh space. Next, we introduce the inverse of the free Green's function,

$$\check{G}_0^{-1}(1,1') = \frac{1}{\hbar}\left(\mathrm{i}\hbar\frac{\partial}{\partial t_1} - \mathcal{H}_0(1)\right)\tau_0\delta(1-1')\,, \tag{2.116}$$

such that the equation of motion (2.114) becomes

$$\left(\check{G}_0^{-1} \otimes \check{G}_0\right)(1,1') = \tau_0 \delta(1-1')\,. \tag{2.117}$$

Left multiplying the first Dyson equation (2.109) by $\check{G}_0^{-1}\otimes$ and rearranging the terms, we obtain

$$\left[\left(\check{G}_0^{-1} - \check{\Sigma}\right) \otimes \check{G}\right](1,1') = \tau_0 \delta(1-1')\,, \tag{2.118}$$

where $\check{\Sigma}$ is the self-energy in Keldysh space due to $\mathcal{H}_{\rm imp}$ which will be discussed in Sec. 2.5. At this point we recall that physical observables, and thus also the distribution function f, are connected to the Green's function at equal time arguments. Therefore, due to the δ-function on the r.h.s., the latter equation has not yet the appropriate form to obtain a Boltzmann equation. However, by right multiplying analogously the second Dyson equation (2.110) by $\otimes\check{G}_0^{-1}$ we get

$$\left[\check{G} \otimes \left(\check{G}_0^{-1} - \check{\Sigma}\right)\right](1,1') = \tau_0 \delta(1-1')\,. \tag{2.119}$$

As a consequence, we can now get rid of the δ-function by subtracting Eqs. (2.118) and (2.119). Rearranging and multiplying with $-\mathrm{i}$ then leads to the quantum kinetic equation

$$-\,\mathrm{i}\left[\check{G}_0^{-1} \underset{,}{\otimes} \check{G}\right](1,1') = \check{K}\,, \tag{2.120}$$

where we call $\check{K} = -\mathrm{i}\left[\check{\Sigma} \underset{,}{\otimes} \check{G}\right]$ the collision kernel. We have also introduced the abbreviation

$$\left[\check{A} \underset{,}{\otimes} \check{B}\right](1,1') = \left(\check{A} \otimes \check{B}\right)(1,1') - \left(\check{B} \otimes \check{A}\right)(1,1') \tag{2.121}$$

for the commutator/convolution of arbitrary objects $\check{A}$ and $\check{B}$ in Keldysh space.

In the following, we concentrate on the l.h.s. of Eq. (2.120) and show how it leads to the l.h.s. of the Boltzmann equation. Analogously, the r.h.s. leads to the collision operator, see Sec. 2.5 for details.

Gradient expansion

It is useful to introduce Wigner coordinates, the center-of-mass coordinates

$$\begin{aligned} t &= \frac{t_1 + t_{1'}}{2}\,, \\ \mathbf{r} &= \frac{\mathbf{r}_1 + \mathbf{r}_{1'}}{2}\,, \end{aligned} \tag{2.122}$$

and the relative coordinates

$$\begin{aligned} t_r &= t_1 - t_{1'} \,, \\ \mathbf{r}_r &= \mathbf{r}_1 - \mathbf{r}_{1'} \,. \end{aligned} \tag{2.123}$$

The center-of-mass (relative) coordinates describe the properties of the system on slowly (fast) varying scales. In order to connect physical observable with Green's functions we send the relative coordinates to zero. This requires Fourier transforming with respect to the relative coordinates and then integrating over the transformed variable. The Fourier transform of the Green's function is given by

$$\check{G}(x,p) = \int \mathrm{d}y \, \check{G}\left(x + \frac{y}{2}, x - \frac{y}{2}\right) \mathrm{e}^{-\frac{\mathrm{i}}{\hbar} y_\mu p^\mu} \,, \tag{2.124}$$

where $\mathrm{d}y = \mathrm{d}^3 r_r \mathrm{d}t_r$. Furthermore, we have introduced the compact relativistic notation [110] with the contravariant four-vectors

$$\begin{aligned} x^\mu &= (t, \mathbf{r}) \,, \\ y^\mu &= (t_r, \mathbf{r}_r) \,, \\ p^\mu &= (\epsilon, \mathbf{p}) \,, \end{aligned} \tag{2.125}$$

the metric $\eta_{\mu\nu} = \mathrm{diag}(-1,1,1,1)$, and the covariant form $a_\mu = \eta_{\mu\nu} a^\nu$ of an arbitrary four-vector a^μ. For the Fourier transform of Eq. (2.120) we utilize the gradient expansion (see App. B.1 for a derivation) which results for the convolution of $\check{A}$ and $\check{B}$ in

$$\left(\check{A} \otimes \check{B}\right)(x,p) = \exp\left[\frac{\mathrm{i}\hbar}{2}\left(\left(\partial_\mu\right)^{\check{A}} \left(\partial_p^\mu\right)^{\check{B}} - \left(\partial_\mu\right)^{\check{B}} \left(\partial_p^\mu\right)^{\check{A}}\right)\right] \check{A}(x,p)\check{B}(x,p) \,. \tag{2.126}$$

Here, the superscript of the partial derivatives

$$\begin{aligned} \partial_\mu &= (\partial_t, \nabla_{\mathbf{r}}) \,, \\ \partial_p^\mu &= (-\partial_\epsilon, \nabla_{\mathbf{p}}) \,, \end{aligned} \tag{2.127}$$

denotes the object on which the respective derivative acts. Since the Fourier transform of a fast varying variable is slowly varying, it is sufficient to expand the exponential function up to linear order in its argument. The Fourier transform of $\left[\check{G}_0^{-1} \mathbin{\overset{\otimes}{,}} \check{G}\right]$, which we encounter on the l.h.s. of Eq. (2.120), thus reads

$$\begin{aligned} \left[\check{G}_0^{-1} \mathbin{\overset{\otimes}{,}} \check{G}\right](x,p) \approx & \left[\check{G}_0^{-1}, \check{G}\right] - \frac{\mathrm{i}\hbar}{2}\Big\{ \left(\partial_p^\mu \check{G}_0^{-1}\right), \left(\partial_\mu \check{G}\right) \Big\} \\ & + \frac{\mathrm{i}\hbar}{2}\Big\{ \left(\partial_\mu \check{G}_0^{-1}\right), \left(\partial_p^\mu \check{G}\right) \Big\} \,. \end{aligned} \tag{2.128}$$

Locally covariant Green's functions

As previously stated, the Green's function is connected to physical observables in the limit of coinciding space-time points. In this case, when performing a gauge transformation, the transformation depends only on *one* space-time point with the quantity under consideration being then called *locally* covariant. Let us consider some gauge transformation $g(1)$, which locally rotates the field operators,

$$\begin{aligned} \hat{\Psi}'(1) &= g(1)\hat{\Psi}(1)\,, \\ \hat{\Psi}'^{\dagger}(1) &= \hat{\Psi}^{\dagger}(1)g^{\dagger}(1)\,, \\ g(1)g^{\dagger}(1) &= 1\,, \end{aligned} \tag{2.129}$$

leaving the Hamiltonian $\hat{H}$ invariant. Under this transformation, the Green's function transforms according to

$$\check{G}(1,1') \longmapsto g(1)\check{G}(1,1')g^{\dagger}(1')\,, \tag{2.130}$$

and therefore the transformation depends on two distinct space-time points, and the Green's function would not be locally covariant. To avoid this problem, we transform the Green's function as

$$\check{\tilde{G}}(1,1') = U_{\Gamma}(x,1)\check{G}(1,1')U_{\Gamma'}(1',x)\,, \tag{2.131}$$

with the Wilson line U_{Γ} given as a line integral of the gauge field [111],

$$U_{\Gamma}(x,1) = \mathcal{P}\exp\left[-\frac{\mathrm{i}e}{\hbar}\int_{\Gamma}\mathrm{d}x'_{\mu}A^{\mu}(x')\right]\,. \tag{2.132}$$

Here, $\mathcal{P}$ is the path-ordering operator, Γ is a curve from 1 to x, and A^{μ} is the four-potential defined by

$$A^{\mu}(1) = \left(\Phi(1) + \Psi^{a}(1)\frac{\sigma^{a}}{2e}, \mathbf{A}(1) + \boldsymbol{\mathcal{A}}^{a}(1)\frac{\sigma^{a}}{2e}\right)\,. \tag{2.133}$$

Since the gauge transformation of the Wilson line is given by

$$U_{\Gamma}(x,1) \longmapsto g(x)U_{\Gamma}(x,1)g^{\dagger}(1)\,, \tag{2.134}$$

the Green's function $\check{\tilde{G}}$ is now a locally covariant object, transforming according to

$$\check{\tilde{G}}(1,1') \longmapsto g(x)\check{\tilde{G}}(1,1')g^{\dagger}(x)\,. \tag{2.135}$$

Let us further examine the Wilson lines in Eq. (2.131). The curve Γ has its starting point at 1 and its ending point at x. Expressed in relative coordinates the difference between these space-time points is therefore given by $-y/2$. Analogously, Γ' is a curve from x to $1'$ and the difference between the ending and starting points is also given by $-y/2$. Similarly to the gradient expansion above, i.e., only considering linear terms in the derivatives in Eq. (2.128), we assume y to be sufficiently small such that we can approximate

$$\begin{aligned} U_\Gamma(x,1) &\approx 1 + \frac{\mathrm{i}e}{2\hbar} y_\mu A^\mu(x)\,, \\ U_{\Gamma'}(1',x) &\approx 1 + \frac{\mathrm{i}e}{2\hbar} y_\mu A^\mu(x)\,. \end{aligned} \tag{2.136}$$

Thus, the Fourier transform with respect to the relative coordinates of the Green's function and its locally covariant definition are linked by

$$\check{\tilde{G}} \approx \check{G} - \frac{1}{2}\Big\{ eA_\mu,\, \partial_p^\mu \check{G} \Big\}\,, \tag{2.137}$$

$$\check{G} \approx \check{\tilde{G}} + \frac{1}{2}\Big\{ eA_\mu,\, \partial_p^\mu \check{\tilde{G}} \Big\}\,. \tag{2.138}$$

Boltzmann equation

Now, we go back to Eq. (2.128) and perform the transformation according to Eq. (2.137) on each term on the r.h.s. of Eq. (2.128), separately:

$$\Big[\check{G}_0^{-1},\, \check{G}\Big] \;\to\; \Big[\check{G}_0^{-1},\, \check{G}\Big] - \frac{1}{2}\Big\{ eA_\mu,\, \partial_p^\mu \Big[\check{G}_0^{-1},\, \check{G}\Big] \Big\}\,, \tag{2.139}$$

$$\begin{aligned} -\frac{\mathrm{i}\hbar}{2}\Big\{ \left(\partial_p^\mu \check{G}_0^{-1}\right),\, \left(\partial_\mu \check{G}\right) \Big\} \;\to\; & -\frac{\mathrm{i}\hbar}{2}\Big\{ \left(\partial_p^\mu \check{G}_0^{-1}\right),\, \left(\partial_\mu \check{G}\right) \Big\} \\ & + \frac{\mathrm{i}\hbar}{4}\Big\{ eA_\mu,\, \partial_p^\mu \Big\{ \left(\partial_p^\mu \check{G}_0^{-1}\right),\, \left(\partial_\mu \check{G}\right) \Big\} \Big\}\,, \end{aligned} \tag{2.140}$$

$$\begin{aligned} \frac{\mathrm{i}\hbar}{2}\Big\{ \left(\partial_\mu \check{G}_0^{-1}\right),\, \left(\partial_p^\mu \check{G}\right) \Big\} \;\to\; & \frac{\mathrm{i}\hbar}{2}\Big\{ \left(\partial_\mu \check{G}_0^{-1}\right),\, \left(\partial_p^\mu \check{G}\right) \Big\} \\ & - \frac{\mathrm{i}\hbar}{4}\Big\{ eA_\mu,\, \partial_p^\mu \Big\{ \left(\partial_\mu \check{G}_0^{-1}\right),\, \left(\partial_p^\mu \check{G}\right) \Big\} \Big\}\,. \end{aligned} \tag{2.141}$$

The procedure is as follows: we rewrite $\check{G}$ in terms of $\check{\tilde{G}}$ via Eq. (2.138), calculate and insert $\check{G}_0^{-1}$ and its respective derivatives, and keep terms up to the next-to-leading-order. The Fourier transform of the inverse of the free Green's function [cf. Eq. (2.116)] is

given by

$$\check{G}_0^{-1} = \frac{1}{\hbar}\left(\epsilon - \frac{\mathbf{p}^2}{2m} - ev^\mu A_\mu - e^2\frac{A_\mu A^\mu - A_0 A^0}{2m}\right), \tag{2.142}$$

from which follows

$$\partial_p^\mu \check{G}_0^{-1} = -\left[v^\mu + e\left(\partial_p^\mu v_\nu\right)A^\nu\right]/\hbar\,, \tag{2.143}$$

$$\partial^\mu \check{G}_0^{-1} = -ev^\nu \partial^\mu A_\nu/\hbar\,, \tag{2.144}$$

where $v^\mu = (1, \mathbf{p}/m)$ is the four-velocity. Following the steps outlined above, we find

$$\left[\check{G}_0^{-1},\, \check{G}\right] \longrightarrow -\frac{v^\mu}{\hbar}\left(\left[eA_\mu,\, \check{\tilde{G}}\right] + \frac{e^2}{2}\Big\{\left[A_\mu,\, A_\nu\right],\, \left(\partial_p^\nu \check{\tilde{G}}\right)\Big\}\right), \tag{2.145}$$

$$-\frac{\mathrm{i}\hbar}{2}\Big\{\left(\partial_p^\mu \check{G}_0^{-1}\right),\, \left(\partial_\mu \check{G}\right)\Big\} \longrightarrow \mathrm{i}v^\mu\left(\partial_\mu \check{\tilde{G}} + \frac{e}{2}\Big\{\left(\partial_\mu A_\nu\right),\, \left(\partial_p^\nu \check{\tilde{G}}\right)\Big\}\right), \tag{2.146}$$

$$\frac{\mathrm{i}\hbar}{2}\Big\{\left(\partial_\mu \check{G}_0^{-1}\right),\, \left(\partial_p^\mu \check{G}\right)\Big\} \longrightarrow -\mathrm{i}v^\mu\frac{e}{2}\Big\{\left(\partial_\nu A_\mu\right),\, \left(\partial_p^\nu \check{\tilde{G}}\right)\Big\}. \tag{2.147}$$

Inserting the summation of Eqs. (2.145)–(2.147) into the covariant form of Eq. (2.120) then leads to

$$v^\mu \tilde{\partial}_\mu \check{\tilde{G}} + v^\mu \frac{e}{2}\Big\{F_{\mu\nu},\, \left(\partial_p^\nu \check{\tilde{G}}\right)\Big\} = \check{\tilde{K}}\,, \tag{2.148}$$

where $\check{\tilde{K}}$ is the locally covariant form of $\check{K}$. Here, we have introduced the covariant four-derivative $\tilde{\partial}_\mu$ and the U(1)×SU(2) electromagnetic tensor $F_{\mu\nu}$, which are defined by

$$\tilde{\partial}_\mu = \partial_\mu + \frac{\mathrm{i}e}{\hbar}\Big[A_\mu,\, \cdot\,\Big]\,, \tag{2.149}$$

$$F_{\mu\nu} = \partial_\mu A_\nu - \partial_\nu A_\mu + \frac{\mathrm{i}e}{\hbar}\Big[A_\mu,\, A_\nu\Big]\,, \tag{2.150}$$

respectively. In order to obtain the generalized Boltzmann equation, we assume that the spectral function is sharply peaked,

$$A(x,p) \approx 2\pi\hbar\delta(\epsilon - \epsilon_{\mathbf{p}})\,, \tag{2.151}$$

and introduce the distribution function in analogy to the equilibrium case, cf. Eq. (2.73):

$$\tilde{G}^K(x,p) = -2\pi\mathrm{i}\hbar\delta(\epsilon - \epsilon_{\mathbf{p}})\big(1 - 2f(x,p)\big)\,. \tag{2.152}$$

As previously stated in Sec. 2.2, this corresponds to the assumption that in the nonequilibrium case only the occupation is affected but not the spectrum itself. Considering

now the Keldysh component of Eq. (2.148) the Boltzmann equation follows by dividing with $4\pi\mathrm{i}\hbar$ and integrating over ϵ. Explicitly, the Boltzmann equation reads

$$\tilde{\partial}_t f + \frac{\mathbf{p}}{m}\cdot\tilde{\nabla}_{\mathbf{r}} f + \frac{1}{2}\Big\{\boldsymbol{\mathcal{F}},\,(\nabla_{\mathbf{p}} f)\Big\} = I[f]\,. \tag{2.153}$$

The collision operator $I[f]$ is given in terms of the Keldysh component of the locally covariant kernel,

$$I[f] = \frac{1}{4\pi\mathrm{i}\hbar}\int \mathrm{d}\epsilon\,\tilde{K}^K\,, \tag{2.154}$$

which will be discussed in detail in Sec. 2.5. The covariant time and spatial derivatives are given by

$$\tilde{\partial}_t = \partial_t - \frac{\mathrm{i}}{\hbar}\Big[\Psi^a\frac{\sigma^a}{2},\,\cdot\,\Big]\,, \tag{2.155}$$

$$\tilde{\nabla}_{\mathbf{r}} = \nabla_{\mathbf{r}} + \frac{\mathrm{i}}{\hbar}\Big[\boldsymbol{\mathcal{A}}^a\frac{\sigma^a}{2},\,\cdot\,\Big]\,, \tag{2.156}$$

respectively. Furthermore, we have introduced the U(1)×SU(2) Lorentz force,

$$\boldsymbol{\mathcal{F}} = -e\left(\boldsymbol{\mathcal{E}} + \frac{\mathbf{p}}{m}\times\boldsymbol{\mathcal{B}}\right)\,, \tag{2.157}$$

with the components of the generalized U(1)×SU(2) electric and magnetic fields defined in terms of the electromagnetic tensor,

$$\mathcal{E}_i = -F_{0i} = E_i + \mathcal{E}_i^a\frac{\sigma^a}{2e}\,, \tag{2.158}$$

$$\mathcal{B}_i = \frac{1}{2}\varepsilon_{ijk}F_{jk} = B_i + \mathcal{B}_i^a\frac{\sigma^a}{2e}\,, \tag{2.159}$$

respectively. Note that in the three-dimensional Euclidean space we use a slightly different notation than in the four-dimensional Minkowski space. In the former, no differentiation between contra- and covariant components, associated with upper and lower indices, is necessary. Hence, in Euclidean space we use lower indices to indicate real space components and upper indices to indicate spin components. Explicitly, the U(1) electric and magnetic fields, $\mathbf{E}$ and $\mathbf{B}$, and their SU(2) correspondents, $\boldsymbol{\mathcal{E}}^a$ and $\boldsymbol{\mathcal{B}}^a$, read

$$\mathbf{E} = -\partial_t\mathbf{A} - \nabla_{\mathbf{r}}\Phi\,, \tag{2.160}$$

$$\mathbf{B} = \nabla_{\mathbf{r}}\times\mathbf{A}\,, \tag{2.161}$$

$$\boldsymbol{\mathcal{E}}^a = -\partial_t\boldsymbol{\mathcal{A}}^a - \nabla_{\mathbf{r}}\Psi^a - \frac{1}{\hbar}\varepsilon^{abc}\Psi^b\boldsymbol{\mathcal{A}}^c\,, \tag{2.162}$$

$$\boldsymbol{\mathcal{B}}^a = \nabla_{\mathbf{r}}\times\boldsymbol{\mathcal{A}}^a - \frac{1}{2\hbar}\varepsilon^{abc}\boldsymbol{\mathcal{A}}^b\times\boldsymbol{\mathcal{A}}^c\,. \tag{2.163}$$

We see that the SU(2) fields compared to the U(1) fields acquire additional terms due to the non-commuting nature of the SU(2) potentials.

2.5. Collision operators

In the following, we discuss the collision operators which take the influence of impurities into account. Both the common case of momentum relaxation [109] and spin-flip relaxation due to the Elliott-Yafet mechanism are considered. Concerning the latter, we rederive the contribution to zeroth order in the four-potential [69, 112], and present new significant SU(2) contributions, first published in Ref. 28.

Preliminary remarks

The effect of impurities is described by the Hamiltonian

$$\mathcal{H}_{\mathrm{imp}}(\mathbf{r}) = V(\mathbf{r}) - \frac{\lambda^2}{4\hbar}\big[\boldsymbol{\sigma} \times \big(\nabla_{\mathbf{r}} V(\mathbf{r})\big)\big] \cdot (-\mathrm{i}\hbar)\, \nabla_{\mathbf{r}}\,, \tag{2.164}$$

where $V(\mathbf{r})$ is the random potential as defined in Eq. (2.93). The second term on the r.h.s. reflects spin-orbit coupling with the impurity potential and λ is the Compton wavelength. Analogously to the quasiclassical assumption we consider small spin-orbit coupling in the sense that $\lambda p_{\mathrm{F}}/\hbar \ll 1$. Let us recall the impurity average, Eq. (2.95),

$$\begin{aligned} \big\langle V(\mathbf{r}) \big\rangle_{\mathrm{imp}} &= 0\,, \\ \big\langle V(\mathbf{r}) V(\mathbf{r}') \big\rangle_{\mathrm{imp}} &= n_i v_0^2 \delta(\mathbf{r} - \mathbf{r}')\,, \end{aligned} \tag{2.165}$$

which, according to $\mathcal{H}_{\mathrm{imp}}$, leads to three types of self-consistent Born approximation diagrams,

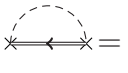
$= \Sigma_0\,,$ (2.166)

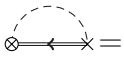
$= \Sigma_{\mathrm{sj}}\,,$ (2.167)

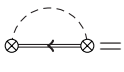
$= \Sigma_{\mathrm{EY}}\,.$ (2.168)

Here, spin-orbit coupling with the impurity potential is represented diagrammatically by

$$\otimes = \mathrm{i}\frac{\lambda^2}{4\hbar}\big[\boldsymbol{\sigma} \times (\nabla_{\mathbf{r}} V(\mathbf{r}))\big] \cdot \overrightarrow{\nabla}_{\mathbf{r}} \,, \tag{2.169}$$

or, since the self-energy features the inner variables within the Dyson equation, by partial integration

$$\otimes = -\mathrm{i}\overleftarrow{\nabla}_{\mathbf{r}} \cdot \frac{\lambda^2}{4\hbar}\big[\boldsymbol{\sigma} \times (\nabla_{\mathbf{r}} V(\mathbf{r}))\big] \,. \tag{2.170}$$

The arrow stacking the spatial derivatives denotes in which direction the derivatives act, respectively. Diagram (2.166) describes momentum relaxation, while (2.168) accounts for Elliott-Yafet spin flips due to scattering at impurities. The middle diagram (2.167) describes instead the side-jump mechanism. We briefly discuss it in Sec. 3.1 and refer to Refs. 17 and 69 for more details.

In the following, we restrict ourselves to two-dimensional space coordinates with regard to Chaps. 4 and 5. This simplified case is sufficient to explain the relevant physical consequences. A generalization to a three-dimensional system with mass anisotropy, such as considered in Chap. 6, is shown in App. G.1. The collision operators are evaluated up to linear order in the SU(2) potentials. However, we remark that when considering both, a Zeeman field and an SU(2) vector potential, it is necessary to include an additional contribution, $I_{\mathrm{EY}}^{\boldsymbol{\mathcal{A}},\Psi}$, which is of second order in the SU(2) potentials. A derivation of $I_{\mathrm{EY}}^{\boldsymbol{\mathcal{A}},\Psi}$ is given in App. C and we further comment on this particular contribution at the end of this section when summarizing the Elliott-Yafet collision operator.

The outline for obtaining the collision operators is as follows: we first rewrite the respective self-energy in Wigner coordinates and perform the Fourier transformation with respect to the relative coordinate. Next, we express the self-energy and the Green's function appearing in the self-energy in their locally covariant form, respectively. The collision kernel is then obtained by the commutator of $\check{\tilde{\Sigma}}$ and $\check{\tilde{G}}$,

$$\check{\tilde{K}} = -\mathrm{i}\Big[\check{\tilde{\Sigma}}, \check{\tilde{G}}\Big] \,. \tag{2.171}$$

Note, that we here neglect the linear order in the derivatives within the gradient expansion (see App. B.2), unlike we did for the l.h.s. of the Boltzmann equation. The reason for this is that the Keldysh component of the resulting terms are $\sim (\tilde{G}^R + \tilde{G}^A)$, which

is essentially the real part of $\tilde{G}^R$. Since within the quasi-particle approximation the real part of the retarded Green's function is the principle value of the fraction $1/(\epsilon - \epsilon_{\mathbf{p}})$ (neglecting the self-energy and contributions due to the potentials), the ϵ integration for obtaining the Boltzmann equation leads to a vanishing of the linear contributions in the derivatives for the self-energies considered here. Analogously, terms $\sim (\tilde{G}^R + \tilde{G}^A)$ which may also appear within the commutator will be neglected in the following as well.

Last, we consider the Keldysh component of $\overset{\scriptscriptstyle\breve{}}{\tilde{K}}$, given by

$$\tilde{K}^K = -\mathrm{i}\left[\tilde{\Sigma}^R\tilde{G}^K - \tilde{G}^K\tilde{\Sigma}^A\right] + 2\pi\hbar\delta(\epsilon - \epsilon_{\mathbf{p}})\tilde{\Sigma}^K\,, \tag{2.172}$$

where we have used the spectral function, Eq. (2.151). The respective collision operator is then obtained according to Eq. (2.154).

Momentum relaxation

In the spatial representation, the diagram (2.166) reads

$$\begin{aligned}\check{\Sigma}_0(1,1') &= \frac{1}{\hbar^2}\left\langle V(\mathbf{r})\check{G}(1,1')V(\mathbf{r}')\right\rangle_{\mathrm{imp}} \\ &= \frac{n_i v_0^2}{\hbar^2}\check{G}(1,1')\delta(\mathbf{r}-\mathbf{r}')\,,\end{aligned} \tag{2.173}$$

where we have performed the impurity average according to Eq. (2.165). Using Wigner coordinates, expressing the Green's function by its Fourier transform, and Fourier transforming with respect to the relative coordinate leads to

$$\check{\Sigma}_0(x,p) = \frac{n_i v_0^2}{\hbar^2}\int\frac{\mathrm{d}^2p'}{(2\pi\hbar)^2}\,\check{G}(\mathbf{p}')\,, \tag{2.174}$$

where we have omitted the variables x and ϵ for the Green's function in the integrand. We transform $\check{\Sigma}_0$ according to Eq. (2.137) and express $\check{G}$ in terms of its locally covariant form via Eq. (2.138). In this particular case, the locally covariant form of $\check{\Sigma}$ has the same structure as in Eq. (2.174), but with $\check{G}$ replaced by $\overset{\scriptscriptstyle\breve{}}{\tilde{G}}$:

$$\overset{\scriptscriptstyle\breve{}}{\tilde{\Sigma}}_0 = \frac{n_i v_0^2}{\hbar^2}\int\frac{\mathrm{d}^2p'}{(2\pi\hbar)^2}\,\overset{\scriptscriptstyle\breve{}}{\tilde{G}}(\mathbf{p}')\,. \tag{2.175}$$

Inserting the components of the self-energy into the Keldysh component of the collision kernel, Eq. (2.172), and using the definition of the distribution function, Eq. (2.152), we obtain

$$\tilde{K}_0^K = -8\pi \mathrm{i} n_i v_0^2 \delta(\epsilon - \epsilon_{\mathbf{p}}) \int \frac{\mathrm{d}^2 p'}{(2\pi\hbar)^2}\, \delta(\epsilon - \epsilon_{\mathbf{p}'}) \big(f_{\mathbf{p}} - f_{\mathbf{p}'}\big)\,. \tag{2.176}$$

Now, the collision operator follows by a division by $4\pi\mathrm{i}\hbar$ and an integration over ϵ,

$$I_0 = -\frac{2\pi n_i v_0^2}{\hbar} \int \frac{\mathrm{d}^2 p'}{(2\pi\hbar)^2}\, \delta(\epsilon_{\mathbf{p}'} - \epsilon_{\mathbf{p}}) \big(f_{\mathbf{p}} - f_{\mathbf{p}'}\big)\,. \tag{2.177}$$

We can write this result in a more condensed form using

$$\int \frac{\mathrm{d}^2 p'}{(2\pi\hbar)^2} \cdots = N_0 \int \mathrm{d}\epsilon_{\mathbf{p}'} \left\langle \ldots \right\rangle\,, \tag{2.178}$$

where $N_0 = m/2\pi\hbar^2$ is the density of states per spin and volume and $\langle \ldots \rangle$ denotes the angular average with respect to the momentum. The collision operator becomes

$$I_0 = -\frac{1}{\tau}\big(f - \langle f \rangle\big)\,, \tag{2.179}$$

where we have introduced the momentum relaxation rate $1/\tau = 2\pi n_i v_0^2 N_0/\hbar$.

Elliott-Yafet collision operator

The Elliott-Yafet self-energy is represented by the diagram (2.168). Rewriting the cross products in the spin-orbit vertices component by component via use of the Levi-Civita symbol, we get

$$\check{\Sigma}_{\text{EY}}(1,1') = -\frac{1}{\hbar^2}\left(\frac{\lambda}{2}\right)^4 \varepsilon_{ijk}\varepsilon_{lmn} \left\langle (\partial_k V)(\partial'_n V) \left(\partial_i \partial'_l \sigma^j \check{G} \sigma^m\right) \right\rangle_{\text{imp}}\,, \tag{2.180}$$

where ∂_i and ∂'_i are the i-th component of $\nabla_{\mathbf{r}}$ and $\nabla_{\mathbf{r}'}$, respectively. Performing the impurity average, expressing the Green's function by its Fourier transform, and further Fourier transforming the self-energy with respect to the relative coordinate then leads to

$$\check{\Sigma}_{\text{EY}}(x,p) = \frac{n_i v_0^2}{\hbar^2}\left(\frac{\lambda}{2\hbar}\right)^4 \int \frac{\mathrm{d}^2 p'}{(2\pi\hbar)^2} \big[\,(\mathbf{p}\times\mathbf{p}')\cdot\boldsymbol{\sigma}\big] \check{G}(\mathbf{p}') \big[\,(\mathbf{p}\times\mathbf{p}')\cdot\boldsymbol{\sigma}\big]\,. \tag{2.181}$$

Since we consider the two-dimensional case, we can set $p_z = p'_z = 0$ such that the self-energy takes the simple form

$$\check{\Sigma}_{\text{EY}}(x,p) = \frac{n_i v_0^2}{\hbar^2}\left(\frac{\lambda}{2\hbar}\right)^4 \int \frac{\mathrm{d}^2 p'}{(2\pi\hbar)^2} \left(\mathbf{p}\times\mathbf{p}'\right)_z^2 \sigma^z \check{G}(\mathbf{p}')\sigma^z \,. \tag{2.182}$$

Transforming $\check{\Sigma}_{\text{EY}}$ according to Eq. (2.137) and inserting Eq. (2.138) leads to

$$\begin{aligned}
\check{\tilde{\Sigma}}_{\text{EY}} =& \frac{n_i v_0^2}{\hbar^2}\left(\frac{\lambda}{2\hbar}\right)^4 \int \frac{\mathrm{d}^2 p'}{(2\pi\hbar)^2} \left(\mathbf{p}\times\mathbf{p}'\right)_z^2 \sigma^z \check{\tilde{G}}(\mathbf{p}')\sigma^z \\
&- \frac{n_i v_0^2}{2\hbar^2}\left(\frac{\lambda}{2\hbar}\right)^4 \Big\{ A_\mu,\, \partial_p^\mu \int \frac{\mathrm{d}^2 p'}{(2\pi\hbar)^2} \left(\mathbf{p}\times\mathbf{p}'\right)_z^2 \sigma^z \check{\tilde{G}}(\mathbf{p}')\sigma^z \Big\} \\
&+ \frac{n_i v_0^2}{2\hbar^2}\left(\frac{\lambda}{2\hbar}\right)^4 \int \frac{\mathrm{d}^2 p'}{(2\pi\hbar)^2} \left(\mathbf{p}\times\mathbf{p}'\right)_z^2 \sigma^z \Big\{ A_\mu,\, \partial_{p'}^\mu \check{\tilde{G}}(\mathbf{p}') \Big\} \sigma^z \,,
\end{aligned} \tag{2.183}$$

where for notational reasons $\partial_{p'}^\mu = (-\partial_\epsilon, \nabla_{\mathbf{p}'})$. Let us further split the contributions to the Elliott-Yafet self-energy according to the type of non-Abelian potential, i.e., no potential (superscript 0), scalar potential (superscript Ψ), and vector potential (superscript $\boldsymbol{\mathcal{A}}$):

$$\check{\tilde{\Sigma}}_{\text{EY}} = \check{\tilde{\Sigma}}^0_{\text{EY}} + \check{\tilde{\Sigma}}^\Psi_{\text{EY}} + \check{\tilde{\Sigma}}^{\boldsymbol{\mathcal{A}}}_{\text{EY}} \,. \tag{2.184}$$

While the derivation of $\check{\tilde{\Sigma}}^0_{\text{EY}}$ and its contribution to the collision operator (as shown next) is well-known [69, 112], the contributions of $\check{\tilde{\Sigma}}^\Psi_{\text{EY}}$ and $\check{\tilde{\Sigma}}^{\boldsymbol{\mathcal{A}}}_{\text{EY}}$ are new [28] and their relevance will be discussed in the summary at the end of this section.

$\boldsymbol{\Sigma}^{\mathbf{0}}_{\text{EY}}$ contribution

To zeroth order in the four-potential, the Elliott-Yafet self-energy is given by

$$\check{\tilde{\Sigma}}^0_{\text{EY}} = \frac{n_i v_0^2}{\hbar^2}\left(\frac{\lambda}{2\hbar}\right)^4 \int \frac{\mathrm{d}^2 p'}{(2\pi\hbar)^2} \left(\mathbf{p}\times\mathbf{p}'\right)_z^2 \sigma^z \check{\tilde{G}}(\mathbf{p}')\sigma^z \,. \tag{2.185}$$

The retarded/advanced and Keldysh components are given by

$$\begin{aligned}
\left[\check{\tilde{\Sigma}}^0_{\text{EY}}\right]^{R/A} =& \frac{1}{2\pi\hbar N_0 \tau}\left(\frac{\lambda}{2\hbar}\right)^4 \int \frac{\mathrm{d}^2 p'}{(2\pi\hbar)^2} \left(\mathbf{p}\times\mathbf{p}'\right)_z^2 \check{\tilde{G}}^{R/A}(\mathbf{p}') \,, \\
\left[\check{\tilde{\Sigma}}^0_{\text{EY}}\right]^{K} =& -\frac{\mathrm{i}}{N_0\tau}\left(\frac{\lambda}{2\hbar}\right)^4 \int \frac{\mathrm{d}^2 p'}{(2\pi\hbar)^2} \delta(\epsilon-\epsilon_{\mathbf{p}'}) \left(\mathbf{p}\times\mathbf{p}'\right)_z^2 \left[1 - 2\sigma^z f_{\mathbf{p}'}\sigma^z\right] ,
\end{aligned} \tag{2.186}$$

respectively, where we have inserted the relaxation rate as defined below Eq. (2.179). Inserting these components into Eq. (2.172), dividing by $4\pi\mathrm{i}\hbar$, and integrating over ϵ yields the following collision operator

$$I^0_{\text{EY}}[f] = -\frac{1}{N_0\tau}\left(\frac{\lambda}{2\hbar}\right)^4 \int \frac{\mathrm{d}^2p'}{(2\pi\hbar)^2}\delta(\epsilon_{\mathbf{p}} - \epsilon_{\mathbf{p}'})\,(\mathbf{p}\times\mathbf{p}')_z^2\,[f_{\mathbf{p}} - \sigma^z f_{\mathbf{p}'}\sigma^z]\,. \tag{2.187}$$

We can simplify this expression by neglecting higher harmonics of f (p-wave approximation) such that we can replace $(\mathbf{p}\times\mathbf{p}')_z^2$ with its angular average with respect to $\mathbf{p}'$, $\langle(\mathbf{p}\times\mathbf{p}')_z^2\rangle' = p^2p'^2/2$. Inserting $f = f^0 + \mathbf{f}\cdot\boldsymbol{\sigma}$ into Eq. (2.187) and using the anticommutation relations for the Pauli matrices,

$$\left\{\sigma^a,\,\sigma^b\right\} = 2\delta_{ab}\,, \tag{2.188}$$

we end up with

$$I^0_{\text{EY}} = -\frac{1}{2N_0\tau}\left(\frac{\lambda p}{2\hbar}\right)^4 \int \frac{\mathrm{d}^2p'}{(2\pi\hbar)^2}\delta(\epsilon_{\mathbf{p}} - \epsilon_{\mathbf{p}'})\left[\Gamma\left(\mathbf{f}_{\mathbf{p}} + \mathbf{f}_{\mathbf{p}'}\right)\right]\cdot\boldsymbol{\sigma}\,. \tag{2.189}$$

Here, $\Gamma = \mathrm{diag}(1,1,0)$ describes the anisotropy of Elliott-Yafet spin relaxation in two dimensions, see also Sec. 3.1. In the derivation of Eq. (2.189), we have neglected terms $\sim (f^{0,z}_{\mathbf{p}} - f^{0,z}_{\mathbf{p}'})$ since these terms are small compared to I_0 [see Eq. (2.179)] due to the assumption $\lambda p_{\text{F}}/\hbar \ll 1$.

$\boldsymbol{\Sigma}^{\boldsymbol{\Psi}}_{\text{EY}}$ contribution

Next, we regard the contributions which are linear in the SU(2) scalar potential. From Eq. (2.183) we obtain

$$\begin{aligned}\check{\tilde{\Sigma}}^{\Psi}_{\text{EY}} = &-\frac{n_i v_0^2}{4\hbar^2}\left(\frac{\lambda}{2\hbar}\right)^4 \\ &\times \partial_\epsilon \int \frac{\mathrm{d}^2p'}{(2\pi\hbar)^2}\,(\mathbf{p}\times\mathbf{p}')_z^2\left(\left\{\sigma^a,\,\sigma^z\check{\tilde{G}}(\mathbf{p}')\sigma^z\right\} - \sigma^z\left\{\sigma^a,\,\check{\tilde{G}}(\mathbf{p}')\right\}\sigma^z\right)\Psi^a\,.\end{aligned} \tag{2.190}$$

With use of the relation

$$\left\{\sigma^a,\,\sigma^z A\sigma^z\right\} = -\sigma^z\left\{\sigma^a,\,A\right\}\sigma^z + 2\delta_{az}\left\{\sigma^z,\,A\right\}, \tag{2.191}$$

we rewrite Eq. (2.190) as follows:

$$\begin{aligned}\check{\tilde{\Sigma}}^{\Psi}_{\text{EY}} =& \frac{n_i v_0^2}{2\hbar^2}\left(\frac{\lambda}{2\hbar}\right)^4 \\ &\times \partial_\epsilon \int \frac{\mathrm{d}^2 p'}{(2\pi\hbar)^2} \left(\mathbf{p}\times\mathbf{p}'\right)_z^2 \left(\sigma^z \left\{\sigma^a,\, \check{\tilde{G}}(\mathbf{p}')\right\}\sigma^z - \delta_{az}\left\{\sigma^z,\, \check{\tilde{G}}(\mathbf{p}')\right\}\right)\Psi^a\,. \quad (2.192)\end{aligned}$$

Again, we replace $\left(\mathbf{p}\times\mathbf{p}'\right)_z^2$ with its angular average and employ the anticommutation relations for the Pauli matrices, Eq. (2.188). The retarded/advanced and Keldysh components of the self-energy become

$$\begin{aligned}\left[\check{\tilde{\Sigma}}^{\Psi}_{\text{EY}}\right]^{R/A} =& -\frac{mp^2}{2\pi\hbar N_0\tau}\left(\frac{\lambda}{2\hbar}\right)^4 \partial_\epsilon \int \frac{\mathrm{d}^2 p'}{(2\pi\hbar)^2}\epsilon_{\mathbf{p}'}\tilde{G}^{R/A}(\mathbf{p}')\,(\Gamma\boldsymbol{\Psi})\cdot\boldsymbol{\sigma}\,, \\ \left[\check{\tilde{\Sigma}}^{\Psi}_{\text{EY}}\right]^{K} =& \frac{\mathrm{i}mp^2}{N_0\tau}\left(\frac{\lambda}{2\hbar}\right)^4 \partial_\epsilon \int \frac{\mathrm{d}^2 p'}{(2\pi\hbar)^2}\delta(\epsilon-\epsilon_{\mathbf{p}'})\epsilon_{\mathbf{p}'}\left[(1-2f^0_{\mathbf{p}'})\boldsymbol{\sigma}^a + 2\mathbf{f}_{\mathbf{p}'}\right]\cdot(\Gamma\boldsymbol{\Psi})\,,\end{aligned} \quad (2.193)$$

respectively. We obtain the associated collision operator by inserting Eq. (2.193) into Eq. (2.172), neglecting terms $\sim (\tilde{G}^R + \tilde{G}^A)$ within the Keldysh component of the collision kernel, and inserting the latter into Eq. (2.154):

$$I^{\Psi}_{\text{EY}} = \frac{mp^2}{N_0\tau}\left(\frac{\lambda}{2\hbar}\right)^4 \int \frac{\mathrm{d}^2 p'}{(2\pi\hbar)^2}\delta(\epsilon_{\mathbf{p}}-\epsilon_{\mathbf{p}'})\left[\left(f^0_{\mathbf{p}}\boldsymbol{\sigma}+\mathbf{f}_{\mathbf{p}}\right) - \partial_{\epsilon_{\mathbf{p}'}}\epsilon_{\mathbf{p}'}\left(f^0_{\mathbf{p}'}\boldsymbol{\sigma}-\mathbf{f}_{\mathbf{p}'}\right)\right]\cdot(\Gamma\boldsymbol{\Psi})\,. \quad (2.194)$$

$\boldsymbol{\Sigma}^{\boldsymbol{\mathcal{A}}}_{\text{EY}}$ contribution

Finally, we consider the linear contribution by $\boldsymbol{\mathcal{A}}^a$ to the Elliott-Yafet collision operator. For the sake of simplicity, we assume that the spin-z component of the SU(2) vector potential vanishes, $\boldsymbol{\mathcal{A}}^z = 0$. Note that Rashba spin-orbit coupling is still contained within this assumption. According to Eq. (2.183) the self-energy under consideration is given by

$$\begin{aligned}\check{\tilde{\Sigma}}^{\boldsymbol{\mathcal{A}}}_{\text{EY}} = \frac{n_i v_0^2}{4\hbar^2}\left(\frac{\lambda}{2\hbar}\right)^4 \int \frac{\mathrm{d}^2 p'}{(2\pi\hbar)^2}\Bigg[&\sigma^z\left\{\sigma^a,\, \boldsymbol{\mathcal{A}}^a\cdot\left(\nabla_{\mathbf{p}'}\check{\tilde{G}}(\mathbf{p}')\right)\right\}\sigma^z\left(\mathbf{p}\times\mathbf{p}'\right)_z^2 \\ &- \left\{\sigma^a,\, \sigma^z\check{\tilde{G}}(\mathbf{p}')\sigma^z\right\}\boldsymbol{\mathcal{A}}^a\cdot\nabla_{\mathbf{p}}\left(\mathbf{p}\times\mathbf{p}'\right)_z^2\Bigg]\,.\end{aligned} \quad (2.195)$$

Utilizing Eq. (2.191) for the second term on the r.h.s. and performing a partial integration for the first term on the r.h.s. , the self-energy can be rewritten as

$$\check{\tilde{\Sigma}}^{\boldsymbol{\mathcal{A}}}_{\text{EY}} = \frac{n_i v_0^2}{2\hbar^2}\left(\frac{\lambda}{2\hbar}\right)^4 \int \frac{\mathrm{d}^2 p'}{(2\pi\hbar)^2} \sigma^z \Big\{\sigma^a,\, \check{\tilde{G}}(\mathbf{p}')\Big\} \sigma^z \boldsymbol{\mathcal{A}}^a \cdot \mathbf{L}_{\mathbf{p},\mathbf{p}'} \tag{2.196}$$

with

$$\begin{aligned}\mathbf{L}_{\mathbf{p},\mathbf{p}'} &= \frac{1}{2}\left(\nabla_{\mathbf{p}} - \nabla_{\mathbf{p}'}\right)\left(\mathbf{p}\times\mathbf{p}'\right)_z^2 \\ &= \Big[\mathbf{p}'^2 + \mathbf{p}\cdot\mathbf{p}'\Big]\mathbf{p} - \Big[\mathbf{p}^2 + \mathbf{p}\cdot\mathbf{p}'\Big]\mathbf{p}' \,. \end{aligned} \tag{2.197}$$

By employing the anticommutation relation (2.188) the retarded, advanced, and Keldysh components are obtained similarly as for $\check{\tilde{\Sigma}}^{\Psi}_{\text{EY}}$ in the previous paragraph. Following the outline around Eq. (2.172) one obtains

$$I^{\boldsymbol{\mathcal{A}}}_{\text{EY}} = \frac{1}{N_0\tau}\left(\frac{\lambda}{2\hbar}\right)^4 \int \frac{\mathrm{d}^2 p'}{(2\pi\hbar)^2} \left[\left(f^0_{\mathbf{p}} - f^0_{\mathbf{p}'}\right)\sigma^a + f^a_{\mathbf{p}} + f^a_{\mathbf{p}'}\right] \boldsymbol{\mathcal{A}}^a \cdot \mathbf{L}_{\mathbf{p},\mathbf{p}'} \,. \tag{2.198}$$

Summary

In order to keep track of the various contributions to the Elliott-Yafet collision operator, let us recall the respective terms and briefly discuss them. The Elliott-Yafet collision operator, including the second-order correction mentioned before, is given by

$$I_{\text{EY}} = I^0_{\text{EY}} + I^{\Psi}_{\text{EY}} + I^{\boldsymbol{\mathcal{A}}}_{\text{EY}} + I^{\boldsymbol{\mathcal{A}},\Psi}_{\text{EY}} \tag{2.199}$$

with

$$\begin{aligned} I^0_{\text{EY}} &= -\frac{1}{2N_0\tau}\left(\frac{\lambda p}{2\hbar}\right)^4 \int \frac{\mathrm{d}^2 p'}{(2\pi\hbar)^2} \delta(\epsilon_{\mathbf{p}} - \epsilon_{\mathbf{p}'}) \big[\Gamma\big(\mathbf{f}_{\mathbf{p}} + \mathbf{f}_{\mathbf{p}'}\big)\big] \cdot \boldsymbol{\sigma} \,, \\ I^{\Psi}_{\text{EY}} &= \frac{mp^2}{N_0\tau}\left(\frac{\lambda}{2\hbar}\right)^4 \int \frac{\mathrm{d}^2 p'}{(2\pi\hbar)^2} \delta(\epsilon_{\mathbf{p}} - \epsilon_{\mathbf{p}'}) \Big[\big(f^0_{\mathbf{p}}\boldsymbol{\sigma} + \mathbf{f}_{\mathbf{p}}\big) - \partial_{\epsilon_{\mathbf{p}'}}\epsilon_{\mathbf{p}'}\left(f^0_{\mathbf{p}'}\boldsymbol{\sigma} - \mathbf{f}_{\mathbf{p}'}\right)\Big] \cdot (\Gamma\boldsymbol{\Psi}) \,, \\ I^{\boldsymbol{\mathcal{A}}}_{\text{EY}} &= \frac{1}{N_0\tau}\left(\frac{\lambda}{2\hbar}\right)^4 \int \frac{\mathrm{d}^2 p'}{(2\pi\hbar)^2} \left[\left(f^0_{\mathbf{p}} - f^0_{\mathbf{p}'}\right)\sigma^a + f^a_{\mathbf{p}} + f^a_{\mathbf{p}'}\right] \boldsymbol{\mathcal{A}}^a \cdot \mathbf{L}_{\mathbf{p},\mathbf{p}'} \,, \\ I^{\boldsymbol{\mathcal{A}},\Psi}_{\text{EY}} &= \frac{1}{2\tau}\left(\frac{\lambda}{2\hbar}\right)^4 \boldsymbol{\Psi}\cdot\boldsymbol{\mathcal{A}}_i p_i p^2 \partial_{\epsilon_{\mathbf{p}}} f^0_{\text{eq}} \,, \end{aligned} \tag{2.200}$$

where f^0_{eq} is the Fermi function. Here, I^0_{EY} describes in-plane spin relaxation due to spin-orbit coupling with impurities. In order to describe Elliott-Yafet spin relaxation

correctly in the presence of a Zeeman field, the collision operator I^{Ψ}_{EY} is essential. The reason is that the collision operator I^{0}_{EY} relaxes the spin density to zero, which is incorrect on physical grounds: instead, the equilibrium spin density must have a finite value due to the Zeeman field. The clue is to take I^{Ψ}_{EY} into account as well, resulting in the correct relaxation of the spin density to its equilibrium value. In addition, I^{Ψ}_{EY} yields a spin filter contribution, $\mathbf{j}_i \sim \mathbf{n} j_i$, and its reciprocal, the inverse spin filter effect, $j_i \sim \mathbf{n} \cdot \mathbf{j}_i$, in a ferromagnetic conductor with magnetization $\mathbf{n}$. To the best of our knowledge, the inverse spin filter effect has been unnoticed so far [28]. However, it yields important contributions to the charge current, e.g., its contribution to the electric field in a spin pumping setup with Rashba spin-orbit coupling is of the same magnitude as the spin galvanic contribution, see Chap. 4. Similarly, $I^{\boldsymbol{\mathcal{A}}}_{\mathrm{EY}}$ contributes significantly to the inverse spin galvanic and the spin galvanic effect [28, 99], reflecting, once more [69], the non-trivial interplay between extrinsic and intrinsic spin-orbit coupling. Considering the presence of a Zeeman field, however, $I^{\boldsymbol{\mathcal{A}}}_{\mathrm{EY}}$ exhibits a similar 'problem' as I^{0}_{EY}. One obtains—incorrectly—a finite effective force acting on the charge carriers due to the equilibrium part of the spin density. The term $I^{\boldsymbol{\mathcal{A}},\Psi}_{\mathrm{EY}}$ fixes this, ensuring that such a force is generated only by a nonequilibrium spin density. The need for including $I^{\boldsymbol{\mathcal{A}},\Psi}_{\mathrm{EY}}$ becomes also plausible by taking a closer look at $I^{\boldsymbol{\mathcal{A}}}_{\mathrm{EY}}$ directly. With the equilibrium spin density being parallel to the Zeeman field, the equilibrium part of the spin distribution function is formally already of first order in the SU(2) scalar potential. Therefore, in order to treat Elliott-Yafet spin relaxation consistently, the second-order contributions have to cancel which is achieved by taking $I^{\boldsymbol{\mathcal{A}},\Psi}_{\mathrm{EY}}$ into account.

3

Spin-orbit physics

In this chapter, we briefly discuss some physical aspects of spin-orbit coupled materials as far as they are relevant for this thesis. Specifically, we consider a metallic system with Rashba spin-orbit interaction in contact with a ferromagnet. We start by discussing the origin of spin-orbit coupling in solids, and consider then the influence of an interface with a ferromagnet, leading to the proximity induced magnetization and the spin-transfer torque.

3.1. Spin-orbit coupling

Spin-orbit coupling in solids can be classified into two types: intrinsic, originating in the band or device structure, and extrinsic due to spin-orbit coupling with impurities or phonons. Regarding the intrinsic contribution, we limit ourselves to the case of Rashba spin-orbit coupling [36, 37]. In the following, we provide a brief overview of the origins and types of Rashba spin-orbit coupling and discuss the mechanisms leading to various extrinsic contributions. For details regarding the explicit derivation of various effective Hamiltonians which describe intrinsic spin-orbit coupling in two-dimensional systems we refer, for instance, to Ref. 42 which employs the $\mathbf{k}\cdot\mathbf{p}$ theory, developed by Luttinger and Kohn [113], and Kane [114].

Rashba spin-orbit coupling

We start by discussing the exemplary case of the GaAs/GaAlAs semiconductor heterostructure [115–118]. In semiconductors, spin-orbit coupling is responsible for a splitting of p-orbital electron states with angular momentum $j = 3/2$ and $j = 1/2$, see Fig. 3.1. The associated spin-orbit splitting Δ_{SO} is small in the sense that

$$\Delta_{\text{SO}} \ll \epsilon_{\text{F}} \,. \tag{3.1}$$

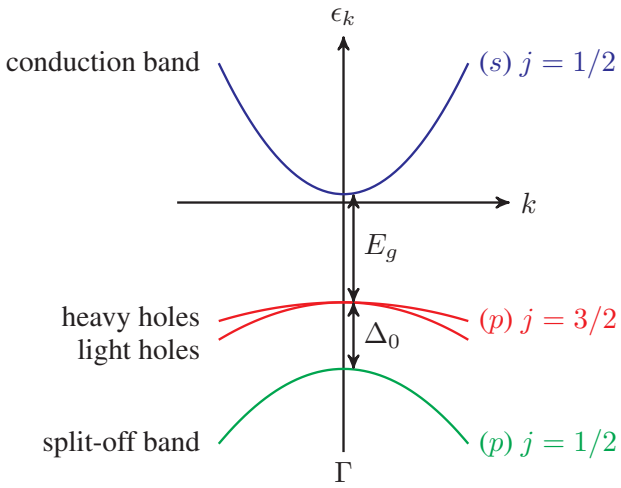

FIG. 3.1.: Sketch of the band structure of GaAs around the Γ point. The conduction band (s) and the valence bands (p) are split by the fundamental gap E_g. There exists another energy gap due to spin-orbit coupling, Δ_0, for the p-orbital electron states between the heavy/light hole bands and the split-off band [42].

GaAs/GaAlAs and similar heterostructures can be described as a quantum well with few energy states which are separated well enough such that the system can be treated as a two-dimensional electron gas. Of particular interest are asymmetrically doped heterostructures which exhibit Rashba spin-orbit coupling in consequence of an asymmetric quantum well, cf. Fig. 3.2. Assuming the structural asymmetry along z direction, the Rashba Hamiltonian is given by

$$\hat{H}_{\text{R}} = -\frac{\alpha}{\hbar}\,(\hat{\mathbf{p}} \times \boldsymbol{\sigma}) \cdot \mathbf{e}_z\,, \tag{3.2}$$

where $\mathbf{e}_z$ is the unit vector along z and α is the Rashba parameter. We remark that the Hamiltonian (3.2) is *not* obtained by simply considering the usual spin-orbit interaction

$$\begin{aligned}\hat{H}_{\text{so}} &= -\frac{\lambda^2}{4\hbar}\big[\boldsymbol{\sigma} \times (\nabla_{\mathbf{r}} V(\mathbf{r}))\big] \cdot \hat{\mathbf{p}} \\ &= -\frac{\lambda^2(\partial_z V)}{4\hbar}\,(\hat{\mathbf{p}} \times \boldsymbol{\sigma}) \cdot \mathbf{e}_z\,.\end{aligned} \tag{3.3}$$

for the asymmetric potential $V(z)$ in the quantum well for the conduction band. Realistic values of α are much larger than one would expect from the factor $\sim \lambda^2 \partial_z V$ [42].

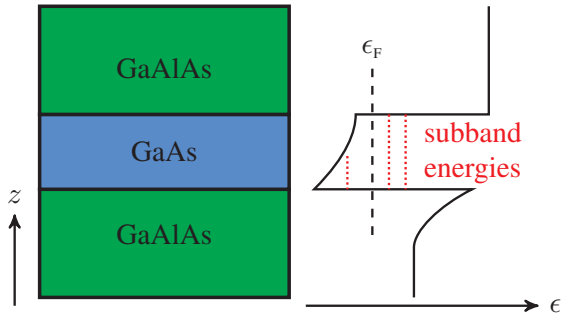

FIG. 3.2.: Example for an asymmertically doped GaAs/GaAlAs heterostructure and a qualitative outline of the condution band profile with indicated subband energies (red dotted lines) and Fermi energy (dashed line). For a quantitative plot of the conduction band profile see Ref. 118.

Instead, the effective 2×2 Hamiltonian $\hat{H}_R$ can be obtained by a multi-band analysis at the Γ point by applying Löwdin partitioning to the 8×8 subband Hamiltonian which describes the four bands depicted in Fig. 3.1, see Ref. 42 for details. As a result, the Rashba parameter is determined by the asymmetry potential in the valance band and by material parameters of the semiconductors such as E_g and Δ_0, see Fig. 3.1.

The Hamiltonian (3.2) can be connected to the SU(2) vector potential in the Hamiltonian (2.112) by

$$\mathcal{A}_y^x = -\mathcal{A}_x^y = \frac{2m\alpha}{\hbar}\,, \tag{3.4}$$

and the other components being zero. The associated spin-orbit splitting is given by $\Delta_{SO} = 2\alpha p_F/\hbar$; for the Rashba parameter of a typical semiconductor quantum well, we thus have

$$\alpha \ll \hbar v_F\,, \tag{3.5}$$

where $v_F = p_F/m$ is the Fermi velocity. Note that condition (3.5) is necessary for employing the gradient expansion in order to obtain the Boltzmann equation, see Sec. 2.4.

The values of the Rashba parameter of semiconductor quantum wells are typically in the range of a few $10\,\mathrm{meV\,Å}$ [119–121]. In addition to semiconductor heterostructures, a Rashba-like spin-orbit coupling due to a structure inversion asymmetry can also be found in single-crystalline Pt thin films [122] and surface alloys like Bi/Ag or Bi/Si [123, 124] which show rather large Rashba parameters, $\alpha \sim 1\,\mathrm{eV\,Å}$. Recently, new types of three-dimensional materials have been found which also host a strong Rashba

field. The so-called 3D Rashba metals BiTeX (X = Br, I) [79–81], GeTe [82, 83], and CH_3 N H_3 Pb X_3 (X = Br, I) [84] offer new and very promising perspectives in spintronics, not only due to their large Rashba coefficient up to $\sim 10\,\mathrm{eV}$ Å, but also due to the possibility of tuning the Fermi energy to values larger or smaller than the Rashba splitting Δ_{SO} [125]. In contrast to their 2D counterparts, the Rashba spin-orbit coupling in 3D Rashba metals is present also in bulk materials, as it does not have its origin in the geometry of the sample but in the noncentrosymmetric crystal structure.

Next, we discuss the Dyakonov-Perel spin relaxation mechanism [126]. Note that the Rashba spin-orbit coupling acts as a momentum-dependent effective magnetic field around which the spin of an electron precesses. In diffusive transport, the momentum dependence of the Rashba spin-orbit field thus leads to a decay of spin polarization, i.e., Dyakonov-Perel spin relaxation. In the dirty limit,

$$\frac{\Delta_{\text{SO}}\tau}{\hbar} \sim \frac{\alpha p_{\text{F}}\tau}{\hbar^2} \ll 1\,, \tag{3.6}$$

as considered in the following, the Boltzmann equation (2.154) leads to the Dyakonov-Perel spin relaxation rate [67],

$$\frac{1}{\tau_{\text{DP}}} = \left(\frac{2m\alpha}{\hbar^2}\right)^2 D\,, \tag{3.7}$$

where $D = v_{\text{F}}^2\tau/d$ is the diffusion constant with $d = 2, 3$ representing the dimensionality. According to condition (3.6), the Dyakonov-Perel relaxation time obeys $\tau_{\text{DP}} \gg \tau$. The length scale associated with τ_{DP} is the Dyakonov-Perel spin diffusion length $l_{\text{DP}} = \sqrt{D\tau_{\text{DP}}}$.

Extrinsic spin-orbit coupling

In Sec. 2.5 we have already introduced the Elliott-Yafet spin relaxation mechanism due to spin-orbit coupling with impurities. One particular goal of this paragraph is to briefly discuss some physical implications of the Elliott-Yafet collision operator. In addition, we would like to mention two other extrinsic mechanisms, side-jump and skew scattering [127]. The relevant self-energy diagrams are depicted in Fig. 3.3.

From the collision operator (2.189), which was obtained from the self-energy (a) in

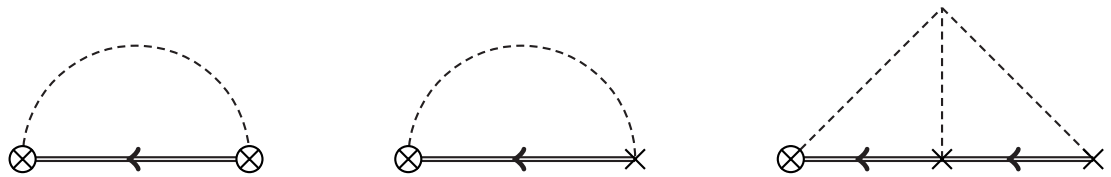

FIG. 3.3.: The impurity averaged self-energy diagrams which account for Elliott-Yafet spin relaxation (a), side-jump (b), and skew scattering (c).

Fig. 3.3, we can read out the Elliott-Yafet relaxation rate in two dimensions,

$$\frac{1}{\tau_s} = \frac{1}{\tau}\left(\frac{\lambda p_{\text{F}}}{2\hbar}\right)^4 . \tag{3.8}$$

The spin diffusion length associated with Elliott-Yafet relaxation is given by $l_s = \sqrt{D\tau_s}$. Furthermore, as already mentioned in Sec. 2.5, the Elliott-Yafet spin relaxation is anisotropic, meaning that the z component of the spin density is preserved in the strictly two-dimensional case, described by the matrix $\Gamma = \text{diag}(1, 1, 0)$. For a three-dimensional electron gas, an isotropic spin relaxation is obtained as can be seen by keeping the z component of the momentum in Eq. (2.181) and below.[1] Hence, in order to account for the transition between two dimensions and three dimensions, as considered in Chap. 4, we introduce a phenomenological parameter $0 \leq \zeta \leq 1$ in the anisotropy matrix,

$$\Gamma = \begin{pmatrix} 1 & 0 & 0 \\ 0 & 1 & 0 \\ 0 & 0 & \zeta \end{pmatrix} . \tag{3.9}$$

Comparing the size of the Elliott-Yafet relaxation with the Dyakonov-Perel relaxation, we note that in typical experiments [22, 122]

$$\frac{1}{\tau_{\text{DP}}} \gg \frac{1}{\tau_s} , \tag{3.10}$$

which will be used in Chaps. 4 and 5.

[1] Besides the fact that Elliott-Yafet spin relaxation becomes isotropic in the three-dimensional case, also the numerical value of $1/\tau_s$ differs slightly from the two-dimensional case as a consequence of the dimensionality when performing the angular average, see also App. G.1.

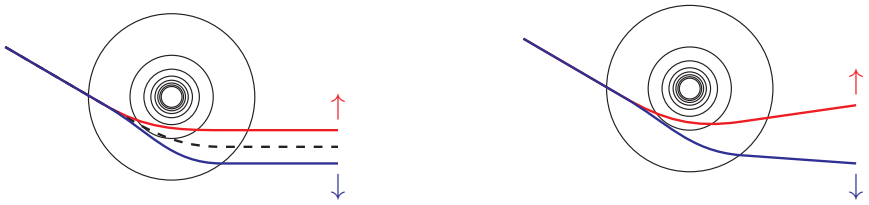

(a) (b)

FIG. 3.4.: Schematic picture of the classical trajectories for scattering of spin-up (↑) and spin-down (↓) electrons with side-jump (a) and skew scattering (b) at a spherical potential [131].

In Chap. 6 we consider a bulk Rashba metal, and thus extend the system to a third spatial dimension and furthermore assume a mass anisotropy. In this case, the anisotropy parameter ζ of the Elliott-Yafet mechanism appearing in Eq. (3.9) is directly determined by the mass anisotropy.

In the following, we present a short introduction to the side-jump and skew scattering mechanisms. In Sec. 2.5, we have already mentioned that side-jump scattering can be described by the self-energy diagram (b) in Fig. 3.3. The name of this spin-dependent scattering has its origin in the semiclassical treatment of an electron-impurity collision process. As depicted in Fig. 3.4 (a), an electron described by a wave packet is displaced from the spinless trajectory by

$$\Delta \mathbf{r}_{\mathrm{sj}} = -2\frac{\lambda^2}{\hbar}\Delta \mathbf{p} \times \boldsymbol{\sigma}\,, \tag{3.11}$$

where $\Delta\mathbf{p}$ is the momentum picked up by the electron during the collision with the impurity [128–130]. Under the action of an electric field $\mathbf{E}$, the momentum change, on average, is proportional to the electric field, $\Delta\mathbf{p} \sim \mathbf{E}$. Thus, the spatial displacement given by Eq. (3.11) is orthogonal to the electric field which in turn leads to a spin current and an additional contribution to the spin Hall effect [2, 131]. A more detailed investigation of this contribution and its extension to spin-thermoelectric effects within the SU(2) Boltzmann theory is given, for instance, in Refs. 69 and 17, respectively.

A further spin-dependent scattering process, skew scattering [131–134], can be taken into account within the SU(2) Boltzmann theory [69]. The corresponding impurity averaged self-energy, diagrammatically depicted in Fig. 3.3 (c), requires the third moment

of the random potential, $\langle V(\mathbf{q}_1)V(\mathbf{q}_2)V(\mathbf{q}_3)\rangle_{\text{imp}} = n_i v_0^3 \delta(\mathbf{q}_1+\mathbf{q}_2+\mathbf{q}_3)$ to be nonzero. Skew scattering is therefore not captured within the Born approximation [127]. The physical mechanism can be explained qualitatively for a two-dimensional system: for a spherical single impurity potential, the spin-orbit Hamiltonian is essentially the product of the orbital and spin angular momentum, L_z and σ_z. Thus, L_z and σ_z are conserved and since the scattering cross section (beyond Born approximation) depends on the relative sign of L_z and σ_z, spin-up electrons are scattered more strongly into states with $L_z > 0$ than into states with $L_z < 0$. For spin-down electrons we have the opposite situation. Altogether, this results in a different scattering angle for spin-up and spin-down electrons. A qualitative picture of a skew scattering process is given in Fig. 3.4 (b).

For Chaps. 4 and 5 we assume

$$\frac{2\alpha}{\hbar v_{\text{F}}} > \frac{\lambda p_{\text{F}}}{2\hbar}\,. \tag{3.12}$$

In this case, the spin Hall effect is dominated by the Rashba spin-orbit coupling. This can be seen from the total spin Hall conductivity as given in Eq. (36) in Ref. 69,

$$\sigma_0^{\text{sH}} = \frac{1}{1+\tau_s/\tau_{\text{DP}}}\left(\sigma_{\text{int}}^{\text{sH}} + \sigma_{\text{sj}}^{\text{sH}} + \sigma_{\text{ss}}^{\text{sH}}\right)\,, \tag{3.13}$$

where $\sigma_{\text{int}}^{\text{sH}} = e\tau/4\pi\hbar\tau_{\text{DP}}$ accounts for the Rashba contribution, $\sigma_{\text{sj}}^{\text{sH}} = e\epsilon_{\text{F}}N_0\lambda^2/2\hbar$ for the side-jump contribution, and $\sigma_{\text{ss}}^{\text{sH}} \sim \epsilon_{\text{F}}\tau\sigma_{\text{sj}}^{\text{sH}}/\hbar$ for the skew-scattering contribution [131]. Condition (3.12), together with $\hbar/\tau \ll \epsilon_{\text{F}}$, then leads to $\sigma_{\text{sj}}^{\text{sH}} \ll \sigma_{\text{ss}}^{\text{sH}} \ll \sigma_{\text{int}}^{\text{sH}}$ such that side-jump and skew scattering can be neglected. However, it is still necessary to take extrinsic spin-orbit coupling, via the Elliott-Yafet spin relaxation mechanism, into account, since its absence ($\tau_s \to \infty$ in Eq. (3.13)) leads to a vanishing of the total spin Hall conductivity in the disordered Rashba system. Note that this vanishing is not trivial and has been intensely debated [12], in particular with regard to the prediction of a universal value $\sigma_0^{\text{sH}} = e/8\pi\hbar$ for the spin Hall conductivity in a clean Rashba system [135]. However, disorder in a Rashba system leads to a cancellation of a reactive and a dissipative contribution, with the dissipative part resulting from vertex corrections for the velocity vertex in the Kubo formalism [136, 137]. For the effect of disorder on the spin Hall effect we refer, for instance, to Ref. 69.

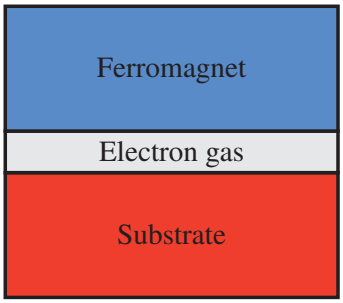

FIG. 3.5.: Schematic picture of the geometry considered in Chap. 4. The Rashba electron gas is sandwiched between a ferromagnet and a nonmagnetic substrate.

3.2. Proximity induced magnetization

In Chap. 4 we consider the geometry as depicted in Fig. 3.5. The Rashba system can either be a two-dimensional electron gas at an interface of a heterostructure or a thin metallic film [122, 138, 139]. For sufficiently thin films of heavy metals like Pt or Pd, it is known that they can be magnetized due to the magnetic proximity effect [140–142]. In either case, it is possible to treat the Rashba system as a ferromagnetic conductor.

Metallic ferromagnetism can be conveniently described within the s-d model [143], which assumes that the itinerant "s" states are coupled to the localized magnetic "d" states. Strictly speaking, the labels "s" and "d" are not correct since the "s" and "d" states are not necessarily associated with particular s and d orbital states, respectively. For instance, in $3d$ metals such as Co, the "s" states represent the $4s$ and $4p$ states and the "d" states the $3d$ states, whereas for $4f$ metals, the "s" states denote the $5d$, $6s$, and $6p$ states and the "d" states are the $4f$ states. Figure 3.6 shows a qualitative sketch of the band structures of this model and a more realistic band structure of face-centered cubic Co.[2] Comparing the realistic band structure (b) to the band structure of the s-d model (a), we see that the s and p bands hybridize with the d bands such that the d

[2]The electronic structure calculations of Co with lattice constant $3.548\,\text{Å}$ were performed in the framework of density functional theory by Wilhelm H. Appelt (private communication). The full-potential augmented-plane wave approach, implemented in ELK, has been used as a basis set (http://elk.sourceforge.net). Exchange and correlation effects were treated with the local density approximation [144]. Spin-orbit effects were neglected and the regular $16 \times 16 \times 16$ Monkhorst-Pack grid for the Brillouin-zone integration was used [145].

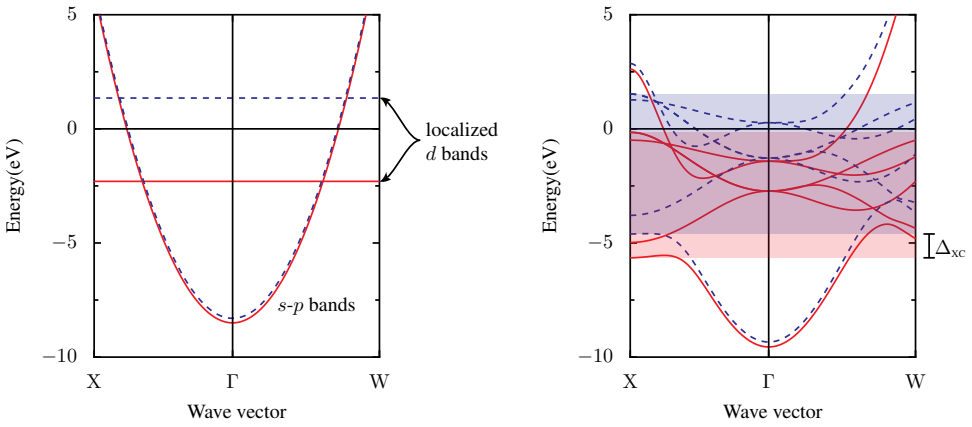

FIG. 3.6.: Comparison of the band structures of the s-d model (a) with a band structure calculated employing the local spin density approximation for face-centered cubic Co (b). The majority (minority) band is depicted by a red solid (blue dashed) line. In panel (b) the bandwidth of the minority and majority d bands are represented by a blue and red shaded area, respectively, and the difference of the bandwidths gives the exchange splitting.

bands generally cannot be considered as localized [146, 147]. Nevertheless, since the realistic situation is far too complex to capture it with an effective Hamiltonian, we stick to the s-d model as our model of choice. Due to the proximity induced magnetization in the Rashba system, we assume that the localized "d" states follow the magnetization direction $\mathbf{n}$ of the attached ferromagnet. The corresponding Hamiltonian reads

$$\mathcal{H}_{\mathrm{sd}} = -\Delta_{\mathrm{xc}}\, \mathbf{n}(\mathbf{r}, t) \cdot \frac{\boldsymbol{\sigma}}{2}\,, \tag{3.14}$$

where Δ_{xc} is the exchange splitting. In the SU(2) language, introduced in Sec. 2.4, the SU(2) scalar potential is therefore given by

$$\boldsymbol{\Psi}(\mathbf{r}, t) = \Delta_{\mathrm{xc}} \mathbf{n}(\mathbf{r}, t)\,. \tag{3.15}$$

The precise value of the proximity induced exchange splitting Δ_{xc} depends on the interface and on the material properties of the various layers. In this work, we assume a large exchange splitting [142] compared to the disorder broadening, $\Delta_{\mathrm{xc}} \gg \hbar/\tau$. Together

with the assumptions (3.6) and (3.10), we thus have the following hierarchy of energy scales:

$$\underbrace{\frac{\hbar}{\Delta_{\mathrm{XC}}\tau_s}}_{\beta_s} \ll \underbrace{\frac{\hbar}{\Delta_{\mathrm{XC}}\tau_{\mathrm{DP}}}}_{\beta_{\mathrm{DP}}} \ll \frac{\hbar}{\Delta_{\mathrm{XC}}\tau} \ll 1 \ll \frac{\hbar}{\Delta_{\mathrm{SO}}\tau}\,. \tag{3.16}$$

Here, we have introduced the spin torque parameters β_s and β_{DP}, which will appear repeatedly in Chap. 4.

3.3. Spin-transfer torque

In the treatment of the spin Hall magnetoresistance in Chaps. 5 and 6, the spin-transfer torque [76, 146, 148] plays a central role since it allows to control the amount of spin current flowing across a ferromagnet/normal-metal interface. The concept of the spin-transfer torque was first introduced by Slonczewski [74] and Berger [149] in 1996 by considering a ferromagnetic-metal/normal-metal/ferromagnetic-metal multilayer, or explicitly, in the case of Ref. 74 a Co/Cu/Co multilayer as depicted in Fig. 3.7.

In order to elucidate the physical origin of the spin-transfer torque, let us consider the spin-polarized current which flows into the right ferromagnetic metal shown in Fig. 3.7. The spins of the electrons entering the ferromagnet eventually align along the magnetization axis of the ferromagnet, and since the exchange interaction is spin conserving, the transversal component of the spin of the incident electrons must be transferred to the total spin angular momentum of the ferromagnet. In other words, the spin-polarized current exerts a torque on the ferromagnet, hence the name spin-transfer torque for the described phenomenon.

The setup depicted in Fig. 3.7 is the typical framework for an irreversible electrical switching of the magnetization. By measuring current-induced resistance changes, a first experimental investigation of the spin-transfer torque was presented by Tsoi et al. in 1998 [150], followed by the observation of a complete current-induced magnetization reversal shortly afterwards in 1999 and 2000 [151, 152]. See, for instance, Ref. 148 for a review.

As mentioned above, the spin-transfer torque can also be used to control the spin current flowing across a normal-metal/ferromagnet interface, and can thus be employed to switch between an open circuit and a closed circuit condition for the spin current.

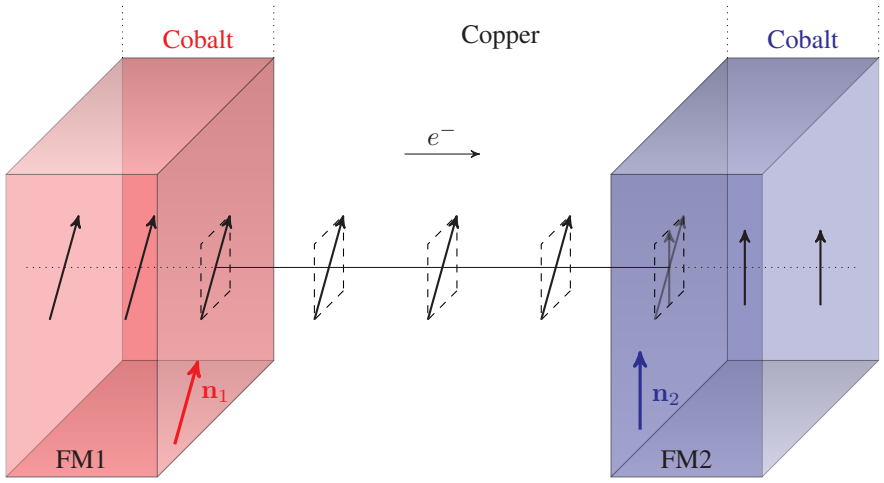

FIG. 3.7.: Visualization of the spin-transfer torque for a Co/Cu/Co multilayer as discussed in Ref. 74. An electric current flows through the first Co layer (FM1) and is polarized along the magnetization direction $\mathbf{n}_1$ of FM1 when flowing into the Cu layer. When the spin-polarized current enters the second Co layer (FM2) the spin of the current will align along the magnetization axis $\mathbf{n}_2$ of FM2 with the transverese component of the spin polarization being transferred to the total spin of FM2 (spin-transfer torque).

Assuming that the interface lies in the xz plane, the boundary condition for the spin current in y direction reads [153, 154]

$$\mathbf{j}_y(y=0) = \frac{1}{2\pi\hbar N_0}\left[g_r^{\uparrow\downarrow}\mathbf{n}\times\big(\mathbf{n}\times\mathbf{s}(y=0)\big) + g_i^{\uparrow\downarrow}\mathbf{n}\times\mathbf{s}(y=0)\right], \tag{3.17}$$

where $\mathbf{s}$ is the spin density. Here, $g_r^{\uparrow\downarrow}$ ($g_i^{\uparrow\downarrow}$) is the real (imaginary) part of the spin mixing conductance, which is defined as [76]

$$g^{\uparrow\downarrow} = \frac{1}{A_{\text{int}}}\sum_{m,n}\left[\delta_{mn} - r_{mn}^{\uparrow}\left(r_{mn}^{\downarrow}\right)^*\right], \tag{3.18}$$

where A_{int} is the area of the normal-metal/ferromagnet interface, and $r_{mn}^{\uparrow}$ ($r_{mn}^{\downarrow}$) is the reflection amplitude for spin up (down) electrons scattered from quantum channel n to quantum channel m.[3] Note that the spin-mixing conductance remains finite even

[3] In the literature, sometimes $g^{\uparrow\downarrow}$ is denoted as "spin mixing conductance," and sometimes $G^{\uparrow\downarrow}$ (as originally introduced by Slonzcewksi [154]). The relation simply is: $G^{\uparrow\downarrow} = (e^2/h)g^{\uparrow\downarrow}$.

when the transmission coefficients vanish. Thus, Eq. (3.17) can also be employed for magnetic insulators like Yttrium Iron Garnet (YIG) [155].

4

Spin-charge dynamics driven by a time-dependent magnetization

In this chapter, the studies on spin-charge coupled dynamics in a thin, magnetized metallic system as published in Ref. 28 are presented. We consider a general inversion-asymmetric substrate/normal-metal/magnet structure as shown in Fig. 3.5, with the magnet inducing a dynamical magnetic texture via the proximity effect, see Sec. 3.2. This magnetic texture, together with Rashba spin-orbit coupling, in turn leads to an effective driving force acting on the charge carriers. In particular, we identify a new term in the effective force, labeled as 'inverse spin filter' contribution, which depends on ζ, the anisotropy parameter in the Elliott-Yafet relaxation, see Eq. (3.9). Furthermore, we discuss the spin pumping configuration of typical experimental setups in order to shed light on the physical meaning of the various contributions, in particular, in the two-dimensional limit where the spin galvanic effect tends to dominate the DC voltage due to the effective force.

Let us briefly discuss the setup, schematically depicted in Fig. 4.1 together with a possible experimental realization. Although determining the value of the physical parameters which enter the s-d Hamiltonian (3.14), the precise nature of the magnetic system (ferro- or ferrimagnet, magnetic insulator) is insignificant for our purposes. Similarly, the substrate may be an ordinary structureless insulator, possibly vacuum, also contributing to an effective Rashba spin-orbit coupling in the normal metal due to inversion symmetry breaking.

Concerning the normal metal, we assume a free electron gas of thickness t_m with static impurities, implying an Elliott-Yafet spin relaxation in the 2D to 3D crossover regime as described in Sec. 3.1. We remark that in this context '2D' or '3D' does not refer to the electron motion. Instead, 2D (3D) is meant in the sense that t_m is small (large) compared to the spin relaxation length $l_s = \sqrt{D\tau_s}$. Regarding transport within the normal metal, we assume the frequency of the magnetization ω to be small compared

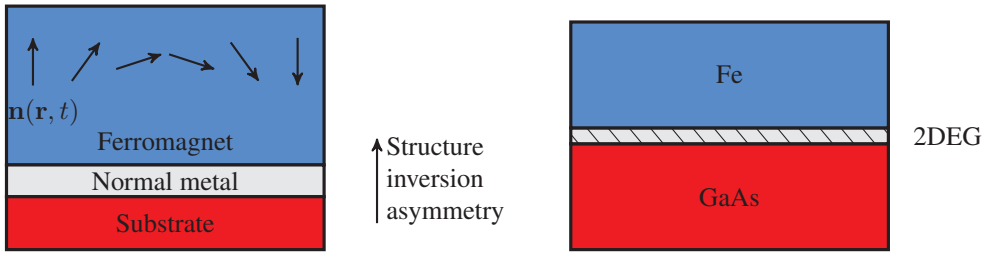

FIG. 4.1.: A sketch of the considered setup. The magnetization $\mathbf{n}(\mathbf{r},t)$ on the left is exemplarily illustrated as a Néel domain wall. The right picture shows a possible experimental realization of the setup, where the spin-charge dynamics in the 2D electron gas, formed at the Fe/GaAs interface, can be driven by a time-dependent Fe magnetization.

to the spin-flip rate,

$$\omega\tau_s \ll 1, \tag{4.1}$$

which corresponds to the typical adiabatic pumping regime. Furthermore, we assume the diffusive regime,

$$\begin{aligned} \omega\tau &\ll 1\,, \\ ql &\ll 1\,, \end{aligned} \tag{4.2}$$

where $l = v_{\mathrm{F}}\tau$ is the mean free path and q is the typical wave vector of the magnetic texture. We recall that the hierarchy of energy scales as defined in relation (3.16) is still valid.

By employing the explicit expressions for the SU(2) vector and scalar potentials, Eqs. (3.4) and (3.15), the i-th component of the generalized force in the Boltzmann equation, Eq. (2.157), reads

$$\mathcal{F}_i = -eE_i + \Delta_{\mathrm{XC}}\left(\tilde{\nabla}_i\mathbf{n}\right)\cdot\frac{\boldsymbol{\sigma}}{2} - \frac{\alpha}{\hbar l_{\mathrm{DP}}}\varepsilon_{ijz}p_j\sigma^z\,. \tag{4.3}$$

Here, the i-th component of the covariant derivative $\tilde{\nabla}_i$ in the 3D-subspace is defined by

$$\tilde{\nabla}_i = \nabla_i - \frac{1}{\hbar}[\boldsymbol{\mathcal{A}}_i]_\times\,, \tag{4.4}$$

where we have introduced the notation for an antisymmetric matrix

$$[\mathbf{v}]_\times = \begin{pmatrix} 0 & -v_3 & v_2 \\ v_3 & 0 & -v_1 \\ -v_2 & v_1 & 0 \end{pmatrix}, \tag{4.5}$$

which corresponds to a cross product in the sense that $[\mathbf{v}]_\times \mathbf{b} = \mathbf{v} \times \mathbf{b}$ for arbitrary vectors $\mathbf{v} = (v_1, v_2, v_3)$ and $\mathbf{b}$. Similarly, the covariant time derivative in the 3D-subspace is given by

$$\tilde{\partial}_t = \partial_t + \frac{\Delta_{\text{xc}}}{\hbar}[\mathbf{n}]_\times . \tag{4.6}$$

4.1. Spin-charge coupled dynamics

In this section, we present the coupled equations for the electron density, the charge current, the spin density, and the spin current, defined via the distribution function as

$$n = 2\int \frac{\mathrm{d}^d p}{(2\pi\hbar)^d} f^0 , \tag{4.7}$$

$$j_i = -2e\int \frac{\mathrm{d}^d p}{(2\pi\hbar)^d} \frac{p_i}{m} f^0 , \tag{4.8}$$

$$\mathbf{s} = \int \frac{\mathrm{d}^d p}{(2\pi\hbar)^d} \mathbf{f} , \tag{4.9}$$

$$j_i^a = \int \frac{\mathrm{d}^d p}{(2\pi\hbar)^d} \frac{p_i}{m} f^a . \tag{4.10}$$

Here, lower indices denote the spatial component, while upper indices refer to the polarization. Throughout the remaining text, the spin current appears also written as a boldface vector consisting of the three components which are not explicitly marked as an index.

Spin sector

First, let us remark that the magnetization leads to a finite spin density even in equilibrium. Thus, the spin density takes the form

$$\mathbf{s} = \mathbf{s}_{\text{eq}} + \delta\mathbf{s} , \tag{4.11}$$

where $\mathbf{s}_{\mathrm{eq}} = (N_0\Delta_{\mathrm{xc}}/2)\mathbf{n}$ is the equilibrium part of $\mathbf{s}$ which follows the magnetization adiabatically, whereas $\delta\mathbf{s}$ accounts for the dynamics of the itinerant electrons, which is typically much faster than the magnetization dynamics. Analogously, it is convenient to split the spin distribution function

$$\mathbf{f} = \mathbf{f}_{\mathrm{eq}} + \delta\mathbf{f}\,, \tag{4.12}$$

with $\mathbf{f}_{\mathrm{eq}} = \left(-\partial_{\epsilon_{\mathbf{p}}} f^0_{\mathrm{eq}}\right)(\Delta_{\mathrm{xc}}/2)\mathbf{n}$.

The spin sector is now obtained by multiplying the Boltzmann equation (2.153) with the Pauli vector $\boldsymbol{\sigma}$ and performing the trace, leading to a 3×3 matrix equation in $\mathbf{f}$. Furthermore, employing the above splitting, the Boltzmann equation in the spin sector can be written as

$$\mathbb{M}\delta\mathbf{f} = \mathbb{N}\langle\delta\mathbf{f}\rangle + \mathbf{S}\,, \tag{4.13}$$

with

$$\mathbb{M} = 1 + \frac{\tau}{2\tau_s}\Gamma + \tau\tilde{\partial}_t + \tau\frac{p_i}{m}\tilde{\nabla}_i\,, \tag{4.14}$$

$$\mathbb{N} = 1 - \frac{\tau}{2\tau_s}\Gamma\,, \tag{4.15}$$

$$\mathbf{S} = \left(\partial_{\epsilon_{\mathbf{p}}} f^0_{\mathrm{eq}}\right)\frac{\tau\Delta_{\mathrm{xc}}}{2}\dot{\mathbf{n}}\,. \tag{4.16}$$

Here, we have also assumed $\langle f^0\rangle \simeq f^0_{\mathrm{eq}}$ and $f^0 \simeq \langle f^0\rangle$, where the latter assumption is motivated by the circumstance that small deviations of f^0 from its angular average are at least first order in the electric field $\mathbf{E}$ or the magnetic texture, i.e., $\nabla_i\mathbf{n}$ or $\dot{\mathbf{n}}$.

Integrating Eq. (4.13) over the momentum yields[1]

$$\tilde{\partial}_t\delta\mathbf{s} + \tilde{\nabla}_i\mathbf{j}_i = -\frac{1}{\tau_s}\Gamma\delta\mathbf{s} - \frac{N_0\Delta_{\mathrm{xc}}}{2}\dot{\mathbf{n}}\,. \tag{4.17}$$

In the following, we consider the quasiadiabatic limit, i.e., $\tau_s\partial_t\delta\mathbf{s} \ll \delta\mathbf{s}$ and $\tau_s\partial_t\delta\mathbf{s} \ll \zeta\delta\mathbf{s}$. In this case, the Boltzmann equation in the spin sector (4.13) can be solved for the nonequilibrium spin density straightforwardly,

$$\delta\mathbf{s} = (\delta\mathbf{s})_{\mathbf{n}} + (\delta\mathbf{s})_{\mathbf{j}_s}\,, \tag{4.18}$$

[1] Equations for the spin density which have a continuity-equation-like form with a covariant time derivative such as Eq. 4.17 can be used as starting point for the derivation of a Landau-Lifshitz-Gilbert equation, see App. D.

which we conveniently separate into two parts, one associated directly with the magnetization,

$$(\delta\mathbf{s})_{\mathbf{n}} = -\frac{N_0\Delta_{\text{xc}}\tau_s}{2}\left(\Gamma + \frac{1}{\beta_s}[\mathbf{n}]_\times\right)^{-1}\dot{\mathbf{n}}\,, \tag{4.19}$$

and the other associated with the spin current,

$$(\delta\mathbf{s})_{\mathbf{j}_s} = -\tau_s\left(\Gamma + \frac{1}{\beta_s}[\mathbf{n}]_\times\right)^{-1}\tilde{\nabla}_i\mathbf{j}_i\,. \tag{4.20}$$

Note that the split in Eq. (4.18) is only of technical nature since the spin current itself depends on the spin density which has to be considered when explicitly solving for the spin density from Eq. (4.17) in terms of the magnetization.

Next, we consider the diffusive regime and calculate the spin current. To do so, we rewrite the matrix $\mathbb{M}$ in Eq. (4.13) as follows:

$$\mathbb{M} = (1+\xi)M\,, \tag{4.21}$$

where

$$M = \left(1 + \frac{\Delta_{\text{xc}}\tau}{\hbar}[\mathbf{n}]_\times\right)\,, \tag{4.22}$$

and

$$\xi = \left(\frac{\tau}{2\tau_s}\Gamma + \tau\partial_t + \tau\frac{p_i}{m}\tilde{\nabla}_i\right)M^{-1}. \tag{4.23}$$

The diffusive regime allows us to approximate $(1+\xi)^{-1} \simeq 1-\xi$, and solving Eq. (4.13) for $\delta\mathbf{f}$ yields

$$\delta\mathbf{f} = M^{-1}(1-\xi)\Big(\mathbb{N}\,\langle\delta\mathbf{f}\rangle + \mathbf{S}\Big)\,. \tag{4.24}$$

Multiplying with p_i/m, and integrating over the momentum, then yields the spin current

$$\mathbf{j}_i = (\mathbf{j}_i)_{\mathbf{n}} + (\mathbf{j}_i)_{\mathbf{s}}\,, \tag{4.25}$$

which we split analogously to the spin density, cf. Eq. (4.18), into one part originating directly in the magnetization,

$$(\mathbf{j}_i)_{\mathbf{n}} = \frac{DN_0\Delta_{\text{xc}}\tau}{2}M^{-1}\tilde{\nabla}_i M^{-1}\,\dot{\mathbf{n}}\,, \tag{4.26}$$

and one part which arises from the spin density,

$$(\mathbf{j}_i)_{\mathbf{s}} = -DM^{-1}\tilde{\nabla}_i M^{-1}\delta\mathbf{s}\,. \tag{4.27}$$

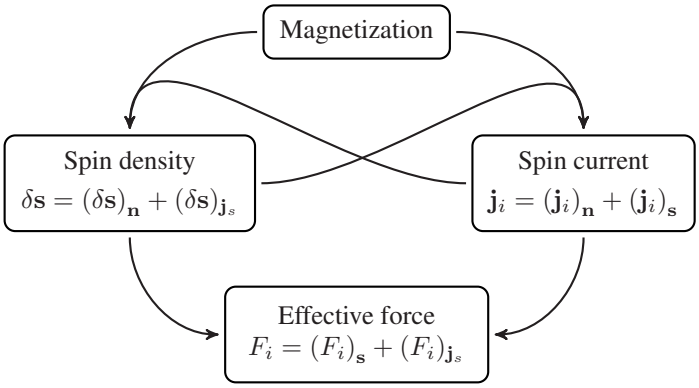

FIG. 4.2.: Overview of the various contributions, and their interrelation, to the effective force.

Charge sector

Similarly to the spin sector, the charge sector is obtained by performing the trace over the Boltzmann equation (2.153). A multiplication with the momentum and a subsequent momentum integration yields

$$(1 + \tau\partial_t)\, j_i - eD\nabla_i n = \sigma_{\text{D}} E_i - \frac{e\tau N_0 \Delta_{\text{xc}}}{m} F_i \,, \tag{4.28}$$

where $\sigma_{\text{D}} = n\tau e^2/m$ is the Drude conductivity. Here, we have introduced an effective force F_i which accounts for contributions of both the nonequilibrium part of the spin density and the spin current,

$$F_i = (F_i)_{\mathbf{s}} + (F_i)_{\mathbf{j}_s} \,. \tag{4.29}$$

The contributions to the effective force from spin densities, $(F_i)_{\mathbf{s}}$, and spin currents, $(F_i)_{\mathbf{j}_s}$, as well as their interrelations, are schematically depicted in Fig. 4.2. Apparently, $(F_i)_{\mathbf{s}}$ is associated with the spin galvanic effect, and $(F_i)_{\mathbf{j}_s}$ with the inverse spin Hall effect. Explicitly, the two parts of the effective force are given by

$$(F_i)_{\mathbf{s}} = \frac{1}{N_0}\left[\left(\tilde{\nabla}_i \mathbf{n}\right)\cdot \delta\mathbf{s} + \frac{\beta_s}{l_{\text{DP}}}(\mathbf{e}_z \times \delta\mathbf{s})_i\right] \,, \tag{4.30}$$

$$(F_i)_{\mathbf{j}_s} = \frac{1}{DN_0}\left[\beta_{\text{DP}}\left(\mathbf{j}^z \times \mathbf{e}_z\right)_i + \frac{\tau}{\tau_s}\mathbf{n}_\zeta \cdot \mathbf{j}_i\right] \,, \tag{4.31}$$

where $\mathbf{n}_\zeta = \Gamma\mathbf{n}$. As discussed in connection with Eq. (2.200), the $\boldsymbol{\mathcal{A}}, \Psi$ part of the Elliott Yafet collision operator is responsible for the appearance of solely the nonequilibrium part of the spin density and not the whole spin density in the second term on the

r.h.s. of Eq. (4.30). Furthermore, we divide

$$(F_i)_{\mathbf{s}} = (F_i)_{\mathbf{s},\mathbf{n}} + (F_i)_{\mathbf{s},\mathbf{j}_s} \tag{4.32}$$

into contributions $(F_i)_{\mathbf{s},\mathbf{n}}$ and $(F_i)_{\mathbf{s},\mathbf{j}_s}$, arising from $(\delta\mathbf{s})_{\mathbf{n}}$ and $(\delta\mathbf{s})_{\mathbf{j}_s}$, respectively. The two contributions have the same form as $(F_i)_{\mathbf{s}}$ in Eq. (4.30), but with $\delta\mathbf{s}$ being replaced by $(\delta\mathbf{s})_{\mathbf{n}}$ and $(\delta\mathbf{s})_{\mathbf{j}_s}$, respectively. Similarly, the spin current part of the effective force, Eq. (4.31), will be further split

$$(F_i)_{\mathbf{j}_s} = (F_i)_{\mathbf{j}_s,\mathbf{n}} + (F_i)_{\mathbf{j}_s,\mathbf{s}}\,, \tag{4.33}$$

where $\mathbf{j}_i$ is replaced by $(\mathbf{j}_i)_{\mathbf{n}}$ and $(\mathbf{j}_i)_{\mathbf{s}}$ in $(F_i)_{\mathbf{j}_s}$ in order to obtain $(F_i)_{\mathbf{j}_s,\mathbf{n}}$ and $(F_i)_{\mathbf{j}_s,\mathbf{s}}$, respectively. The idea behind this separation is to indicate the respective origins of the force via the subscripts. In the following, we shall therefore express the effective force in terms of $\dot{\mathbf{n}}$ and $(j_i^a)_{\mathbf{n}}$, respectively.

The contribution $(F_i)_{\mathbf{s},\mathbf{n}}$

According to Eq. (4.19), the spin density directly related to the dynamical magnetization explicitly reads

$$(\delta\mathbf{s})_{\mathbf{n}} = \frac{\hbar N_0}{2}\frac{1}{\mathbf{n}_\zeta^2}\left[\mathbf{n}_\zeta \times \dot{\mathbf{n}} - \beta_s\zeta\Gamma^{-1}\dot{\mathbf{n}}\right]. \tag{4.34}$$

Inserting Eq. (4.34) into Eq. (4.30) leads to the following effective force contribution:

$$\begin{aligned}(F_i)_{\mathbf{s},\mathbf{n}} = \frac{\hbar}{2}\frac{1}{\mathbf{n}_\zeta^2}\Bigg\{ &(\nabla_i\mathbf{n})\cdot\left(\mathbf{n}_\zeta\times\dot{\mathbf{n}} - \beta_s\zeta\Gamma^{-1}\dot{\mathbf{n}}\right)\\ &+\frac{1}{l_{\text{DP}}}\Big[\,(\mathbf{n}\cdot\mathbf{n}_\zeta)\,\mathbf{e}_z\times\dot{\mathbf{n}} + \beta_s\mathbf{e}_z\times\left(\mathbf{n}_\zeta\times\dot{\mathbf{n}} + \zeta\mathbf{n}\times\Gamma^{-1}\dot{\mathbf{n}}\right)\Big]_i\Bigg\}.\end{aligned} \tag{4.35}$$

In the case $\zeta = 1$, Eq. (4.35) coincides with Eq. (11) in Ref. 156; see also Refs. 71, 157–161 for preceding work. We recall that, regarding the spin-flip relaxation, the parameter ζ describes the anisotropy and that $\zeta = 1$ corresponds to the isotropic case. To the best of our knowledge, such an anisotropy ($\zeta < 1$) was first explicitly taken into account in Ref. 28. However, it is necessary to include this effect since experiments on thin films typically deal with samples on the scale of a few nanometers, hence the thickness is on the same length scale as the spin relaxation length l_s.

The contributions $(F_i)_{\mathbf{s},\mathbf{j}_s}$ and $(F_i)_{\mathbf{j}_s,\mathbf{n}}$ (homogeneous case)

In the following, we assume a spatially homogeneous situation, i.e., $\tilde{\nabla}_i \approx -(1/\hbar)[\boldsymbol{\mathcal{A}}_i]_\times$ in Eqs. (4.20) and (4.30). We consider this case, first due to the sake of simplicity, and second in order to focus on the Rashba contribution with the motivation to show the competition between the spin galvanic effect and the (in-plane) inverse spin Hall effect. Up to first order in the spin torque parameters, the effective force contribution $(F_i)_{\mathbf{s},\mathbf{j}_s}$ according to its definition in Eq. (4.32) is obtained as

$$(F_i)_{\mathbf{s},\mathbf{j}_s} = \frac{\beta_{\text{DP}}}{DN_0}\frac{1}{\mathbf{n}_\zeta^2}\Big\{ (\mathbf{n}\cdot\mathbf{n}_\zeta)\left[\mathbf{e}_z \times (\mathbf{j}^z)_\mathbf{n}\right]_i + 2\sum_{a=x,y}\left[n_z\,(j_a^a)_\mathbf{n} - n_a\,(j_a^z)_\mathbf{n}\right](\mathbf{e}_z\times\mathbf{n})_i\Big\}. \tag{4.36}$$

Adding the spin current contribution with $\mathbf{j}_i \to (\mathbf{j}_i)_\mathbf{n}$ in Eq. (4.31),

$$(F_i)_{\mathbf{j}_s,\mathbf{n}} = \frac{1}{DN_0}\left\{\beta_{\text{DP}}\Big[\,(\mathbf{j}^z)_\mathbf{n}\times\mathbf{e}_z\Big]_i + \frac{\tau}{\tau_s}\mathbf{n}_\zeta\cdot(\mathbf{j}_i)_\mathbf{n}\right\}, \tag{4.37}$$

we obtain

$$(F_i)_{\mathbf{s},\mathbf{j}_s} + (F_i)_{\mathbf{j}_s,\mathbf{n}} = \frac{1}{DN_0}\Big\{\frac{\beta_{\text{DP}}\zeta(1-\zeta)n_z^2}{\mathbf{n}_\zeta^2}\left[\mathbf{e}_z\times(\mathbf{j}^z)_\mathbf{n}\right]_i + 2\beta_{\text{DP}}\sum_{a=x,y}\left[n_z\,(j_a^a)_\mathbf{n} - n_a\,(j_a^z)_\mathbf{n}\right](\mathbf{e}_z\times\mathbf{n})_i + \frac{\tau}{\tau_s}\mathbf{n}_\zeta\cdot(\mathbf{j}_i)_\mathbf{n}\Big\}. \tag{4.38}$$

The first term on the r.h.s. of Eq. (4.38) results from a non-trivial interplay of these two 'origins', spin density versus spin current, since the first term on the r.h.s. of Eq. (4.36) is canceled to some extent by the first term on the r.h.s. of Eq. (4.37). This demonstrates once more that the interplay between the spin galvanic effect and the inverse spin Hall effect is non-trivial.

Discussion: effective forces

We remark the general validity of the above expressions, Eqs. (4.30) and (4.31), obtained by properly integrating the kinetic equation. Let us comment on the relation of

these equations to previous results before continuing with discussing the spin pumping configuration (Sec. 4.2). First, in the isotropic case ($\zeta = 1$) and with vanishing Rashba spin-orbit coupling, the resulting spin density

$$\delta\mathbf{s} = \frac{\hbar N_0}{2}[\mathbf{n} \times \dot{\mathbf{n}} - \beta_s \dot{\mathbf{n}}] \tag{4.39}$$

inserted into Eq. (4.30) leads to a force term which agrees with the result given in Ref. 71. Second, neglecting the spin current contribution to $\delta\mathbf{s}$ in Eq. (4.20), including the Rashba contribution, and again for $\zeta = 1$, Eq. (4.30) reduces to Eq. (11) in Ref. 156. Third, the first term on the r.h.s. of Eq. (4.31), arising due to Rashba spin-orbit coupling, describes the inverse spin Hall effect: a spin current in the xy plane and polarized in z direction generates an in-plane charge current which flows perpendicular to the spin current direction, $\sim \mathbf{j}^z \times \mathbf{e}_z$, cf. Ref. 24.

However, we remark that the various terms are not independent from each other. In particular, as already pointed out in Ref. 69, the interplay of Rashba coupling and Elliott-Yafet relaxation implies a close relation between spin density and spin current. This becomes apparent for time-independent and spatially homogeneous situations, where Eq. (4.17) reads

$$\frac{\Delta_{\text{xc}}}{\hbar}\mathbf{n} \times \delta\mathbf{s} - \frac{1}{\hbar}\boldsymbol{\mathcal{A}}_i \times \mathbf{j}_i = -\frac{1}{\tau_s}\Gamma\delta\mathbf{s}\,. \tag{4.40}$$

The total effective force in this situation, based on the latter equation, can be related to the one discussed in Ref. 66, see Eq. (12) therein. In addition, considering the limit $\Delta_{\text{xc}} \to 0$, leaves only the second term in Eq. (4.30) and the first term in Eq. (4.31), while the latter can be readily identified with the 'Hall-like' force in Ref. 66. However, our result appears to be larger by a factor of two since the contributions $\sim \boldsymbol{\mathcal{A}}$ and $\sim \Psi \cdot \boldsymbol{\mathcal{A}}_i$ to the Elliott-Yafet collision operator, Eq. (2.200), result in an additional, previously unknown term [28], the second term on the r.h.s. of Eq. (4.30). Further differences become apparent for finite Δ_{xc}.

Finally, let us focus on the second term on the r.h.s. of Eq. (4.31). Since it describes a force arising from a spin current which is polarized parallel to the magnetization (roughly speaking), we denote this term as 'inverse spin filter' force, its strength being $\sim \tau_s^{-1}$. To the best of our knowledge, such a term was first explicitly considered in Ref. 28 as a result from the new I_{EY}^{Ψ} contribution of the total Elliott-Yafet collision operator, see Eq. (2.200). However, in case of a non-zero ζ it can be related to the anomalous

Hall effect: imagine a spin current j_y^z created via the spin Hall effect by an electric field in x direction. This spin current in turn induces a charge current in y direction via the inverse spin filter term. In this context, see also the discussions in Refs. 162 and 142.

4.2. Spin pumping configuration

In this section, we consider a homogeneous magnetization which precesses with a cone angle θ and angular frequency ω about an axis fixed by an external static and homogeneous magnetic field.[2] We parametrize the magnetization as

$$\mathbf{n}(t) = R_\phi \begin{pmatrix} n_0 \\ \delta n_y(t) \\ \delta n_z(t) \end{pmatrix} = R_\phi \begin{pmatrix} \cos\theta \\ \sin\theta\cos\omega t \\ \sin\theta\sin\omega t \end{pmatrix} , \tag{4.41}$$

where R_ϕ is a rotation matrix around the z-axis,

$$R_\phi = \begin{pmatrix} \cos\phi & -\sin\phi & 0 \\ \sin\phi & \cos\phi & 0 \\ 0 & 0 & 1 \end{pmatrix} , \tag{4.42}$$

with ϕ describing the angle between the x axis and the cone axis, see Fig. 4.3.

In order to determine the electric field along these directions, we furthermore assume open circuit conditions in x and y direction. Note that we can expect the particle current to be homogeneous since the driving source, the magnetization, is also homogeneous. Thus, together with the open circuit condition, we consider $j_{x,y} = 0$ in the whole sample. From the drift-diffusion equation (4.28), we obtain

$$\sigma_{\text{D}} E_{x,y} = \frac{e\tau N_0 \Delta_{\text{XC}}}{m} F_{x,y} . \tag{4.43}$$

According to Ref. 69 the spin Hall conductivity in the limit $\tau_s \gg \tau_{\text{DP}}$ can be expressed as[3] $\sigma_0^{\text{sH}} = e\hbar\tau N_0/2m\tau_s$, hence we may rewrite Eq. (4.43) as

$$eE_{x,y} = \frac{\theta_{\text{sH}}}{\beta_s} F_{x,y} , \tag{4.44}$$

[2] Experimentally, the setup employed to excite the magnetization dynamics has to be carefully chosen, see the discussion in Ref. 49.

[3] The result given here can be obtained from Eq. (36) in Ref. 69 for $\tau_s \gg \tau_{\text{DP}}$, and by disregarding side-jump and skew scattering contributions. According to Ref. 69, the spin Hall conductivity is then given by $\sigma_0^{\text{sH}} = (\tau_{\text{DP}}/\tau_s)\sigma_{\text{int}}^{\text{sH}}$ with $\sigma_{\text{int}}^{\text{sH}} = e\tau/4\pi\tau_{\text{DP}}$.

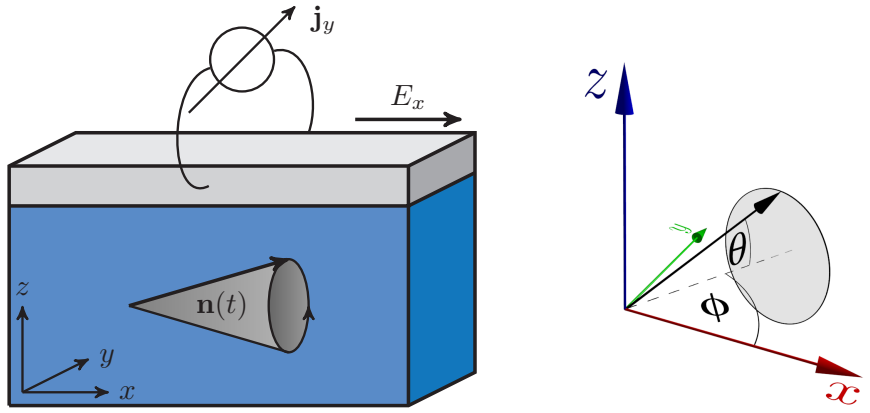

(a) (b)

FIG. 4.3.: (a) The setup under investigation, a metallic film on top of a magnetic material (shown in blue). (b) Sketch of the conical precession of the magnetization, defining the angles θ and ϕ.

where we have introduced the spin Hall angle $\theta_{\text{SH}} = 2e\sigma_0^{\text{SH}}/\sigma_{\text{D}}$, which is of the order of magnitude $\sim \hbar/\epsilon_{\text{F}}\tau_s$. Our aim is to study the DC contribution to the electric field, hence we average Eq. (4.44) with respect to time.

Before performing the time average, let us explicitly consider the x component of the effective force. It is given as the sum of the x component of Eqs. (4.35) and (4.38), as well as Eq. (4.31) with $\mathbf{j}_i \to (\mathbf{j}_i)_{\mathbf{s}}$, leading to

$$(F_x)_{\mathbf{s},\mathbf{n}} = -\frac{\hbar}{2l_{\text{DP}}}\left[\dot{n}_y + \beta_s\left(1+\zeta\right)\left(\mathbf{n}\times\dot{\mathbf{n}}\right)_y\right], \tag{4.45}$$

$$\begin{aligned}(F_x)_{\mathbf{s},\mathbf{j}_s} + (F_x)_{\mathbf{j}_s,\mathbf{n}} = &-\frac{\beta_{\text{DP}}}{DN_0}\left\{\zeta(1-\zeta)n_z^2\left(j_y^z\right)_{\mathbf{n}} + 2n_y\sum_{a=x,y}\left[n_z\left(j_a^a\right)_{\mathbf{n}} - n_a\left(j_a^z\right)_{\mathbf{n}}\right]\right\} \\ &+ \frac{1}{DN_0}\frac{\tau}{\tau_s}\mathbf{n}_\zeta\cdot\left(\mathbf{j}_x\right)_{\mathbf{n}},\end{aligned} \tag{4.46}$$

$$(F_x)_{\mathbf{j}_s,\mathbf{s}} = \frac{1}{DN_0}\left[\beta_{\text{DP}}\left(j_y^z\right)_{\mathbf{s}} + \frac{\tau}{\tau_s}\mathbf{n}_\zeta\cdot\left(\mathbf{j}_x\right)_{\mathbf{s}}\right]. \tag{4.47}$$

Note that the cone angle θ is usually small [48]. Thus, we have approximated $\mathbf{n}_\zeta^2 \simeq 1$ and $\mathbf{n}_\zeta\cdot\mathbf{n} \simeq 1$ in order to derive Eqs. (4.45) and (4.46). For the same reason, we also allow only terms up to $\sin^2\theta$ when performing the time average. Thus, the first term on the r.h.s. of Eq. (4.46), which has its origin in the interplay of the spin density and the

spin current, is negligible since the spin current $\left(j_y^z\right)_{\mathbf{n}}$ is at least proportional to $\dot{n}_z$, see Eq. (4.26), and thus the angular average of $n_z^2 \left(j_y^z\right)_{\mathbf{n}}$ is at least of order $\sim \sin^4\theta$.

Let us now rewrite Eqs. (4.45)–(4.47) in order to identify the different effects:

$$F_x^{(A)} = \frac{\beta_{\text{DP}}}{DN_0} \left(j_y^z\right)_{\mathbf{s}} , \tag{4.48}$$

$$\begin{aligned} F_x^{(B)} =& -\frac{\hbar}{2l_{\text{DP}}} \left[\dot{n}_y + \beta_s \left(1+\zeta\right) \left(\mathbf{n} \times \dot{\mathbf{n}}\right)_y \right] \\ & - \frac{2\beta_{\text{DP}}}{DN_0} n_y \sum_{a=x,y} \left[n_z \left(j_a^a\right)_{\mathbf{n}} - n_a \left(j_a^z\right)_{\mathbf{n}} \right] , \end{aligned} \tag{4.49}$$

$$F_x^{(C)} = \frac{1}{DN_0} \frac{\tau}{\tau_s} \mathbf{n}_\zeta \cdot \mathbf{j}_x \, . \tag{4.50}$$

Here, $F_x^{(A)}$ can be related to the inverse spin Hall effect since it originates in the first term on the r.h.s. of Eq. (4.31), and $F_x^{(B)}$ to the spin galvanic effect since it originates in Eq. (4.30). The last term, $F_x^{(C)}$, is the inverse spin filter force as discussed in the previous section, i.e., the build-up of an effective force due to the spin current polarized parallel to the magnetization, or more precisely, parallel to $\mathbf{n}_\zeta$.

Similarly, the y component can be decomposed as follows:

$$F_y^{(A)} = -\frac{\beta_{\text{DP}}}{DN_0} \left(j_x^z\right)_{\mathbf{s}} , \tag{4.51}$$

$$\begin{aligned} F_y^{(B)} =& \frac{\hbar}{2l_{\text{DP}}} \left[\dot{n}_x + \beta_s \left(1+\zeta\right) \left(\mathbf{n} \times \dot{\mathbf{n}}\right)_x \right] \\ & + \frac{2\beta_{\text{DP}}}{DN_0} n_x \sum_{a=x,y} \left[n_z \left(j_a^a\right)_{\mathbf{n}} - n_a \left(j_a^z\right)_{\mathbf{n}} \right] , \end{aligned} \tag{4.52}$$

$$F_y^{(C)} = \frac{1}{DN_0} \frac{\tau}{\tau_s} \mathbf{n}_\zeta \cdot \mathbf{j}_y \, . \tag{4.53}$$

In the following, we study the electric field in a narrow wire (see Fig. 4.4) that will be considered in a longitudinal and an orthogonal measurement setup. The wire is assumed to be 'narrow' in such a way that the width of the wire is smaller than the spin diffusion length l_s. Then, the spin current contribution polarized parallel to the magnetization and flowing orthogonal to the wire vanishes, see App. E.

Longitudinal measurement

Here, we consider a longitudinal measurement of the electrical field of a narrow wire as sketched in the left panel of Fig. 4.4. In this case, we find a homogeneous spin current flowing in x direction. In particular, the spin current has a contribution polarized along $\mathbf{n}$, giving rise to the inverse spin filter force according to Eq. (4.50). Performing the time average of Eqs. (4.48)–(4.50) and inserting the results into Eq. (4.44) yields the following DC electric fields:

$$\left\langle E_x^{(A)} \right\rangle_t \sim \beta_{\text{DP}} \theta_{\text{sH}} \frac{F_\alpha}{e} \ll \theta_{\text{sH}} \frac{F_\alpha}{e} \,, \tag{4.54}$$

$$\left\langle E_x^{(B)} \right\rangle_t = -\theta_{\text{sH}} \frac{F_\alpha}{e} (1+\zeta) \sin\phi \sin^2\theta \,, \tag{4.55}$$

$$\left\langle E_x^{(C)} \right\rangle_t = -\theta_{\text{sH}} \frac{F_\alpha}{2e} (1-\zeta) \sin\phi \sin^2\theta \,, \tag{4.56}$$

where $F_\alpha \equiv \hbar\omega / 2 l_{\text{DP}}$. The inverse spin Hall term (A) plays only a minor role for the total electric field $\langle E_x \rangle_t = \langle E_x^{(A)} + E_x^{(B)} + E_x^{(C)} \rangle_t$. We remark that in the two-dimensional limit, $\zeta \simeq 0$, the inverse spin filter contribution is of the same order of magnitude as the spin galvanic term, whereas it vanishes in the three-dimensional limit, $\zeta = 1$.

Orthogonal measurement

Next, we consider the case of an orthogonal measurement, see right panel of Fig. 4.4. In this case, the contribution given in Eq. (4.53) vanishes since the spin current $\mathbf{j}_y$ lacks a contribution parallel to the magnetization ($\ell_y \ll l_s$). The DC electric field along y direction is given by

$$\left\langle E_y^{(\text{A})} \right\rangle_t \sim \beta_{\text{DP}} \theta_{\text{sH}} \frac{F_\alpha}{e} \ll \theta_{\text{sH}} \frac{F_\alpha}{e} \,, \tag{4.57}$$

$$\left\langle E_y^{(\text{B})} \right\rangle_t = -\theta_{\text{sH}} \frac{F_\alpha}{e} (1+\zeta) \cos\phi \sin^2\theta \,, \tag{4.58}$$

$$\left\langle E_y^{(\text{C})} \right\rangle_t = 0 \,, \tag{4.59}$$

leaving only the spin galvanic term (B) to contribute to the total DC electric field.

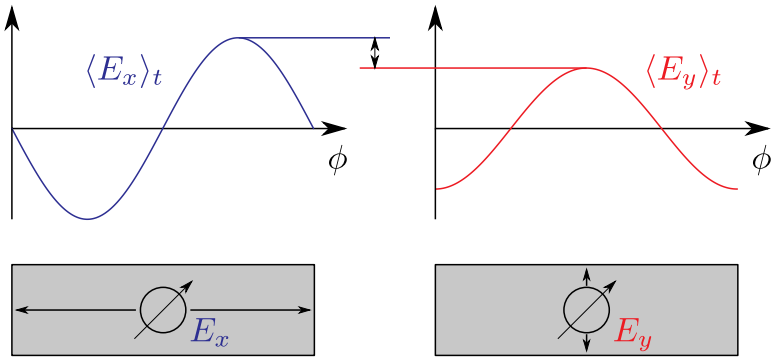

FIG. 4.4.: The top view of the setup is sketched in the bottom part of the figure. Here, the length is denoted as ℓ_x and the width as ℓ_y with $\ell_y \ll \ell_x$. The top part of figure shows a qualitative plot of the DC electric fields, $\langle eE_x \rangle_t$ and $\langle eE_y \rangle_t$, for a longitudinal (left) and an orthogonal (right) measurement, respectively. In both cases we set $\zeta = 0$.

Discussion

Comparing the results for the longitudinal and the orthogonal measurement, we realize that the signal can be up to 1.5 times larger in the longitudinal measurement in the limit $\zeta = 0$, see Fig. 4.4. Thus, for a two-dimensional electron gas one should be able to probe a Rashba-induced spin galvanic effect. Additionally, one can obtain estimates of α and ζ by comparing samples of different thicknesses.

Recent articles [44, 48, 49, 76] discussed spin pumping and the induced ISHE on the basis of a spin current $\mathbf{j}_z$ which flows perpendicular to the interface, i.e., in z direction into the normal-metal film. This situation differs significantly from the one discussed here and in Ref. 28 with this particular spin current being zero, $\mathbf{j}_z = 0$. Nevertheless, the electric field estimated in such a way [48] shows the same angular-dependence of the magnetization as our result:

$$\text{Ref. 48} \quad \Rightarrow \quad E_x \sim F_{g^{\uparrow\downarrow}} \sin\phi \sin^2\theta \,, \tag{4.60}$$

$$\text{Eq. (4.55)} \quad \Rightarrow \quad E_x \sim F_{\alpha} \sin\phi \sin^2\theta \,. \tag{4.61}$$

Comparing the relevant forces, $F_{g^{\uparrow\downarrow}} = e^2\omega g^{\uparrow\downarrow}/4\sigma_{\text{D}}$ and F_α, for reasonable parameter values, $g^{\uparrow\downarrow} \approx 2.1 \times 10^{19}\,\text{m}^{-2}$ and $\sigma_{\text{D}} \approx 2.4 \times 10^{6}\,\Omega^{-1}\,\text{m}^{-1}$ for a Pt film [48], we find the forces to be of the same order of magnitude for $\alpha \approx 0.3\,\text{eV Å}$. Therefore, as stated

in Ref. 28, it is important to take the spin galvanic contribution, as well as the inverse spin filter effect, into account when interpreting experiments where Rashba-induced spin currents and spin accumulations are likely to exist.

4.3. Conclusions

In this chapter, we have presented our findings [28] on the spin-charge coupled dynamics in a magnetized thin metallic film with Rashba spin-orbit coupling.

We have found significant modifications of the kinetic equations which describe spin and charge transport. These modifications are due to the very general form of the Elliott-Yafet collision operator, presented in Sec. 2.5, which results in anisotropic spin-flip processes. Analyzing the charge sector of the Boltzmann equation, we have derived a very general form of an effective force acting on the charge carriers due to a time-dependent magnetic texture. The various contributions to the effective force and their respective relation to the inverse spin Hall effect and the spin galvanic effect have been discussed in detail, as well as a new contribution, denoted as 'inverse spin filter' contribution.

In order to illustrate the significance of the various contributions, we have applied the general approach to the particular case of the typical spin pumping configuration for a narrow wire. It is found that for the generation of an in-plane electric field the spin galvanic effect is crucial, whereas the in-plane inverse spin Hall effect turns out to be negligible. However, the additional contribution from the inverse spin filter effect is found to be of similar magnitude for a longitudinal measurement, while it vanishes for an orthogonal measurement. This suggests the possibility of determining the strength of the spin galvanic effect and the spin-orbit coupling parameter—Rashba in our specific scenario—, as well as probing the anisotropy of the spin-flip relaxation, by performing both measurements on the same sample.

5

Spin Hall magnetoresistance and spin Nernst magnetothermopower

In this chapter, we present the results published in Ref. 78, where a Rashba two-dimensional electron gas in contact with a ferromagnetic insulator has been considered. Due to the sensitivity of the boundary conditions with respect to the magnetization direction it is possible to control spin currents entering the ferromagnet. As a consequence of the Rashba spin-orbit coupling a bulk inverse spin galvanic effect is present which in turn leads to a non-trivial and asymmetric angular-dependence of the spin Hall magnetoresistance and the spin Nernst magnetothermopower.

The system under consideration consists of a 2DEG in the xy plane with finite width ℓ_y in y direction, and an interface to an insulating ferromagnet at $y = 0$. An exemplary realization of the system is sketched in Fig. 5.1. As discussed in Sec. 3.3 one can control the spin current across the interface by varying the magnetization direction $\mathbf{n}$ of the ferromagnet due to the spin-transfer torque. By recalling Eq. (3.17) the boundary conditions read

$$\mathbf{j}_y(y=0) = \frac{g_r^{\uparrow\downarrow}}{2\pi\hbar N_0}\mathbf{n}\times\big(\mathbf{n}\times\mathbf{s}(y=0)\big)\,, \tag{5.1}$$

where in two dimensions $g_r^{\uparrow\downarrow}$ has the dimension of an inverse length. We neglect the imaginary part of the spin mixing conductance and its influence on the spin-transfer torque since it is estimated to be one to two orders of magnitude smaller compared to the real part for three-dimensional ferromagnet/metal interfaces [155, 163]. We are aware that the situation is less obvious in the case of a ferromagnet/2DEG interface. However, since results concerning the magnitude of the imaginary part of the spin mixing conductance are not available to the best of our knowledge, we have chosen to neglect the imaginary part of the spin mixing conductance and its influence on the spin-transfer torque.

In the literature [12, 77] the resulting spin Hall magnetoresistance due to the boundary

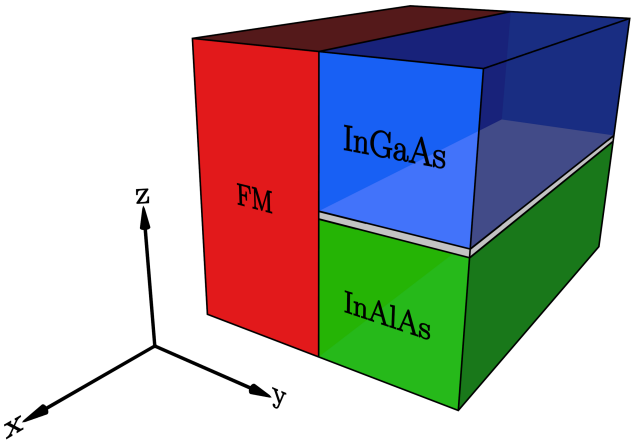

FIG. 5.1.: Schematic view of a 2DEG, here visualized in grey in a InAlAs/InGaAs heterostructure, in contact with a ferromagnetic insulator (FM). The InAlAs/InGaAs heterostructure is used as an example only: for an experimental realization the materials need to be chosen so as to minimize upward band bending at the interface with the FM, which could otherwise deplete the 2DEG in the FM contact region. Alternatively, single-crystalline Pt thin films [122] could be used instead of the semiconductor heterostructure.

condition (5.1) is estimated as follows: assuming a spin polarization $\mathbf{s} \sim \mathbf{e}_z$ generated by an electrical field $\mathbf{E} = E_x \mathbf{e}_x$, one obtains a spin current $\mathbf{j}_y \sim \mathbf{n} \times (\mathbf{n} \times \mathbf{e}_z)$, according to the boundary condition. This spin current in turn induces an additional electrical field $\mathbf{E} \sim \mathbf{e}_y \times \mathbf{j}_y$ with a magnetization dependence $E_x \sim 1 - n_z^2$ due to the inverse spin Hall effect. Thus, considering a magnetization within the yz plane, $\mathbf{n} = (0, \cos\phi, \sin\phi)$, the resulting spin Hall magnetoresistance signal as function of ϕ should be symmetric around $\phi = \pi/2$. The above argumentation is the standard explanation of the spin Hall magnetoresistance observed in thin heavy-metal films deposited on ferromagnetic insulators [50, 54, 55]. However, taking into account an additional in-plane spin polarization s^y due to the inverse spin galvanic effect, it is obvious from Eq. (5.1) that the resulting spin Hall magnetoresistance signal does not necessarily have this symmetry property.

In the following we consider the static case, i.e., $\partial_t f = 0$ in the Boltzmann equation (2.153). With an electric field $E_x \mathbf{e}_x$ and taking into account Rashba spin-orbit coupling,

the SU(2) Lorentz force, Eq. (2.157), is given by

$$\mathcal{F}_i = -eE_x\delta_{ix} - \frac{\alpha}{\hbar l_{\text{DP}}}\varepsilon_{ijz}p_j\sigma^z\,. \tag{5.2}$$

5.1. Linear response in the spin sector

Similarly to Chap. 4, we first consider the spin sector of the (static) Boltzmann equation, here with the aim to discuss the spin Hall effect and the inverse spin galvanic effect due to an electrical field applied along the x direction. The system is assumed to be homogeneous in x direction but inhomogeneous in y direction due to the presence of boundaries. For a magnetization $\mathbf{n} = (0, \cos\phi, \sin\phi)$ it is possible to restrict ourselves to the y and z components of the spin current since the boundary condition (5.1) for the x component of $\mathbf{s}$ and $\mathbf{j}_y$ is decoupled from the y and z components. As derived in detail in App. F.1 we obtain for the y and z components of $\mathbf{j}_y$ the following coupled differential equations:

$$\left(2 - l_s^2\nabla_y^2\right) j_y^y = \frac{l_s^2 + l_{\text{DP}}^2}{l_{\text{DP}}}\nabla_y j_y^z\,, \tag{5.3}$$

$$\left(1 + \frac{\tau_s}{\tau_{\text{DP}}} - l_{\text{DP}}^2\nabla_y^2\right) j_y^z = -\frac{l_s^2 + l_{\text{DP}}^2}{l_{\text{DP}}}\nabla_y j_y^y + \frac{\hbar\sigma_{\text{D}}}{2e\epsilon_{\text{F}}\tau_{\text{DP}}}E_x\,. \tag{5.4}$$

Once Eqs. (5.3) and (5.4) are solved it is straightforward to obtain the spin densities s^y and s^z given in terms of the spin currents:

$$s^y = -\tau_s\nabla_y j_y^y - \frac{\tau_s}{l_{\text{DP}}}j_y^z + \frac{\hbar\sigma_{\text{D}}}{4e\epsilon_{\text{F}}l_{\text{DP}}}E_x\,, \tag{5.5}$$

$$s^z = -\tau_{\text{DP}}\nabla_y j_y^z + \frac{\tau_{\text{DP}}}{l_{\text{DP}}}j_y^y\,. \tag{5.6}$$

Considering the homogeneous case Eqs. (5.3)–(5.6) are solved by

$$j_y^y = s^z = 0\,, \tag{5.7}$$

$$j_y^z = j_0^z = \frac{\hbar\sigma_{\text{D}}}{2e\epsilon_{\text{F}}(\tau_{\text{DP}} + \tau_s)}E_x\,, \tag{5.8}$$

$$s^y = s_0^y = -\frac{\tau_s - \tau_{\text{DP}}}{2l_{\text{DP}}}j_0^z\,. \tag{5.9}$$

The corresponding transport coefficients, the bulk spin Hall conductivity σ_0^{sH} and bulk polarization coefficient P_0^{E} are defined by $j_0^z = \sigma_0^{\text{sH}}E_x$ and $s_0^y = P_0^{\text{E}}E_x$, respectively.

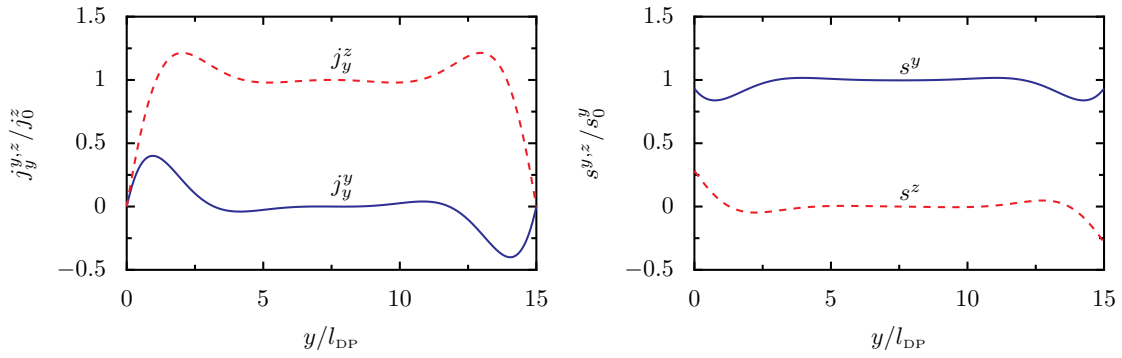

(a) (b)

FIG. 5.2.: Spatial profile of the spin currents, (a), and the spin polarizations, (b), for symmetric boundary conditions ($g_r^{\uparrow\downarrow} = 0$); $\ell_y/l_{\mathrm{DP}} = 15$, $\tau_s/\tau_{\mathrm{DP}} = 10$.

From Eqs. (5.8) and (5.9) we see that the spin Hall effect vanishes in the limit $\tau_s \to \infty$, while the inverse spin galvanic effect is absent in the case $\tau_s = \tau_{\mathrm{DP}}$. Note that the latter is no longer the case when side-jump or skew scattering are included [99].

Next, we discuss the influence of the boundary conditions. First, the spatial profile of the spin polarization and the spin currents will be investigated, and second we determine the spatial averages of the resulting spin Hall conductivity and the polarization coefficient as function of the magnetization direction.

Spatial profile

The coupled differential equations (5.3)–(5.6) can be solved under given appropriate boundary conditions both analytically, see App. F.1, and numerically. First, we consider a symmetric setup with $\mathbf{j}_y(0) = \mathbf{j}_y(\ell_y) = 0$, which corresponds to an isolated stripe of width ℓ_y. The vanishing of the normal component of the spin current can be justified from the Boltzmann equation when assuming spin-conserving scattering, see Ref. 164. Second, we consider asymmetric boundary conditions, with $\mathbf{j}_y(\ell_y) = 0$ and $\mathbf{j}_y(0)$ given in Eq. (5.1), which corresponds to the setup with a ferromagnetic insulator attached to the "left" side ($y = 0$) of the stripe. Apparently, by setting $g_r^{\uparrow\downarrow} = 0$ the symmetric boundary conditions are recovered.

The spatial profile of the spin currents and the spin polarizations for symmetric

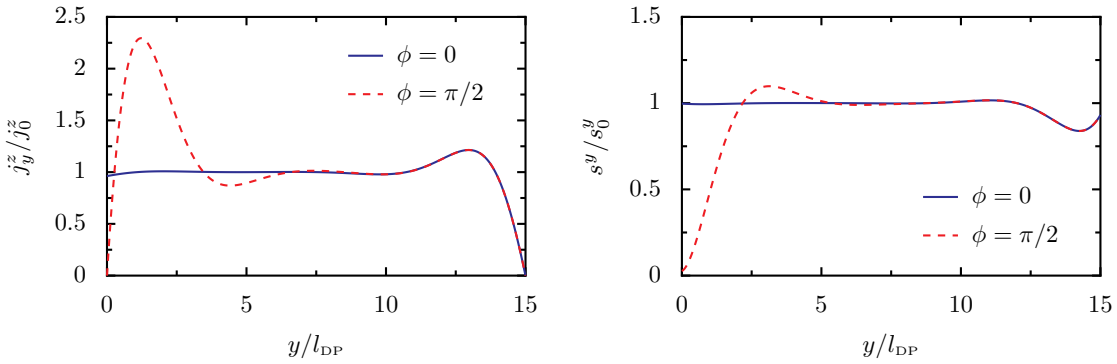

(a) (b)

FIG. 5.3.: Spatial profile of the spin current j_y^z, (a), and the spin polarization s^y, (b), for asymmetric boundary conditions with $g_r^{\uparrow\downarrow}\alpha\tau_{\mathrm{DP}}/\hbar = 10$ and $\phi = 0, \pi/2$. The parameters ℓ_y/l_{DP} and $\tau_s/\tau_{\mathrm{DP}}$ are the same as in Fig. 5.2.

boundary conditions is shown in Fig. 5.2. As seen from panel (a) the spin currents exhibit the symmetry $j_y^y(y) = -j_y^y(\ell_y - y)$ and $j_y^z(y) = j_y^z(\ell_y - y)$, which is consistent with Eqs. (5.3) and (5.4). Analogously, panel (b) shows $s^y(y) = s^y(\ell_y - y)$ and $s^z(y) = -s^z(\ell_y - y)$ according to Eqs. (5.5) and (5.6). Note that the influence of the boundaries is restricted to a range of $\sim 3\, l_{\mathrm{DP}}$. Therefore, assuming larger system sizes it is justified to solve the diffusion equations for a semi-infinite system, see App. F.2. In this case, we obtain

$$j_y^y = \frac{j_0^z}{2 + l_s^2|q|^2} \frac{l_{\mathrm{DP}}|q|^2}{q_+} \left(1 + \frac{\tau_s}{\tau_{\mathrm{DP}}}\right) \exp\left(-q_- y\right) \sin(q_+ y)\,, \tag{5.10}$$

$$j_y^z = j_0^z - j_0^z \exp\left(-q_- y\right) \left[\cos(q_+ y) + \frac{q_-}{q_+} \frac{2 - l_s^2|q|^2}{2 + l_s^2|q|^2} \sin(q_+ y)\right], \tag{5.11}$$

where

$$q_\pm = \frac{1}{2l_{\mathrm{DP}}} \sqrt{\sqrt{8 + 8\frac{\tau_{\mathrm{DP}}}{\tau_s}} \pm \left(1 - \frac{\tau_{\mathrm{DP}}}{\tau_s}\right)} \tag{5.12}$$

and $|q|^2 = q_+^2 + q_-^2$. The symmetrized analytical result deviates by less than 10^{-5} from the numerical data shown in Fig. 5.2, and even for $\ell_y \approx 5 l_{\mathrm{DP}}$ analytical and numerical results are still in fair agreement.

In the case of the asymmetric setup with the boundary condition to the ferromagnet given by Eq. (5.1), we assume that the magnetization direction $\mathbf{n}$ lies within the yz plane

and is parametrized by $\mathbf{n} = (0, \cos\phi, \sin\phi)$. The spatial profile of the spin current j_y^z and the spin polarization s^y for two orientations of the ferromagnetic polarization, $\phi = 0$ and $\phi = \pi/2$, is depicted in Fig. 5.3. A remarkable feature is the hump of j_y^z close to the left boundary for $\phi = \pi/2$. Due to this hump the spin current averaged over the whole system can be enhanced compared to the average spin current in the $\phi = 0$ case, even though the spin current vanishes at the interface. The implications of this observation will be discussed in the following.

Spatial averages

Here, we examine the spatial averages of the spin polarization s^y and the spin current j_y^z, from which we define an averaged spin Hall conductivity and polarization coefficient, respectively. In particular, we focus on their dependence on the polarization angle ϕ of the attached ferromagnet. For a stripe of width ℓ_y, the spatial averages of s^y and j_y^z, and the corresponding averaged transport coefficients P_{sE} and σ_{sE}, are defined as

$$\langle s^y \rangle_y = \frac{1}{\ell_y} \int_0^{\ell_y} \mathrm{d}y \, s^y = P_{\text{sE}} E_x \tag{5.13}$$

$$\langle j_y^z \rangle_y = \frac{1}{\ell_y} \int_0^{\ell_y} \mathrm{d}y \, j_y^z = \sigma_{\text{sE}} E_x \, . \tag{5.14}$$

The subscript "sE" indicates the linear response of the spin (current or polarization) to an applied electrical field. Similarly, in Sec. 5.2, the linear spin response to a temperature gradient will be labeled by "sT".

The averaged spin Hall conductivity and the averaged polarization coefficient normalized to their respective bulk values versus the magnetization angle ϕ for $\ell_y/l_{\text{DP}} = 10$ and various values of the spin mixing conductance $g_r^{\uparrow\downarrow}$ are shown in Fig. 5.4. The averaged spin Hall conductivity, panel (a), increases with increasing $g_r^{\uparrow\downarrow}$ for nearly all angles ϕ, peaked in the range $\pi/2 \lesssim \phi \lesssim 3\pi/4$, whereas the averaged polarization coefficient, panel (b), is enhanced or reduced, depending on ϕ.

Let us compare the numerical results shown in Fig. 5.4 with the analytical result in the limit $\ell_y \gg l_{\text{DP}}$. The "ferromagnetic" contribution of the spin current, defined as

$$\Delta j_y^z = j_y^z - j_y^z(g_r^{\uparrow\downarrow} = 0) \, , \tag{5.15}$$

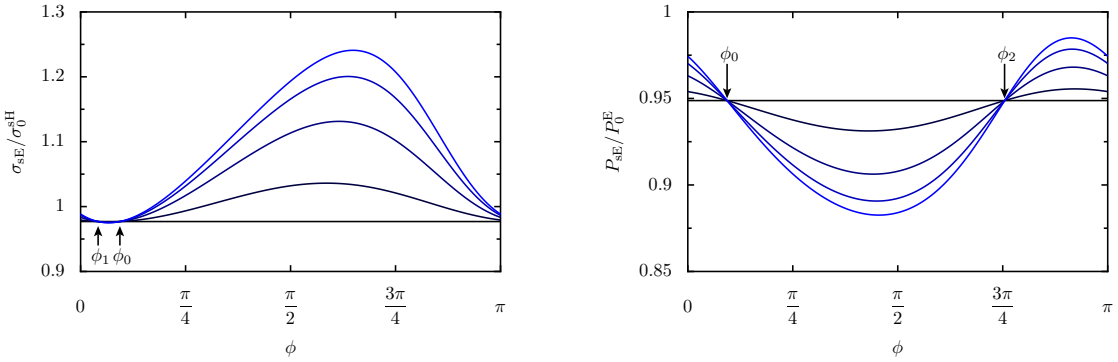

(a) (b)

FIG. 5.4.: Averaged spin Hall conductivity, (a), and polarization coefficient, (b), versus ϕ, normalized by their respective bulk values, for $\tau_s/\tau_{DP} = 10$, $\ell_y/l_{DP} = 10$, and $g_r^{\uparrow\downarrow}\alpha\tau_{DP}/\hbar = 0, 0.2, 0.5, 2, 100$ from black to blue.

see Eq. (F.27) in App. F.2, yields the ferromagnetic contribution to the spin Hall conductivity by performing the spatial average,

$$\frac{\Delta\sigma_{sE}}{\sigma_0^{sH}} = \frac{2\,(1+\tau_s/\tau_{DP})\,j_y^y(0) + 4l_{DP}q_- j_y^z(0)}{\ell_y l_{DP}|q|^2\,(2+l_s^2|q|^2)\,j_0^z}\,. \tag{5.16}$$

The boundary values of the spin current, $j_y^y(0)$ and $j_y^z(0)$, that can be controlled by the magnetization angle ϕ fully determine $\Delta\sigma_{sE}$. From Eq. (5.1) we see that for $\phi = 0$ the spin current $j_y^y(0)$ vanishes and $j_y^z(0) \sim s^z(0)$, while for $\phi = \pi/2$ the spin current $j_y^z(0)$ vanishes and $j_y^y(0) \sim s^y(0)$. This explains why in the limit $\tau_s/\tau_{DP} \gg 1$ the averaged spin Hall conductivity σ_{sE} is enhanced for $\phi \approx \pi/2$ compared to $\phi \approx 0$ as observed in Fig. 5.4 (a) due to the presence of a nonvanishing in-plane spin polarization s^y, i.e., the inverse spin galvanic effect.

Remarkably, one finds a magnetization angle $\phi_0 \approx 0.294$ where σ_{sE} and P_{sE} are both independent of $g_r^{\uparrow\downarrow}$. The reason for this is that the spin polarization at the interface, $\mathbf{s}(g_r^{\uparrow\downarrow} = 0, y = 0)$, is proportional to the magnetization direction $\mathbf{n}$ at ϕ_0, and thus the spin current $\mathbf{j}_y(0)$ vanishes according to Eq. (5.1), independently of $g_r^{\uparrow\downarrow}$. In the limit $\ell_y \gg l_{DP}$, the analytical result derived in App. F.2 is given by

$$\tan\phi_0 = \frac{4\tau_{DP}l_{DP}q_-}{\tau_s + \tau_{DP}(1 - l_{DP}^2|q|^2)}\,, \tag{5.17}$$

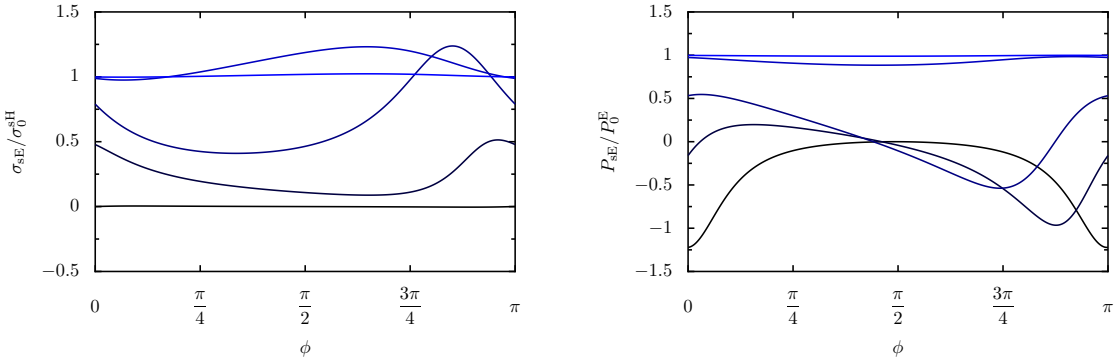

(a) (b)

FIG. 5.5.: Averaged spin Hall conductivity, (a), and polarization coefficient, (b), versus ϕ, normalized by their respective bulk values, for $\tau_s/\tau_{DP} = 10$, $g_r^{\uparrow\downarrow}\alpha\tau_{DP}/\hbar = 10$, and $\ell_y/l_{DP} = 0.01, 0.5, 1, 10, 100$ from black to blue.

which yields $\phi_0 \approx 0.2934$, very close to the numerical result for $\ell_y = 10 l_{DP}$. Furthermore, there are two more magnetization angles, $\phi_1 \approx 0.131$ and $\phi_2 \approx 2.37$, where σ_{sE} and P_{sE} are also independent of $g_r^{\uparrow\downarrow}$, respectively, as indicated by the arrows in Fig. 5.4. According to Eq. (5.16), $\Delta\sigma_{sE}$ vanishes if the condition

$$\frac{j_y^y(0)}{j_y^z(0)} = -\frac{2\tau_{DP} l_{DP} q_-}{\tau_{DP} + \tau_s} \tag{5.18}$$

is fulfilled. On the other hand, from the boundary condition (5.1) we know $\mathbf{j}_y(0) \sim (0, -\sin\phi, \cos\phi)$ which leads to

$$\tan\phi_1 = \frac{2\tau_{DP} l_{DP} q_-}{\tau_{DP} + \tau_s}\,. \tag{5.19}$$

A similar kind of reasoning for the $g_r^{\uparrow\downarrow}$-dependent part of P_{sE} yields

$$\tan\phi_2 = -\frac{2q_-}{l_{DP}|q|^2}\,. \tag{5.20}$$

Even though Eqs. (5.19) and (5.20) are strictly valid only in the limit $\ell_y \gg l_{DP}$, for a system of size $\ell_y = 10\, l_{DP}$ the values for ϕ_1 and ϕ_2 obtained from Eqs. (5.19) and (5.20) are very close to the numerical results.

Figure 5.5 shows the averaged spin Hall conductivity, panel (a), and polarization coefficient, panel (b), for fixed spin mixing conductance $g_r^{\uparrow\downarrow}\alpha\tau_{DP}/\hbar = 10$ and several

values of ℓ_y. Clearly, for very narrow systems, σ_{sE} goes to zero due to the vanishing spin current at $y = \ell_y$. On the other hand, for very wide systems the influence of the boundary conditions becomes negligible and thus σ_{sE} approaches the bulk value σ_0^{sH}. In between, the averaged spin Hall conductivity depends non-trivially on the magnetization angle ϕ. Similarly, the averaged polarization coefficient P_{sE} also approaches its bulk value for $\ell_y \gg l_{\text{DP}}$. However, in contrast to σ_{sE}, it does not vanish for very narrow systems. By assuming that spin densities and spin currents depend only linearly on y, which is justified for $\ell_y \ll l_{\text{DP}}$, we find that P_{sE} approaches

$$\frac{P_{\text{sE}}}{P_0^{\text{E}}} = -\frac{\tau_{\text{DP}}(\tau_{\text{DP}} + \tau_s)}{(\tau_s - \tau_{\text{DP}})(\tau_{\text{DP}} + \tau_s \tan^2\phi)}\,, \tag{5.21}$$

which is symmetric around $\phi = \pi/2$.

5.2. Linear response in the charge sector

Spin signatures (polarization and currents) are notoriously difficult to detect directly in experiment. Thus, we shall now consider the signals in the charge current associated with the spin polarization and spin currents in response to an applied electrical field as discussed in the previous section. In addition, we extend our analysis by including also thermal effects, i.e., contributions due to a temperature gradient. In particular, our discussion focuses on the spin Hall magnetoresistance and the spin Nernst magnetothermopower, namely the fingerprint of the magnetization dependent spin Hall and spin Nernst effect [17] in the conductivity and the thermopower, respectively.

The thermal gradient $\nabla_x T$ is taken into account in terms of the x spatial derivative of the local charge distribution function,

$$\nabla_x f^0 \approx \left(-\frac{\partial f^0_{\text{eq}}}{\partial \epsilon_{\mathbf{p}}}\right) \frac{\epsilon_{\mathbf{p}} - \epsilon_{\text{F}}}{T} \nabla_x T\,. \tag{5.22}$$

Then, similar to Sec. 4.1, the momentum integrated charge sector of the Boltzmann equation yields the following expression for the width-averaged charge current in linear response to an electrical field E_x and a thermal gradient $\nabla_x T$:

$$\langle j_x \rangle_y = \sigma_{\text{D}} E_x - \sigma_{\text{D}} S_0 \nabla_x T - 2e\frac{\alpha}{\hbar}\frac{\tau}{l_{\text{DP}}}\left(\langle j_y^z \rangle_y - \frac{l_{\text{DP}}}{\tau_s}\langle s^y \rangle_y\right)\,, \tag{5.23}$$

where $S_0 = -\pi^2 k_B^2 T/(3e\epsilon_{\text{F}})$ is the Seebeck coefficient of the free electron gas. The corresponding expressions for the spin current and the spin polarization, see App. F.3, are given by

$$\langle j_y^z \rangle_y = \sigma_{\text{sE}} E_x + \sigma_{\text{sT}} \nabla_x T \,, \tag{5.24}$$

$$\langle s^y \rangle_y = P_{\text{sE}} E_x + P_{\text{sT}} \nabla_x T \,, \tag{5.25}$$

respectively, where the direct spin Nernst and the direct thermal polarization coefficients read [17]

$$\sigma_{\text{sT}} = -S_0 \epsilon_{\text{F}} \sigma'_{\text{sE}}(\epsilon_{\text{F}}) \,, \tag{5.26}$$

$$P_{\text{sT}} = -S_0 \epsilon_{\text{F}} P'_{\text{sE}}(\epsilon_{\text{F}}) \,. \tag{5.27}$$

Apparently, the only ingredients necessary to fully determine the thermoelectric linear response in the charge sector are the coefficients σ_{sE} and P_{sE}, which have already been investigated in detail in the previous section.

Spin Hall magnetoresistance

In order to describe the spin Hall magnetoresistance we assume a vanishing temperature gradient, $\nabla_x T = 0$. The corresponding resistivity, ρ, is defined by

$$E_x = \rho \langle j_x \rangle_y \,. \tag{5.28}$$

In analogy to Eq. (5.15) we define the ferromagnetic contribution by

$$\Delta\rho = \rho - \rho(g_r^{\uparrow\downarrow} = 0) \tag{5.29}$$

in order to focus on the angular dependence. Employing Eq. (5.23) and assuming $\Delta\rho \ll \rho(g_r^{\uparrow\downarrow} = 0)$, we obtain

$$\Delta\rho = -\Delta\sigma \rho^2 (g_r^{\uparrow\downarrow} = 0) \,, \tag{5.30}$$

where

$$\Delta\sigma = -2e \frac{\alpha}{\hbar} \frac{\tau}{l_{\text{DP}}} \left(\Delta\sigma_{\text{sE}} - \frac{l_{\text{DP}}}{\tau_s} \Delta P_{\text{sE}} \right) \tag{5.31}$$

is the ferromagnetic contribution to the conductivity. Analogously, $\Delta\sigma_{\text{sE}}$ and ΔP_{sE} are the ferromagnetic contributions to the spin Hall conductivity and the polarization coefficient, respectively. At this point we remark that one should be aware of the fact

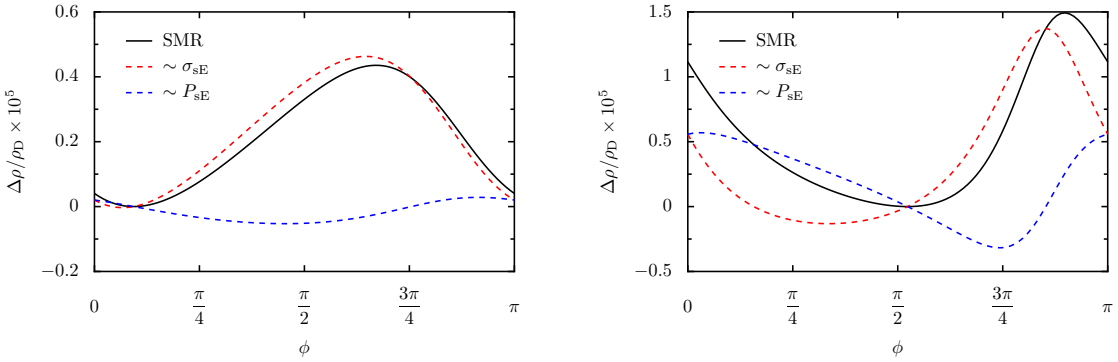

(a) (b)

FIG. 5.6.: Ferromagnetic contribution to the spin Hall magnetoresistance (SMR) as function of ϕ with $\tau_s/\tau_{DP} = 10$, $\alpha\tau/\hbar l_{DP} = 0.01$, and $g_r^{\uparrow\downarrow}\alpha\tau_{DP}/\hbar = 10$ for $\ell_y = 10\, l_{DP}$, (a), and $\ell_y = l_{DP}$, (b). The dashed curves represent the contributions proportional to σ_{sE} (red) and P_{sE} (blue), respectively. All data are normalized by $\rho_D = 1/\sigma_D$.

that both, $\Delta\sigma_{sE}$ and ΔP_{sE}, contribute linearly to $\Delta\rho$. Therefore, the notion "spin Hall" magnetoresistance might be misleading in a Rashba system as the one we consider. Nevertheless, it is extremely difficult to distinguish between the spin Hall and the inverse spin galvanic contributions in an experiment and thus we shall further use this terminology.

The ferromagnetic contribution to the resistivity $\Delta\rho$ versus the magnetization angle ϕ is depicted in Fig. 5.6. Panel (a) corresponds to a wide system and we see that the spin Hall magnetoresistance is dominated by the spin Hall (σ_{sE}) contribution. On the other hand, in case of a narrow system, (b), both contributions appear equally important. Remarkably, at the universal crossing point ϕ_0, that has already been discussed in the previous section, $\Delta\rho$ has a local minimum since the contributions $\sim \Delta\sigma_{sE}$ and $\sim \Delta P_{sE}$ cancel up to linear order. In the limit $\ell_y \gg l_{DP}$ it is easily possible to verify this cancellation analytically. Note that by employing Eq. (5.17) the ratio τ_s/τ_{DP} can be calculated once ϕ_0 is known. Thus, it is in principle possible to extract this ratio experimentally by measuring ϕ_0.

Finally, let us discuss the special case $\tau_s/\tau_{DP} = 1$ where the bulk inverse spin galvanic effect is absent, see Eq. (5.9). In the limit $\ell_y \gg l_{DP}$, the spin Hall magnetoresistance

simplifies to

$$\frac{\Delta\rho}{\rho_{\mathrm{D}}} = \theta_{\mathrm{sH}}^2 \cos^2\phi\,, \tag{5.32}$$

where $\rho_{\mathrm{D}} = 1/\sigma_{\mathrm{D}}$, and $\theta_{\mathrm{sH}} = 2e\sigma_0^{\mathrm{sH}}/\sigma_{\mathrm{D}}$ is the spin Hall angle. Equation (5.32) agrees with the result given in Ref. 77, which has been derived based on phenomenological spin diffusion equations in three dimensions. However, for $\tau_s \neq \tau_{\mathrm{DP}}$ the angular dependence is more complex as discussed above, cf. Fig. 5.6.

Spin Nernst magnetothermopower

In the following, we consider a finite thermal gradient in x direction and study the spin Nernst magnetothermopower under an open circuit condition, i.e., $\langle j_x\rangle_y = 0$. The thermopower S is defined by

$$E_x = S\nabla_x T\,. \tag{5.33}$$

Using Eqs. (5.23)–(5.25) we obtain

$$S = \rho\sigma_{\mathrm{D}}\left[1 + 2\frac{\alpha\tau}{\hbar l_{\mathrm{DP}}}\frac{e}{S_0\sigma_{\mathrm{D}}}\left(\sigma_{\mathrm{sT}} - \frac{l_{\mathrm{DP}}}{\tau_s}P_{\mathrm{sT}}\right)\right]S_0\,, \tag{5.34}$$

where

$$\rho = \frac{1}{\sigma_{\mathrm{D}}}\left[1 - 2\frac{\alpha\tau}{\hbar l_{\mathrm{DP}}}\frac{e}{\sigma_{\mathrm{D}}}\left(\sigma_{\mathrm{sE}} - \frac{l_{\mathrm{DP}}}{\tau_s}P_{\mathrm{sE}}\right)\right]^{-1} \tag{5.35}$$

is the resistivity corresponding to the spin Hall magnetoresistance as discussed in the previous subsection. In analogy to Eq. (5.15), we define the ferromagnetic contribution to the thermopower by

$$\Delta S = S - S(g_r^{\uparrow\downarrow} = 0)\,. \tag{5.36}$$

Keeping only terms linear in σ_{sE} and P_{sE}, respectively, it is possible and convenient to split ΔS into two parts, an electrical part, associated with σ_{sE} and P_{sE}, and a thermal part, associated with σ_{sT} and P_{sT}. We obtain

$$\Delta S = \Delta S_{\mathrm{sE}} + \Delta S_{\mathrm{sT}} \tag{5.37}$$

with the electrical and thermal parts given by

$$\Delta S_{\mathrm{sE}} = \Delta\rho\sigma_{\mathrm{D}} S_0\,, \tag{5.38}$$

$$\Delta S_{\mathrm{sT}} = 2e\frac{\alpha}{\hbar}\frac{\tau}{l_{\mathrm{DP}}}\left(\Delta\sigma_{\mathrm{sT}} - \frac{l_{\mathrm{DP}}}{\tau_s}\Delta P_{\mathrm{sT}}\right)\rho(g_r^{\uparrow\downarrow} = 0)\,, \tag{5.39}$$

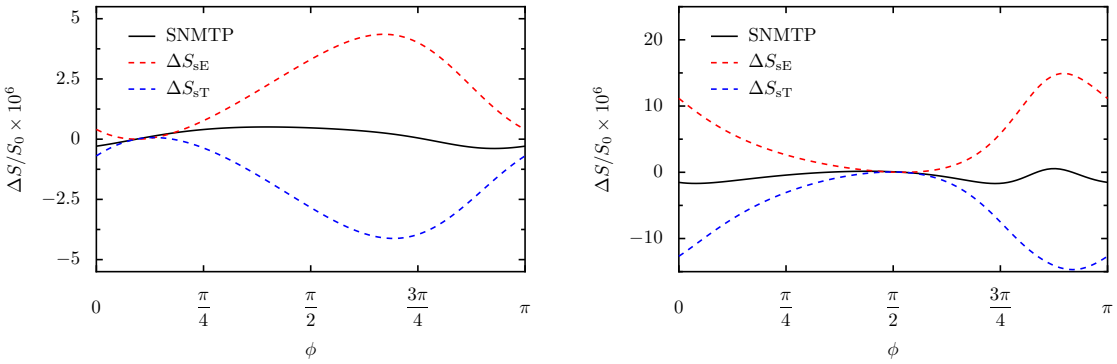

FIG. 5.7.: Ferromagnetic contribution to the spin Nernst magnetothermopower (SNMTP) as function of ϕ with $\tau_s/\tau_{DP} = 10$, $\alpha\tau/\hbar l_{DP} = 0.01$, and $g_r^{\uparrow\downarrow}\alpha\tau_{DP}/\hbar = 10$ for $\ell_y = 10\, l_{DP}$, (a), and $\ell_y = l_{DP}$, (b). The dashed curves represent the electrical part (red) and the thermal part (blue), respectively.

where $\Delta\sigma_{sT}$ and ΔP_{sT} are the corresponding ferromagnetic contributions to the direct spin Nernst conductivity and the direct thermal polarization coefficient, respectively.

Figure 5.7 shows the spin Nernst magnetothermopower with its respective electrical and thermal parts as function of the magnetization angle ϕ. Interestingly, since the electrical and thermal contributions nearly cancel each other, the resulting spin Nernst fingerprint in the thermopower is rather small for both a wide, (a), and a narrow, (b), system. For the parameters considered in Fig. 5.7 we find that $\Delta S/S_0$ is of the order of 10^{-6}. In addition, in the limit of infinitely large spin mixing conductance $g_r^{\uparrow\downarrow} \to \infty$, and for $\tau_{DP}/\tau_s \to 0$, one can show that this cancellation is exact, and thus the spin Nernst magnetothermopower is completely absent in this limit.

5.3. Conclusions

In this chapter, we have presented the results published in Ref. 78, where the spin and charge transport properties of a two-dimensional electron gas with Rashba spin-orbit coupling and Elliott-Yafet spin relaxation have been discussed with focus on the spin Hall magnetoresistance and the spin Nernst magnetothermopower.

From the generalized Boltzmann equation we have derived a set of coupled spin diffu-

sion equations and solved them for boundary conditions that correspond to the presence of a ferromagnetic insulator attached to one side of the two-dimensional electron gas. It was shown that the two main effects which are associated with spin-orbit coupling, the spin Hall effect and the inverse spin galvanic effect, are significantly affected by the magnetization direction of the ferromagnet due to the spin-transfer torque across the interface. Interestingly, for a particular polarization direction both effects turn out to be independent of the spin mixing conductance, which leads to a local minimum in the spin Hall magnetoresistance signature. The spin Nernst magnetothermopower turns out to be extremely small compared to the bulk thermopower since electrical and thermal contributions partly cancel each other and in the limit of infinite spin mixing conductance it even vanishes completely if Elliott-Yafet spin relaxation is neglected.

Finally, we want to point out that it is hardly possible to quantitatively compare our results with experiments on heavy-metal/magnetic-insulator bilayers, e.g., Pt/YIG, due to the lack of an accepted microscopic model of the spin-orbit coupling in heavy metals and due to the different geometry in these experiments. Thus, as suggested in Ref. 78, it would be interesting to measure the spin Hall magnetoresistance and the spin Nernst magnetothermopower in a pure Rashba systems as realized in semiconductor heterostructures.

6

Magnetoresistance in 3D Rashba metals

This chapter is devoted to the investigation of the magnetoresistance in a three-dimensional Rashba metal placed on top of a ferromagnet [85]. The system under consideration is schematically depicted in Fig. 6.1, with the interface between the Rashba metal and the ferromagnet at $z = 0$ and d the thickness of the Rashba metal. In Chap. 5 we have studied the magnetoresistance in a two-dimensional Rashba system, where one side is in contact with a ferromagnet [78]. Here, we extend the Rashba system to a third spatial dimension; the setup, the spin-orbit system residing on top of a ferromagnet, corresponds to the typical setup in experiments on heavy-metal/ferromagnet bilayers. In this context, "ferromagnet" is used as a generic term for ferromagnetic insulators, e.g., YIG [50, 52, 53, 165–167], $CoFe_2O_4$ [168], or Fe_3O_4 [165, 169], ferromagnetic metals such as Co [170] or CoFeB [171, 172], and even antiferromagnetic materials like $SrMnO_3$ [173] or FeMn [174]. In the following, we focus on ferromagnetic insulators that the only function of the ferromagnet is to manipulate the spin transport in the Rashba metal, and not providing an additional contribution to the magnetoresistance as it is the case for ferromagnetic metals. Analogously to Chap. 5, the boundary condition at the interface ($z = 0$) is then determined by the spin-transfer torque, Eq. (3.17),

$$\mathbf{j}_z(z=0) = \frac{1}{2\pi\hbar N_0}\left[g_r^{\uparrow\downarrow}\mathbf{n}\times\big(\mathbf{n}\times\mathbf{s}(z=0)\big) + g_i^{\uparrow\downarrow}\mathbf{n}\times\mathbf{s}(z=0)\right]. \tag{6.1}$$

Here, as another extension compared to Chap. 5, we also consider the imaginary part of the spin mixing conductance $g_i^{\uparrow\downarrow}$. In addition, in a 3D Rashba metal, which is discussed next, the density of states per spin and volume at the Fermi energy is given by $N_0 = m_\parallel\sqrt{2m_\perp\epsilon_\mathrm{F}}/2\pi^2\hbar^3$.

As mentioned in Chap. 3, the recently discovered bulk Rashba metals [79–84] exhibit a Rashba spin-orbit coupling due to their noncentrosymmetric crystal structure. We account for the resulting inversion symmetry breaking along $\mathbf{e}_z$ direction by different

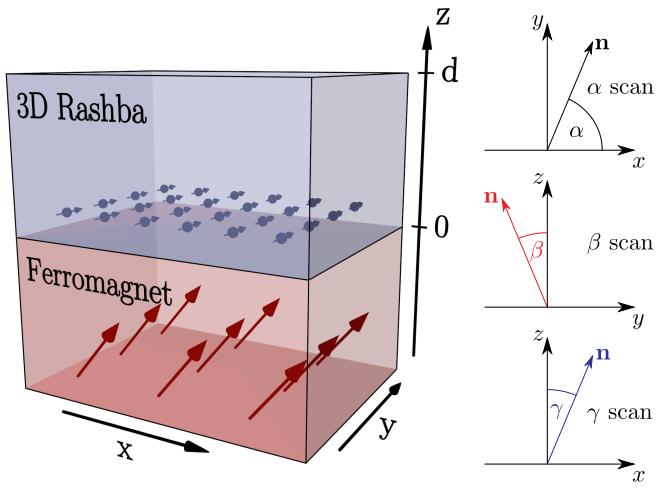

FIG. 6.1.: Left: Schematic picture of the setup with a three-dimensional Rashba system (3D Rashba) placed on top of a ferromagnet. Right: Definition of the angles α, β, and γ which describe the rotation of the magnetization direction in the xy, yz, and xz planes, respectively.

in-plane and out-of-plane effective masses, $m_\parallel$ and $m_\perp$. Accordingly, we describe the Rashba system by the model Hamiltonian

$$\hat{H} = \frac{\hat{p}_x^2 + \hat{p}_y^2}{2m_\parallel} + \frac{\hat{p}_z^2}{2m_\perp} - \frac{\alpha_\mathrm{R}}{\hbar}\left(\hat{\mathbf{p}} \times \boldsymbol{\sigma}\right) \cdot \mathbf{e}_z + \hat{H}_\mathrm{imp}\,. \tag{6.2}$$

In this chapter, we denote the Rashba parameter by α_R since we want to avoid confusion with the angle α defined in Fig. 6.1. Note that our model is not restricted to Rashba metals with a noncentrosymmetric crystal structure. It can also be used to describe Rashba spin-orbit coupling occuring in thin Pt films [122] and to some extend for metallic thin film bilayers on top of a ferromagnet, such as a Bi/Ag bilayer on top of CoFeB [175, 176] or Cu with Pt nanoislands on top of YIG [177]. In addition, we take side-jump and skew scattering, see Sec. 3.1, into account since the precise value of the effective spin-orbit coupling constant λ in metals is unknown, to the best of our knowledge, and could be large enough such that side-jump and skew scattering cannot be neglected [127].

Due to the mass anisotropy, the definition of some quantities in this chapter differs from the notation used in Chaps. 4 and 5. The charge and spin current in $i = x, y, z$

direction are now defined by

$$j_i = -2e \int \frac{\mathrm{d}^3 p}{(2\pi\hbar)^3}\, v_i f^0 \,, \tag{6.3}$$

$$\mathbf{j}_i = \int \frac{\mathrm{d}^3 p}{(2\pi\hbar)^3}\, v_i \mathbf{f} \,, \tag{6.4}$$

where v_i is the i-th component of the velocity $\mathbf{v} = (p_x/m_\parallel, p_y/m_\parallel, p_z/m_\perp)$. The same anisotropy in the velocity comes into play in the generalized Boltzmann equation which in the static case is given by

$$\frac{\mathrm{i}}{\hbar}\frac{\mathbf{p}}{m_\parallel} \cdot \left[\boldsymbol{\mathcal{A}}^a \frac{\sigma^a}{2}, f\right] + \frac{p_z}{m_\perp}\nabla_z f + \frac{1}{2}\left\{\boldsymbol{\mathcal{F}} \cdot \nabla_{\mathbf{p}}, f\right\} = I_0 + I_{\text{EY}} + I_{\text{ext}} \,, \tag{6.5}$$

where the second term on the l.h.s. accounts for the inhomogeneity due to the presence of the ferromagnet. Since the Rashba spin-orbit coupling depends only on the in-plane components of the momentum, the nonzero components of the SU(2) vector potential and the SU(2) Lorentz force with the electrical field $E_x \mathbf{e}_x$ are of the same form as in Chap. 5, i.e.,

$$\mathcal{A}_y^x = -\mathcal{A}_x^y = \frac{\hbar}{l_{\text{DP}}} \,, \tag{6.6}$$

$$\mathcal{F}_i = -eE_x\delta_{ix} - \frac{\alpha_{\text{R}}}{\hbar l_{\text{DP}}}\varepsilon_{ijz}p_j\sigma^z \,, \tag{6.7}$$

where $l_{\text{DP}} = \hbar^2/2m_\parallel\alpha_{\text{R}}$ is the Dyakonov-Perel spin diffusion length which amounts to simply renaming $m \to m_\parallel$ compared to the isotropic case. Analogously, the Dyakonov-Perel relaxation rate reads

$$\frac{1}{\tau_{\text{DP}}} = \frac{D_\parallel}{l_{\text{DP}}^2} \tag{6.8}$$

with the in-plane diffusion constant $D_\parallel = 2\epsilon_{\text{F}}\tau/3m_\parallel$. The Elliott-Yafet collision operator I_{EY} for the anisotropic Rashba metal is discussed in App. G.1. The collision operator I_{ext} corresponds to side-jump and skew scattering, see Ref. 69 for details.[1] Here, we briefly discuss, how the mass anisotropy affects the Elliott-Yafet relaxation mechanism. In Chap. 4 we have introduced the phenomenological parameter ζ which accounts for a reduction of the momentum in z direction for quasi two-dimensional systems. Here, we

[1] Compared to Ref. 69, in the resulting spin Hall conductivities $\sigma_{\text{sj}}^{\text{sH}}$ and $\sigma_{\text{ss}}^{\text{sH}}$ the mass m has to be replaced by $2m_\parallel/3$ with the factor $2/3$ due to the dimensionality.

encounter a similar situation since the Fermi surface is an ellipsoid and the momentum in z direction at the Fermi energy differs from the in-plane momentum at the Fermi energy. Indeed, the total anisotropic spin relaxation is obtained as follows:

$$\partial_t \mathbf{s} \sim -\frac{1}{\tau_{\text{DP}}} \begin{pmatrix} 1 & 0 & 0 \\ 0 & 1 & 0 \\ 0 & 0 & 2 \end{pmatrix} \mathbf{s} - \frac{1}{\tau_s} \begin{pmatrix} 1 & 0 & 0 \\ 0 & 1 & 0 \\ 0 & 0 & \zeta \end{pmatrix} \mathbf{s} \,, \tag{6.9}$$

where $\zeta = 2m_\perp/(m_\perp + m_\parallel)$ and

$$\frac{1}{\tau_s} = \frac{8}{9(2-\zeta)} \left(\frac{\lambda p_{\text{F}}}{2\hbar} \right)^4 \frac{1}{\tau} \tag{6.10}$$

with $p_{\text{F}} = \sqrt{2m_\parallel \epsilon_{\text{F}}}$. We would like to mention that besides necessary generalizations of some quantities due to the mass anisotropy, in the following there will be additional changes in the notation compared to previous chapters. This has practical reasons due to the inclusion of side-jump and skew scattering with the goal to facilitate the comparison with published work on the heavy-metal/ferromagnet system.

6.1. Current-induced spin polarization

In this section, we calculate the current-induced and magnetization-dependent spin polarization in the spin diffusive limit, $p_{\text{F}}\tau/m_\parallel l_{\text{DP}} \ll 1$. Analogously to Sec. 4.1 and 5.1, we thus consider the spin sector of the Boltzmann equation. Neglecting spin-dependent contributions to the charge current, $j_x \approx \sigma_{\text{D}} E_x$, the momentum integrated spin sector yields

$$\Gamma \mathbf{s} + \tau_s \nabla_z \mathbf{j}_z - \tau_s \frac{\boldsymbol{\mathcal{A}}_i}{\hbar} \times \mathbf{j}_i = \mathbf{e}_y \theta_{\text{int}}^{\text{sH}} \frac{\tau_{\text{DP}}}{l_{\text{DP}}} \left(1 - \frac{3\zeta}{4} \right) \frac{\sigma_{\text{D}} E_x}{2e} \,, \tag{6.11}$$

where $\Gamma = \text{diag}(1, 1, \zeta)$ and $\theta_{\text{int}}^{\text{sH}} = \alpha_{\text{R}}\tau/\hbar l_{\text{DP}}$ accounts for the Rashba contribution to the spin Hall angle.[2] Similarly, by a multiplication with p_i prior to the momentum

[2] Note that $\theta_{\text{int}}^{\text{sH}}$ is not the bulk spin Hall angle in case of a pure Rashba system [69].

integration we obtain the spin current in $i = x, y, z$ direction, respectively,

$$\mathbf{j}_x = -\frac{l_{\text{DP}}}{\tau_{\text{DP}}}\mathbf{e}_y \times \mathbf{s}\,, \tag{6.12}$$

$$\mathbf{j}_y = \frac{l_{\text{DP}}}{\tau_{\text{DP}}}\mathbf{e}_x \times \mathbf{s} + \mathbf{e}_z \left(\theta_{\text{int}}^{\text{sH}} + \theta_{\text{ext}}^{\text{sH}}\right) \frac{\sigma_{\text{D}} E_x}{2e}\,, \tag{6.13}$$

$$\mathbf{j}_z = -D_\perp \nabla_z \mathbf{s} - \mathbf{e}_y \theta_{\text{ext}}^{\text{sH}} \frac{m_\parallel}{m_\perp} \frac{\sigma_{\text{D}} E_x}{2e}\,, \tag{6.14}$$

where $D_\perp = 2\epsilon_{\text{F}}\tau/3m_\perp$ is the out-of-plane diffusion constant. Side-jump and skew scattering are taken into account via the parameter $\theta_{\text{ext}}^{\text{sH}} = 2e(\sigma_{\text{sj}}^{\text{sH}} + \sigma_{\text{ss}}^{\text{sH}})/\sigma_{\text{D}}$, the extrinsic contribution to the spin Hall angle. We insert Eqs. (6.12)–(6.14) into Eq. (6.11) and obtain the following set of diffusion equations for the spin density:

$$q_1^2 s^x = \nabla_z^2 s^x\,, \tag{6.15}$$

$$q_1^2 s^y = \nabla_z^2 s^y + q_1^2 s_0^y\,, \tag{6.16}$$

$$q_2^2 s^z = \nabla_z^2 s^z\,. \tag{6.17}$$

The inverse spin relaxation lengths,

$$q_1 = \frac{1}{l_{\text{DP}}}\sqrt{\frac{m_\perp}{m_\parallel}\left(1 + \frac{\tau_{\text{DP}}}{\tau_s}\right)}\,, \tag{6.18}$$

$$q_2 = \frac{1}{l_{\text{DP}}}\sqrt{\frac{m_\perp}{m_\parallel}\left(2 + \zeta\frac{\tau_{\text{DP}}}{\tau_s}\right)}\,, \tag{6.19}$$

reflect the anisotropy of the spin relaxation rates. In addition, we have introduced the bulk current-induced spin polarization in the homogeneous case,

$$s_0^y = -\frac{1}{D_\parallel q_{\text{ISGE}}}\frac{\sigma_{\text{D}} E_x}{2e}\,, \tag{6.20}$$

which describes the inverse spin galvanic effect in an anisotropic Rashba metal. The wavenumber q_{ISGE} is defined by

$$\frac{1}{D_\parallel q_{\text{ISGE}}} = \frac{\tau_s/l_{\text{DP}}}{1 + \tau_s/\tau_{\text{DP}}}\left(\xi_{\text{int}}\theta_{\text{int}}^{\text{sH}} + \theta_{\text{ext}}^{\text{sH}}\right)\,, \tag{6.21}$$

where

$$\xi_{\text{int}} = 1 - \frac{\tau_{\text{DP}}}{\tau_s}\left(1 - \frac{3\zeta}{4}\right)\,. \tag{6.22}$$

In the following step, we explicitly solve Eqs. (6.15)–(6.17) by taking into account proper boundary conditions at $z = 0$ and $z = d$. These are given by Eq. (6.1) for the spin current $\mathbf{j}_z(0)$ across the interface to the ferromagnet and by the condition $\mathbf{j}_z(d) = 0$, corresponding to spin-conserving scattering at the opposite boundary. Via Eq. (6.14) we see that the boundary conditions for the spin current can be transformed to boundary conditions for the spin density. Applying these boundary conditions to Eqs. (6.15)–(6.17) we obtain the current-induced spin polarization

$$s^y(z) = s_0^y + \Delta s_{\mathrm{sc}}^y(z) + \Delta s^y(z, \mathbf{n})\,, \tag{6.23}$$

where

$$\Delta s_{\mathrm{sc}}^y(z) = \frac{\theta_{\mathrm{ext}}^{\mathrm{sH}}}{D_\parallel q_1} \frac{\sigma_{\mathrm{D}} E_x}{2e} \frac{\sinh\big(q_1(d/2 - z)\big)}{\cosh(q_1 d/2)} \tag{6.24}$$

is the spin accumulation which is the source for the spin current j_z^y in the absence of the ferromagnet. The magnetization dependence of the spin density is contained in $\Delta s^y(z, \mathbf{n})$. Let us now focus on $\Delta s^y(z, \mathbf{n})$ with the magnetization vector $\mathbf{n}$ lying in the xy, yz, and xz plane, respectively, i.e., the α, β, and γ scans as defined in Fig. 6.1. After some algebra, see App. G.2 for details, we obtain

$$\Delta s_{\alpha,\beta,\gamma}^y(z) = -A(z) f_{\alpha,\beta,\gamma}\,, \tag{6.25}$$

with

$$A(z) = s_0^y \left[1 - \tanh\left(q_1 d/2\right) \theta_{\mathrm{ext}}^{\mathrm{sH}} \frac{q_{\mathrm{ISGE}}}{q_1}\right] \frac{\cosh\big(q_1(d - z)\big)}{\cosh(q_1 d)}\,. \tag{6.26}$$

The angular dependence is given by

$$f_\alpha = \frac{(q_i^2 + q_r^2 + q_r \tilde{q}_2)\cos^2\alpha}{q_i^2 + (\tilde{q}_1 + q_r)(\tilde{q}_2 + q_r)}\,, \tag{6.27}$$

$$f_\beta = \frac{(q_i^2 + q_r^2 + q_r \tilde{q}_1)\cos^2\beta}{\frac{\tilde{q}_1}{\tilde{q}_2}\left[q_i^2 + (\tilde{q}_1 + q_r)(\tilde{q}_2 + q_r)\right]\sin^2\beta + \left[q_i^2 + (\tilde{q}_1 + q_r)^2\right]\cos^2\beta}\,, \tag{6.28}$$

$$f_\gamma = \frac{q_i^2 + q_r^2 + q_r \tilde{q}_1 - (q_i^2 + q_r^2)\left(1 - \frac{\tilde{q}_1}{\tilde{q}_2}\right)\sin^2\gamma}{\frac{\tilde{q}_1}{\tilde{q}_2}\left[q_i^2 + (\tilde{q}_1 + q_r)(\tilde{q}_2 + q_r)\right]\sin^2\gamma + \left[q_i^2 + (\tilde{q}_1 + q_r)^2\right]\cos^2\gamma}\,, \tag{6.29}$$

where the respective scan is indicated by the subscript. Here, we have introduced $q_{r,i} = g_{r,i}^{\uparrow\downarrow}/2\pi\hbar N_0 D_\perp$ and $\tilde{q}_{1,2} = q_{1,2}\tanh(q_{1,2}d)$, reflecting a decrease of the wave numbers q_1 and q_2 due to the finite thickness. Equations (6.25)–(6.29) explicitly describe how

the spatially resolved spin polarization in an anisotropic Rashba metal depends on the magnetization direction of the adjacent ferromagnet. We wish to emphasize that these equations fully determine the magnetoresistance signals, as we shall see in the following section.

6.2. Magnetoresistance

Analogously to the spin Hall magnetoresistance consideration in Sec. 5.2, we investigate the magnetization dependence of the resistivity. For an electrical field E_x the resistivity reads

$$E_x = \rho j_x \,, \tag{6.30}$$

where $j_x = 1/d \int_0^d \mathrm{d}z j_x(z)$ is the current density averaged over the thickness of the Rashba system. In the following, quantities without explicit z dependence are considered as thickness-averaged. Similarly to Sec. 5.2, it is convenient to the split the resistivity,

$$\rho = \rho_0 + \Delta\rho(\mathbf{n}) \,, \tag{6.31}$$

where $\rho_0 \approx 1/\sigma_\mathrm{D}$ is the resistivity for vanishing spin-mixing conductance, $g_r^{\uparrow\downarrow} = g_i^{\uparrow\downarrow} = 0$, and $\Delta\rho$ captures the magnetization dependence. The charge sector of the generalized Boltzmann equation yields the charge current

$$j_x(z) = \sigma_\mathrm{D} E_x + 2e \left[\frac{l_\mathrm{DP}}{\tau_s} \left(1 - \frac{3\zeta}{4} \right) \theta_\mathrm{int}^\mathrm{sH} s^y(z) - \left(\theta_\mathrm{int}^\mathrm{sH} + \theta_\mathrm{ext}^\mathrm{sH} \right) j_y^z(z) + \frac{m_\perp}{m_\parallel} \theta_\mathrm{ext}^\mathrm{sH} j_z^y(z) \right] . \tag{6.32}$$

Loosely speaking, the first term in the square brackets corresponds to a spin galvanic or inverse Edelstein effect, the second term to an in-plane inverse spin Hall effect, and the third term to an out-of-plane inverse spin Hall effect. Interestingly, the relevant spin currents,

$$j_y^z(z) = \frac{l_\mathrm{DP}}{\tau_\mathrm{DP}} s^y(z) + \left(\theta_\mathrm{int}^\mathrm{sH} + \theta_\mathrm{ext}^\mathrm{sH} \right) \frac{\sigma_\mathrm{D} E_x}{2e} \,, \tag{6.33}$$

$$j_z^y(z) = -D_\perp \nabla_z s^y(z) - \theta_\mathrm{ext}^\mathrm{sH} \frac{m_\parallel}{m_\perp} \frac{\sigma_\mathrm{D} E_x}{2e} \,, \tag{6.34}$$

are completely determined by $\Delta s^y(z, \mathbf{n})$ regarding their dependence on the magnetization of the ferromagnet. Hence, inserting Eqs. (6.33) and (6.34) into Eq. (6.32), the

angular dependence of $j_x(z)$, and thus the magnetoresistance, can be traced back to $\Delta s^y(z, \mathbf{n})$. With the definition of the conductivity, $j_x = \sigma E_x$, where $\sigma = \sigma_0 + \Delta\sigma(\mathbf{n})$, cf. Eq. (6.31), we obtain

$$\Delta\sigma(\mathbf{n}) E_x = -2eD_{\parallel} q_{\text{SGE}} \Delta s^y(\mathbf{n}) \,. \tag{6.35}$$

Similarly to q_{ISGE} defined in Eq. (6.21), we have introduced

$$q_{\text{SGE}} = \frac{1}{l_{\text{DP}}} \left[\xi_{\text{int}} \theta^{\text{sH}}_{\text{int}} + \xi_{\text{ext}} \theta^{\text{sH}}_{\text{ext}} \right] , \tag{6.36}$$

a wave number which represents the efficiency of the spin galvanic effect. The parameter ξ_{ext}, the extrinsic analogue to ξ_{int} defined in Eq. (6.22), reads

$$\xi_{\text{ext}} = 1 - q_1 l_{\text{DP}} \tanh(q_1 d/2) \,. \tag{6.37}$$

Assuming $\sigma_0 \approx \sigma_{\text{D}} \gg \Delta\sigma$, the magnetization-dependent contribution to the resistivity is given by

$$\frac{\Delta\rho(\mathbf{n})}{\rho_0} \approx -\frac{\Delta\sigma(\mathbf{n})}{\sigma_{\text{D}}} \,. \tag{6.38}$$

We insert Eq. (6.35) together with the thickness average of $\Delta s^y_{\alpha,\beta,\gamma}(z)$, Eq. (6.25), and obtain the magnetoresistance ratio

$$\frac{\Delta\rho_{\alpha,\beta,\gamma}}{\rho_0} = C f_{\alpha,\beta,\gamma} \tag{6.39}$$

for the α, β, and γ scans. The magnitude of the effect is determined by

$$C = \frac{\tanh(q_1 d)}{q_1 d} \frac{q_{\text{SGE}}}{q_{\text{ISGE}}} \left[1 - \tanh\left(q_1 d/2\right) \theta^{\text{sH}}_{\text{ext}} \frac{q_{\text{ISGE}}}{q_1} \right] \tag{6.40}$$

with the ratio $q_{\text{SGE}}/q_{\text{ISGE}}$ being quadratic in the spin Hall angles. However, due to the simultaneous contributions from s^y, j^z_y, and j^y_z, the magnetoresistance can generally not be expressed in terms of the square of a single total spin Hall angle, as in the phenomenological approach of Ref. 77. Only in the special case where intrinsic spin-orbit coupling is negligible we can express the magnetoresistance in terms of a single squared spin Hall angle. In the following subsections, we discuss the magnetoresistance for a purely damping-like torque, $g_i^{\uparrow\downarrow} = 0$, and a purely field-like torque, $g_r^{\uparrow\downarrow} = 0$, respectively.

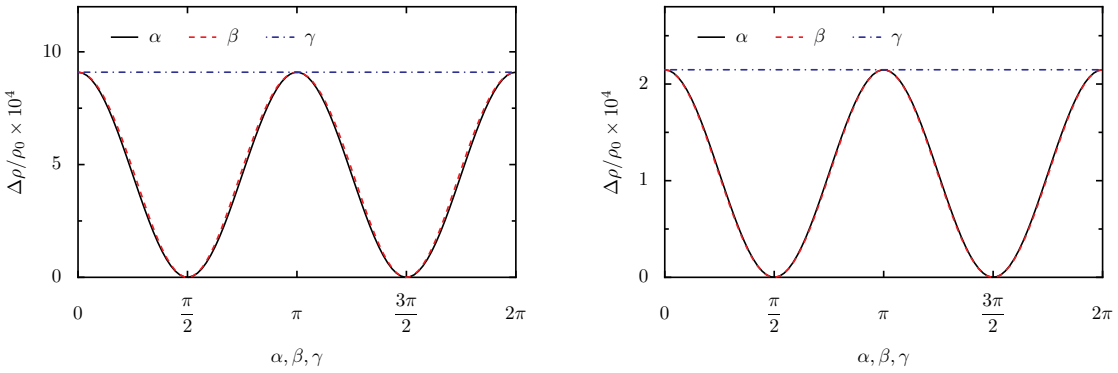

(a) (b)

FIG. 6.2.: Magnetoresistance for a damping-like torque as function of α, β, and γ with $\zeta = 0.5$, $q_r l_{\text{DP}} = 0.5$, and $d = 2l_{\text{DP}}$. The left panel (a) corresponds to the case of strong Rashba spin-orbit coupling ($\tau_{\text{DP}}/\tau_s = 0.5$, $\theta^{\text{sH}}_{\text{int}} = 0.1$, $\theta^{\text{sH}}_{\text{ext}} = 0.01$), and the right panel (b) to the case of dominant extrinsic spin-orbit coupling ($\tau_{\text{DP}}/\tau_s = 5$, $\theta^{\text{sH}}_{\text{int}} = 0.01$, $\theta^{\text{sH}}_{\text{ext}} = 0.1$).

Damping-like torque

In the case of vanishing imaginary part of the spin mixing conductance, $g_i^{\uparrow\downarrow} = 0$, which corresponds to a damping-like torque, the angular-dependent magnetoresistances are given by

$$\frac{\Delta\rho_\alpha}{\rho_0} = \frac{Cq_r}{q_r + \tilde{q}_1} \cos^2\alpha\,, \tag{6.41}$$

$$\frac{\Delta\rho_\beta}{\rho_0} = \frac{Cq_r \cos^2\beta}{q_r + \tilde{q}_1 - q_r\left(1 - \frac{\tilde{q}_1}{\tilde{q}_2}\right)\sin^2\beta}\,, \tag{6.42}$$

$$\frac{\Delta\rho_\gamma}{\rho_0} = \frac{Cq_r}{q_r + \tilde{q}_1}\,. \tag{6.43}$$

We see that $\Delta\rho_\gamma$ is constant and that $\Delta\rho_\beta$ has a similar angular dependence as $\Delta\rho_\alpha$ for a wide range of parameters. More precisely, in the case $|1 - \tilde{q}_1/\tilde{q}_2| \ll 1$, the $\sin^2\beta$ term in the denominator in Eq. (6.42) leads to higher harmonics in β of small magnitude,

$$\frac{\Delta\rho_\beta}{\rho_0} \approx \frac{Cq_r}{q_r + \tilde{q}_1}\left[\cos^2\beta + \frac{1 - \tilde{q}_1/\tilde{q}_2}{4(1 + \tilde{q}_1/q_r)}\sin^2(2\beta)\right]\,. \tag{6.44}$$

Hence, the ratio $\tilde{q}_1/\tilde{q}_2$ determines the sign of the next-to-leading harmonic of the signal.

Figure 6.2 shows the magnetoresistance according to Eqs. (6.41)–(6.43). Panel (a) corresponds to the case where Rashba spin-orbit coupling is large compared to the extrinsic spin-orbit coupling, whereas (b) corresponds to the opposite situation. Although qualitatively there is no difference, we see that the magnitude of the signal is larger in the case where the Rashba spin-orbit coupling dominates compared to the case of a stronger extrinsic contribution.

Field-like torque

In order to focus on a purely field-like torque, we now neglect the real part of the spin mixing conductance, $g_r^{\uparrow\downarrow} = 0$. The angular-dependent magnetoresistances are then given by

$$\frac{\Delta\rho_\alpha}{\rho_0} = \frac{Cq_i^2}{q_i^2 + \tilde{q}_1\tilde{q}_2}\cos^2\alpha\,, \tag{6.45}$$

$$\frac{\Delta\rho_\beta}{\rho_0} = \frac{Cq_i^2\cos^2\beta}{q_i^2 + \tilde{q}_1^2 - q_i^2\left(1-\frac{\tilde{q}_1}{\tilde{q}_2}\right)\sin^2\beta}\,, \tag{6.46}$$

$$\frac{\Delta\rho_\gamma}{\rho_0} = \frac{Cq_i^2\left[1-\left(1-\frac{\tilde{q}_1}{\tilde{q}_2}\right)\sin^2\gamma\right]}{q_i^2 + \tilde{q}_1^2 - q_i^2\left(1-\frac{\tilde{q}_1}{\tilde{q}_2}\right)\sin^2\gamma}\,. \tag{6.47}$$

The ratio $\tilde{q}_1/\tilde{q}_2$ defines the sign of the $\sin^2\gamma$ contribution in Eq. (6.47). It also determines whether the ratio of the amplitudes of $\Delta\rho_\alpha$ and $\Delta\rho_\beta$,

$$\frac{\Delta\rho_\alpha(0)}{\Delta\rho_\beta(0)} = 1 - \frac{\tilde{q}_1\tilde{q}_2}{q_i^2 + \tilde{q}_1\tilde{q}_2}\left(1-\frac{\tilde{q}_1}{\tilde{q}_2}\right)\,, \tag{6.48}$$

is larger or smaller than one. In the case $\tilde{q}_2 \gg q_i$ and $\tilde{q}_1 \gg q_i$, Eq. (6.48) reduces to

$$\frac{\Delta\rho_\alpha(0)}{\Delta\rho_\beta(0)} \approx \frac{\tilde{q}_1}{\tilde{q}_2}\,, \tag{6.49}$$

such that the ratio $\tilde{q}_1/\tilde{q}_2$ can be read off directly from the measured amplitudes of the α and β signal. Inserting the definitions of $\tilde{q}_1$ and $\tilde{q}_2$, Eqs. (6.18) and (6.19), into Eq. (6.49) we can solve for

$$\frac{\tau_{\text{DP}}}{\tau_s} = \frac{2\left(\frac{\Delta\rho_\alpha(0)}{\Delta\rho_\beta(0)}\right)^2 - 1}{1-\zeta\left(\frac{\Delta\rho_\alpha(0)}{\Delta\rho_\beta(0)}\right)^2}\,, \tag{6.50}$$

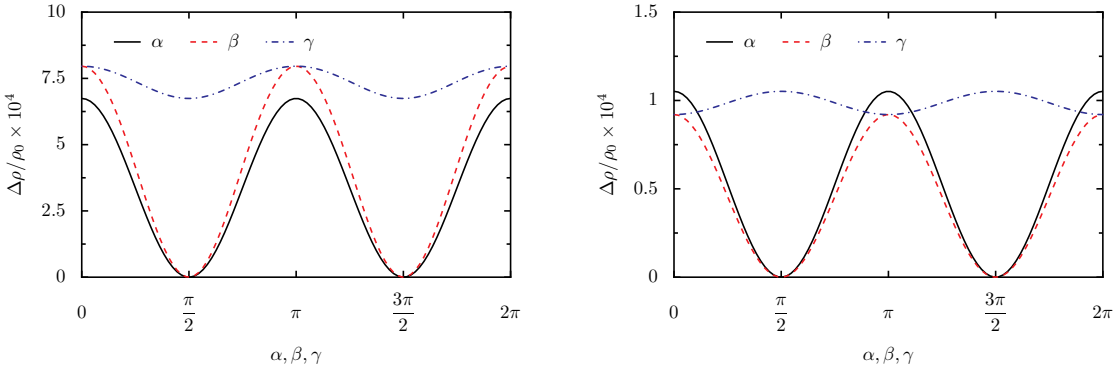

(a) (b)

FIG. 6.3.: Magnetoresistance for a field-like torque as function of α, β, and γ with $\zeta = 0.5$, $q_r l_{\text{DP}} = 0.5$, and $d = 2l_{\text{DP}}$. The left panel (a) corresponds to the case of strong Rashba spin-orbit coupling ($\tau_{\text{DP}}/\tau_s = 0.5$, $\theta^{\text{sH}}_{\text{int}} = 0.1$, $\theta^{\text{sH}}_{\text{ext}} = 0.01$), and the right panel (b) to the case of dominant extrinsic spin-orbit coupling ($\tau_{\text{DP}}/\tau_s = 5$, $\theta^{\text{sH}}_{\text{int}} = 0.01$, $\theta^{\text{sH}}_{\text{ext}} = 0.1$).

or, in the case $\tau_{\text{DP}} \gg \tau_s$, directly extract the anisotropy parameter of the Elliott-Yafet spin relaxation,

$$\zeta \approx \left(\frac{\Delta\rho_\alpha(0)}{\Delta\rho_\beta(0)}\right)^{-2} . \tag{6.51}$$

Analogously to the damping-like case, up to linear order in $(1 - \tilde{q}_1/\tilde{q}_2)$ we can expand $\Delta\rho_\beta$ in terms of higher harmonics in β,

$$\frac{\Delta\rho_\beta}{\rho_0} \approx \frac{Cq_i^2}{q_i^2 + \tilde{q}_1^2}\left[\cos^2\beta + \frac{1}{4}\left(\frac{1 - \tilde{q}_1/\tilde{q}_2}{1 + \tilde{q}_1^2/q_i^2}\right)\sin^2(2\beta)\right] , \tag{6.52}$$

and similarly, $\Delta\rho_\gamma$ can be expressed as

$$\frac{\Delta\rho_\gamma}{\rho_0} \approx \frac{Cq_i^2}{q_i^2 + \tilde{q}_1^2}\left[1 - \frac{\tilde{q}_1^2}{q_i^2}\left(\frac{1 - \tilde{q}_1/\tilde{q}_2}{1 + \tilde{q}_1^2/q_i^2}\right)\sin^2\gamma\right] . \tag{6.53}$$

We see that one can obtain the ratio $q_i/\tilde{q}_1$ by dividing the amplitude of the second-harmonic of $\Delta\rho_\beta$ by the amplitude of the γ scan of the magnetoresistance.

Figure 6.3 shows the magnetoresistance according to Eqs. (6.45)–(6.47). Analogously to Fig. 6.2, panel (a) corresponds to the case where Rashba spin-orbit coupling dominates and (b) to the case where extrinsic spin-orbit coupling is more important.

Similarly to the damping-like boundary condition, the signal is stronger in the situation with dominant Rashba spin-orbit coupling. In addition, there is a noticeable qualitative difference between (a) and (b) namely the change of the sign of the γ oscillation. This follows from Eq. (6.47) with $\tilde{q}_1/\tilde{q}_2 < 1$ in the case (a), and $\tilde{q}_1/\tilde{q}_2 > 1$ in the case (b).

Discussion

First of all, we remark that this work provides the first microscopical theory of the magnetoresistance in anisotropic Rashba metals, to the best of our knowledge. Apart from the obvious application to real Rashba metals such as discussed at the beginning of this chapter, our theory is also applicable to heavy-metal/ferromagnet bilayers and goes beyond common phenomenological approaches [77], which are however contained in our result by setting $\zeta = 1$, $\alpha_{\text{R}} = 0$, and $\theta_{\text{ext}}^{\text{sH}} \to \theta_{\text{sH}}$. Here, two points stand out: (1) the consideration of a mass anisotropy and (2) the inclusion of Rashba spin-orbit coupling.

The mass anisotropy, point (1), leads to an anisotropic spin relaxation, even in the case of vanishing Rashba spin-orbit coupling $\alpha_{\text{R}} = 0$, and thus $\tilde{q}_1/\tilde{q}_2 \neq 1$. In this case, according to Eq. (6.29) the γ scan acquires a finite amplitude $\Delta\rho_\gamma$ for a nonzero imaginary part of the spin mixing constant, $g_i^{\uparrow\downarrow} \neq 0$. Hence, using a ferromagnetic insulator, one could extract the ratio of the reduced spin relaxation lengths $1/\tilde{q}_1$ and $1/\tilde{q}_2$ by a precise measurement of $\Delta\rho_\gamma$. Indeed, experimental results for a Cu[Pt]/YIG bilayer structure, where the Cu/YIG interface is sputtered with Pt nanosize islands, show a noticeable oscillation in the γ scan [177], which can be explained within our theory for a nonzero $g_i^{\uparrow\downarrow}$ and $\tilde{q}_1/\tilde{q}_2 > 1$, cf. Fig. 6.3 (b). This effect is pronounced due to an enhancement of the anisotropy of the spin relaxation mechanism as the sputtered Pt exhibits a Rashba spin-orbit coupling [177]. This directly brings us to point (2). There exists evidence that also thin Pt films can exhibit a strong Rashba spin-orbit coupling [122]. In this case, the inverse spin galvanic effect strongly influences spin transport and the magnetoresistance signal cannot be interpreted as a 'simple' interplay between the spin Hall and the inverse spin Hall effect, resulting in $\Delta\rho \sim \theta_{\text{sH}}^2$, namely the spin Hall magnetoresistance. Instead, one should focus on the spin polarization s^y, described by the wavenumbers q_{ISGE} and q_{SGE}, which represent the efficiency of the conversion of an electric field to a spin polarization and vice versa. This approach is more general than to focus on the spin Hall angle and the spin currents.

Last, we would like to compare our results with experiments on hybrid structures of spin-orbit active materials and a ferromagnetic metal. In these measurements, the angular dependent γ scan is usually explained by the additional contribution from the anisotropic magnetoresistance to the total signal [170–172]. Note however, that the measured signals qualitatively agree well with the magnetoresistance obtained in this work for a field-like torque, see Fig. 6.3. Since the spin mixing conductance is determined by interface properties, it is not perfectly clear that its imaginary part is always negligible. Therefore, special care is required when interpreting the measured signals. For example, the magnetoresistance in a Bi(15nm)/Ag/CoFeB trilayer, where a Rashba 2DEG is present at the Bi/Ag interface,[3] shows a sign reversal in the oscillation of the γ scan when comparing the low-temperature with the room-temperature measurements [176]. Qualitatively, the signals in the first case agree with Fig. 6.3 (a) and in the second case with 6.3 (b). Since $1/\tau$ is typically an increasing function of the temperature and $\tau_{\text{DP}}/\tau_s \sim 1/\tau^2$, the ratio $\tilde{q}_1/\tilde{q}_2$ is also temperature dependent. Hence, Fig. 6.3 (a) with $\tilde{q}_1/\tilde{q}_2 < 1$ due to a small ratio $\tau_{\text{DP}}/\tau_s = 0.5$ corresponds to the low-temperature regime and, vice versa, Fig. 6.3 (b) with $\tilde{q}_1/\tilde{q}_2 > 1$ to the high-temperature regime.

6.3. Conclusions

In this chapter, we have presented a microscopic theory of the magnetoresistance in Rashba-metal/ferromagnetic-insulator bilayer structures, where the Rashba metal exhibits a mass anisotropy. Extrinsic spin-orbit coupling due to impurities has been taken into account via Elliott-Yafet spin relaxation as well as side-jump and skew scattering.

We have found that the mass anisotropy of the Rashba metal results in an anisotropic Elliott-Yafet spin relaxation mechanism. Consequently, and enhanced by Dyakonov-Perel spin relaxation, the spin diffusion equations derived from the spin sector of the generalized Boltzmann equation have resulted in two different spin relaxation lengths. We have solved these equations for the current-induced spin polarization and, in particular, we have focused on its dependence on the magnetization direction of the adjacent ferromagnet.

[3] Due to the Rashba spin-orbit coupling and the associated Edelstein effect (inverse spin galvanic effect) the measured magnetoresistance is named Rashba-Edelstein magnetoresistance in Refs. 175 and 176.

It has been shown that the angular dependence of the magnetoresistance is fully determined by the current-induced spin polarization. In order to illustrate the relevance of the Rashba-metal/ferromagnet interface, we have considered the special cases of a purely damping-like and a purely field-like torque. In both cases, it turned out that the magnitude of the magnetoresistance is strongly enhanced when Rashba spin-orbit coupling is large compared to extrinsic contributions. Interestingly, for a field-like torque the γ scan becomes non-constant, with the sign of its oscillation being determined by the ratio of the two spin relaxation lengths, and thus the anisotropy of the spin relaxation. Due to the temperature dependence of the spin relaxation lengths, a sign change in the amplitude of the γ scan is predicted which would explain the experimentally observed temperature dependence. Carefully analyzing the experimental data could therefore provide important information concerning the anisotropy of the spin relaxation mechanism and its temperature dependence.

7

Summary and outlook

In this thesis, we have studied spin-charge coupled transport in systems with Rashba spin-orbit coupling and Elliott-Yafet spin relaxation, in particular, regarding the possibility of its manipulation by means of an adjacent insulating ferromagnet. More specifically, we have focused on signatures in the charge sector which are related to effects due to spin-orbit coupling, providing the basis for indirectly measuring these spin-related effects.

Our investigations are based on a generalized Boltzmann equation which takes spin-orbit coupling in the form of SU(2) gauge fields into account. For a review of its derivation, a perturbation theory on the basis of the Keldysh (nonequilibrium) Green's function formalism has been introduced. The Boltzmann equation then follows by a generalization of the gradient expansion for locally covariant Green's functions. In order to account for scattering processes, collision integrals have been derived from their associated self-energy diagrams. More precisely, we have derived collision integrals describing momentum relaxation and Elliott-Yafet spin relaxation. In particular, the latter crucially depends on the proper treatment of the SU(2) gauge fields, resulting in novel contributions which were previously overlooked.

As an application of the theoretical formalism to experimentally relevant situations, three geometries have been considered: (1) a ferromagnet on top of a (quasi) two-dimensional electron gas, (2) a ferromagnet being attached laterally to a two-dimensional Rashba system, and (3) a bilayer structure which consists of a 3D Rashba metal on top of a ferromagnetic insulator.

Regarding the first geometry, the influence of the ferromagnet has been assumed as a proximity-induced time-dependent magnetic texture. Furthermore, the system was assumed to be in the crossover regime between a two-dimensional and a three-dimensional system with respect to the Elliott-Yafet spin relaxation, which is anisotropic in the transition regime and isotropic in the three-dimensional case. As response to the time dependence of the localized spins an effective force acting on the charge carriers has

been derived, with contributions by both the spin current (inverse spin Hall effect) and the spin density (spin galvanic effect); in particular, we have discussed a novel 'inverse spin filter' contribution which results from one of the new SU(2) terms in the Elliott-Yafet collision operator. As a concrete example, the typical spin pumping setup for a narrow wire has been discussed. We have found that the inverse spin Hall contribution to a generated in-plane electric field is negligible, whereas the spin galvanic effect is dominant. In addition, the inverse spin filter effect is found to depend crucially on the anisotropy of the Elliott-Yafet spin relaxation, with the consequence that in the strictly two-dimensional case the inverse spin filter contribution is of similar magnitude as the spin galvanic contribution in a longitudinal measurement, whereas the inverse spin filter effect is absent in an orthogonal measurement.

In the second geometry, the ferromagnetic insulator is laterally attached to a two-dimensional Rashba system, hence it can be used to modify the boundary conditions for the spin current flowing across the interface. On the basis of coupled spin diffusion equations, we have shown that the spin Hall effect and the inverse spin galvanic effect are non-trivially affected by the magnetization direction due to the interplay of spin currents and spin density in a two-dimensional Rashba system. In particular, there exists a polarization direction where the ferromagnetic boundary condition with finite spin mixing conductance is equivalent to the case with a vanishing spin mixing conductance. This, in turn, leads to a local minimum in the angular dependence of the spin Hall magnetoresistance. In addition, we have shown that the ratio of the Dyakonov-Perel and Elliott-Yafet relaxation rates are associated with this particular polarization direction, which offers the possibility to extract this ratio by measuring the spin Hall magnetoresistance and the location of its minimum. Last, we have extended our investigation to thermal effects by discussing the spin Nernst magnetothermopower. It was found that due to a partial cancellation of electrical and thermal contributions the spin Nernst magnetothermopower becomes very small, and even vanishes when Elliott-Yafet spin relaxation is neglected.

In the third geometry we have extended the metallic system to a bulk three-dimensional Rashba metal with mass anisotropy. Here, we have focused on the magnetoresistance and its angular dependence due to the presence of an insulating ferromagnet. In addition, side-jump and skew scattering have been taken into account. It was shown

that the current-induced spin polarization fully determines the magnetoresistance. In general, the amplitude of the magnetoresistance is enhanced in the case of dominating Rashba spin-orbit coupling. In the special case of a field-like torque at the interface, the qualitative behavior of the angular-dependent magnetoresistance depends on two different spin relaxation lengths due to the anisotropy of the spin relaxation mechanisms. As a consequence, a sign change in the amplitude of the γ scan is predicted as function of temperature due to the temperature-dependent ratio of the two spin relaxation lengths. Our theoretical results provide a simple and consistent interpretation of magnetoresistance measurements for various systems without resorting to additional assumptions.

Clearly, there are still many open questions in the fields of spintronics and spin caloritronics which could be addressed. In relation to the present work, which focused on the manipulation of spin-charge dynamics in a Rashba system interfaced with a ferromagnet, let us provide the following (by far incomplete) list:

- In Chap. 4 we have introduced the phenomenological parameter ζ in order to account for the two-dimensional to three-dimensional crossover regime regarding the anisotropy of the Elliott-Yafet relaxation rate. A microscopic theory with quantized momenta along the constrained direction and an appropriate random potential model for the impurities should shed light on how such an anisotropy parameter depends on the thickness of the system.

- As a concrete example, the conical precession of the magnetization has been discussed for the typical spin pumping configuration. Certainly, more complicated time-dependent magnetic textures such as moving domain walls or optically excited skyrmions [178–180] are also of considerable interest.

- Chapters 5 and 6 could be extended, for example, by replacing the ferromagnetic insulator by a non-collinear magnet [181, 182] or by considering an additional ferromagnet attached to the Rashba system vis-à-vis to the first one. Furthermore, the imaginary part of the spin mixing conductance could be included in Chap. 5, as well as other contributions such as interfacial spin-orbit coupling [183].

- In Chaps. 4 and 5 extrinsic spin-orbit coupling could be included in addition, e.g., side-jump and skew scattering. In general, other extrinsic contributions such as spin-orbit coupling at rough surfaces [184] or grain boundaries are of interest as

well, which could be considered by proper boundary conditions or by additional collision operators.

- In order to study the interplay between localized and itinerant spins, a very general approach would be to study coupled Boltzmann equations for the respective spin distribution functions. As shown in App. D it is possible to derive a Landau-Lifshitz-Gilbert equation and obtain torque terms for the two subsystems.

Despite intense efforts of numerous scientists during recent years, it is apparent from the few specific cases studied in this thesis that spintronics and spin caloritronics are still most lively fields, characterized by a close interplay between experiment and theory. In particular, it is hoped that the theoretical developments presented above will initiate further experimental investigations.

A

Time-evolution operator

A.1. Separation of the time-evolution operator

In this appendix, we proof the separation

$$\hat{U}_H(t,t_0) = \hat{U}_{H_1}(t,t_0)\hat{S}(t,t_0) \tag{A.1}$$

of the time-evolution operator

$$\hat{U}_H(t,t_0) = T\left\{\exp\left(-\frac{\mathrm{i}}{\hbar}\int_{t_0}^{t}\mathrm{d}t'\,\hat{H}(t')\right)\right\} \tag{A.2}$$

for a given Hamiltonian $\hat{H}(t) = \hat{H}_1 + \hat{H}'(t)$, where $\hat{H}'(t) = 0$ for $t \leq t_0$. Here, $\hat{U}_{H_1}$ is the time-evolution operator with respect to the time-independent Hamiltonian $\hat{H}_1$,

$$\hat{U}_{H_1}(t,t_0) = \exp\left(-\frac{\mathrm{i}}{\hbar}\hat{H}_1(t-t_0)\right)\,, \tag{A.3}$$

and

$$\hat{S}(t,t_0) = T\left\{\exp\left(-\frac{\mathrm{i}}{\hbar}\int_{t_0}^{t}\mathrm{d}t'\,\hat{H}'_{H_1}(t')\right)\right\}, \tag{A.4}$$

where

$$\hat{H}'_{H_1}(t) = \hat{U}^{\dagger}_{H_1}(t,t_0)\hat{H}'(t)\hat{U}_{H_1}(t,t_0) \tag{A.5}$$

is the time-evolution of $\hat{H}'$ with respect to $\hat{H}_1$.

In the following, we present two approaches for proofing that Eq. (A.1) is correct together with the definitions above: first, a combinatorial proof with use of the time-evolution of $\hat{U}$ and second, a proof by discretization of the time-evolution operator. For both approaches we consider $t > t_0$ as the proof of Eq. (A.1) is trivial for $t \leq t_0$, since $\hat{H}' = 0$ in this case.

Combinatorial proof

Let us consider the Schrödinger equation for some state $|\psi\rangle$:

$$\mathrm{i}\hbar\frac{\partial}{\partial t}\,|\psi(t)\rangle = \hat{H}\,|\psi(t)\rangle\ . \tag{A.6}$$

Expressing $|\psi\rangle$ by

$$|\psi(t)\rangle = \hat{U}(t,t_0)\,|\psi(t_0)\rangle\ , \tag{A.7}$$

the Schrödinger equation leads to the time-evolution of $\hat{U}$ given by

$$\mathrm{i}\hbar\frac{\partial}{\partial t}\hat{U}(t,t_0) = \hat{H}\hat{U}(t,t_0)\,. \tag{A.8}$$

Inserting the ansatz (A.1) results in the differential equation

$$\mathrm{i}\hbar\frac{\partial}{\partial t}\hat{S}(t,t_0) = \hat{H}'_{H_1}(t)\hat{S}(t,t_0)\,, \tag{A.9}$$

which by integration gives

$$\hat{S}(t,t_0) = 1 - \frac{\mathrm{i}}{\hbar}\int_{t_0}^{t}\mathrm{d}t_1\,\hat{H}'_{H_1}(t_1)\hat{S}(t_1,t_0)\,. \tag{A.10}$$

Equation (A.10) can now be iterated, leading to the infinite sum

$$\hat{S}(t,t_0) = 1 - \frac{\mathrm{i}}{\hbar}\int_{t_0}^{t}\mathrm{d}t_1\,\hat{H}'_{H_1}(t_1) + \left(\frac{\mathrm{i}}{\hbar}\right)^2\int_{t_0}^{t}\mathrm{d}t_1\int_{t_0}^{t_1}\mathrm{d}t_2\,\hat{H}'_{H_1}(t_1)\hat{H}'_{H_1}(t_2) + \dots\ . \tag{A.11}$$

It is now possible to utilize the combinatorial properties of a multidimensional integration over a time-ordered product of operators such that the n-th order term in $\hat{H}'_{H_1}$ can be rewritten as

$$\begin{aligned}\left(-\frac{\mathrm{i}}{\hbar}\right)^n &\int_{t_0}^{t}\mathrm{d}t_1\int_{t_0}^{t_1}\mathrm{d}t_2\cdots\int_{t_0}^{t_{n-1}}\mathrm{d}t_n\,\hat{H}'_{H_1}(t_1)\hat{H}'_{H_1}(t_2)\dots\hat{H}'_{H_1}(t_n)\\ &= \frac{1}{n!}\left(-\frac{\mathrm{i}}{\hbar}\right)^n\int_{t_0}^{t}\mathrm{d}t_1\int_{t_0}^{t}\mathrm{d}t_2\cdots\int_{t_0}^{t}\mathrm{d}t_n\,T\left\{\hat{H}'_{H_1}(t_1)\hat{H}'_{H_1}(t_2)\dots\hat{H}'_{H_1}(t_n)\right\}\ .\end{aligned} \tag{A.12}$$

Thus, Eq. (A.11) reduces to

$$\begin{aligned}\hat{S}(t,t_0) &= 1 + \sum_{n=1}^{\infty}\frac{1}{n!}\left(-\frac{\mathrm{i}}{\hbar}\right)^n\int_{t_0}^{t}\mathrm{d}t_1\dots\mathrm{d}t_n\,T\left\{\hat{H}'_{H_1}(t_1)\dots\hat{H}'_{H_1}(t_n)\right\}\\ &= T\left\{\exp\left(-\frac{\mathrm{i}}{\hbar}\int_{t_0}^{t}\mathrm{d}t'\,\hat{H}'_{H_1}(t')\right)\right\},\end{aligned} \tag{A.13}$$

coinciding with Eq. (A.4) such that Eq. (A.1) is proven to be correct together with the definitions (A.2)–(A.5).

Proof by discretization

Note that the definition of the time-evolution operator in Eq. (A.2) must be equivalent to an infinite product of time-evolutions over infinitesimal times [89]:

$$\hat{U}_H(t,t_0) = \lim_{M\to\infty} \mathrm{e}^{-\frac{\mathrm{i}}{\hbar}\epsilon\hat{H}(t_{M-1})}\mathrm{e}^{-\frac{\mathrm{i}}{\hbar}\epsilon\hat{H}(t_{M-2})}\dots\mathrm{e}^{-\frac{\mathrm{i}}{\hbar}\epsilon\hat{H}(t_1)}\mathrm{e}^{-\frac{\mathrm{i}}{\hbar}\epsilon\hat{H}(t_0)}\,, \tag{A.14}$$

where $\epsilon = (t-t_0)/M$ and $t_n = t_0 + n\epsilon$. Inserting $1 = \hat{U}_{H_1}\hat{U}_{H_1}^\dagger$ with proper time arguments between the exponential functions results in

$$\begin{aligned}\hat{U}_H(t,t_0) = \lim_{M\to\infty} \mathrm{e}^{-\frac{\mathrm{i}}{\hbar}\epsilon\hat{H}(t_{M-1})}\hat{U}_{H_1}(t_{M-1},t_0)\hat{U}_{H_1}^\dagger(t_{M-1},t_0)\mathrm{e}^{-\frac{\mathrm{i}}{\hbar}\epsilon\hat{H}(t_{M-2})}\dots\\ \times\dots\hat{U}_{H_1}^\dagger(t_{n+1},t_0)\mathrm{e}^{-\frac{\mathrm{i}}{\hbar}\epsilon\hat{H}(t_n)}\hat{U}_{H_1}(t_n,t_0)\dots\\ \times\dots\mathrm{e}^{-\frac{\mathrm{i}}{\hbar}\epsilon\hat{H}(t_1)}\hat{U}_{H_1}(t_1,t_0)\hat{U}_{H_1}^\dagger(t_1,t_0)\mathrm{e}^{-\frac{\mathrm{i}}{\hbar}\epsilon\hat{H}(t_0)}\,.\end{aligned} \tag{A.15}$$

The explicit evaluation of some term inside the product, e.g., the second line on the r.h.s. of Eq. (A.15), is given by

$$\begin{aligned}\hat{U}_{H_1}^\dagger(t_{n+1},t_0)\mathrm{e}^{-\frac{\mathrm{i}}{\hbar}\epsilon\hat{H}(t_n)}\hat{U}_{H_1}(t_n,t_0) &= \mathrm{e}^{\frac{\mathrm{i}}{\hbar}\hat{H}_1(t_{n+1}-t_0)}\mathrm{e}^{-\frac{\mathrm{i}}{\hbar}\epsilon(\hat{H}_1+\hat{H}'(t_n))}\mathrm{e}^{\frac{\mathrm{i}}{\hbar}\hat{H}_1(t_n-t_0)}\\ &= \mathrm{e}^{\frac{\mathrm{i}}{\hbar}\hat{H}_1(t_{n+1}-\epsilon-t_0)}\mathrm{e}^{-\frac{\mathrm{i}}{\hbar}\epsilon\hat{H}'(t_n)}\mathrm{e}^{\frac{\mathrm{i}}{\hbar}\hat{H}_1(t_n-t_0)}\\ &= \mathrm{e}^{\frac{\mathrm{i}}{\hbar}\hat{H}_1(t_n-t_0)}\mathrm{e}^{-\frac{\mathrm{i}}{\hbar}\epsilon\hat{H}'(t_n)}\mathrm{e}^{\frac{\mathrm{i}}{\hbar}\hat{H}_1(t_n-t_0)}\\ &= \mathrm{e}^{-\frac{\mathrm{i}}{\hbar}\epsilon\hat{H}'_{H_1}(t_n)}\,,\end{aligned} \tag{A.16}$$

where we have used $\exp[\epsilon(\hat{A}+\hat{B})] = \exp(\epsilon\hat{A})\exp(\epsilon\hat{B}) + \mathcal{O}(\epsilon^2)$ for the step from the first to the second line. Thus, by also inserting $1 = \hat{U}_{H_1}(t,t_0)\hat{U}_{H_1}^\dagger(t,t_0)$ on the left of the $\lim$ operation, we obtain

$$\hat{U}_H(t,t_0) = \hat{U}_{H_1}(t,t_0)\lim_{M\to\infty} \mathrm{e}^{-\frac{\mathrm{i}}{\hbar}\epsilon\hat{H}'_{H_1}(t_{M-1})}\mathrm{e}^{-\frac{\mathrm{i}}{\hbar}\epsilon\hat{H}'_{H_1}(t_{M-2})}\dots\mathrm{e}^{-\frac{\mathrm{i}}{\hbar}\epsilon\hat{H}'_{H_1}(t_1)}\mathrm{e}^{-\frac{\mathrm{i}}{\hbar}\epsilon\hat{H}'_{H_1}(t_0)}\,. \tag{A.17}$$

Similarly to the definition of the time-evolution operator according to Eq. (A.14), the limes on the r.h.s. reduces to

$$\lim_{M\to\infty} \mathrm{e}^{-\frac{\mathrm{i}}{\hbar}\epsilon\hat{H}'_{H_1}(t_{M-1})}\mathrm{e}^{-\frac{\mathrm{i}}{\hbar}\epsilon\hat{H}'_{H_1}(t_{M-2})}\dots\mathrm{e}^{-\frac{\mathrm{i}}{\hbar}\epsilon\hat{H}'_{H_1}(t_1)}\mathrm{e}^{-\frac{\mathrm{i}}{\hbar}\epsilon\hat{H}'_{H_1}(t_0)} = \hat{S}(t,t_0)\,, \tag{A.18}$$

such that Eq. (A.17) yields Eq. (A.1).

A.2. Contour-ordering

Next, we show the equivalence between

$$\hat{O}_H(t) = \hat{S}^\dagger(t,t_0)\hat{O}_{H_1}(t)\hat{S}(t,t_0) \tag{A.19}$$

and

$$\hat{O}_H(t) = T_c\left\{ \exp\left[-\frac{\mathrm{i}}{\hbar}\int_c \mathrm{d}\tau\, \hat{H}'_{H_1}(\tau)\right]\hat{O}_{H_1}(t)\right\}. \tag{A.20}$$

Here, $\hat{O}_H(t)$ is the time-evolution of an arbitrary operator $\hat{O}$ under the influence of the Hamiltonian $\hat{H}(t) = \hat{H}_1 + \hat{H}'(t)$ with $\hat{H}'(t) = 0$ for $t \leq t_0$. Analogously, $\hat{O}_{H_1}(t)$ is the time-evolution with respect to $\hat{H}_1$. The operator T_c is the contour-ordering operator along the contour c as depicted in Fig. A.1. For our proof it is convenient to recall the definition (A.18) for the operator $\hat{S}$:

$$\hat{S}(t,t_0) = \lim_{M\to\infty} \mathrm{e}^{-\frac{\mathrm{i}}{\hbar}\epsilon\hat{H}'_{H_1}(t_{M-1})}\mathrm{e}^{-\frac{\mathrm{i}}{\hbar}\epsilon\hat{H}'_{H_1}(t_{M-2})}\ldots\mathrm{e}^{-\frac{\mathrm{i}}{\hbar}\epsilon\hat{H}'_{H_1}(t_1)}\mathrm{e}^{-\frac{\mathrm{i}}{\hbar}\epsilon\hat{H}'_{H_1}(t_0)}. \tag{A.21}$$

Analogously to the time-ordering, Eq. (A.14), the contour-ordering in Eq. (A.20) can be discretized as an infinite product over infinitesimal steps along the contour. Equation (A.20) can therefore be rewritten as follows:

$$\begin{aligned}\hat{O}_H(t) = &\lim_{N\to\infty} \mathrm{e}^{\frac{\mathrm{i}}{\hbar}\epsilon'\hat{H}'_{H_1}(t'_0)}\mathrm{e}^{\frac{\mathrm{i}}{\hbar}\epsilon'\hat{H}'_{H_1}(t'_1)}\ldots\mathrm{e}^{\frac{\mathrm{i}}{\hbar}\epsilon'\hat{H}'_{H_1}(t'_{N-1})}\\ &\times\hat{O}_{H_1}(t)\lim_{M\to\infty}\mathrm{e}^{-\frac{\mathrm{i}}{\hbar}\epsilon\hat{H}'_{H_1}(t_{M-1})}\mathrm{e}^{-\frac{\mathrm{i}}{\hbar}\epsilon\hat{H}'_{H_1}(t_{M-2})}\ldots\mathrm{e}^{-\frac{\mathrm{i}}{\hbar}\epsilon\hat{H}'_{H_1}(t_0)},\end{aligned} \tag{A.22}$$

where $\epsilon = (t-t_0)/M$, $\epsilon' = (t-t_0)/N$, $t_n = t_0 + n\epsilon$, and $t'_n = t_0 + n\epsilon'$. Equation (A.19) now follows immediately by inserting Eq. (A.21) and its adjunct, thus the equivalence of Eqs. (A.19) and (A.20) is shown. Note, that also a combinatorial proof similar to the first proof in App. A.1 is possible, see Ref. 96 for instance.

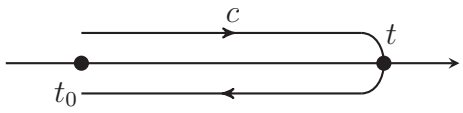

FIG. A.1.: The closed time path contour c.

B

Gradient expansion

The gradient expansion is a convenient form of the Fourier transform of some convolution

$$\left(\check{A} \otimes \check{B}\right)(1,1') = \left(\check{A} \otimes \check{B}\right)\left(x + \frac{y}{2}, x - \frac{y}{2}\right) \tag{B.1}$$

with respect to the relative coordinate y as defined in Eq. (2.125). Here, we first derive the gradient expansion of ordinary objects in Keldysh space and second, directly for locally covariant objects as defined in Sec. 2.4.

B.1. Common gradient expansion

In Wigner coordinates, the integrand which we find in the convolution (B.1) reads

$$\begin{aligned}\check{A}\left(x + \frac{y}{2}, 2\right)\check{B}\left(2, x - \frac{y}{2}\right) \\ = \check{A}\left(x_1 + \frac{y_1}{2}, x_1 - \frac{y_1}{2}\right)\check{B}\left(x_2 + \frac{y_2}{2}, x_2 - \frac{y_2}{2}\right),\end{aligned} \tag{B.2}$$

where $x_1 = (1+2)/2$, $x_2 = (2+1')/2$, $y_1 = 1-2$, and $y_2 = 2-1'$. By comparison of the variables we have

$$x + \frac{y}{2} = x_1 + \frac{y_1}{2} = 1\,, \tag{B.3}$$

$$x_1 - \frac{y_1}{2} = x_2 + \frac{y_2}{2} = 2\,, \tag{B.4}$$

$$x - \frac{y}{2} = x_2 - \frac{y_2}{2} = 1'\,, \tag{B.5}$$

thus the inner variable can be expressed by

$$2 = x - \frac{y_1 - y_2}{2}\,. \tag{B.6}$$

The differential volume element $\mathrm{d}y_1\mathrm{d}y_2$ equals $\mathrm{d}y\mathrm{d}2$ and therefore the Fourier transform of the convolution (B.1) can be rewritten as

$$\left(\check{A}\otimes\check{B}\right)(x,p)=\int\mathrm{d}y_1\int\mathrm{d}y_2\,\check{A}\left(x+\frac{y_1+y_2}{2},x-\frac{y_1-y_2}{2}\right)\\ \times\check{B}\left(x-\frac{y_1-y_2}{2},x-\frac{y_1+y_2}{2}\right)\mathrm{e}^{-\frac{\mathrm{i}}{\hbar}p_\mu y_1^\mu}\mathrm{e}^{-\frac{\mathrm{i}}{\hbar}p_\nu y_2^\nu}\,. \tag{B.7}$$

The next step is to perform the Taylor expansion of $\check{A}$ and $\check{B}$ in powers of $y_2/2$ and $-y_1/2$, respectively. Explicitly, the Taylor expansion of $\check{A}$ reads

$$\check{A}\left(x+\frac{y_1+y_2}{2},x-\frac{y_1-y_2}{2}\right)=\sum_{n=0}^{\infty}\frac{1}{n!}\left(\frac{y_2^\mu}{2}\partial_\mu\right)^n\check{A}\left(x+\frac{y_1}{2},x-\frac{y_1}{2}\right)\,. \tag{B.8}$$

In addition, we utilize

$$\left(\frac{y_2^\mu}{2}\right)^n\mathrm{e}^{-\frac{\mathrm{i}}{\hbar}p_\nu y_2^\nu}=\left(\frac{\mathrm{i}\hbar}{2}\partial_p^\mu\right)^n\mathrm{e}^{-\frac{\mathrm{i}}{\hbar}p_\nu y_2^\nu}\,, \tag{B.9}$$

and with the analogous expressions for $\check{B}$ the Fourier transform (B.7) becomes

$$\left(\check{A}\otimes\check{B}\right)(x,p)=\sum_{m=0}^{\infty}\sum_{n=0}^{\infty}\frac{1}{m!}\frac{1}{n!}\left(\frac{\mathrm{i}\hbar}{2}\right)^m\left(-\frac{\mathrm{i}\hbar}{2}\right)^n\\ \times\int\mathrm{d}y_1\,\left[(\partial_\mu)^m\check{A}\left(x+\frac{y_1}{2},x-\frac{y_1}{2}\right)\right]\left((\partial_p^\nu)^n\mathrm{e}^{-\frac{\mathrm{i}}{\hbar}p_\rho y_1^\rho}\right)\\ \times\int\mathrm{d}y_2\,\left[(\partial_\nu)^n\check{B}\left(x+\frac{y_2}{2},x-\frac{y_2}{2}\right)\right]\left((\partial_p^\mu)^m\mathrm{e}^{-\frac{\mathrm{i}}{\hbar}p_\lambda y_2^\lambda}\right)\,. \tag{B.10}$$

Since the integrals are now separated we are able to perform the Fourier transformation, respectively, and we finally obtain

$$\left(\check{A}\otimes\check{B}\right)(x,p)=\mathrm{e}^{\frac{\mathrm{i}\hbar}{2}\left[(\partial_\mu)^{\check{A}}(\partial_p^\mu)^{\check{B}}-(\partial_\nu)^{\check{B}}(\partial_p^\nu)^{\check{A}}\right]}\check{A}(x,p)\check{B}(x,p)\,, \tag{B.11}$$

where the superscript of the partial derivatives denotes the object on which the respective derivative acts.

B.2. Gradient expansion of locally covariant objects

According to Eq. (2.131) the locally covariant forms of $\check{A}(1,2)$ and $\check{B}(2,1')$ are given by

$$\check{\tilde{A}}(1,2) = U_{\Gamma_A}(x,1)\check{A}(1,2)U_{\Gamma'_A}(2,x)\,, \tag{B.12}$$

$$\check{\tilde{B}}(2,1') = U_{\Gamma_B}(x,2)\check{B}(2,1')U_{\Gamma'_B}(1',x)\,, \tag{B.13}$$

respectively. The Wilson lines up to first order in the four-potential A^μ read

$$U_{\Gamma_A}(x,1) \approx 1 - \frac{\mathrm{i}e}{\hbar}(x_\mu - 1_\mu)A^\mu(x)\,, \tag{B.14}$$

$$U_{\Gamma'_A}(2,x) \approx 1 - \frac{\mathrm{i}e}{\hbar}(2_\mu - x_\mu)A^\mu(x)\,, \tag{B.15}$$

$$U_{\Gamma_B}(x,2) \approx 1 - \frac{\mathrm{i}e}{\hbar}(x_\mu - 2_\mu)A^\mu(x)\,, \tag{B.16}$$

$$U_{\Gamma'_B}(1',x) \approx 1 - \frac{\mathrm{i}e}{\hbar}(1'_\mu - x_\mu)A^\mu(x)\,. \tag{B.17}$$

Using Wigner coordinates analogously to App. B.1 with $x-1 = 1'-x = -(y_1+y_2)/2$ and $2-x = -(x-2) = -(y_1-y_2)/2$ we obtain

$$\check{\tilde{A}} \approx \check{A} + \frac{\mathrm{i}e}{2\hbar}y_1^\mu\Big\{A_\mu,\,\check{A}\Big\} + \frac{\mathrm{i}e}{2\hbar}y_2^\nu\Big[A_\nu,\,\check{A}\Big]\,, \tag{B.18}$$

$$\check{\tilde{B}} \approx \check{B} + \frac{\mathrm{i}e}{2\hbar}y_2^\mu\Big\{A_\mu,\,\check{B}\Big\} - \frac{\mathrm{i}e}{2\hbar}y_1^\nu\Big[A_\nu,\,\check{B}\Big]\,. \tag{B.19}$$

Inserting the Taylor expansion of $\check{A}$ and $\check{B}$, and allowing terms up to linear order in y_2 and y_1, respectively, then leads to

$$\check{\tilde{A}} \approx \check{\tilde{A}}(0) + \frac{y_2^\mu}{2}\tilde{\partial}_\mu\check{A}(0)\,, \tag{B.20}$$

$$\check{\tilde{B}} \approx \check{\tilde{B}}(0) - \frac{y_1^\mu}{2}\tilde{\partial}_\mu\check{B}(0)\,, \tag{B.21}$$

where the argument of $\check{\tilde{A}}$, $\check{A}$ and $\check{\tilde{B}}$, $\check{B}$ on the r.h.s. of Eqs. (B.20) and (B.21) is meant in the sense that $y_2 = 0$ and $y_1 = 0$, respectively. Here,

$$\tilde{\partial}_\mu = \partial_\mu + \frac{\mathrm{i}e}{\hbar}\Big[A_\mu,\,\cdot\,\Big] \tag{B.22}$$

is the covariant derivative. Employing Eqs. (B.20) and (B.21), the Fourier transform of the convolution of $\check{A}$ and $\check{B}$ with respective to the relative coordinate reads

$$\left(\check{\tilde{A}} \otimes \check{\tilde{B}}\right)(x,p) \approx \check{\tilde{A}}\check{\tilde{B}} + \frac{\mathrm{i}\hbar}{2}\left(\tilde{\partial}_\mu \check{A}\right)\left(\partial_p^\mu \check{B}\right) - \frac{\mathrm{i}\hbar}{2}\left(\partial_p^\nu \check{A}\right)\left(\tilde{\partial}_\nu \check{B}\right). \tag{B.23}$$

Allowing terms up to the order $\mathcal{O}(\tilde{\partial}_\mu \partial_p^\mu)$ we can replace $\check{A}$ and $\check{B}$ on the r.h.s. of Eq. (B.23) with $\check{\tilde{A}}$ and $\check{\tilde{B}}$, respectively, and obtain

$$\left(\check{\tilde{A}} \otimes \check{\tilde{B}}\right)(x,p) \approx \check{\tilde{A}}\check{\tilde{B}} + \frac{\mathrm{i}\hbar}{2}\left(\tilde{\partial}_\mu \check{\tilde{A}}\right)\left(\partial_p^\mu \check{\tilde{B}}\right) - \frac{\mathrm{i}\hbar}{2}\left(\partial_p^\nu \check{\tilde{A}}\right)\left(\tilde{\partial}_\nu \check{\tilde{B}}\right). \tag{B.24}$$

Therefore, the gradient expansion up to $\mathcal{O}(\tilde{\partial}_\mu \partial_p^\mu)$ for locally covariant objects has the same form as the usual gradient expansion with the only difference that the derivative ∂_μ is replaced by the covariant derivative $\tilde{\partial}_\mu$.

We remark that the above expression is usually sufficient when $\check{A}$ and $\check{B}$ are self-energies and/or full Green's functions. However, it turns out to that the expansion (B.24) is insufficient for obtaining the l.h.s. of the Boltzmann equation (2.153). In this case, we encounter the inverse of the free Green's function, Eq. (2.142), whose locally covariant form is given by

$$\check{\tilde{G}}_0^{-1} = \epsilon - \frac{\mathbf{p}^2}{2m}. \tag{B.25}$$

Thus, using Eq. (B.24) in order to obtain the l.h.s. of the Boltzmann equation, see Eq. (2.120), gives only

$$-\mathrm{i}\left[\check{\tilde{G}}_0^{-1} \overset{\otimes}{,} \check{\tilde{G}}\right] = v^\mu \tilde{\partial}_\mu \check{\tilde{G}}, \tag{B.26}$$

such that the force term is missing compared to Eq. (2.148). We recall that we have allowed terms up to the next-to-leading order $\sim \mathcal{O}(A_\mu A_\nu \partial^\mu, A_\mu A_\nu \partial_p^\mu)$ in the derivation of Eq. (2.148). Since $\check{\tilde{G}}_0^{-1}$ is not at least linear in the four-potential, the gradient expansion (B.24) obviously cannot deliver terms $\sim \mathcal{O}(A_\mu A_\nu \partial^\mu, A_\mu A_\nu \partial_p^\mu)$. Therefore, we have to consider the Wilson line up to the second order in the potential, which leads to

the following expressions for $\overset{\scriptscriptstyle\diamond}{\tilde{A}}$ and $\overset{\scriptscriptstyle\diamond}{\tilde{B}}$,[1]

$$\overset{\scriptscriptstyle\diamond}{\tilde{A}} \approx \overset{\scriptscriptstyle\diamond}{\tilde{A}}(0) + \frac{y_2^\mu}{2}\tilde{\partial}_\mu \overset{\scriptscriptstyle\diamond}{\tilde{A}}(0) - \frac{y_1^\nu y_2^\mu}{4\hbar^2}\left(\mathrm{i}e\hbar\Big\{ (\partial_\mu A_\nu)\,,\, \overset{\scriptscriptstyle\diamond}{\tilde{A}}(0)\Big\} - \frac{e^2}{2}\Big\{\Big[A_\mu,\, A_\nu\Big],\, \overset{\scriptscriptstyle\diamond}{\tilde{A}}(0)\Big\}\right)\,, \tag{B.27}$$

$$\overset{\scriptscriptstyle\diamond}{\tilde{B}} \approx \overset{\scriptscriptstyle\diamond}{\tilde{B}}(0) - \frac{y_1^\mu}{2}\tilde{\partial}_\mu \overset{\scriptscriptstyle\diamond}{\tilde{B}}(0) + \frac{y_1^\mu y_2^\nu}{4\hbar^2}\left(\mathrm{i}e\hbar\Big\{ (\partial_\mu A_\nu)\,,\, \overset{\scriptscriptstyle\diamond}{\tilde{B}}(0)\Big\} - \frac{e^2}{2}\Big\{\Big[A_\mu,\, A_\nu\Big],\, \overset{\scriptscriptstyle\diamond}{\tilde{B}}(0)\Big\}\right)\,. \tag{B.28}$$

As a consequence, the gradient expansion features additional terms in the four-potential,

$$\begin{aligned}\left(\overset{\scriptscriptstyle\diamond}{\tilde{A}} \otimes \overset{\scriptscriptstyle\diamond}{\tilde{B}}\right)(x,p) =& \overset{\scriptscriptstyle\diamond}{\tilde{A}}\overset{\scriptscriptstyle\diamond}{\tilde{B}} + \frac{\mathrm{i}\hbar}{2}\left(\tilde{\partial}_\mu \overset{\scriptscriptstyle\diamond}{\tilde{A}}\right)\left(\partial_p^\mu \overset{\scriptscriptstyle\diamond}{\tilde{B}}\right) - \frac{\mathrm{i}\hbar}{2}\left(\partial_p^\mu \overset{\scriptscriptstyle\diamond}{\tilde{A}}\right)\left(\tilde{\partial}_\mu \overset{\scriptscriptstyle\diamond}{\tilde{B}}\right) \\ &+ \frac{\mathrm{i}e\hbar}{4}\left[\Big\{ (\partial_\mu A_\nu)\,,\, \left(\partial_p^\nu \overset{\scriptscriptstyle\diamond}{\tilde{A}}\right)\Big\} + \frac{\mathrm{i}e}{2\hbar}\Big\{\Big[A_\mu,\, A_\nu\Big],\, \left(\partial_p^\nu \overset{\scriptscriptstyle\diamond}{\tilde{A}}\right)\Big\}\right]\left(\partial_p^\mu \overset{\scriptscriptstyle\diamond}{\tilde{B}}\right) \\ &- \frac{\mathrm{i}e\hbar}{4}\left(\partial_p^\mu \overset{\scriptscriptstyle\diamond}{\tilde{A}}\right)\left[\Big\{ (\partial_\mu A_\nu)\,,\, \left(\partial_p^\nu \overset{\scriptscriptstyle\diamond}{\tilde{B}}\right)\Big\} + \frac{\mathrm{i}e}{2\hbar}\Big\{\Big[A_\mu,\, A_\nu\Big],\, \left(\partial_p^\nu \overset{\scriptscriptstyle\diamond}{\tilde{B}}\right)\Big\}\right]\,.\end{aligned} \tag{B.29}$$

This form of the gradient expansion then results in the same expression as the l.h.s. of Eq. (2.148) for $-\mathrm{i}\left[\overset{\scriptscriptstyle\diamond}{\tilde{G}_0^{-1}} \underset{\diamond}{\otimes} \overset{\scriptscriptstyle\diamond}{\tilde{G}}\right]$.

[1] Note that we have neglected quadratic terms $\sim y_1^\mu y_1^\nu$ and $\sim y_2^\mu y_2^\nu$ since these terms lead to a second momentum four-derivative acting on a single object.

C

Elliott-Yafet collision operator

Appendix B.2 allows us to obtain the needed second-order correction for the Elliott-Yafet collision operator fairly easy. Here, we are interested in the contribution to the charge sector by the product of Ψ^a and $\mathcal{A}_i^a$ (mixed second-order in the following), together with the equilibrium particle distribution function. Regarding the last point, we assume the Keldysh component of the Green's function to be given by

$$\tilde{G}^K_{\mathrm{eq}}(x,p) \approx -2\pi \mathrm{i}\hbar\delta(\epsilon-\epsilon_{\mathbf{p}})\big(1-2f^0_{\mathrm{eq}}\big)\,. \tag{C.1}$$

Here, with the nonzero components of eA^μ being either given by $\Psi^a\sigma^a/2$ or $\mathcal{A}_i^a\sigma^a/2$, and $\check{\tilde{G}}_{\mathrm{eq}}$ featuring no spin component, the only relevant second-order contribution to the collision kernel is

$$-\,\mathrm{i}\left[\check{\tilde{\Sigma}}_{\mathrm{EY}} \mathbin{\overset{\otimes}{,}} \check{\tilde{G}}_{\mathrm{eq}}\right]^{\boldsymbol{\mathcal{A}},\Psi} = -\mathrm{i}\Big[\check{\tilde{\Sigma}}^{\boldsymbol{\mathcal{A}},\Psi}_{\mathrm{EY}},\, \check{\tilde{G}}_{\mathrm{eq}}\Big]\,, \tag{C.2}$$

since the other mixed second-order terms in Eq. (B.29) appear linear in the Pauli vector and thus do not contribute to the charge sector. Expanding the Wilson line up to the second order in the four-potential and Fourier transforming with respect to the relative coordinate yields the following covariant form of the Elliott-Yafet self-energy:

$$\check{\tilde{\Sigma}}_{\mathrm{EY}} = \check{\Sigma}_{\mathrm{EY}} + \frac{e}{2}\Big\{A_\mu,\, \partial_p^\mu\check{\Sigma}_{\mathrm{EY}}\Big\} + \frac{e^2}{4}A_\mu\partial_p^\mu\partial_p^\nu\check{\Sigma}_{\mathrm{EY}}A_\nu + \frac{e^2}{8}\Big\{A_\mu A_\nu,\, \partial_p^\mu\partial_p^\nu\check{\Sigma}_{\mathrm{EY}}\Big\}\,. \tag{C.3}$$

Inserting the corresponding Green's function

$$\check{G}_{\mathrm{eq}} = \check{\tilde{G}}_{\mathrm{eq}} - \frac{e}{2}\Big\{A_\mu,\, \partial_p^\mu\check{\tilde{G}}_{\mathrm{eq}}\Big\} + \frac{e^2}{4}A_\mu\partial_p^\mu\partial_p^\nu\check{\tilde{G}}_{\mathrm{eq}}A_\nu + \frac{e^2}{8}\Big\{A_\mu A_\nu,\, \partial_p^\mu\partial_p^\nu\check{\tilde{G}}_{\mathrm{eq}}\Big\} \tag{C.4}$$

into $\check{\Sigma}_{\mathrm{EY}}$, see Eq. (2.182), leads to the following second-order contribution:

$$\begin{aligned}\check{\tilde{\Sigma}}^{A_\mu,A_\nu}_{\mathrm{EY}} = -\frac{n_i v_0^2 e^2}{4\hbar^2}\left(\frac{\lambda}{2\hbar}\right)^4\int\frac{\mathrm{d}^2p'}{(2\pi\hbar)^2}\Bigg[&\Big\{A_\mu,\, \partial_p^\mu(\mathbf{p}\times\mathbf{p}')_z^2\sigma^z\Big\{A_\nu,\, \partial_{p'}^\nu\check{\tilde{G}}_{\mathrm{eq}}\Big\}\sigma^z\Big\}\\ &- A_\mu\partial_p^\mu\partial_p^\nu(\mathbf{p}\times\mathbf{p}')_z^2\sigma^z\check{\tilde{G}}_{\mathrm{eq}}\sigma^z A_\nu\\ &- \frac{1}{2}\Big\{A_\mu A_\nu,\, \partial_p^\mu\partial_p^\nu(\mathbf{p}\times\mathbf{p}')_z^2\sigma^z\check{\tilde{G}}_{\mathrm{eq}}\sigma^z\Big\}\Bigg]\,,\end{aligned} \tag{C.5}$$

Equation (C.5) reduces to

$$\check{\check{\Sigma}}^{\boldsymbol{\mathcal{A}},\Psi}_{\mathrm{EY}} = \frac{1}{4\pi\tau}\left(\frac{\lambda}{2\hbar}\right)^4 \boldsymbol{\Psi}\cdot\boldsymbol{\mathcal{A}}_i p_i \int \mathrm{d}\epsilon_{\mathbf{p}'} p'^2 \partial_\epsilon \check{\check{G}}_{\mathrm{eq}}\,, \tag{C.6}$$

when employing that $\check{\check{G}}_{\mathrm{eq}}$ has no spin component, only considering the mixed terms, preforming the angular average, and neglecting terms $\sim \sigma^a$. Inserting Eq. (C.6) into Eq. (C.2) and following the outline given in Sec. 2.5 then leads to the collision operator $I^{\boldsymbol{\mathcal{A}},\Psi}_{\mathrm{EY}}$ as given in Eq. (2.200).

D

Landau-Lifshitz-Gilbert equation

In this appendix, we derive a Landau-Lifshitz-Gilbert equation which describes the spin density dynamics of itinerant electrons coupled to an effective magnetic field $\mathbf{H}_{\text{eff}}$ via a magnetic exchange interaction. The Hamiltonian is given by

$$\mathcal{H}_{\text{mag}} = -\mu_0 \boldsymbol{\mu} \cdot \mathbf{H}_{\text{eff}}(\mathbf{r}, t)\,, \tag{D.1}$$

where μ_0 is the magnetic constant and $\boldsymbol{\mu}$ is the spin magnetic moment of an electron given by

$$\boldsymbol{\mu} = \frac{\hbar\gamma}{2}\boldsymbol{\sigma}\,, \tag{D.2}$$

with the gyromagnetic ratio $\gamma = -g_e e/2m$, where $g_e \approx 2$ is the electron g-factor. In this case, the SU(2) scalar potential reads

$$\boldsymbol{\Psi}(\mathbf{r}, t) = -\hbar\mu_0|\gamma|\mathbf{H}_{\text{eff}}(\mathbf{r}, t)\,, \tag{D.3}$$

which corresponds to $\Delta_{\text{xc}}\mathbf{n} \to -\hbar\mu_0|\gamma|\mathbf{H}_{\text{eff}}$ in Chap. 4. Analogously to Eq. (4.17), a momentum integration over the spin sector of the Boltzmann equation leads to

$$\tilde{\partial}_t \delta\mathbf{s} = -\frac{1}{\tau_s}\delta\mathbf{s} + \frac{\hbar\mu_0|\gamma|N_0}{2}\dot{\mathbf{H}}_{\text{eff}} + \mathbf{T}[\mathbf{s}, \mathbf{j}^a, n, \mathbf{j}]\,. \tag{D.4}$$

For the sake of simplicity, we assume an isotropic spin-flip relaxation. Furthermore, we have introduced $\mathbf{T}$ as a general functional of the spin density, the spin current, the electron density, and the charge current, which in the end corresponds to a torque term in the Landau-Lifshitz-Gilbert equation. For example, in case of Rashba spin-orbit coupling, $\mathbf{T}$ can be identified with $-\tilde{\nabla}_i \mathbf{j}_i$, cf. Eq. (4.17). By inserting $\delta\mathbf{s} = \mathbf{s} + \hbar\mu_0|\gamma|N_0\mathbf{H}_{\text{eff}}/2$, cf. Eq. (4.11), into Eq. (D.4), and rearranging the terms we obtain

$$\partial_t \hat{\mathbf{s}} + \frac{1}{\tau_s}\hat{\mathbf{s}} = -\mu_0|\gamma|\alpha_{\text{G}}\left(1 + \frac{1}{\alpha_{\text{G}}}[\hat{\mathbf{s}}]_\times\right)\mathbf{H}_{\text{eff}} + \frac{\mathbf{T}}{|\mathbf{s}|}\,, \tag{D.5}$$

where $\alpha_{\mathrm{G}} = \hbar N_0/2\tau_s|\mathbf{s}|$ is the Gilbert damping constant and $\hat{\mathbf{s}} = \mathbf{s}/|\mathbf{s}|$ is the direction of the spin density. A multiplication of Eq. (D.5) with the matrix

$$\frac{1+\alpha_{\mathrm{G}}^2}{\alpha_{\mathrm{G}}}[\hat{\mathbf{s}}]_\times \left(1 + \frac{1}{\alpha_{\mathrm{G}}}[\hat{\mathbf{s}}]_\times\right)^{-1} = (\alpha_{\mathrm{G}} - [\hat{\mathbf{s}}]_\times)\,[\hat{\mathbf{s}}]_\times\,, \tag{D.6}$$

use of $\hat{\mathbf{s}} \times (\hat{\mathbf{s}} \times \partial_t \hat{\mathbf{s}}) = -\partial_t \hat{\mathbf{s}}$, and a rearrangement of the terms then finally leads to a Landau-Lifshitz-Gilbert-like equation,

$$\partial_t \hat{\mathbf{s}} = -\mu_0|\gamma|(1+\alpha_{\mathrm{G}}^2)\,\hat{\mathbf{s}} \times \mathbf{H}_{\mathrm{eff}} - \alpha_{\mathrm{G}}\,\hat{\mathbf{s}} \times \partial_t \hat{\mathbf{s}} + \boldsymbol{\tau}\,. \tag{D.7}$$

The torque $\boldsymbol{\tau}$ is associated with the functional $\mathbf{T}$ and given by

$$\boldsymbol{\tau} = \frac{1}{|\mathbf{s}|}\,(\alpha_{\mathrm{G}} - [\hat{\mathbf{s}}]_\times)\,(\hat{\mathbf{s}} \times \mathbf{T})\,. \tag{D.8}$$

Note that the procedure outlined in this appendix, taking a continuity equation (D.5) and transforming it to a Landau-Lifshitz-Gilbert equation (D.7), is quite general. Thus, a microscopic derivation of a Landau-Lifshitz-Gilbert equation, including torques, is possible once one has microscopically derived a kinetic equation such as Eq. (D.5).

E

Appendix to chapter 4

In this appendix, we assume the narrow wire setup as introduced in Sec. 4.2 in the homogeneous case and show that the contribution which is polarized parallel to the magnetization of the spin current flowing in the narrow direction vanishes. The narrow wire is considered to be aligned along x direction, i.e., $\ell_y \ll l_s$ and $\ell_x \gg l_s$. Furthermore, we assume an open circuit condition, $\mathbf{j}_y(y=0) = \mathbf{j}_y(y=\ell_y) = 0$ as well as, for the sake of simplicity, isotropic spin-flip relaxation ($\zeta = 1$).

Due to the homogeneous situation it is reasonable to assume that the spin current which flows in x direction is homogeneous as well, thus given by Eqs. (4.25)–(4.27) with $\tilde{\nabla}_x \to -(1/\hbar)[\boldsymbol{\mathcal{A}}_x]_\times$. According to Eqs. (4.18)–(4.20) the spin density can be expressed as

$$\delta\mathbf{s}(y) = \delta\mathbf{s}_0 - \tau_s M_s^{-1}\tilde{\nabla}_y \mathbf{j}_y(y) \tag{E.1}$$

with

$$\delta\mathbf{s}_0 = (\delta\mathbf{s})_\mathbf{n} + \frac{\tau_s}{\hbar} M_s^{-1}[\boldsymbol{\mathcal{A}}_x]_\times \mathbf{j}_x \,. \tag{E.2}$$

In addition, we have introduced $M_s = M(\tau \to \tau_s)$, where M, according to Eq. (4.22), is explicitly given by

$$M = 1 + \frac{\Delta_{\text{xc}}\tau}{\hbar}[\mathbf{n}]_\times = \beta_\tau^{-1} \begin{pmatrix} \beta_\tau & -n_z & n_y \\ n_z & \beta_\tau & -n_x \\ -n_y & n_x & \beta_\tau \end{pmatrix} , \tag{E.3}$$

where $\beta_\tau = \hbar/\Delta_{\text{xc}}\tau$. Given by Eqs. (4.25)–(4.27), the spin current which flows in y direction reads

$$\mathbf{j}_y(y) = DM^{-1}\tilde{\nabla}_y M^{-1}\left[N_0\beta_\tau^{-1}\dot{\mathbf{n}} - \delta\mathbf{s}(y)\right] . \tag{E.4}$$

Inserting Eq. (E.1) into Eq. (E.4) leads approximately ($\tilde{\nabla}_y \mathbf{j}_y \simeq \nabla_y \mathbf{j}_y$) to the following differential equation:

$$\left(1 - l_s^2 M_s^{-1} M^{-2}\nabla_y^2\right)\mathbf{j}_y(y) = \mathbf{j}_{y,0} \,, \tag{E.5}$$

where the r.h.s. is given by the spatially constant spin current

$$\mathbf{j}_{y,0} = -\frac{D}{\hbar} M^{-1} [\boldsymbol{\mathcal{A}}_y]_\times M^{-1} \left(N_0 \beta_\tau^{-1} \dot{\mathbf{n}} - \delta \mathbf{s}_0 \right) . \tag{E.6}$$

Apparently, $\mathbf{j}_{y,0}$ is a particular solution of the differential equation (E.5). In order to determine the complete solution $\mathbf{j}_y = \mathbf{j}_{y,h} + \mathbf{j}_{y,0}$, we have to add the solution of the homogeneous differential equation, which can be written as follows:

$$\left(M_s M^2 - l_s^2 \nabla_y^2 \right) \mathbf{j}_{y,h}(y) = 0 \, . \tag{E.7}$$

In order to solve Eq. (E.7) it is convenient to change the basis by the following transformation:

$$\mathbb{R} = \begin{pmatrix} n_x & \dot{n}_x/|\dot{\mathbf{n}}| & (\mathbf{n} \times \dot{\mathbf{n}})_x/|\dot{\mathbf{n}}| \\ n_y & \dot{n}_y/|\dot{\mathbf{n}}| & (\mathbf{n} \times \dot{\mathbf{n}})_y/|\dot{\mathbf{n}}| \\ n_z & \dot{n}_z/|\dot{\mathbf{n}}| & (\mathbf{n} \times \dot{\mathbf{n}})_z/|\dot{\mathbf{n}}| \end{pmatrix} , \tag{E.8}$$

which replaces $\mathbf{n}$ with $\mathbf{e}_x$ in Eq. (E.7),

$$\left[\left(1 + \beta_s^{-1} [\mathbf{e}_x]_\times \right) \left(1 + \beta_\tau^{-1} [\mathbf{e}_x]_\times \right)^2 - l_s^2 \nabla_y^2 \right] \tilde{\boldsymbol{j}}_{y,h}(y) = 0, \tag{E.9}$$

where $\tilde{\boldsymbol{j}}_{y,h} = \mathbb{R}^T \mathbf{j}_{y,h}$. Note that in this basis, the x component of $\tilde{\boldsymbol{j}}_{y,h}$ represents the contribution of the spin current which is parallel to the magnetization. The matrix in Eq. (E.9) has the eigenvalue 1 with eigenvector $\mathbf{e}_x$, thus leading to

$$\tilde{j}_{y,h}^x = A \exp\left(-\frac{y}{l_s} \right) + B \exp\left(-\frac{y}{l_s} \right) . \tag{E.10}$$

Therefore, the general solution in the case $\ell_y \ll l_s$ is given by

$$\tilde{j}_y^x = A \left(1 - \frac{y}{l_s} \right) + B \left(1 + \frac{y}{l_s} \right) + \tilde{j}_{y,0}^x \, , \tag{E.11}$$

where $\tilde{j}_{y,0}^x$ is the x component of $\mathbb{R}^T \mathbf{j}_{y,0}$. Employing the boundary conditions, i.e., $\mathbf{j}_y(y = 0) = \mathbf{j}_y(y = \ell_y) = 0$, results in the coefficients

$$A = B = -\frac{1}{2} \tilde{j}_{y,0}^x \, . \tag{E.12}$$

Finally, we insert A and B into Eq. (E.11) and obtain $\tilde{j}_y^x = 0$. Therefore the spin current contribution which is parallel to the magnetization vanishes, $\mathbf{n} \cdot \mathbf{j}_y = 0$.

Last, we remark that the transverse-polarization components of the spin current, i.e., $\tilde{j}_y^y$ and $\tilde{j}_y^z$, do not vanish since the transverse spin relaxation length $l_s^\perp$ is orders of magnitude smaller than l_s [185]. Assuming $\Delta_{\text{xc}} \tau / \hbar \gg 1$ one obtains an explicit solution of the above diffusion equations which yields ${l_s}^\perp < l_s \beta_\tau$.

F

Appendix to chapter 5

In this appendix, we present supplement information for Chap. 5. First, we derive the coupled differential equations (5.3) and (5.4) and present their general solution. Next, we explicitly solve for the spin polarization and the spin currents by assuming a large system and considering the ferromagnet insulator as a boundary condition via the spin transfer torque. Last, Mott-like formulas for the spin-thermoelectric response coefficients are derived and employed, as an example, for the description of the bulk spin Nernst effect.

F.1. Spin diffusion equations

Analogously to Sec. 4.1, the spin sector of the (static) Boltzmann equation can be written as

$$\mathbb{M}\mathbf{f} = \mathbb{N}\langle\mathbf{f}\rangle + \mathbf{S}\,, \tag{F.1}$$

with

$$\mathbb{M} = 2 - \mathbb{N} + \frac{\tau p_y}{m}\nabla_y + \frac{2\alpha\tau}{\hbar^2}\begin{pmatrix} 0 & 0 & p_x \\ 0 & 0 & p_y \\ -p_x & -p_y & 0 \end{pmatrix}\,, \tag{F.2}$$

$$\mathbb{N} = 1 - \frac{\tau}{2\tau_s}\begin{pmatrix} 1 & 0 & 0 \\ 0 & 1 & 0 \\ 0 & 0 & 0 \end{pmatrix}\,, \tag{F.3}$$

$$\begin{aligned} S^a =& \frac{\tau B_z^z}{2m}\left(\mathbf{p}\times\mathbf{e}_z\right)\cdot\left(\nabla_{\mathbf{p}} f^0\right)\delta_{az} \\ &+ \frac{1}{N_0}\left(\frac{\lambda}{2\hbar}\right)^4 \int \frac{\mathrm{d}^2 p'}{(2\pi\hbar)^2}\,\boldsymbol{\mathcal{A}}^a\cdot\mathbf{L}_{\mathbf{p},\mathbf{p}'}\left(f^0_{\mathbf{p}} - f^0_{\mathbf{p}'}\right)\delta(\epsilon_{\mathbf{p}} - \epsilon'_{\mathbf{p}})\,. \end{aligned} \tag{F.4}$$

We integrate Eq. (F.1) over the momentum and by using $j_x = \sigma_{\text{D}} E_x$ we obtain the following equations for the y and z component:

$$s^y = -\tau_s \nabla_y j_y^y - \frac{\tau_s}{l_{\text{DP}}} j_y^z + \frac{\hbar \sigma_{\text{D}}}{4e\epsilon_F l_{\text{DP}}} E_x \,, \tag{F.5}$$

$$\nabla_y j_y^z = \frac{1}{l_{\text{DP}}} \left(j_x^x + j_y^y \right) \,, \tag{F.6}$$

where Eq. (F.5) coincides with Eq. (5.5) in Sec. 5.1. Furthermore, Eq. (F.1) can be rewritten as

$$\mathbf{f} = \mathbb{M}^{-1} \left(\mathbb{N} \langle \mathbf{f} \rangle + \mathbf{S} \right) \,, \tag{F.7}$$

where, in the diffusive limit and with $\tau_s \gg \tau$,

$$\mathbb{M}^{-1} \approx 1 - \frac{\tau p_y}{m} \nabla_y - \frac{2\alpha\tau}{\hbar^2} \begin{pmatrix} 0 & 0 & p_x \\ 0 & 0 & p_y \\ -p_x & -p_y & 0 \end{pmatrix} \,. \tag{F.8}$$

A multiplication of Eq. (F.7) with $p_{x,y}/m$ and an integration over the momentum yields

$$j_x^x = -\frac{D s^z}{l_{\text{DP}}} \,, \tag{F.9}$$

$$j_y^y = -D \nabla_y s^y - \frac{D s^z}{l_{\text{DP}}} \,, \tag{F.10}$$

$$j_y^z = -D \nabla_y s^z + \frac{D s^y}{l_{\text{DP}}} + \frac{\hbar \sigma_{\text{D}}}{4e\epsilon_F \tau_{\text{DP}}} E_x \,. \tag{F.11}$$

We insert Eq. (F.9) into Eq. (F.6) and obtain

$$s^z = -\tau_{\text{DP}} \nabla_y j_y^z + \frac{\tau_{\text{DP}}}{l_{\text{DP}}} j_y^y \,, \tag{F.12}$$

as presented by Eq. (5.6). Inserting Eqs. (F.5) and (F.12) into Eqs. (F.10) and (F.11), respectively, leads to the following coupled differential equations:

$$\left(2 - l_s^2 \nabla_y^2 \right) j_y^y = \frac{l_s^2 + l_{\text{DP}}^2}{l_{\text{DP}}} \nabla_y j_y^z \,, \tag{F.13}$$

$$\left(1 + \frac{\tau_s}{\tau_{\text{DP}}} - l_{\text{DP}}^2 \nabla_y^2 \right) j_y^z = -\frac{l_s^2 + l_{\text{DP}}^2}{l_{\text{DP}}} \nabla_y j_y^y + \frac{\hbar \sigma_{\text{D}}}{2e\epsilon_F \tau_{\text{DP}}} E_x \,, \tag{F.14}$$

cf. Eqs. (5.3) and (5.4) in Sec. 5.1. The general solution of the latter set of equations reads[1]

$$\begin{aligned} j_y^y =& \exp(q_- y)\left[(A_- + B_+)\cos(q_+ y) - (A_+ - B_-)\sin(q_+ y)\right] \\ & - \exp(-q_- y)\left[(C_- - D_+)\cos(q_+ y) + (C_+ + D_-)\sin(q_+ y)\right], \end{aligned} \tag{F.15}$$

$$\begin{aligned} j_y^z =& j_0^z + \exp(q_- y)\left[A\cos(q_+ y) + B\sin(q_+ y)\right] \\ & + \exp(-q_- y)\left[C\cos(q_+ y) + D\sin(q_+ y)\right], \end{aligned} \tag{F.16}$$

where $q_\pm$ is given in Eq. (5.12), and

$$A_\pm = \frac{\tau_{\text{DP}}}{\tau_{\text{DP}} + \tau_s}\frac{q_\pm}{2}\left(2 \pm l_s^2|q|^2\right) A\,, \tag{F.17}$$

with $|q|^2 \equiv q_+^2 + q_-^2$; $B_\pm$, $C_\pm$, and $D_\pm$ are defined analogously to $A_\pm$.

F.2. Large system sizes

In the case $\ell_y \gg l_{\text{DP}}$ it is possible to consider a semi-infinite system with appropriate boundary conditions at $y = 0$, and formulate a approximate solution for finite systems by applying the symmetry relations discussed in Sec. 5.1.

Assuming $g_r^{\uparrow\downarrow} = 0$ the spin currents must vanish at the interface, and thus the boundary conditions are given by

$$j_y^y(0) = 0\,, \quad j_y^y(y \to \infty) = 0\,, \tag{F.18}$$

$$j_y^z(0) = 0\,, \quad j_y^z(y \to \infty) = j_0^z\,. \tag{F.19}$$

Employing the general solution of Eqs. (F.15) and (F.16) with use of these boundary conditions we obtain the spin currents as follows:

$$j_y^y = \frac{j_0^z}{2 + l_s^2|q|^2}\frac{l_{\text{DP}}|q|^2}{q_+}\left(1 + \frac{\tau_s}{\tau_{\text{DP}}}\right)\exp(-q_- y)\sin(q_+ y)\,, \tag{F.20}$$

$$\begin{aligned} j_y^z =& j_0^z - \frac{j_0^z}{2 + l_s^2|q|^2}\exp(-q_- y) \\ & \times\left[\left(2 + l_s^2|q|^2\right)\cos(q_+ y) + \frac{q_-}{q_+}\left(2 - l_s^2|q|^2\right)\sin(q_+ y)\right]. \end{aligned} \tag{F.21}$$

[1] The solutions presented here are valid for $\tau_s \gg \tau_{\text{DP}}$. More generally, these solutions are still correct when the requirement $\tau_s/\tau_{\text{DP}} > 1/(5 + 4\sqrt{2})$ is fulfilled such that q_+ is real.

According to Eqs. (F.5) and (F.12) the corresponding expressions for the spin densities are given by

$$\begin{aligned} s^y =& s_0^y + \frac{2s_0^y}{2+l_s^2|q|^2}\frac{\tau_s}{\tau_{\text{DP}}-\tau_s}\exp(-q_-y) \\ &\times\left[\left(2-l_{\text{DP}}^2|q|^2\right)\cos(q_+y)+\frac{q_-}{q_+}\left(2+l_{\text{DP}}^2|q|^2\right)\sin(q_+y)\right], \end{aligned} \tag{F.22}$$

$$\begin{aligned} s^z =& -\frac{s_0^y}{2+l_s^2|q|^2}\frac{\tau_s}{\tau_{\text{DP}}-\tau_s}\exp(-q_-y) \\ &\times\left[4l_{\text{DP}}^3q_-|q|^2\cos(q_+y)+\frac{\tau_{\text{DP}}-\tau_s}{\tau_s}\frac{l_{\text{DP}}|q|^2}{q_+}\sin(q_+y)\right]. \end{aligned} \tag{F.23}$$

In the case $g_r^{\uparrow\downarrow} > 0$ the boundary conditions for a semi-infinite system read

$$j_y^y(0) = j_{\text{FM}}^y\,,\quad j_y^y(y\to\infty) = 0\,, \tag{F.24}$$

$$j_y^z(0) = j_{\text{FM}}^z\,,\quad j_y^z(y\to\infty) = j_0^z\,, \tag{F.25}$$

where, for the time being, we assume that the boundary values of the spin currents, j_{FM}^y and j_{FM}^z, are given. Adjusting the general solution, Eqs. (F.15) and (F.16), to the boundary conditions we get

$$\begin{aligned} \Delta j_y^y = \frac{\exp(-q_-y)}{2+l_s^2|q|^2}\Bigg\{& j_{\text{FM}}^y\Big[\left(2+l_s^2|q|^2\right)\cos(q_+y)-\frac{q_-}{q_+}\left(2-l_s^2|q|^2\right)\sin(q_+y)\Big] \\ &- j_{\text{FM}}^z\left(1+\frac{\tau_s}{\tau_{\text{DP}}}\right)\frac{l_{\text{DP}}|q|^2}{q_+}\sin(q_+y)\Bigg\}, \end{aligned} \tag{F.26}$$

$$\begin{aligned} \Delta j_y^z = \frac{\exp(-q_-y)}{2+l_s^2|q|^2}\Bigg\{& j_{\text{FM}}^y\left(1+\frac{\tau_s}{\tau_{\text{DP}}}\right)\frac{2}{l_{\text{DP}}q_+}\sin(q_+y) \\ &+ j_{\text{FM}}^z\Big[\left(2+l_s^2|q|^2\right)\cos(q_+y)+\frac{q_-}{q_+}\left(2-l_s^2|q|^2\right)\sin(q_+y)\Big]\Bigg\}. \end{aligned} \tag{F.27}$$

where $\Delta\mathbf{j}_y = \mathbf{j}_y(g_r^{\uparrow\downarrow}) - \mathbf{j}_y(g_r^{\uparrow\downarrow}=0)$ denotes the additional contribution due to the coupling to the ferromagnet.

Let us now focus on the boundary values j_{FM}^y and j_{FM}^z which we recall from Eq. (5.1):

$$\mathbf{j}_{\text{FM}} = \mathbf{j}_y(0) = \frac{g_r^{\uparrow\downarrow}}{2\pi\hbar N_0}\mathbf{n}\times\big(\mathbf{n}\times\mathbf{s}(0)\big)\,. \tag{F.28}$$

When inserting Eqs. (F.26) and (F.27) into Eqs. (F.5) and (F.12), one obtains the ferromagnetic contribution to the spin density, which depends through $\mathbf{j}_{\mathrm{FM}}$ on the total spin density $\mathbf{s}(0)$. Therefore, it is possible to relate $\mathbf{s}(0)$ to the $g_r^{\uparrow\downarrow}=0$ contribution:

$$\begin{pmatrix} s^y(0) \\ s^z(0) \end{pmatrix} = \begin{pmatrix} s^y(0) \\ s^z(0) \end{pmatrix}\Bigg|_{g_r^{\uparrow\downarrow}=0} + \mathbb{F} \begin{pmatrix} s^y(0) \\ s^z(0) \end{pmatrix}, \tag{F.29}$$

where

$$\begin{aligned} \mathbb{F} = &- \frac{2g_r^{\uparrow\downarrow}\alpha\tau_{\mathrm{DP}}}{\hbar} \frac{2\tau_s/\tau_{\mathrm{DP}} - l_s^2|q|^2}{2+l_s^2|q|^2} \\ &\times n_y n_z \begin{pmatrix} 1+\dfrac{4l_{\mathrm{DP}}q_-}{2-l_{\mathrm{DP}}^2|q|^2}\dfrac{n_z}{n_y} & -\dfrac{n_y}{n_z} - \dfrac{4l_{\mathrm{DP}}q_-}{2-l_{\mathrm{DP}}^2|q|^2} \\ -\dfrac{n_z}{n_y} - \dfrac{2l_{\mathrm{DP}}^3|q|^2q_-}{2-l_{\mathrm{DP}}^2|q|^2} & 1+\dfrac{2l_{\mathrm{DP}}^3|q|^2q_-}{2-l_{\mathrm{DP}}^2|q|^2}\dfrac{n_y}{n_z} \end{pmatrix} \end{aligned} \tag{F.30}$$

corresponds to the influence of the ferromagnetic boundary. Solving Eq. (F.29) for $\mathbf{s}(0)$ yields

$$\begin{pmatrix} s^y(0) \\ s^z(0) \end{pmatrix} = (1-\mathbb{F})^{-1} \begin{pmatrix} s^y(0) \\ s^z(0) \end{pmatrix}\Bigg|_{g_r^{\uparrow\downarrow}=0}. \tag{F.31}$$

Conveniently, we rewrite the inverse matrix in the form

$$(1-\mathbb{F})^{-1} = \frac{1}{d}\left(1+\mathbb{G}\right), \tag{F.32}$$

where

$$d = 1 + \frac{4g_r^{\uparrow\downarrow}\alpha\tau_{\mathrm{DP}}}{\hbar}\frac{\tau_s/\tau_{\mathrm{DP}}}{2+l_s^2|q|^2}\left[l_{\mathrm{DP}}q_-\left(2n_z^2 + l_{\mathrm{DP}}^2|q|^2n_y^2\right) + \left(2-l_{\mathrm{DP}}^2|q|^2\right)n_yn_z\right] \tag{F.33}$$

is the determinant of $1-\mathbb{F}$, and

$$\begin{aligned} \mathbb{G} = &\frac{2g_r^{\uparrow\downarrow}\alpha\tau_{\mathrm{DP}}}{\hbar}\frac{2\tau_s/\tau_{\mathrm{DP}} - l_s^2|q|^2}{2+l_s^2|q|^2} \\ &\times n_y n_z \begin{pmatrix} 1+\dfrac{2l_{\mathrm{DP}}^3|q|^2q_-}{2-l_{\mathrm{DP}}^2|q|^2}\dfrac{n_y}{n_z} & \dfrac{n_y}{n_z} + \dfrac{4l_{\mathrm{DP}}q_-}{2-l_{\mathrm{DP}}^2|q|^2} \\ \dfrac{n_z}{n_y} + \dfrac{2l_{\mathrm{DP}}^3|q|^2q_-}{2-l_{\mathrm{DP}}^2|q|^2} & 1+\dfrac{4l_{\mathrm{DP}}q_-}{2-l_{\mathrm{DP}}^2|q|^2}\dfrac{n_z}{n_y} \end{pmatrix}. \end{aligned} \tag{F.34}$$

Remarkably, the matrix $\mathbb{G}$ has the property

$$\mathbb{G}\begin{pmatrix} s^y(0) \\ s^z(0) \end{pmatrix}\Bigg|_{g_r^{\uparrow\downarrow}=0} \sim \begin{pmatrix} n_y \\ n_z \end{pmatrix}. \tag{F.35}$$

Hence, by inserting Eqs. (F.31) and (F.32) into the boundary condition, Eq. (F.28), we obtain

$$\mathbf{j}_{\mathrm{FM}} = \frac{g_r^{\uparrow\downarrow}}{2\pi\hbar d N_0}\mathbf{n}\times\left(\mathbf{n}\times\mathbf{s}(g_r^{\uparrow\downarrow}=0,y=0)\right), \tag{F.36}$$

which means that the spin polarization for $g_r^{\uparrow\downarrow}=0$ fixes the boundary condition for the spin current in the case $g_r^{\uparrow\downarrow}>0$. It is now straightforward to determine the magnetization angle ϕ_0 for which the spin current across the interface vanishes independently of $g_r^{\uparrow\downarrow}$: the cross product vanishes when $\mathbf{s}(g_r^{\uparrow\downarrow}=0,y=0)$ is parallel to $\mathbf{n}$. Therefore, the ratio of $s^z(0)$ and $s^y(0)$ for $g_r^{\uparrow\downarrow}=0$ equals the tangent of ϕ_0. Using Eqs. (F.22) and (F.23), we obtain the result given in Eq. (5.17).

F.3. Spin-thermoelectrics

In the following, we show that the response coefficients of the spin polarizations and spin currents due to a thermal gradient, such as Eqs. (5.26) and (5.27), are given by Mott-like formulas in terms of the energy derivative of the response coefficients due to an electrical field [17, 134]. For this, we first consider the charge sector of the static Boltzmann equation by taking into account the thermal gradient via Eq. (5.22):

$$\left(-\frac{\partial f_{\mathrm{eq}}^0}{\partial\epsilon_{\mathbf{p}}}\right)\frac{p_x}{m}\frac{\epsilon_{\mathbf{p}}-\epsilon_{\mathrm{F}}}{T}\nabla_x T - eE_x\nabla_{p_x}f = -\frac{1}{\tau}\left(f-\langle f\rangle\right). \tag{F.37}$$

Furthermore, we have neglected spin contributions since our aim is to derive spin response coefficients on basis of the charge sector and thus spin contributions in the last equation lead to higher order contributions in the spin sector which can be neglected. Assuming $\langle f\rangle\approx f_{\mathrm{eq}}^0$, the solution of the linearized form of Eq. (F.37) is given by

$$f^0 = f_{\mathrm{eq}}^0 + \frac{\tau p_x}{m}\left(eE_x+\frac{\epsilon_{\mathbf{p}}-\epsilon_{\mathrm{F}}}{T}\nabla_x T\right)\frac{\partial f_{\mathrm{eq}}^0}{\partial\epsilon_{\mathbf{p}}}. \tag{F.38}$$

Next, let us consider the spin sector, Eq. (F.1). With use of Eq. (F.38) the spin sector can be rewritten as follows:

$$\mathbf{f} = \mathbb{M}^{-1}\mathbb{N}\langle\mathbf{f}\rangle + \left(E_x+\frac{\epsilon_{\mathbf{p}}-\epsilon_{\mathrm{F}}}{eT}\nabla_x T\right)\frac{\partial f_{\mathrm{eq}}^0}{\partial\epsilon_{\mathbf{p}}}\boldsymbol{\mathcal{S}} \tag{F.39}$$

where

$$\left(E_x+\frac{\epsilon_{\mathbf{p}}-\epsilon_{\mathrm{F}}}{eT}\nabla_x T\right)\frac{\partial f_{\mathrm{eq}}^0}{\partial\epsilon_{\mathbf{p}}}\boldsymbol{\mathcal{S}} = \mathbb{M}^{-1}\mathbf{S}. \tag{F.40}$$

By performing the angular average on Eq. (F.39) it is now possible to obtain $\langle \mathbf{f} \rangle$ in terms of the energy derivative of f^0_{eq}, and thus also $\mathbf{f}$ in terms of $\partial_{\epsilon_\mathbf{p}} f^0_{\mathrm{eq}}$ by explicitly inserting $\langle \mathbf{f} \rangle$ into Eq. (F.39). One ends up with an expression of the following kind

$$\mathbf{f} = \mathbf{g}(\mathbf{p}) \left(E_x + \frac{\epsilon_\mathbf{p} - \epsilon_\mathrm{F}}{eT} \nabla_x T \right) \frac{\partial f^0_{\mathrm{eq}}}{\partial \epsilon_\mathbf{p}} \,, \tag{F.41}$$

where the momentum (and energy) dependent vector $\mathbf{g}$ is to be obtained by the approach described above. By integrating Eq. (F.41) over the momentum one obtains the spin polarization $\mathbf{s}$ or, by a prior multiplication with p_i/m, the spin current $\mathbf{j}_i$. According to

$$\int \frac{\mathrm{d}^2 p}{(2\pi\hbar)^2} \cdots = N_0 \int \mathrm{d}\epsilon_\mathbf{p} \langle \ldots \rangle \tag{F.42}$$

the problem of obtaining the response coefficients comes down to an energy integration. Employing the low temperature ($k_\mathrm{B} T \ll \epsilon_\mathrm{F}$) expansion (also known as Sommerfeld expansion) [186] we obtain

$$\int \mathrm{d}\epsilon_\mathbf{p} \mathbf{L}(\epsilon_\mathbf{p}) \left(E_x + \frac{\epsilon_\mathbf{p} - \epsilon_\mathrm{F}}{eT} \nabla_x T \right) \frac{\partial f^0_{\mathrm{eq}}}{\partial \epsilon_\mathbf{p}} \approx \mathbf{L}(\epsilon_\mathrm{F}) E_x - S_0 \epsilon_\mathrm{F} \mathbf{L}'(\epsilon_\mathrm{F}) \nabla_x T \,, \tag{F.43}$$

where $\mathbf{L} = N_0 \langle \mathbf{g} \rangle$ corresponds to the response coefficients of $\mathbf{s}$, or $\mathbf{L} = N_0 \langle p_i \mathbf{g} \rangle / m$ for the response coefficients of $\mathbf{j}_i$. Therefore, Eq. (F.43) yields the Mott like formulas (5.26) and (5.27) by considering the y component of $\mathbf{L} = N_0 \langle \mathbf{g} \rangle$ and the z component of $\mathbf{L} = N_0 \langle p_y \mathbf{g} \rangle / m$, respectively.

As an example, let us consider the bulk spin Nernst effect of the system regarded in Chap. 5. Note that this is a special case of the investigations published in Ref. 17 since we here neglect side-jump contributions. The spin Nernst conductivity σ_{sN} is defined by

$$j^z_y = \sigma_{\mathrm{sN}} \nabla_x T \,, \tag{F.44}$$

under the boundary condition $j_x = 0$, i.e., an open circuit condition for the charge current. We obtain σ_{sN} by recalling the general expression of the spin current given in Eq. (5.24),

$$j^z_y = \sigma_{\mathrm{sE}} E_x + \sigma_{\mathrm{sT}} \nabla_x T \,. \tag{F.45}$$

The bulk spin Hall conductivity σ_{sE} is given in Eq. (5.8) and by employing the Mott-like

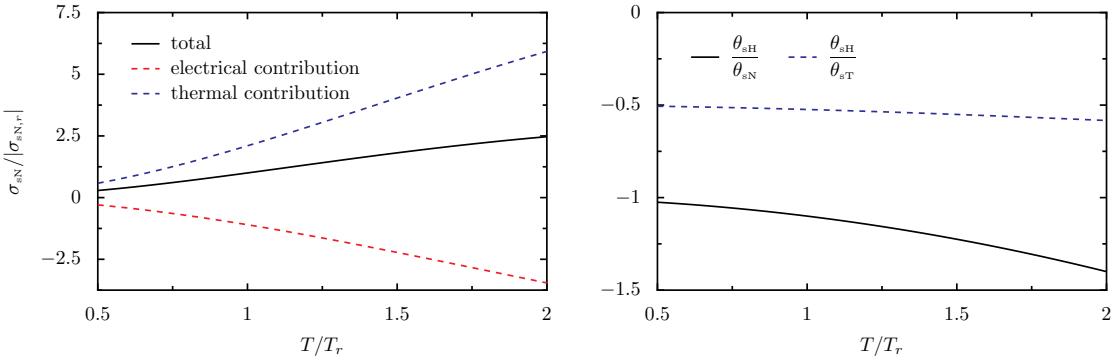

(a) (b)

FIG. F.1.: The spin Nernst conductivity (a) and the spin Hall angle over the (direct) spin Nernst angle (b) against the temperature with $\tau_{s,r}/\tau_{\mathrm{DP},r} = 10$. The spin Nernst conductivity is normalized by its absolute value at room temperature T_r. For a given quantity the subscript r indicates that its value is taken at room temperature.

formula (5.26) the transport coefficients in Eq. (F.45) read

$$\sigma_{\mathrm{sE}} = \frac{\hbar\sigma_{\mathrm{D}}}{2e\epsilon_{\mathrm{F}}(\tau_{\mathrm{DP}} + \tau_s)}\,, \tag{F.46}$$

$$\sigma_{\mathrm{sT}} = -\frac{2\tau_s + \tau_{\mathrm{DP}}}{\tau_s + \tau_{\mathrm{DP}}} S_0\sigma_{\mathrm{sE}}\,. \tag{F.47}$$

Due to the open circuit condition we can express the electric field in terms of the thermal gradient, i.e., $E_x \approx S_0\nabla_x T$ by neglecting spin-dependent contributions to the Seebeck coefficient. Thus, the spin Nernst conductivity is the sum of an electrical contribution, $S_0\sigma_{\mathrm{sE}}$, and a thermal contribution, σ_{sT}. We obtain

$$\sigma_{\mathrm{sN}} = -\frac{\tau_s}{\tau_s + \tau_{\mathrm{DP}}} S_0\sigma_{\mathrm{sE}}\,. \tag{F.48}$$

Analogously to the definition of the spin Hall angle $\theta_{\mathrm{sH}} = 2e\sigma_{\mathrm{sE}}/\sigma_{\mathrm{D}}$, we introduce the spin Nernst angle

$$\begin{aligned}\theta_{\mathrm{sN}} &= \frac{2e\sigma_{\mathrm{sN}}}{S_0\sigma_{\mathrm{D}}} \\ &= -\frac{\tau_s}{\tau_s + \tau_{\mathrm{DP}}}\theta_{\mathrm{sH}}\,.\end{aligned} \tag{F.49}$$

Note that the spin Nernst angle is sometimes also referred only to the direct thermal contribution [27] which we denote the direct spin Nernst angle

$$\begin{aligned}\theta_{\text{sT}} &= \frac{2e\sigma_{\text{sT}}}{S_0\sigma_{\text{D}}} \\ &= -\frac{2\tau_s + \tau_{\text{DP}}}{\tau_s + \tau_{\text{DP}}}\theta_{\text{sH}}\,.\end{aligned} \tag{F.50}$$

Figure F.1 shows the spin Nernst conductivity (a) and the spin Hall angle over the (direct) spin Nernst angle (b) as function of the temperature. The temperature dependences of the spin Nernst conductivity and the (direct) spin Nernst angle are essentially given by the temperature dependence of the momentum relaxation rate, respectively. Here, we assume $1/\tau \sim T$ which corresponds to the typical case of a metal in the high-temperature regime, $k_{\text{B}}T \gg \hbar\omega_{\text{D}}$ with the Debye frequency ω_{D}. As discussed in Ref. 17, and analogously to the spin Nernst magnetothermopower discussed in Ref. 78 and Chap. 5, we see in panel (a) that electrical and thermal contributions compete each other. In addition, the spin Nernst conductivity generally has a nonlinear temperature dependence due to the interplay of intrinsic and extrinsic spin-orbit coupling [17], in our case determined by the ratio τ_s/τ_{DP}. The spin Hall angle over the direct and total spin Nernst angles, panel (b), also show a nonlinear temperature-dependence. In the case $\tau_s/\tau_{\text{DP}} \gg 1$ we obtain from Eq. (F.50) the ratio $\theta_{\text{sH}}/\theta_{\text{sT}} \approx -0.5$, which is in agreement with experimental results [27].

G

Appendix to chapter 6

G.1. Elliott-Yafet collision operator

In this appendix we derive the Elliott-Yafet collision operator for the anisotropic Rashba metal as considered in Chap. 5 by following the lines of Sec. 2.5. Our starting point is the impurity averaged Elliott-Yafet self-energy in three dimensions,

$$\check{\Sigma}_{\text{EY}} = \frac{n_i v_0^2}{\hbar^2} \left(\frac{\lambda}{2\hbar}\right)^4 \int \frac{\mathrm{d}^3 p'}{(2\pi\hbar)^3} \left[(\mathbf{p}\times\mathbf{p}')\cdot\boldsymbol{\sigma}\right] G(\mathbf{p}') \left[(\mathbf{p}\times\mathbf{p}')\cdot\boldsymbol{\sigma}\right] , \tag{G.1}$$

similar to the two-dimensional case, cf. Eq. (2.181). The locally covariant form of the self-energy is given by $\check{\tilde{\Sigma}}_{\text{EY}} = \check{\tilde{\Sigma}}^0_{\text{EY}} + \check{\tilde{\Sigma}}^{\mathcal{A}}_{\text{EY}}$ with

$$\check{\tilde{\Sigma}}^0_{\text{EY}} = \frac{n_i v_0^2}{\hbar^2} \left(\frac{\lambda}{2\hbar}\right)^4 \int \frac{\mathrm{d}^3 p'}{(2\pi\hbar)^3} \left[(\mathbf{p}\times\mathbf{p}')\cdot\boldsymbol{\sigma}\right] \tilde{G}(\mathbf{p}') \left[(\mathbf{p}\times\mathbf{p}')\cdot\boldsymbol{\sigma}\right] , \tag{G.2}$$

$$\begin{aligned}\check{\tilde{\Sigma}}^{\mathcal{A}}_{\text{EY}} =& \frac{n_i v_0^2}{2\hbar^2} \left(\frac{\lambda}{2\hbar}\right)^4 \left\{\sigma^a,\, \boldsymbol{\mathcal{A}}^a\cdot\nabla_{\mathbf{p}} \int \frac{\mathrm{d}^3 p'}{(2\pi\hbar)^3} \left[(\mathbf{p}\times\mathbf{p}')\cdot\boldsymbol{\sigma}\right] \tilde{G}(\mathbf{p}') \left[(\mathbf{p}\times\mathbf{p}')\cdot\boldsymbol{\sigma}\right] \right\} \\ & - \frac{n_i v_0^2}{2\hbar^2} \left(\frac{\lambda}{2\hbar}\right)^4 \int \frac{\mathrm{d}^3 p'}{(2\pi\hbar)^3} \left[(\mathbf{p}\times\mathbf{p}')\cdot\boldsymbol{\sigma}\right] \left\{\sigma^a, \left[\boldsymbol{\mathcal{A}}^a\cdot\nabla_{\mathbf{p}'}\tilde{G}(\mathbf{p}')\right]\right\} \left[(\mathbf{p}\times\mathbf{p}')\cdot\boldsymbol{\sigma}\right] .\end{aligned} \tag{G.3}$$

Regarding the $\check{\tilde{\Sigma}}^{\mathcal{A}}_{\text{EY}}$ contribution, it is convenient to split the Keldysh Green's function into a charge and a spin contribution, $\tilde{G}^K = \tilde{G}^K_0 + \boldsymbol{\sigma}\cdot\tilde{\mathbf{G}}^K$, and make use of the anticommutation relations (2.188) for the Pauli matrices in order to analogously split $\check{\tilde{\Sigma}}^{\mathcal{A}}_{\text{EY}}$ into a charge contribution $\check{\tilde{\Sigma}}^{\mathcal{A}}_{\text{EY},c}$ and a spin contribution $\check{\tilde{\Sigma}}^{\mathcal{A}}_{\text{EY},s}$, where the latter is

linear in the Pauli matrices. The corresponding collision operators become

$$I^{\mathcal{A}}_{\mathrm{EY},c} = \frac{1}{N_0\tau}\left(\frac{\lambda}{2\hbar}\right)^4 \mathcal{A}^a_i \varepsilon_{ijk}\varepsilon_{lmn} \int \frac{\mathrm{d}^3p'}{(2\pi\hbar)^3}\, \delta(\epsilon_{\mathbf{p}} - \epsilon_{\mathbf{p}'}) p'_k p'_n p_m \times \left[f^b_{\mathbf{p}'}(\delta_{al}\delta_{bj} + \delta_{aj}\delta_{bl}) - \delta_{ab}\delta_{jl}\left(f^b_{\mathbf{p}'} + f^b_{\mathbf{p}}\right)\right], \tag{G.4}$$

$$I^{\mathcal{A}}_{\mathrm{EY},s} = \frac{1}{N_0\tau}\left(\frac{\lambda}{2\hbar}\right)^4 \mathcal{A}^a_i \varepsilon_{ijk}\varepsilon_{lmn} \int \frac{\mathrm{d}^3p'}{(2\pi\hbar)^3}\, \delta(\epsilon_{\mathbf{p}} - \epsilon_{\mathbf{p}'}) \left(f^0_{\mathbf{p}'} - f^0_{\mathbf{p}}\right) \times \left[p'_k p'_n p_m \delta_{jl}\sigma^a - p'_n p_k p_m \left(\delta_{aj}\sigma^l + \delta_{al}\sigma^j - \delta_{jl}\sigma^a\right)\right], \tag{G.5}$$

where $\epsilon_{\mathbf{p}} = (p_x^2 + p_y^2)/2m_\parallel + p_z^2/m_\perp$ is the band energy.

The $\check{\tilde{\Sigma}}^0_{\mathrm{EY}}$ contribution, Eq. (G.2), results in the compact collision operator

$$I^0_{\mathrm{EY}} = -\frac{1}{\tau_s}\boldsymbol{\sigma}\cdot(\Gamma\langle\mathbf{f}\rangle)\,. \tag{G.6}$$

We recall that $\langle\dots\rangle$ denotes the angular average and $\Gamma = \mathrm{diag}(1,1,\zeta)$ accounts for the anisotropy of Elliott-Yafet spin relaxation with $\zeta = 2m_\perp/(m_\perp + m_\parallel)$ due to the mass anisotropy. In order to obtain Eq. (G.6) it is convenient to parametrize the momentum by

$$\begin{aligned} p_x &= \sqrt{2m_\parallel\epsilon_{\mathbf{p}}}\sin\theta\cos\phi\,,\\ p_y &= \sqrt{2m_\parallel\epsilon_{\mathbf{p}}}\sin\theta\sin\phi\,.\\ p_z &= \sqrt{2m_\perp\epsilon_{\mathbf{p}}}\cos\theta \end{aligned} \tag{G.7}$$

and rewrite the momentum integral,

$$\int\frac{\mathrm{d}^3p}{(2\pi\hbar)^3}\,\cdots = \int\mathrm{d}\epsilon_{\mathbf{p}}\,\mathcal{N}(\epsilon_{\mathbf{p}})\langle\dots\rangle\,, \tag{G.8}$$

where $\mathcal{N}(\epsilon) = m_\parallel\sqrt{2m_\perp\epsilon}/2\pi^2\hbar^3$ is the density of states per spin and volume. Neglecting terms beyond the harmonic contribution, $\tilde{G}$ and quadratic terms in the momentum p_ip_j or $p'_ip'_j$ can be replaced by their angular average in Eq. (G.2), respectively. We obtain the collision operator

$$I^0_{\mathrm{EY}} = -\frac{4}{\tau}\left(\frac{\lambda}{2\hbar}\right)^4 \boldsymbol{\sigma}\cdot\Big[\begin{pmatrix} \langle p_x^2\rangle[\langle p_y^2\rangle + \langle p_z^2\rangle] & 0 & 0\\ 0 & \langle p_y^2\rangle[\langle p_x^2\rangle + \langle p_z^2\rangle] & 0\\ 0 & 0 & \langle p_z^2\rangle[\langle p_x^2\rangle + \langle p_y^2\rangle] \end{pmatrix}\langle\mathbf{f}\rangle\Big]\,. \tag{G.9}$$

Assuming that $\langle \mathbf{f} \rangle$ is sharply peaked at ϵ_F, we can set $\langle p_x^2 \rangle = \langle p_y^2 \rangle = 2m_\parallel \epsilon_\mathrm{F}/3$ and $\langle p_z^2 \rangle = 2m_\perp \epsilon_\mathrm{F}/3$. Then, we can rewrite Eq. (G.9) as Eq. (G.6) with the Elliott-Yafet spin relaxation rate

$$\frac{1}{\tau_s} = \frac{8}{9(2-\zeta)} \frac{1}{\tau} \left(\frac{\lambda p_F}{2\hbar} \right)^4 , \tag{G.10}$$

as given in Eq. (6.10). Note that Eq. (G.9) also yields the strictly two-dimensional case, $p_z = 0$, with $\zeta = 0$ and $1/\tau_s = (\lambda p_F/2\hbar)^4/\tau$.

G.2. Spin polarization

Next, we present a detailed description of solving the set of diffusion equations (6.15)–(6.17),

$$q_1^2 s^x = \nabla_z^2 s^x \,, \tag{G.11}$$

$$q_1^2 s^y = \nabla_z^2 s^y + q_1^2 s_0^y \,, \tag{G.12}$$

$$q_2^2 s^z = \nabla_z^2 s^z \,, \tag{G.13}$$

for s^y with the boundary conditions

$$\mathbf{j}_z(z=0) = D_\perp q_r \mathbf{n} \times \big[\mathbf{n} \times \mathbf{s}(z=0)\big] + D_\perp q_i \mathbf{n} \times \mathbf{s}(z=0) \,, \tag{G.14}$$

$$\mathbf{j}_z(z=d) = 0 \,. \tag{G.15}$$

We recall Eq. (6.14),

$$\mathbf{j}_z = -D_\perp \nabla_z \mathbf{s} - \mathbf{e}_y \theta_\mathrm{ext}^\mathrm{sH} \frac{m_\parallel}{m_\perp} \frac{\sigma_\mathrm{D} E_x}{2e} \,, \tag{G.16}$$

which allows us to transform the boundary conditions (G.14) and (G.15) for the spin current to boundary conditions for the spin density. The general solution of Eqs. (G.11)–(G.13) is given by

$$s^x = a_1 \mathrm{e}^{-q_1 z} + a_2 \mathrm{e}^{q_1 z} \,, \tag{G.17}$$

$$s^y = b_1 \mathrm{e}^{-q_1 z} + b_2 \mathrm{e}^{q_1 z} + s_0^y \,, \tag{G.18}$$

$$s^z = c_1 \mathrm{e}^{-q_2 z} + c_2 \mathrm{e}^{q_2 z} \,. \tag{G.19}$$

First, we consider the boundary $z = d$. In this case, inserting Eqs. (G.17)–(G.19) into Eq. (G.16) yields

$$a_1 \mathrm{e}^{-q_1 d} - a_2 \mathrm{e}^{q_1 d} = 0\,, \tag{G.20}$$

$$b_1 \mathrm{e}^{-q_1 d} - b_2 \mathrm{e}^{q_1 d} = \frac{\theta_{\mathrm{ext}}^{\mathrm{sH}}}{D_\parallel q_1} \frac{\sigma_{\mathrm{D}} E_x}{2e}\,, \tag{G.21}$$

$$c_1 \mathrm{e}^{-q_2 d} - c_2 \mathrm{e}^{q_2 d} = 0\,. \tag{G.22}$$

We can now reduce the number of unknown parameters by setting

$$a_1 = a\frac{\mathrm{e}^{q_1 d}}{2}\,, \qquad a_2 = a\frac{\mathrm{e}^{-q_1 d}}{2}\,, \tag{G.23}$$

$$b_1 = \left(b + \frac{\theta_{\mathrm{ext}}^{\mathrm{sH}}}{D_\parallel q_1} \frac{\sigma_{\mathrm{D}} E_x}{2e}\right) \frac{\mathrm{e}^{q_1 d}}{2}\,, \qquad b_2 = \left(b - \frac{\theta_{\mathrm{ext}}^{\mathrm{sH}}}{D_\parallel q_1} \frac{\sigma_{\mathrm{D}} E_x}{2e}\right) \frac{\mathrm{e}^{-q_1 d}}{2}\,, \tag{G.24}$$

$$c_1 = c\frac{\mathrm{e}^{q_2 d}}{2}\,, \qquad c_2 = c\frac{\mathrm{e}^{-q_2 d}}{2}\,, \tag{G.25}$$

which results in the spin density

$$s^x = a\cosh\big(q_1(d-z)\big)\,, \tag{G.26}$$

$$s^y = b\cosh\big(q_1(d-z)\big) + \frac{\theta_{\mathrm{ext}}^{\mathrm{sH}}}{D_\parallel q_1} \frac{\sigma_{\mathrm{D}} E_x}{2e} \sinh\big(q_1(d-z)\big) + s_0^y\,, \tag{G.27}$$

$$s^z = c\cosh\big(q_2(d-z)\big)\,. \tag{G.28}$$

Let us now consider the boundary $z = 0$, for the time being in the absence of the ferromagnet, i.e., $q_r = q_i = 0$ and thus $\mathbf{j}(z=0) = 0$ according to Eq. (G.14). Inserting Eq. (G.27) into Eq. (G.16) and setting $z = 0$ then leads to the following solution for s^y:

$$s^y(z)\big|_{q_r = q_i = 0} = s_0^y + \Delta s_{sc}^y(z)\,, \tag{G.29}$$

where

$$\Delta s_{\mathrm{sc}}^y(z) = \frac{\theta_{\mathrm{ext}}^{\mathrm{sH}}}{D_\parallel q_1} \frac{\sigma_{\mathrm{D}} E_x}{2e} \frac{\sinh\big(q_1(d/2-z)\big)}{\cosh(q_1 d/2)}\,, \tag{G.30}$$

as given in Eq. (6.24).

In the presence of the ferromagnet, $q_r \neq 0$, $q_i \neq 0$, the spin density acquires an additional, magnetization dependent, contribution,

$$\mathbf{s}(z, \mathbf{n}) = [s_0^y + \Delta s_{\mathrm{sc}}^y(z)]\, \mathbf{e}_y + \Delta\mathbf{s}(z, \mathbf{n}) \tag{G.31}$$

with

$$\Delta\mathbf{s}(z,\mathbf{n}) = \begin{pmatrix} \tilde{a}\cosh\big(q_1(d-z)\big) \\ \tilde{b}\cosh\big(q_1(d-z)\big) \\ \tilde{c}\cosh\big(q_2(d-z)\big) \end{pmatrix} . \tag{G.32}$$

Analogously, we can rewrite the spin current

$$\mathbf{j}_z(z,\mathbf{n}) = \big[j^y_{z,0} + \Delta j^y_{z,\mathrm{sc}}(z)\big]\,\mathbf{e}_y + \Delta\mathbf{j}_z(z,\mathbf{n})\,, \tag{G.33}$$

where

$$j^y_{z,0} = \theta^{\mathrm{sH}}_{\mathrm{ext}}\frac{m_\parallel}{m_\perp}\frac{\sigma_{\mathrm{D}}E_x}{2e}\,, \tag{G.34}$$

$$\Delta j^y_{z,\mathrm{sc}}(z) = -D_\perp\nabla_z\Delta s^y_{\mathrm{sc}}(z)\,, \tag{G.35}$$

$$\Delta\mathbf{j}_z(z,\mathbf{n}) = -D_\perp\nabla_z\Delta\mathbf{s}(z,\mathbf{n})\,. \tag{G.36}$$

From the derivation of Δs^y_{sc} we know that $j^y_{z,0} + \Delta j^y_{z,\mathrm{sc}}(0) = 0$ and thus the boundary condition (G.14) can be easily rewritten as a boundary condition for the magnetization-dependent contribution $\Delta\mathbf{j}_z$. By explicitly inserting Eq. (G.32) into Eq. (G.36) and setting $z = 0$ we obtain

$$\begin{pmatrix} q_1\tilde{a}\sinh(q_1 d) \\ q_1\tilde{b}\sinh(q_1 d) \\ q_2\tilde{c}\sinh(q_2 d) \end{pmatrix} = q_r\mathbf{n}\times\big[\mathbf{n}\times\mathbf{s}(z=0)\big] + q_i\mathbf{n}\times\mathbf{s}(z=0) \tag{G.37}$$

with

$$\mathbf{s}(z=0) = \left[s^y_0 + \Delta s^y_{\mathrm{sc}}(0)\right]\mathbf{e}_y + \begin{pmatrix} \tilde{a}\cosh(q_1 d) \\ \tilde{b}\cosh(q_1 d) \\ \tilde{c}\cosh(q_2 d) \end{pmatrix} . \tag{G.38}$$

The remaining task is now to solve the set of equations (G.37) for $\tilde{b}$ in order to obtain the complete solution for s^y. For this it is convenient to rewrite the magnetization direction in spherical coordinates,

$$\mathbf{n} = \begin{pmatrix} \sin\theta\cos\phi \\ \sin\theta\sin\phi \\ \cos\theta \end{pmatrix} , \tag{G.39}$$

and rotate Eq. (G.37) with the transformation matrix

$$\mathbb{D} = \begin{pmatrix} \sin\theta\cos\phi & \sin\theta\sin\phi & \cos\theta \\ \cos\theta\cos\phi & \cos\theta\sin\phi & -\sin\theta \\ -\sin\phi & \cos\phi & 0 \end{pmatrix} \tag{G.40}$$

with the consequence $\mathbb{D}\mathbf{n} = \mathbf{e}_x$. By a proper choice of θ and ϕ, Eq. (G.37) can be rewritten for the α, β, γ scans, respectively,

$$\alpha \text{ scan: } \theta = \frac{\pi}{2}, \phi = \alpha\,; \qquad \mathbb{M}_\alpha \begin{pmatrix} \tilde{a} \\ \tilde{b} \\ \tilde{c} \end{pmatrix} = -\cos\alpha \left[s_0^y + \Delta s_{\mathrm{sc}}^y(0)\right] \begin{pmatrix} 0 \\ q_i \\ q_r \end{pmatrix}, \tag{G.41}$$

$$\beta \text{ scan: } \theta = \beta, \phi = -\frac{\pi}{2}\,; \qquad \mathbb{M}_\beta \begin{pmatrix} \tilde{a} \\ \tilde{b} \\ \tilde{c} \end{pmatrix} = -\cos\beta \left[s_0^y + \Delta s_{\mathrm{sc}}^y(0)\right] \begin{pmatrix} 0 \\ -q_r \\ q_i \end{pmatrix}, \tag{G.42}$$

$$\gamma \text{ scan: } \theta = \gamma, \phi = 0\,; \qquad \mathbb{M}_\gamma \begin{pmatrix} \tilde{a} \\ \tilde{b} \\ \tilde{c} \end{pmatrix} = -\left[s_0^y + \Delta s_{\mathrm{sc}}^y(0)\right] \begin{pmatrix} 0 \\ q_i \\ q_r \end{pmatrix}. \tag{G.43}$$

The matrices $\mathbb{M}_\alpha$, $\mathbb{M}_\beta$, and $\mathbb{M}_\gamma$ are given by

$$\begin{aligned}
\mathbb{M}_\alpha &= \begin{pmatrix} q_1\sinh(q_1 d)\cos\alpha & q_1\sinh(q_1 d)\sin\alpha & 0 \\ -q_i\cosh(q_1 d)\sin\alpha & q_i\cosh(q_1 d)\cos\alpha & -[q_2\sinh(q_2 d)+q_r\cosh(q_2 d)] \\ -[q_1\sinh(q_1 d)+q_r\cosh(q_1 d)]\sin\alpha & [q_1\sinh(q_1 d)+q_r\cosh(q_1 d)]\cos\alpha & q_i\cosh(q_2 d) \end{pmatrix}, \\
\mathbb{M}_\beta &= \begin{pmatrix} 0 & -q_1\sinh(q_1 d)\sin\beta & q_2\sinh(q_2 d)\cos\beta \\ q_i\cosh(q_1 d) & -[q_1\sinh(q_1 d)+q_r\cosh(q_1 d)]\cos\beta & -[q_2\sinh(q_2 d)+q_r\cosh(q_2 d)]\sin\beta \\ q_1\sinh(q_1 d)+q_r\cosh(q_1 d) & q_i\cosh(q_1 d)\cos\beta & q_i\cosh(q_2 d)\sin\beta \end{pmatrix}, \\
\mathbb{M}_\gamma &= \begin{pmatrix} q_1\sinh(q_1 d)\sin\gamma & 0 & q_2\sinh(q_2 d)\cos\gamma \\ [q_1\sinh(q_1 d)+q_r\cosh(q_1 d)]\cos\gamma & q_i\cosh(q_1 d) & -[q_2\sinh(q_2 d)+q_r\cosh(q_2 d)]\sin\gamma \\ -q_i\cosh(q_1 d)\cos\gamma & q_1\sinh(q_1 d)+q_r\cosh(q_1 d) & q_i\cosh(q_2 d)\sin\gamma \end{pmatrix}.
\end{aligned} \tag{G.44}$$

It is now straightforward to solve for $\tilde{b}$ in the respective case, and hence obtain $\Delta s_{\alpha,\beta,\gamma}^y$, Eq. (6.25), which reads

$$\Delta s_{\alpha,\beta,\gamma}^y(z) = -A(z) f_{\alpha,\beta,\gamma} \tag{G.45}$$

with

$$A(z) = s_0^y \left[1 - \tanh\left(q_1 d/2\right)\theta_{\mathrm{ext}}^{\mathrm{sH}} \frac{q_{\mathrm{ISGE}}}{q_1}\right] \frac{\cosh\big(q_1(d-z)\big)}{\cosh(q_1 d)}, \tag{G.46}$$

$$f_\alpha = \frac{(q_i^2 + q_r^2 + q_r\tilde{q}_2)\cos^2\alpha}{q_i^2 + (\tilde{q}_1 + q_r)(\tilde{q}_2 + q_r)}, \tag{G.47}$$

$$f_\beta = \frac{(q_i^2 + q_r^2 + q_r\tilde{q}_1)\cos^2\beta}{\frac{\tilde{q}_1}{\tilde{q}_2}\left[q_i^2 + (\tilde{q}_1 + q_r)(\tilde{q}_2 + q_r)\right]\sin^2\beta + \left[q_i^2 + (\tilde{q}_1 + q_r)^2\right]\cos^2\beta}, \tag{G.48}$$

$$f_\gamma = \frac{q_i^2 + q_r^2 + q_r\tilde{q}_1 - (q_i^2 + q_r^2)\left(1 - \frac{\tilde{q}_1}{\tilde{q}_2}\right)\sin^2\gamma}{\frac{\tilde{q}_1}{\tilde{q}_2}\left[q_i^2 + (\tilde{q}_1 + q_r)(\tilde{q}_2 + q_r)\right]\sin^2\gamma + \left[q_i^2 + (\tilde{q}_1 + q_r)^2\right]\cos^2\gamma}. \tag{G.49}$$

Notation and symbols

Notation	Description
$1 = (t_1, \mathbf{r}_1)$	space-time point
$A(z)$	magnitude and spatial dependence of $\Delta s^y_{\alpha,\beta,\gamma}$
A	spectral function
$\mathbf{A}$	vector potential
$\boldsymbol{\mathcal{A}}^a$	SU(2) vector potential
$\boldsymbol{\mathcal{B}}$	U(1)×SU(2) magnetic field
$\boldsymbol{\mathcal{B}}^a$	SU(2) magnetic field
$\mathbf{B}$	magnetic field
C	magnitude of the magnetoresistance ratio
$\hat{c}_k$	creation operator for state k
d	thickness of the system
D	diffusion constant
$D_\parallel$	in-plane diffusion constant
$D_\perp$	out-of-plane diffusion constant
$e > 0$	elementary charge
e	base of the natural logarithm
$\boldsymbol{\mathcal{E}}$	U(1)×SU(2) electric field
$\boldsymbol{\mathcal{E}}^a$	SU(2) electric field
$\mathbf{E}$	electric field
$\mathbf{F}$	effective force in Chap. 4
F_α	frequency-dependent force in the spin-pumping configuration
$\boldsymbol{\mathcal{F}}$	U(1)×SU(2) Lorentz force
$F^{(A)}, E^{(A)}$	force and electric field related to the inverse spin Hall effect
$F^{(B)}, E^{(B)}$	force and electric field related to the spin galvanic effect
$F^{(C)}, E^{(C)}$	force and electric field related to the inverse spin filter effect
$F_{\mu\nu}$	U(1)×SU(2) electromagnetic field tensor
f	distribution function

Notation	Description
f^0	charge distribution function
f^0_{eq}	equilibrium charge distribution function, Fermi function
$\mathbf{f}$	spin distribution function
$\mathbf{f}_{\mathrm{eq}}$	equilibrium spin distribution function
$\delta\mathbf{f}$	nonequilibrium part of the spin distribution function
$f_{\alpha,\beta,\gamma}$	angular dependence of $\Delta s^y_{\alpha,\beta,\gamma}$
G^T	time-ordered Green's function
$G^{\tilde{T}}$	anti-time-ordered Green's function
G^R	retarded Green's function
G^A	advanced Green's function
$G^<$	lesser Green's function
$G^>$	greater Green's function
$G^K, \tilde{G}^K$	Keldysh Green's function and its locally covariant form
G_c, G_{c_i}, G_{c_K}	contour-ordered Green's function on contours c, c_i, and c_K
$\tilde{G}, \check{G}, \check{\tilde{G}}$	full Green's function: in 2×2 space, in Keldysh space, locally covariant form
$G_0, \check{G}_0$	free Green's function: contour-ordered (c_K), in Keldysh space
$G_n, \tilde{G}_n, \check{G}_n$	n-th order Green's function: contour-ordered (c_K), in 2×2 space, in Keldysh space
$\check{G}_0^{-1}, \check{\tilde{G}}_0^{-1}$	inverse of the free Green's function: in Keldysh space, locally covariant form
g	gauge transformation
g_e	electron g-factor
$g^{\uparrow\downarrow}$	spin mixing conductance
$g_r^{\uparrow\downarrow}$	real part of the spin mixing conductance
$g_i^{\uparrow\downarrow}$	imaginary part of the spin mixing conductance
$\hbar$	Planck's constant
$\mathbf{H}_{\mathrm{eff}}$	effective magnetic field
$\hat{H}$	Hamilton operator
$\hat{H}_0$	Hamilton operator which is quadratic in the field operators

Notation	Description
$\hat{H}_1$	time-independent Hamilton operator before a disturbance is switched on
$\hat{H}^i$	part of the Hamilton operator which represents interaction
$\hat{H}'$	part of the Hamilton operator which represents a disturbance
$\mathcal{H}$	Hamiltonian $\hat{H}$ in spatial representation
$\mathcal{H}_0$	Hamiltonian $\hat{H}_0$ in spatial representation
$\mathcal{H}_{\mathrm{imp}}$	Hamiltonian which describes the effect of impurities
$\mathcal{H}_{\mathrm{sd}}$	s-d Hamiltonian
I	collision operator
I_0	collision operator which describes momentum relaxation
I_{ext}	collision operator which corresponds to side-jump and skew scattering
I_{EY}	collision operator which describes Elliott-Yafet spin relaxation
I^0_{EY}	contribution of zeroth-order in the four-potential to I_{EY}
$I^{\boldsymbol{\mathcal{A}}}_{\mathrm{EY}}$, $I^{\boldsymbol{\mathcal{A}}}_{\mathrm{EY},c}$, $I^{\boldsymbol{\mathcal{A}}}_{\mathrm{EY},s}$	contribution linear in $\boldsymbol{\mathcal{A}}^a$ to I_{EY} and its contribution in the charge (c) and spin (s) sector, respectively
$I^{\boldsymbol{\Psi}}_{\mathrm{EY}}$	contribution linear in $\boldsymbol{\Psi}$ to I_{EY}
$I^{\boldsymbol{\mathcal{A}},\boldsymbol{\Psi}}_{\mathrm{EY}}$	mixed second-order contribution to I_{EY}
i	imaginary unit
$\mathbf{j}$	charge current density
$\mathbf{j}^a$	a-polarized spin current density
j^z_0	homogeneous spin current (bulk spin Hall effect)
$\Delta\mathbf{j}^a$	magnetization-dependent part of $\mathbf{j}^a$
k_{B}	Boltzmann constant
$\check{K}$, $\check{\check{K}}$	collision kernel: in Keldysh space, locally covariant form
l	mean free path
l_{DP}	Dyakonov-Perel spin diffusion length
l_s	Elliott-Yafet spin diffusion length
ℓ_x, ℓ_y	length and width of the system
m	effective mass
$m_{\parallel}$	in-plane effective mass

Notation	Description
$m_\perp$	out-of-plane effective mass
n	electron density
$\mathcal{N}$	density of states per area (volume) and spin
N_0	density of states per area (volume) and spin at the Fermi energy
N_i	number of impurities
n_i	impurity density
$\hat{n}_k$	occupation number operator for state k
n_k	occupation number for state k
$\mathbf{n}$	magnetization direction
$\mathbf{n}_\zeta$	abbreviation for $\Gamma\mathbf{n}$
$\hat{N}$	total number operator
$\hat{O}_H, \hat{O}_{H_0}, \hat{O}_{H_1}$	time-evolution of some operator $\hat{O}$ with respect to $\hat{H}$, $\hat{H}_0$, and $\hat{H}_1$
$\mathcal{P}$	path-ordering operator
p_{F}	Fermi momentum
$\mathbf{p}$	momentum
p^μ	four-momentum
P_{sE}	polarization coefficient
P_0^{E}	bulk polarization coefficient
ΔP_{sE}	magnetization-dependent contribution to P_{sE}
P_{sT}	thermal polarization coefficient
ΔP_{sT}	magnetization-dependent contribution to P_{sT}
q	wavenumber of the magnetic texture
q_-	wavenumber describing the exponential decay of the spin current
q_+	wavenumber describing the oscillation of the spin current
q_1	inverse spin relaxation length of the in-plane spin density
q_2	inverse spin relaxation length of the out-of-plane spin density
$\tilde{q}_1$	decrease of q_1 due to a finite thickness
$\tilde{q}_2$	decrease of q_2 due to a finite thickness
q_i	wavenumber associated with $g_i^{\uparrow\downarrow}$
q_r	wavenumber associated with $g_r^{\uparrow\downarrow}$
q_{ISGE}	inverse spin galvanic wavenumber

Notation	Description
q_{SGE}	spin galvanic wavenumber
$\mathbf{r}$	position vector
S	thermopower or Seebeck coefficient
S_0	thermopower of a free electron gas
ΔS	magnetization-dependent part of S (magnetothermopower)
ΔS_{sE}	electrical part of ΔS
ΔS_{sT}	thermal part of ΔS
$\hat{S}$	factorization of the time-evolution operator, $\hat{U}_H = \hat{U}_{H_1}\hat{S}$
$\mathbf{s}$	spin density
$\mathbf{s}_{\text{eq}}$	equilibrium part of $\mathbf{s}$
$\delta\mathbf{s}$	nonequilibrium part of $\mathbf{s}$
$\Delta\mathbf{s}$	magnetization-dependent part of $\mathbf{s}$
Δs^y_{sc}	spin accumulation due to j^z_y
s^y_0	current-induced spin polarization (inverse spin galvanic effect)
$\Delta s^y_{\alpha,\beta,\gamma}$	magnetization-dependent part of s^y for the α, β, and γ scans
t	time
∇T	temperature gradient
$T\{\dots\}$	time-ordering operator
$T_c\{\dots\}$	contour-ordering operator for a contour c
$\mathbf{T}$	spin torque functional
T	temperature
U	potential
$\hat{U}_H, \hat{U}_{H_0}, \hat{U}_{H_1}$	time-evolution operator with respect to $\hat{H}$, $\hat{H}_0$, and $\hat{H}_1$
U_Γ	Wilson line with curve Γ
$\check{U}$	potential in Keldysh space
V	potential; random potential
$\mathbf{v}$	velocity
v_0	amplitude of a δ-shaped impurity potential
v_{F}	Fermi velocity
V_{imp}	single impurity potential
v^μ	four-velocity

Notation	Description
$x^\mu = (t, \mathbf{r})$	four-vector with the center-of-mass coordinates t and $\mathbf{r}$
$y^\mu = (t_r, \mathbf{r}_r)$	four-vector with the relative coordinates t_r and $\mathbf{r}_r$
α	Rashba parameter; magnetization angle in the xy plane (α scan)
α_{R}	Rashba parameter in Chap. 6
α_{G}	Gilbert damping constant
$\beta = 1/k_{\text{B}}T$	inverse temperature
β	magnetization angle in the yz plane (β scan)
β_{DP}	spin torque parameter associated with τ_{DP}
β_s	spin torque parameter associated with τ_s
Γ	anisotropy matrix of the Elliott-Yafet mechanism
γ	gyromagnetic ratio; magnetization angle in the xz plane (γ scan)
Δ_{SO}	spin-orbit energy splitting
Δ_{XC}	exchange energy splitting
ϵ	energy, Fourier transform of the time variable
ϵ_{F}	Fermi energy
ϵ_k	single-particle energy for state k
$\epsilon_{\mathbf{p}}$	energy at momentum $\mathbf{p}$
ζ	anisotropy parameter of the Elliott-Yafet mechanism
$\eta_{\mu\nu}$	metric
θ_{sH}	spin Hall angle
$\theta^{\text{sH}}_{\text{ext}}$	extrinsic contribution to the spin Hall angle
$\theta^{\text{sH}}_{\text{int}}$	intrinsic contribution to the spin Hall angle
θ_{sN}	spin Nernst angle
θ_{sT}	direct spin Nernst angle
λ	effective Compton wavelength
μ_0	magnetic constant
μ	chemical potential
$\boldsymbol{\mu}$	spin magnetic moment of an electron
$\xi_{\text{int}}, \xi_{\text{ext}}$	abbreviations used in the definitions of q_{ISGE} and q_{SGE}
ρ	resistivity
ρ_0	resistivity in the absence of a ferromagnet

Notation	Description
ρ_{D}	inverse of the Drude conductivity
$\Delta\rho$	magnetization-dependent part of ρ (magnetoresistance)
$\Delta\rho_{\alpha,\beta,\gamma}$	magnetoresistance for the α, β, and γ scan
$\hat{\rho}$	statistical operator
$\hat{\rho}_1$	statistical operator with Hamiltonian $\hat{H}_1$
$\boldsymbol{\sigma} = (\sigma^x, \sigma^y, \sigma^z)$	vector of Pauli matrices
σ_0	conductivity in the absence of a ferromagnet
σ_{D}	Drude conductivity
$\Delta\sigma$	magnetization dependence of the conductivity
$\Sigma, \check{\Sigma}, \check{\check{\Sigma}}$	self-energy: contour-ordered (c_K), in Keldysh space, locally covariant form
$\check{\Sigma}_0, \check{\check{\Sigma}}_0$	momentum relaxation self-energy: in Keldysh space, locally covariant form
$\check{\Sigma}_{\mathrm{EY}}, \check{\check{\Sigma}}_{\mathrm{EY}}$	Elliott-Yafet self-energy: in Keldysh space, locally covariant form
$\check{\check{\Sigma}}^0_{\mathrm{EY}}$	contribution of zeroth-order in the four-potential to $\check{\check{\Sigma}}_{\mathrm{EY}}$
$\check{\check{\Sigma}}^{\boldsymbol{\mathcal{A}}}_{\mathrm{EY}}$	contribution linear in $\boldsymbol{\mathcal{A}}^a$ to $\check{\check{\Sigma}}_{\mathrm{EY}}$
$\check{\check{\Sigma}}^{\Psi}_{\mathrm{EY}}$	contribution linear in $\boldsymbol{\Psi}$ to $\check{\check{\Sigma}}_{\mathrm{EY}}$
$\check{\check{\Sigma}}^{\boldsymbol{\mathcal{A}},\Psi}_{\mathrm{EY}}$	mixed second-order contribution to $\check{\check{\Sigma}}_{\mathrm{EY}}$
σ_{sE}	spin Hall conductivity
$\Delta\sigma_{\mathrm{sE}}$	magnetization-dependent part of σ_{sE}
σ_0^{sH}	bulk spin Hall conductivity
$\sigma_{\mathrm{int}}^{\mathrm{sH}}$	intrinsic contribution to the spin Hall conductivity
$\sigma_{\mathrm{sj}}^{\mathrm{sH}}$	side-jump contribution to the spin Hall conductivity
$\sigma_{\mathrm{ss}}^{\mathrm{sH}}$	skew-scattering contribution to the spin Hall conductivity
σ_{sN}	bulk spin Nernst conductivity
σ_{sT}	direct spin Nernst conductivity
$\Delta\sigma_{\mathrm{sT}}$	magnetization-dependent part of σ_{sT}
τ	momentum relaxation time with associated rate $1/\tau$; contour time
τ_{DP}	Dyakonov-Perel spin relaxation time with associated rate $1/\tau_{\mathrm{DP}}$
τ_s	Elliott-Yafet spin relaxation time with associated rate $1/\tau_s$
τ_x, τ_y, τ_z	Pauli matrices

Notation	Description
τ_0	2×2 unit matrix
$\boldsymbol{\tau}$	spin torque
ϕ	magnetization angle
ϕ_0	magnetization angle where σ_{sE} and P_{sE} are independent of $g_r^{\uparrow\downarrow}$
ϕ_1, ϕ_2	magnetization angle where σ_{sE} and P_{sE} are independent of $g_r^{\uparrow\downarrow}$, respectively
φ_k	single-particle wave function
Φ	scalar potential
$\hat{\Psi}$	fermionic field operator
$\boldsymbol{\Psi}$	SU(2) scalar potential
ω	frequency of the magnetic texture
ω_{D}	Debye frequency
∂_p^μ	momentum four-derivative
∂_μ	spatial four-derivative
$\tilde{\partial}_\mu$	covariant four-derivative
$\tilde{\nabla}_{\mathbf{r}}$	covariant spatial derivative
$\tilde{\partial}_t$	covariant time derivative
δ_{ij}	Kronecker delta
$\delta(x)$	Dirac delta function
ε_{ijk}	Levi-Civita symbol
$\theta(x)$	Theta function
$\langle \dots \rangle$	angular average; expectation value
$\langle \dots \rangle_{\text{imp}}$	impurity average
$\langle \dots \rangle_y$	spatial average
$[A, B]$	commutator of A and B
$\{A, B\}$	anticommutator of A and B
$A \otimes B$	convolution and matrix multiplication of A and B
$[A \overset{\otimes}{,} B]$	commutator/convolution of A and B

Bibliography

[1] M. Dyakonov and V. Perel, "Current-induced spin orientation of electrons in semiconductors," Phys. Lett. A **35**, 459 (1971).

[2] J. E. Hirsch, "Spin Hall effect," Phys. Rev. Lett. **83**, 1834 (1999).

[3] Y. K. Kato, R. C. Myers, A. C. Gossard, and D. D. Awschalom, "Observation of the spin Hall effect in semiconductors," Science **306**, 1910 (2004).

[4] J. Wunderlich, B. Kaestner, J. Sinova, and T. Jungwirth, "Experimental observation of the spin-Hall effect in a two-dimensional spin-orbit coupled semiconductor system," Phys. Rev. Lett. **94**, 047204 (2005).

[5] E. L. Ivchenko and G. E. Pikus, "New photogalvanic effect in gyrotropic crystals," JETP Lett. **27**, 604 (1978).

[6] F. T. Vas'ko and N. A. Prima, "Spin splitting of spectrum of 2-dimensional electrons," Sov. Phys. Solid State **21**, 994 (1979).

[7] A. G. Aronov and Y. B. Lyanda-Geller, "Nuclear electric resonance and orientation of carrier spins by an electric field," JETP Lett. **50**, 431 (1989).

[8] V. Edelstein, "Spin polarization of conduction electrons induced by electric current in two-dimensional asymmetric electron systems," Solid State Commun. **73**, 233 (1990).

[9] Y. K. Kato, R. C. Myers, A. C. Gossard, and D. D. Awschalom, "Current-induced spin polarization in strained semiconductors," Phys. Rev. Lett. **93**, 176601 (2004).

[10] A. Y. Silov, P. A. Blajnov, J. H. Wolter, R. Hey, K. H. Ploog, and N. S. Averkiev, "Current-induced spin polarization at a single heterojunction," Appl. Phys. Lett. **85**, 5929 (2004).

[11] I. Žutić, J. Fabian, and S. Das Sarma, "Spintronics: Fundamentals and applications," Rev. Mod. Phys. **76**, 323 (2004).

[12] J. Sinova, S. O. Valenzuela, J. Wunderlich, C. H. Back, and T. Jungwirth, "Spin Hall effects," Rev. Mod. Phys. **87**, 1213 (2015).

[13] S.-g. Cheng, Y. Xing, Q.-f. Sun, and X. C. Xie, "Spin Nernst effect and Nernst effect in two-dimensional electron systems," Phys. Rev. B **78**, 045302 (2008).

[14] Z. Ma, "Spin Hall effect generated by a temperature gradient and heat current in a two-dimensional electron gas," Solid State Commun. **150**, 510 (2010).

[15] K. Tauber, M. Gradhand, D. V. Fedorov, and I. Mertig, "Extrinsic spin Nernst effect from first principles," Phys. Rev. Lett. **109**, 026601 (2012).

[16] J. Borge, C. Gorini, and R. Raimondi, "Spin thermoelectrics in a disordered Fermi gas," Phys. Rev. B **87**, 085309 (2013).

[17] S. Tölle, C. Gorini, and U. Eckern, "Room-temperature spin thermoelectrics in metallic films," Phys. Rev. B **90**, 235117 (2014).

[18] C. M. Wang and M. Q. Pang, "Thermally induced spin polarization and thermal conductivities in a spin–orbit-coupled two-dimensional electron gas," Solid State Commun. **150**, 1509 (2010).

[19] A. Dyrdał, M. Inglot, V. K. Dugaev, and J. Barnaś, "Thermally induced spin polarization of a two-dimensional electron gas," Phys. Rev. B **87**, 245309 (2013).

[20] G. E. W. Bauer, E. Saitoh, and B. J. Van Wees, "Spin caloritronics," Nat. Mater. **11**, 391 (2012).

[21] S. D. Ganichev, E. L. Ivchenko, S. N. Danilov, J. Eroms, W. Wegscheider, D. Weiss, and W. Prettl, "Conversion of spin into directed electric current in quantum wells," Phys. Rev. Lett. **86**, 4358 (2001).

[22] J. C. Rojas Sánchez, L. Vila, G. Desfonds, S. Gambarelli, J. P. Attané, J. M. De Teresa, C. Magén, and A. Fert, "Spin-to-charge conversion using Rashba coupling at the interface between non-magnetic materials," Nat. Commun. **4**, 2944 (2013).

[23] H. Zhao, E. J. Loren, H. M. van Driel, and A. L. Smirl, "Coherence control of Hall charge and spin currents," Phys. Rev. Lett. **96**, 246601 (2006).

[24] E. Saitoh, M. Ueda, H. Miyajima, and G. Tatara, "Conversion of spin current into charge current at room temperature: Inverse spin-Hall effect," Appl. Phys. Lett. **88**, 182509 (2006).

[25] S. O. Valenzuela and M. Tinkham, "Direct electronic measurement of the spin Hall effect," Nature **442**, 176 (2006).

[26] P. Sheng, Y. Sakuraba, Y.-C. Lau, S. Takahashi, S. Mitani, and M. Hayashi, "The spin Nernst effect in tungsten," Sci. Adv. **3**, e1701503 (2017).

[27] S. Meyer, Y.-T. Chen, S. Wimmer, M. Althammer, T. Wimmer, S. Geprägs, H. Huebl, D. Ködderitzsch, H. Ebert, G. E. W. Bauer, et al., "Observation of the spin Nernst effect," Nat. Mater. **16**, 977 (2017).

[28] S. Tölle, U. Eckern, and C. Gorini, "Spin-charge coupled dynamics driven by a time-dependent magnetization," Phys. Rev. B **95**, 115404 (2017).

[29] K. v. Klitzing, G. Dorda, and M. Pepper, "New method for high-accuracy determination of the fine-structure constant based on quantized Hall resistance," Phys. Rev. Lett. **45**, 494 (1980).

[30] V. L. Berezinskiĭ, "Destruction of long-range order in one-dimensional and two-dimensional systems having a continuous symmetry group I. Classical systems," Sov. Phys. JETP **32**, 493 (1971).

[31] V. L. Berezinskiĭ, "Destruction of long-range order in one-dimensional and two-dimensional systems possessing a continuous symmetry group. II. Quantum systems," Sov. Phys. JETP **34**, 610 (1972).

[32] J. M. Kosterlitz and D. J. Thouless, "Ordering, metastability and phase transitions in two-dimensional systems," J. Phys. C: Solid State Phys. **6**, 1181 (1973).

[33] P. W. Anderson, "Absence of diffusion in certain random lattices," Phys. Rev. **109**, 1492 (1958).

[34] E. Abrahams, P. W. Anderson, D. C. Licciardello, and T. V. Ramakrishnan, "Scaling theory of localization: Absence of quantum diffusion in two dimensions," Phys. Rev. Lett. **42**, 673 (1979).

[35] P. A. Lee and T. V. Ramakrishnan, "Disordered electronic systems," Rev. Mod. Phys. **57**, 287 (1985).

[36] É. I. Rashba, "Properties of semiconductors with an extremum loop, I. cyclotron and combinational resonance in a magnetic field perpendicular to the plane of the loop," Sov. Phys. Solid State **2**, 1109 (1960), *Rashba spin-orbit coupling was named in honour of the Soviet-American theoretical physicist Emmanuel I. Rashba (born October 30, 1927, Kiev) who worked in Ukraine, Russia, and the USA*.

[37] Y. A. Bychkov and É. I. Rashba, "Properties of a 2d electron gas with lifted spectral degeneracy," JETP Lett. **39**, 78 (1984).

[38] A. Ohtomo and H. Y. Hwang, "A high-mobility electron gas at the $LaAlO_3$/$SrTiO_3$ heterointerface," Nature **427**, 423 (2004).

[39] S. Thiel, G. Hammerl, A. Schmehl, C. W. Schneider, and J. Mannhart, "Tunable quasi-two-dimensional electron gases in oxide heterostructures," Science **313**, 1942 (2006).

[40] J. Mannhart and D. G. Schlom, "Oxide interfaces–an opportunity for electronics," Science **327**, 1607 (2010).

[41] G. Khalsa, B. Lee, and A. H. MacDonald, "Theory of t_{2g} electron-gas Rashba interactions," Phys. Rev. B **88**, 041302 (2013).

[42] R. Winkler, *Spin-orbit coupling effects in two-dimensional electron and hole systems* (Springer, Berlin, 2003).

[43] R. Urban, G. Woltersdorf, and B. Heinrich, "Gilbert damping in single and multilayer ultrathin films: Role of interfaces in nonlocal spin dynamics," Phys. Rev. Lett. **87**, 217204 (2001).

[44] Y. Tserkovnyak, A. Brataas, and G. E. W. Bauer, "Enhanced gilbert damping in thin ferromagnetic films," Phys. Rev. Lett. **88**, 117601 (2002).

[45] A. Azevedo, L. H. Vilela-Leão, R. L. Rodríguez-Suárez, A. F. Lacerda Santos, and S. M. Rezende, "Spin pumping and anisotropic magnetoresistance voltages in magnetic bilayers: Theory and experiment," Phys. Rev. B **83**, 144402 (2011).

[46] F. D. Czeschka, L. Dreher, M. S. Brandt, M. Weiler, M. Althammer, I.-M. Imort, G. Reiss, A. Thomas, W. Schoch, W. Limmer, et al., "Scaling behavior of the spin pumping effect in ferromagnet-platinum bilayers," Phys. Rev. Lett. **107**, 046601 (2011).

[47] T. Kimura, Y. Otani, T. Sato, S. Takahashi, and S. Maekawa, "Room-temperature reversible spin Hall effect," Phys. Rev. Lett. **98**, 156601 (2007).

[48] O. Mosendz, V. Vlaminck, J. E. Pearson, F. Y. Fradin, G. E. W. Bauer, S. D. Bader, and A. Hoffmann, "Detection and quantification of inverse spin Hall effect from spin pumping in permalloy/normal metal bilayers," Phys. Rev. B **82**, 214403 (2010).

[49] M. Obstbaum, M. Härtinger, H. G. Bauer, T. Meier, F. Swientek, C. H. Back, and G. Woltersdorf, "Inverse spin Hall effect in $Ni_{81}Fe_{19}$/normal-metal bilayers," Phys. Rev. B **89**, 060407(R) (2014).

[50] H. Nakayama, M. Althammer, Y.-T. Chen, K. Uchida, Y. Kajiwara, D. Kikuchi, T. Ohtani, S. Geprägs, M. Opel, S. Takahashi, et al., "Spin Hall magnetoresistance induced by a nonequilibrium proximity effect," Phys. Rev. Lett. **110**, 206601 (2013).

[51] N. Vlietstra, J. Shan, V. Castel, J. Ben Youssef, G. E. W. Bauer, and B. J. Van Wees, "Exchange magnetic field torques in YIG/Pt bilayers observed by the spin-Hall magnetoresistance," Appl. Phys. Lett. **103**, 032401 (2013).

[52] C. Hahn, G. de Loubens, O. Klein, M. Viret, V. V. Naletov, and J. Ben Youssef, "Comparative measurements of inverse spin Hall effects and magnetoresistance in YIG/Pt and YIG/Ta," Phys. Rev. B **87**, 174417 (2013).

[53] S. Meyer, M. Althammer, S. Geprägs, M. Opel, R. Gross, and S. T. B. Goennenwein, "Temperature dependent spin transport properties of platinum inferred from spin Hall magnetoresistance measurements," Appl. Phys. Lett. **104**, 242411 (2014).

[54] S. T. B. Goennenwein, R. Schlitz, M. Pernpeintner, K. Ganzhorn, M. Althammer, R. Gross, and H. Huebl, "Non-local magnetoresistance in Yig/Pt nanostructures," Appl. Phys. Lett. **107**, 172405 (2015).

[55] S. Vélez, V. N. Golovach, A. Bedoya-Pinto, M. Isasa, E. Sagasta, M. Abadia, C. Rogero, L. E. Hueso, F. S. Bergeret, and F. Casanova, "Hanle magnetoresistance in thin metal films with strong spin-orbit coupling," Phys. Rev. Lett. **116**, 016603 (2016).

[56] L. Vila, T. Kimura, and Y. Otani, "Evolution of the spin Hall effect in Pt nanowires: Size and temperature effects," Phys. Rev. Lett. **99**, 226604 (2007).

[57] T. Seki, Y. Hasegawa, S. Mitani, S. Takahashi, H. Imamura, S. Maekawa, J. Nitta, and K. Takanashi, "Giant spin Hall effect in perpendicularly spin-polarized FePt/Au devices," Nat. Mater. **7**, 1476 (2008).

[58] L. Liu, T. Moriyama, D. C. Ralph, and R. A. Buhrman, "Spin-torque ferromagnetic resonance induced by the spin Hall effect," Phys. Rev. Lett. **106**, 036601 (2011).

[59] L. Liu, C.-F. Pai, Y. Li, H. W. Tseng, D. C. Ralph, and R. A. Buhrman, "Spin-torque switching with the giant spin Hall effect of tantalum," Science **336**, 555 (2012).

[60] M. Isasa, E. Villamor, L. E. Hueso, M. Gradhand, and F. Casanova, "Temperature dependence of spin diffusion length and spin Hall angle in Au and Pt," Phys. Rev. B **91**, 024402 (2015).

[61] Q. Hao, W. Chen, and G. Xiao, "Beta (β) tungsten thin films: structure, electron transport, and giant spin Hall effect," Appl. Phys. Lett. **106**, 182403 (2015).

[62] M. Gmitra, A. Matos-Abiague, C. Draxl, and J. Fabian, "Magnetic control of spin-orbit fields: A first-principles study of Fe/GaAs junctions," Phys. Rev. Lett. **111**, 036603 (2013).

[63] T. Hupfauer, A. Matos-Abiague, M. Gmitra, F. Schiller, J. Loher, D. Bougeard, C. H. Back, J. Fabian, and D. Weiss, "Emergence of spin–orbit fields in magnetotransport of quasi-two-dimensional iron on gallium arsenide," Nat. Comm. **6**, 7374 (2015).

[64] S. D. Ganichev, E. L. Ivchenko, V. V. Bel'kov, S. A. Tarasenko, M. Sollinger, D. Weiss, W. Wegscheider, and W. Prettl, "Spin-galvanic effect," Nature **417**, 153 (2002).

[65] S. D. Ganichev, M. Trushin, and J. Schliemann, in *Handbook of spin transport and magnetism*, edited by E. Y. Tsymbal and I. Žutić (CRC Press, Boca Raton, FL, 2012), pp. 487–497.

[66] K. Shen, G. Vignale, and R. Raimondi, "Microscopic theory of the inverse Edelstein effect," Phys. Rev. Lett. **112**, 096601 (2014).

[67] R. Raimondi, C. Gorini, P. Schwab, and M. Dzierzawa, "Quasiclassical approach to the spin Hall effect in the two-dimensional electron gas," Phys. Rev. B **74**, 035340 (2006).

[68] C. Gorini, P. Schwab, M. Dzierzawa, and R. Raimondi, "Spin polarizations and spin Hall currents in a two-dimensional electron gas with magnetic impurities," Phys. Rev. B **78**, 125327 (2008).

[69] R. Raimondi, P. Schwab, C. Gorini, and G. Vignale, "Spin-orbit interaction in a two-dimensional electron gas: SU(2) formulation," Ann. Phys. (Berlin) **524**, 153 (2012).

[70] Y. Tserkovnyak, A. Brataas, and G. E. W. Bauer, "Theory of current-driven magnetization dynamics in inhomogeneous ferromagnets," J. Magn. Magn. Mater. **320**, 1282 (2008).

[71] Y. Tserkovnyak and M. Mecklenburg, "Electron transport driven by nonequilibrium magnetic textures," Phys. Rev. B **77**, 134407 (2008).

[72] V. Vlaminck and M. Bailleul, "Current-induced spin-wave Doppler shift," Science **322**, 410 (2008).

[73] Y. Kajiwara, K. Harii, S. Takahashi, J. Ohe, K. Uchida, M. Mizuguchi, H. Umezawa, H. Kawai, K. Ando, K. Takanashi, et al., "Transmission of electrical signals by spin-wave interconversion in a magnetic insulator," Nature **464**, 262 (2010).

[74] J. Slonczewski, "Current-driven excitation of magnetic multilayers," J. Magn. Magn. Mater. **159**, L1 (1996).

[75] A. Brataas, Y. V. Nazarov, and G. E. W. Bauer, "Finite-element theory of transport in ferromagnet–normal metal systems," Phys. Rev. Lett. **84**, 2481 (2000).

[76] Y. Tserkovnyak, A. Brataas, G. E. W. Bauer, and B. I. Halperin, "Nonlocal magnetization dynamics in ferromagnetic heterostructures," Rev. Mod. Phys. **77**, 1375 (2005).

[77] Y.-T. Chen, S. Takahashi, H. Nakayama, M. Althammer, S. T. B. Goennenwein, E. Saitoh, and G. E. W. Bauer, "Theory of spin Hall magnetoresistance," Phys. Rev. B **87**, 144411 (2013).

[78] S. Tölle, M. Dzierzawa, U. Eckern, and C. Gorini, "Spin Hall magnetoresistance and spin Nernst magnetothermopower in a Rashba system: Role of the inverse spin galvanic effect," Ann. Phys. (Berlin) **530**, 1700303 (2018).

[79] K. Ishizaka, M. S. Bahramy, H. Murakawa, M. Sakano, T. Shimojima, T. Sonobe, K. Koizumi, S. Shin, H. Miyahara, A. Kimura, et al., "Giant Rashba-type spin splitting in bulk BiTeI," Nat. Mater. **10**, 521 (2011).

[80] G. Landolt, S. V. Eremeev, Y. M. Koroteev, B. Slomski, S. Muff, T. Neupert, M. Kobayashi, V. N. Strocov, T. Schmitt, Z. S. Aliev, et al., "Disentanglement of surface and bulk Rashba spin splittings in noncentrosymmetric BiTeI," Phys. Rev. Lett. **109**, 116403 (2012).

[81] C. Martin, A. V. Suslov, S. Buvaev, A. F. Hebard, P. Bugnon, H. Berger, A. Magrez, and D. B. Tanner, "Experimental determination of the bulk Rashba parameters in BiTeBr," EPL **116**, 57003 (2017).

[82] D. Di Sante, P. Barone, R. Bertacco, and S. Picozzi, "Electric control of the giant Rashba effect in bulk GeTe," Adv. Mater. **25**, 509 (2013).

[83] M. Liebmann, C. Rinaldi, D. Di Sante, J. Kellner, C. Pauly, R. N. Wang, J. E. Boschker, A. Giussani, S. Bertoli, M. Cantoni, et al., "Giant Rashba-type spin splitting in ferroelectric GeTe (111)," Adv. Mater. **28**, 560 (2016).

[84] D. Niesner, M. Wilhelm, I. Levchuk, A. Osvet, S. Shrestha, M. Batentschuk, C. Brabec, and T. Fauster, "Giant Rashba splitting in $CH_3NH_3PbBr_3$ organic-inorganic perovskite," Phys. Rev. Lett. **117**, 126401 (2016).

[85] S. Tölle, M. Dzierzawa, U. Eckern, and C. Gorini, "Quasiclassical theory of the spin-orbit magnetoresistance of three-dimensional Rashba metals," arXiv:1805.10245 (2018).

[86] L. P. Kadanoff and G. A. Baym, *Quantum statistical mechanics* (Benjamin, New York, NY, 1962).

[87] A. A. Abrikosov and L. P. Gor'kov, *Quantum field theoretical methods in statistical physics* (Pergamon Press, Oxford, 1965).

[88] J. M. Ziman, *Elements of advanced quantum theory* (Cambridge University Press, Cambridge, 1995).

[89] J. W. Negele and H. Orland, *Quantum many-particle systems* (Westview Press, Boulder, CO, 1998).

[90] A. L. Fetter and J. D. Walecka, *Quantum theory of many-particle systems* (Dover Publications, Mineola, NY, 2003).

[91] G. D. Mahan, *Many-particle physics* (Plenum Press, New York, NY, 1990).

[92] A. M. Tsvelik, *Quantum field theory in condensed matter physics* (Cambridge University Press, Cambridge, 2003).

[93] A. Kamenev and A. Levchenko, "Keldysh technique and non-linear σ-model: basic principles and applications," Adv. Phys. **58**, 197 (2009).

[94] J. Rammer and H. Smith, "Quantum field-theoretical methods in transport theory of metals," Rev. Mod. Phys. **58**, 323 (1986).

[95] H. Haug and A.-P. Jauho, *Quantum kinetics in transport and optics of semiconductors* (Springer, Berlin, 1996).

[96] J. Rammer, *Quantum field theory of non-equilibrium states* (Cambridge University Press, Cambridge, 2007).

[97] C. Gorini, P. Schwab, R. Raimondi, and A. L. Shelankov, "Non-Abelian gauge fields in the gradient expansion: Generalized Boltzmann and Eilenberger equations," Phys. Rev. B **82**, 195316 (2010).

[98] U. Eckern and A. Schmid, "Quasiclassical Green's function in the BCS pairing theory," J. Low Temp. Phys. **45**, 137 (1981).

[99] C. Gorini, A. Maleki Sheikhabadi, K. Shen, I. V. Tokatly, G. Vignale, and R. Raimondi, "Theory of current-induced spin polarization in an electron gas," Phys. Rev. B **95**, 205424 (2017).

[100] R. J. Elliott, "Theory of the effect of spin-orbit coupling on magnetic resonance in some semiconductors," Phys. Rev. **96**, 266 (1954).

[101] Y. Yafet, "g factors and spin-lattice relaxation of conduction electrons," Solid State Physics **14**, 1 (1963).

[102] H. B. Callen and T. A. Welton, "Irreversibility and generalized noise," Phys. Rev. **83**, 34 (1951).

[103] R. Kubo, M. Toda, and N. Hashitsume, *Statistical physics II: nonequilibrium statistical mechanics* (Springer, Berlin, 1985).

[104] L. V. Keldysh, "Diagram technique for nonequilibrium processes," Sov. Phys. JETP **20**, 1018 (1965).

[105] J. Schwinger, "Brownian motion of a quantum oscillator," J. Math. Phys. **2**, 407 (1961).

[106] A. I. Larkin and Y. Ovchinnikov, "Nonlinear conductivity of superconductors in the mixed state," Sov. Phys. JETP **41**, 960 (1975).

[107] G. C. Wick, "The evaluation of the collision matrix," Phys. Rev. **80**, 268 (1950).

[108] R. P. Feynman, "Space-time approach to quantum electrodynamics," Phys. Rev. **76**, 769 (1949).

[109] J. Rammer, *Quantum transport theory* (Perseus Books, Reading, MA, 1998).

[110] R. Raimondi, C. Gorini, and S. Tölle, in *Spin orbitronics and topological transport properties*, edited by V. Dugaev, I. Tralle, A. Wal, and J. Barnaś (World Scientific, Singapore, 2018), pp. 80–109.

[111] M. E. Peskin and D. V. Schroeder, *An introduction to quantum field theory* (Perseus Books, Reading, MA, 1995).

[112] R. Raimondi and P. Schwab, "Tuning the spin Hall effect in a two-dimensional electron gas," EPL **87**, 37008 (2009).

[113] J. M. Luttinger and W. Kohn, "Motion of electrons and holes in perturbed periodic fields," Phys. Rev. **97**, 869 (1955).

[114] E. O. Kane, "Band structure of indium antimonide," J. Phys. Chem. Solids **1**, 249 (1957).

[115] D. Stein, K. v. Klitzing, and G. Weimann, "Electron spin resonance on GaAs-$Al_xGa_{1-x}As$ heterostructures," Phys. Rev. Lett. **51**, 130 (1983).

[116] H. L. Stormer, Z. Schlesinger, A. Chang, D. C. Tsui, A. C. Gossard, and W. Wiegmann, "Energy structure and quantized Hall effect of two-dimensional holes," Phys. Rev. Lett. **51**, 126 (1983).

[117] R. Lassnig, "$\mathbf{k} \cdot \mathbf{p}$ theory, effective-mass approach, and spin splitting for two-dimensional electrons in GaAs-GaAlAs heterostructures," Phys. Rev. B **31**, 8076 (1985).

[118] L. Wissinger, U. Rössler, R. Winkler, B. Jusserand, and D. Richards, "Spin splitting in the electron subband of asymmetric GaAs/$Al_xGa_{1-x}As$ quantum wells: The multiband envelope function approach," Phys. Rev. B **58**, 15375 (1998).

[119] J. Nitta, T. Akazaki, H. Takayanagi, and T. Enoki, "Gate control of spin-orbit interaction in an inverted $In_{0.53}Ga_{0.47}As/In_{0.52}Al_{0.48}As$ heterostructure," Phys. Rev. Lett. **78**, 1335 (1997).

[120] T. Schäpers, G. Engels, J. Lange, T. Klocke, M. Hollfelder, and H. Lüth, "Effect of the heterointerface on the spin splitting in modulation doped $In_xGa_{1-x}As$/InP quantum wells for $B \to 0$," J. Appl. Phys. **83**, 4324 (1998).

[121] D. Grundler, "Large Rashba splitting in InAs quantum wells due to electron wave function penetration into the barrier layers," Phys. Rev. Lett. **84**, 6074 (2000).

[122] J. Ryu, M. Kohda, and J. Nitta, "Observation of the D'yakonov-Perel' spin relaxation in single-crystalline Pt thin films," Phys. Rev. Lett. **116**, 256802 (2016).

[123] C. R. Ast, J. Henk, A. Ernst, L. Moreschini, M. C. Falub, D. Pacilé, P. Bruno, K. Kern, and M. Grioni, "Giant spin splitting through surface alloying," Phys. Rev. Lett. **98**, 186807 (2007).

[124] I. Gierz, T. Suzuki, E. Frantzeskakis, S. Pons, S. Ostanin, A. Ernst, J. Henk, M. Grioni, K. Kern, and C. R. Ast, "Silicon surface with giant spin splitting," Phys. Rev. Lett. **103**, 046803 (2009).

[125] V. Brosco and C. Grimaldi, "Anisotropy of transport in bulk Rashba metals," Phys. Rev. B **95**, 195164 (2017).

[126] M. I. Dyakonov and V. I. Perel, "Spin relaxation of conduction electrons in noncentrosymmetric semiconductors," Sov. Phys. Solid State **13**, 3023 (1972).

[127] G. Vignale, "Ten years of spin Hall effect," J. Supercond. Nov. Magn. **23**, 3 (2010).

[128] L. Berger, "Side-jump mechanism for the Hall effect of ferromagnets," Phys. Rev. B **2**, 4559 (1970).

[129] S. K. Lyo and T. Holstein, "Side-jump mechanism for ferromagnetic Hall effect," Phys. Rev. Lett. **29**, 423 (1972).

[130] A. Crépieux and P. Bruno, "Theory of the anomalous Hall effect from the Kubo formula and the Dirac equation," Phys. Rev. B **64**, 014416 (2001).

[131] H.-A. Engel, B. I. Halperin, and E. I. Rashba, "Theory of spin Hall conductivity in n-doped GaAs," Phys. Rev. Lett. **95**, 166605 (2005).

[132] N. F. Mott and H. S. W. Massey, *The theory of atomic collisions*, vol. 35 (Clarendon Press, Oxford, 1965).

[133] C. Gorini, U. Eckern, and R. Raimondi, "Spin Hall effects due to phonon skew scattering," Phys. Rev. Lett. **115**, 076602 (2015).

[134] U. Eckern, C. Gorini, and S. Tölle, "Room-temperature transport properties of spin-robit coupled Fermi systems: Spin thermoelectric effects, phonon skew scattering," arXiv:1609.00561 (2016).

[135] J. Sinova, D. Culcer, Q. Niu, N. A. Sinitsyn, T. Jungwirth, and A. H. MacDonald, "Universal intrinsic spin Hall effect," Phys. Rev. Lett. **92**, 126603 (2004).

[136] R. Raimondi and P. Schwab, "Spin-Hall effect in a disordered two-dimensional electron system," Phys. Rev. B **71**, 033311 (2005).

[137] O. V. Dimitrova, "Spin-Hall conductivity in a two-dimensional Rashba electron gas," Phys. Rev. B **71**, 245327 (2005).

[138] I. M. Miron, K. Garello, G. Gaudin, P.-J. Zermatten, M. V. Costache, S. Auffret, S. Bandiera, B. Rodmacq, A. Schuhl, and P. Gambardella, "Perpendicular switching of a single ferromagnetic layer induced by in-plane current injection," Nature **476**, 189 (2011).

[139] D. A. Pesin and A. H. MacDonald, "Quantum kinetic theory of current-induced torques in Rashba ferromagnets," Phys. Rev. B **86**, 014416 (2012).

[140] W. J. Antel, M. M. Schwickert, T. Lin, W. L. O'Brien, and G. R. Harp, "Induced ferromagnetism and anisotropy of Pt layers in Fe/Pt(001) multilayers," Phys. Rev. B **60**, 12933 (1999).

[141] F. Wilhelm, P. Poulopoulos, G. Ceballos, H. Wende, K. Baberschke, P. Srivastava, D. Benea, H. Ebert, M. Angelakeris, N. K. Flevaris, et al., "Layer-resolved magnetic moments in Ni/Pt multilayers," Phys. Rev. Lett. **85**, 413 (2000).

[142] G. Y. Guo, Q. Niu, and N. Nagaosa, "Anomalous Nernst and Hall effects in magnetized platinum and palladium," Phys. Rev. B **89**, 214406 (2014).

[143] D. C. Langreth and J. W. Wilkins, "Theory of spin resonance in dilute magnetic alloys," Phys. Rev. B **6**, 3189 (1972).

[144] J. P. Perdew and Y. Wang, "Accurate and simple analytic representation of the electron-gas correlation energy," Phys. Rev. B **45**, 13244 (1992).

[145] H. J. Monkhorst and J. D. Pack, "Special points for brillouin-zone integrations," Phys. Rev. B **13**, 5188 (1976).

[146] D. Ralph and M. Stiles, "Spin transfer torques," J. Magn. Magn. Mater. **320**, 1190 (2008).

[147] M. Pickel, A. B. Schmidt, F. Giesen, J. Braun, J. Minár, H. Ebert, M. Donath, and M. Weinelt, "Spin-orbit hybridization points in the face-centered-cubic cobalt band structure," Phys. Rev. Lett. **101**, 066402 (2008).

[148] A. Fert, "Nobel lecture: Origin, development, and future of spintronics," Rev. Mod. Phys. **80**, 1517 (2008).

[149] L. Berger, "Emission of spin waves by a magnetic multilayer traversed by a current," Phys. Rev. B **54**, 9353 (1996).

[150] M. Tsoi, A. G. M. Jansen, J. Bass, W.-C. Chiang, M. Seck, V. Tsoi, and P. Wyder, "Excitation of a magnetic multilayer by an electric current," Phys. Rev. Lett. **80**, 4281 (1998).

[151] E. B. Myers, D. C. Ralph, J. A. Katine, R. N. Louie, and R. A. Buhrman, "Current-induced switching of domains in magnetic multilayer devices," Science **285**, 867 (1999).

[152] J. A. Katine, F. J. Albert, R. A. Buhrman, E. B. Myers, and D. C. Ralph, "Current-driven magnetization reversal and spin-wave excitations in Co/Cu/Co pillars," Phys. Rev. Lett. **84**, 3149 (2000).

[153] A. A. Kovalev, A. Brataas, and G. E. W. Bauer, "Spin transfer in diffusive ferromagnet–normal metal systems with spin-flip scattering," Phys. Rev. B **66**, 224424 (2002).

[154] J. C. Slonczewski, "Currents and torques in metallic magnetic multilayers," J. Magn. Magn. Mater. **247**, 324 (2002).

[155] X. Jia, K. Liu, K. Xia, and G. E. Bauer, "Spin transfer torque on magnetic insulators," EPL **96**, 17005 (2011).

[156] M. E. Knoester, J. Sinova, and R. A. Duine, "Phenomenology of current-skyrmion interactions in thin films with perpendicular magnetic anisotropy," Phys. Rev. B **89**, 064425 (2014).

[157] A. Stern, "Berry's phase, motive forces, and mesoscopic conductivity," Phys. Rev. Lett. **68**, 1022 (1992).

[158] S. E. Barnes and S. Maekawa, "Generalization of Faraday's law to include nonconservative spin forces," Phys. Rev. Lett. **98**, 246601 (2007).

[159] R. A. Duine, "Spin pumping by a field-driven domain wall," Phys. Rev. B **77**, 014409 (2008).

[160] G. Tatara, N. Nakabayashi, and K.-J. Lee, "Spin motive force induced by Rashba interaction in the strong sd coupling regime," Phys. Rev. B **87**, 054403 (2013).

[161] Y. Yamane, J. Ieda, and S. Maekawa, "Spinmotive force with static and uniform magnetization induced by a time-varying electric field," Phys. Rev. B **88**, 014430 (2013).

[162] P. Schwab, R. Raimondi, and C. Gorini, "Inverse spin Hall effect and anomalous Hall effect in a two-dimensional electron gas," EPL **90**, 67004 (2010).

[163] M. Zwierzycki, Y. Tserkovnyak, P. J. Kelly, A. Brataas, and G. E. W. Bauer, "First-principles study of magnetization relaxation enhancement and spin transfer in thin magnetic films," Phys. Rev. B **71**, 064420 (2005).

[164] P. Schwab, M. Dzierzawa, C. Gorini, and R. Raimondi, "Spin relaxation in narrow wires of a two-dimensional electron gas," Phys. Rev. B **74**, 155316 (2006).

[165] M. Althammer, S. Meyer, H. Nakayama, M. Schreier, S. Altmannshofer, M. Weiler, H. Huebl, S. Geprägs, M. Opel, R. Gross, et al., "Quantitative study of the spin Hall magnetoresistance in ferromagnetic insulator/normal metal hybrids," Phys. Rev. B **87**, 224401 (2013).

[166] T. Lin, C. Tang, H. M. Alyahayaei, and J. Shi, "Experimental investigation of the nature of the magnetoresistance effects in Pd-YIG hybrid structures," Phys. Rev. Lett. **113**, 037203 (2014).

[167] Y. Yang, B. Wu, K. Yao, S. Shannigrahi, B. Zong, and Y. Wu, "Investigation of magnetic proximity effect in Ta/YIG bilayer Hall bar structure," J. Appl. Phys. **115**, 17C509 (2014).

[168] M. Isasa, A. Bedoya-Pinto, S. Vélez, F. Golmar, F. Sánchez, L. E. Hueso, J. Fontcuberta, and F. Casanova, "Spin Hall magnetoresistance at Pt/$CoFe_2O_4$ interfaces and texture effects," Appl. Phys. Lett. **105**, 142402 (2014).

[169] Z. Ding, B. L. Chen, J. H. Liang, J. Zhu, J. X. Li, and Y. Z. Wu, "Spin Hall magnetoresistance in Pt/Fe_3O_4 thin films at room temperature," Phys. Rev. B **90**, 134424 (2014).

[170] C. O. Avci, K. Garello, A. Ghosh, M. Gabureac, S. F. Alvarado, and P. Gambardella, "Unidirectional spin Hall magnetoresistance in ferromagnet/normal metal bilayers," Nat. Phys. **11**, 570 (2015).

[171] J. Liu, T. Ohkubo, S. Mitani, K. Hono, and M. Hayashi, "Correlation between the spin Hall angle and the structural phases of early 5d transition metals," Appl. Phys. Lett. **107**, 232408 (2015).

[172] J. Kim, P. Sheng, S. Takahashi, S. Mitani, and M. Hayashi, "Spin Hall magnetoresistance in metallic bilayers," Phys. Rev. Lett. **116**, 097201 (2016).

[173] J. H. Han, C. Song, F. Li, Y. Y. Wang, G. Y. Wang, Q. H. Yang, and F. Pan, "Antiferromagnet-controlled spin current transport in $SrMnO_3$Pt hybrids," Phys. Rev. B **90**, 144431 (2014).

[174] Y. Yang, Y. Xu, K. Yao, and Y. Wu, "Thickness dependence of spin Hall magnetoresistance in FeMn/Pt bilayers," AIP Advances **6**, 065203 (2016).

[175] H. Nakayama, Y. Kanno, H. An, T. Tashiro, S. Haku, A. Nomura, and K. Ando, "Rashba-Edelstein magnetoresistance in metallic heterostructures," Phys. Rev. Lett. **117**, 116602 (2016).

[176] H. Nakayama, H. An, A. Nomura, Y. Kanno, S. Haku, Y. Kuwahara, H. Sakimura, and K. Ando, "Temperature dependence of Rashba-Edelstein magnetoresistance in Bi/Ag/CoFeB trilayer structures," Appl. Phys. Lett. **110**, 222406 (2017).

[177] L. Zhou, H. Song, K. Liu, Z. Luan, P. Wang, L. Sun, S. Jiang, H. Xiang, Y. Chen, J. Du, et al., "Observation of spin-orbit magnetoresistance in metallic thin films on magnetic insulators," Sci. Adv. **4**, eaao3318 (2018).

[178] S. Mühlbauer, B. Binz, F. Jonietz, C. Pfleiderer, A. Rosch, A. Neubauer, R. Georgii, and P. Böni, "Skyrmion lattice in a chiral magnet," Science **323**, 915 (2009).

[179] Y. Onose, Y. Okamura, S. Seki, S. Ishiwata, and Y. Tokura, "Observation of magnetic excitations of skyrmion crystal in a helimagnetic insulator Cu_2OSeO_3," Phys. Rev. Lett. **109**, 037603 (2012).

[180] D. Hirobe, Y. Shiomi, Y. Shimada, J.-i. Ohe, and E. Saitoh, "Generation of spin currents in the skyrmion phase of a helimagnetic insulator Cu_2OSeO_3," J. Appl. Phys. **117**, 053904 (2015).

[181] A. Aqeel, N. Vlietstra, J. A. Heuver, G. E. W. Bauer, B. Noheda, B. J. van Wees, and T. T. M. Palstra, "Spin-Hall magnetoresistance and spin Seebeck effect in

spin-spiral and paramagnetic phases of multiferroic $CoCr_2O_4$ films," Phys. Rev. B **92**, 224410 (2015).

[182] A. Aqeel, N. Vlietstra, A. Roy, M. Mostovoy, B. J. van Wees, and T. T. M. Palstra, "Electrical detection of spiral spin structures in Pt|Cu_2OSeO_3 heterostructures," Phys. Rev. B **94**, 134418 (2016).

[183] K.-W. Kim, K.-J. Lee, J. Sinova, H.-W. Lee, and M. D. Stiles, "Spin-orbit torques from interfacial spin-orbit coupling for various interfaces," Phys. Rev. B **96**, 104438 (2017).

[184] L. Zhou, V. L. Grigoryan, S. Maekawa, X. Wang, and J. Xiao, "Spin Hall effect by surface roughness," Phys. Rev. B **91**, 045407 (2015).

[185] A. Shpiro, P. M. Levy, and S. Zhang, "Self-consistent treatment of nonequilibrium spin torques in magnetic multilayers," Phys. Rev. B **67**, 104430 (2003).

[186] N. W. Ashcroft and N. D. Mermin, *Solid state physics* (Saunders, Philadelphia, PA, 1976).

Publications and preprints

2018 [85] S. Tölle, M. Dzierzawa, U. Eckern, and C. Gorini, "Quasiclassical theory of the spin-orbit magnetoresistance of three-dimensional Rashba metals," arXiv:1805.10245 (2018).

[78] S. Tölle, M. Dzierzawa, U. Eckern, and C. Gorini, "Spin Hall magnetoresistance and spin Nernst magnetothermopower in a Rashba system: Role of the inverse spin galvanic effect," Ann. Phys. (Berlin) **530**, 1700303 (2018).

[110] R. Raimondi, C. Gorini, and S. Tölle, in *Spin orbitronics and topological transport properties*, edited by V. Dugaev, I. Tralle, A. Wal, and J. Barnas (World Scientific, Singapore, 2018), pp. 80–109.

2017 [28] S. Tölle, U. Eckern, and C. Gorini, "Spin-charge coupled dynamics driven by a time-dependent magnetization," Phys. Rev. B **95**, 115404 (2017).

2016 [134] U. Eckern, C. Gorini, and S. Tölle, "Room-temperature transport properties of spin-orbit coupled Fermi systems: Spin thermoelectric effects, phonon skew scattering," arXiv:1609.00561 (2016).

2014 [17] S. Tölle, C. Gorini, and U. Eckern, "Room-temperature spin thermoelectrics in metallic films," Phys. Rev. B **90**, 235117 (2014).

Acknowledgements

I wish to express my gratitude to those persons who contributed in one way or another to the successful completion of this thesis.

First and foremost I thank my doctoral advisor Prof. Dr. Ulrich Eckern for his excellent mentoring and for giving me the opportunity to work on this interesting topic in his group. I have benefited a lot on his knowledge, his experience, and his professional guidance.

I consider it an honor to work with Dr. Cosimo Gorini and I am deeply grateful for his continuous support and his commitment during my time as a Ph.D. student. Despite the regional distance, he always found time to answer my emails patiently or to setup a Skype conference, even during his (sometimes busy) free time at home.

Prof. Dr. Thilo Kopp kindly agreed to be the secondary referee of this thesis. For this, and for being my second mentor during my time in the IGS of the Transregio, I thank him a lot.

A special gratitude goes out to Dr. Michael Dzierzawa for proofreading this thesis and the fruitful collaboration. I very much appreciate our sophisticated discussions, not only on physical grounds ("Ball gespielt!").

I would like to thank my colleagues for creating the pleasant atmosphere in the workplace, Andreas Prinz-Zwick, Patrick Seiler, Christian Schiegg, Ralf Utermann, Dr. Johannes Wanner, Prof. Dr. Gert-Ludwig Ingold, and Prof. Dr. Dr. h.c. mult. Peter Hänggi. A special thanks to Michael Hartmann for organizing the Kaffeeseminar and helping me with computer problems, and Wilhelm Appelt for supporting me with DFT calculations for this thesis.

Last but by no means least, I am especially indebted to my parents, Jutta and Wolfram Tölle, my brother, Benjamin Tölle, and my wife, Ramona Tölle, for supporting me spiritually without any if, ands or buts. Thanks for all your encouragement!

No pain!
Tony "Duke" Evers to Rocky Balboa
Rocky IV (1985)